The Thesis Committee for Trenton Blake Ellis
Certifies that this is the approved version of the following thesis:

A Subsurface Investigation in Taylor Clay

APPROVED BY
SUPERVISING COMMITTEE:

Supervisor:

Chadi S. El Mohtar

Robert B. Gilbert

A Subsurface Investigation in Taylor Clay

by

Trenton Blake Ellis, B.S.C.E.

Thesis

Presented to the Faculty of the Graduate School of

The University of Texas at Austin

in Partial Fulfillment

of the Requirements

for the Degree of

Master of Science in Engineering

The University of Texas at Austin

August 2011

Acknowledgements

The author is indebted to many people for their help and support throughout this research project. Many thanks are in order to Fugro Consultants, Inc. for their help with the subsurface investigation and valuable laboratory guidance. This project would not have been possible without funding from the Texas Department of Transportation. Though not directly related to the research presented herein, it was also a pleasure to work with Lymon C. Reese and Associates, McKinney Drilling Company and HVJ and Associates. Perhaps most importantly, the author wishes to thank Roy Lee for allowing the research team to dig holes in his property over the past two years.

The author's advisors, Dr. Chadi El Mohtar and Dr. Robert Gilbert, have provided meaningful insight throughout the study. The author would also like to thank the other two students involved with this research project, Andrew Brown and Greg Dellinger, for their help in the laboratory and the field. Thanks also extend to the University of Texas soil dynamics research group for braving extreme heat to run seismic tests on site. Finally, the author offers his thanks to friends and family who have kept life interesting and lively in the midst of long hours in the field and the lab.

Abstract

A Subsurface Investigation in Taylor Clay

Trenton Blake Ellis, M.S.E.

The University of Texas at Austin, 2011

Supervisor: Chadi S. El Mohtar

A comprehensive field and laboratory investigation at the location of the Lymon C. Reese Research Wall is presented. Soil at the site is a stiff, fissured and heavily overconsolidated clay from the Taylor Group. Index properties such as Atterberg limits and clay fractions were used with common empirical guidelines to assess the qualitative swell potential. The soil's compressibility and strength characteristics were difficult to measure in the lab, owing to the stiff soil's secondary structure. Measured values were compared to well established correlations and test results from similar soils sampled from locations near the present test site. Cyclic swell tests were to predict the soil's lateral swell potential after multiple cycles of wetting and drying. Empirical guidelines indicated the soil has a "high" to "very high" swell potential. This was validated by the swelling that was observed during consolidation and cyclic swell tests. The soil's drained and undrained strengths were both rather large, often more typical of rock than soil. The stress history was not evident from consolidation results, either due to disturbance, cementation or extreme overconsolidation. The hydraulic conductivity was particularly elusive, again due to the soil's secondary structure.

Table of Contents

1 Introduction

1. 1 Background

Highly plastic and overconsolidated clay soils can present many challenges for geotechnical engineers. Over geologic time, these soils have experienced stresses that impart a secondary structure of slickensided fissures, mineral-filled bands and micro-cracks. This chaotic matrix of discontinuities significantly affects the soil's strength and permeability. The process of overconsolidation – whether by evapotranspiration or static loading – also locks some amount of stress into the soil structure, which can vary in magnitude depending on direction. For soils rich in montmorillonite, the swell potential associated with a strong affinity for water also influences the soil's behavior.

Researchers have attempted to understand the combined effect of these factors for decades, but the field behavior of this type of soil remains shrouded in uncertainty. By and large, the associated design procedures for any application are limited to empirical guidelines, local experience and engineering judgment. The laboratory methods that are available for measuring expansion potential and permeability must be carefully planned to model site conditions, typically involve several weeks of testing time and require careful interpretation.

1. 2 Setting: Lymon C. Reese Research Wall

The Lymon C. Reese Research Wall is a drilled shaft retaining wall that was installed in the Taylor clay of Manor, TX. The drilled shafts were instrumented with optical strain gages and inclinometers to measure the wall's movement as moisture

fluctuations cause the retained soil to shrink and swell. Time domain reflectrometry (TDR) sensors were installed in soil around the retaining wall to measure changes in volumetric moisture content, and a piezometer was installed near the retaining wall to monitor the groundwater level (Dellinger, 2011). The purpose of the project as a whole is to gain a better understanding of the magnitude and distribution of lateral pressures that an expansive soil may exert on a retaining structure. This thesis describes the subsurface investigation and soil properties at the test site.

1. 3 Scope

The research presented in this thesis applies to clays from the Taylor Group in central Texas. The clays are very stiff, highly overconsolidated, highly plastic and fissured. In a qualitative sense, Taylor clay has properties that could pertain to either a hard blocky soil or a very soft rock. All of the test samples for this project were obtained from the Lymon C. Reese Research Wall test site in Manor, TX.

1. 4 Objectives

This research was conducted to study the lateral pressures that can develop in shallow regions of the Taylor clay. This involved several approaches. First, a number of index properties such as Atterberg limits and clay fractions were measured. These values are commonly used to characterize this type of soil on an empirical basis. Standard engineering tests were also conducted to quantify the compressibility and strength properties of the soil at the Lymon C. Reese Research Wall test site. In addition, more

specialized tests were conducted to measure the lateral swell pressure under cyclic wetting and drying. The objective is to combine field and laboratory tests with a thorough review of local experience to gain a better understanding of the soil at the test site.

1. 5 Thesis Organization

The thesis is organized into seven chapters. Chapter 2 is a literature review that provides background on expansive soils and stiff-fissured clays. Chapter 3 reviews the geology and engineering properties of Taylor clays near the test site. Chapter 4 summarizes the sampling and testing that occurred during the subsurface investigation. Chapter 5 describes the laboratory tests that were conducted and summarizes the results. Test results from Chapters 2, 3, 4 and 5 were compared in Chapter 6. General conclusions from the study are presented in Chapter 7.

1. 6 Sign Convention

Measurements of axial strain are presented throughout the thesis in the discussion of various laboratory tests. In each case, positive strains refer to compression while negative strains refer to swelling. This is consistent with the geotechnical tradition of referring to compressive forces in the positive sense.

2 Literature Review

2. 1 Swell Potential in Expansive Clays

2.1.1 Overview

In the presence of water, expansive clays can expand by sucking free water molecules into their mineral structure. This phenomenon causes volumetric strains and/or the exertion of swell pressures, depending on boundary conditions. The boundary conditions – which may include stress history, in-situ confinement, structural boundaries and a seasonally imposed system of dynamic moisture pathways – are difficult, if not impossible to replicate in the lab with small-scale samples.

Expansive soils are also prone to shrinking as water molecules are removed from the mineral structure. This process occurs much slower than swelling under normal field conditions because of the attraction between the clay and the water. During swelling, the clay pulls free water molecules into its structure and locks them into place. The water molecules are no longer "free" during shrinking, and external factors such as heat and air flow are required to overcome the attraction. As the clay minerals are robbed of water molecules, the soil exhibits volumetric shrinkage and cracking. Meanwhile, the surface tension in the water imparts negative pore pressures to the clay's skeletal structure. The negative pore pressures can be very large in magnitude – corresponding to the large tensile forces required to remove the water molecules – which results in high effective stress and stiffness. The potential for a clay soil to swell is therefore a function of climate as well as clay mineralogy.

Katti (1994) ran large-scale laboratory tests to measure the lateral pressure exerted by a column of expansive Black Cotton soil. The researchers built a 9-ft tall stiffened steel frame, fitted for the measurement of lateral pressure at several depths and lined with a thin sand layer to distribute water. The lateral pressure was around zero near the surface after wetting for 60 to 90 days, but lateral pressures increased rapidly up to a 1.2-meter depth, thereafter remaining constant. The largest lateral stresses exceeded vertical stresses by 18 times, far greater than typical at-rest or passive earth pressures. Katti attributes this deviation from typical Coulomb and Rankine assumptions to physical and physiochemical alterations within the clay that occur during and after saturation. This may or may not be typical for other expansive soils with different mineralogies. It does, however, indicate that expansive soils can exhibit fundamentally different behavior than we expect from typical soils.

It has been also been shown that stress history can also influence the swell potential of expansive clays. Laboratory tests by Joshi and Katti (1980) have shown that, for a given surcharge, overconsolidated clays can exert larger lateral swell pressures than their normally consolidated counterparts. This change in swell potential caused by preloading was shown by measuring the lateral swell pressures that developed upon wetting under various surcharge loads. The higher surcharge loads were gradually reduced, overconsolidating the soil. The authors surmised that overconsolidation can cause a subtle rearrangement of the matrix of clay minerals and water molecules, essentially locking some amount of stress into the soil, Figure 1.

These concepts are not well understood, but designers mostly agree that highly overconsolidated soils are prone to exhibit additional swell potential that cannot be predicted based solely on the clay minerology and climate. The same holds true for most aspects of design involving expansive soils.

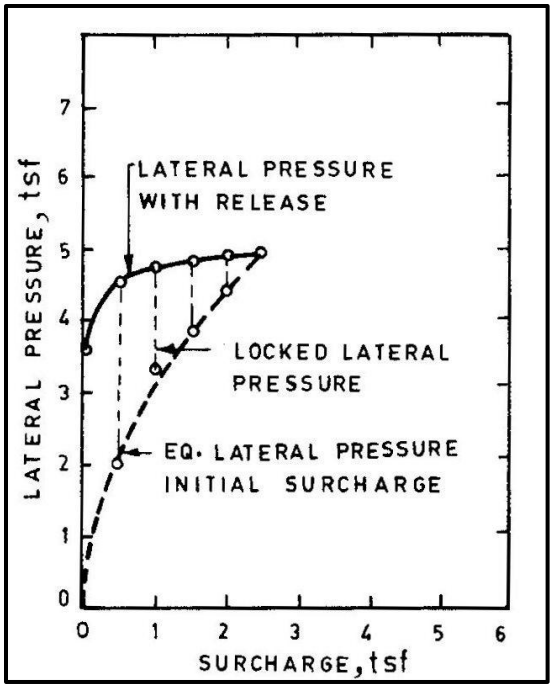

Figure 1. Locked-In Swell Potential from Overconsolidation, Joshi and Katti (1980)

2.1.2 Effects of Mineral Structure and Orientation

Expansive soils owe their swell potential to a unique aluminosilicate mineral structure that has been well documented extensively in the literature (Mitchell 2005). Smectite minerals, including montmorillonite, generally contain the most swell potential. Smectite's mineral sheets are connected to one another by weak van der Waals forces,

allowing cations within the mineral structure to be substituted with ease during formation. Isomorphic substitution, as the process is called, tends to replace silicon and aluminum with other cations. These cations are attracted to the region between mineral plates, whose surfaces are covered with negative charges. The interplate space is mostly populated with dipolar water molecules; the exchangeable cations bond with the negative ends of those water molecules. Owing to the weak van der Waals forces that connect the mineral plates, additional water can infiltrate between a mature soil's mineral plates as boundary conditions such as confinement and climate change. The influx of water into the mineral structure is the genesis for expansive behavior.

Young soils often have a neat arrangement of flatly stacked clay mineral sheets that would be expected to swell essentially perpendicular to the faces of the mineral plates. The particle arrangement of young soils is modified by processes including over-consolidation, weathering, shearing and cycles of wetting and drying. This process – termed ripening – creates a more complicated microstructure. The ripened microstructure first becomes more chaotic, then rearranges to a more stable pattern through multiple wetting and drying cycles. The microstructure of ripened clays becomes more random, consisting of a matrix of various structural arrangements (Kodikara et al., 1999). The resulting swell potential is difficult to predict, but is certainly three-dimensional.

2.1.3 Empirical Correlations

It is usually more practical to predict expansive potential with inexpensive index tests than to invest in a limited number of more robust laboratory methods. Index

properties do not measure any mechanistic aspect of swell potential, but they correlate well enough with swell potential to provide a qualitative indicator of what to expect. Laboratory tests, although complicated and expensive, do not generally replicate field conditions well enough to provide high quality predictions of field behavior.

Atterberg limits are widely used to estimate various aspects of clay behavior. Atterberg limits essentially measure the amount of water a soil can hold under specific – and arbitrary – dynamic loading conditions. The ability to hold more water under these arbitrary conditions is analogous to the weakness of the soil's interlayer bonds and its ability to add water to its mineral structure. Table 1 (Chen, 1988) and Figure 2 (Daksanamurthy and Raman, 1973) present two guidelines that are used to qualitatively predict swell potential with Atterberg limits.

Table 1. Qualitative Relationship between PI and Swell Potential, Chen (1988)

Swell Potential	Plasticity Index
Low	0 – 15
Medium	10 – 35
High	20 – 55
Very High	35 and above

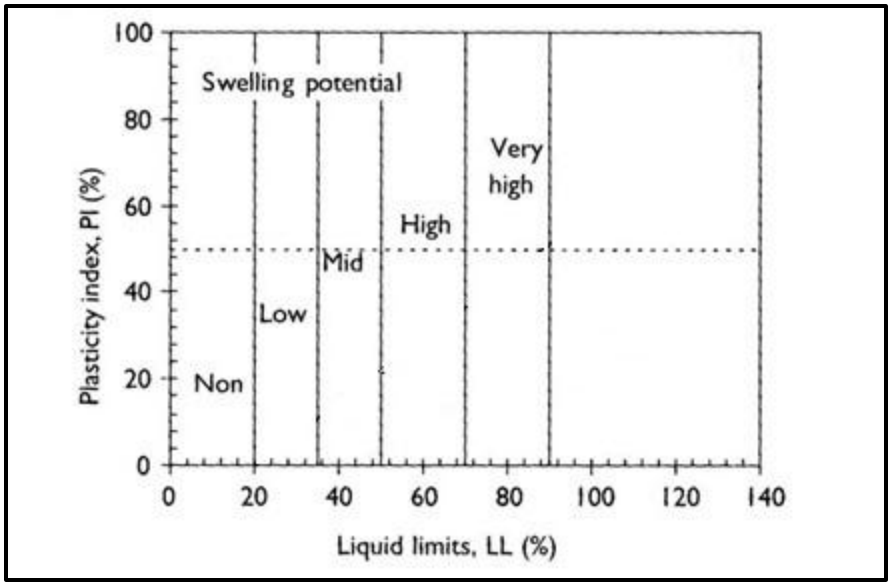

Figure 2. Qualitative Relationship Between PI, LL and Swelling Potential, Daksanamurthy and Raman (1973)

Swell potential is similarly related to the amount of suction that a soil can exert to bring water into its structure. Both measures (water carrying capacity and suction) are essentially functions of the physico-chemical structure of the soil. A soil's physico-chemical structure can be quantified by a parameter termed colloidal activity (A_c). Skempton (1953) defined colloidal activity as the ratio of plasticity index (PI) to clay fraction (CF), Equation 1. Clay fraction is the percent of particles smaller in diameter than 0.002 mm. Higher A_c values indicate higher swelling potential, and Table 2 provides a simple guideline for classifying A_c values.

$$A_c = \frac{PI}{CF} \qquad \text{..... Eq. 1}$$

The physico-chemical structure is also quantified by its cation exchange capacity (CEC), which is the milliequivalent of exchangeable cations per 100 grams of dry clay. Table 3 lists ranges of CEC and A_c values for the common clay minerals. As the table suggests, montmorillonite – particularly, sodium montmorillonite – possesses much greater swell potential than any other common clay mineral.

Table 2. Guideline for Interpreting Colloidal Activity (A_c) Values

A_c	Activity Class
< 0.75	Inactive
0.75 – 1.25	Normal
> 1.25	Active

Table 3. Cation Exchange Capacities and Activities of Common Clay Minerals, Nelson and Miller (1992)

Clay Mineral	CEC (meq/100 g)	A_c
Kaolinite	3 – 15	0.33 – 0.46
Illite	10 – 40	0.9
Montmorillonite (Ca)	80 - 150	1.5
Montmorillonite (Na)		7.2

2.1.4 Mechanistic Predictions

The swell potential of expansive soils is most commonly measured with the same type of equipment used to conduct one-dimensional consolidation tests. A remolded or undisturbed specimen is prepared in a rigid ring, typically 2.5 inches in diameter and 0.5 – 1.0 inches thick. An appropriate normal stress is applied to the specimen for a short time to allow seating and the closing of fissures and microcracks in the specimen. The specimen is then wetted, and the resulting strains from swelling are measured. ASTM D4546 describes several standard methods for conducting these types of tests.

In other cases the normal load is progressively increased to prevent swelling strains. The load required to achieve and maintain constant volume is a measure of the soil's heave potential. Fredlund (1980) has reported that heave measurements on trimmed specimens may lead to very unconservative results owing to sampling disturbance. Fredlund reports that measured heave values can be as low as half of the heave to be expected in-situ, and he has presented a method for correcting those errors.

According to Fredlund, the effects of disturbance during heave tests may be corrected as follows. The method applies to heave tests that involve swelling under constant volume, then loading up to a very large vertical effective stress and finally unloading back to some token load. First, the machine deflections are subtracted from the analysis and the resulting e-log-P' curve is plotted. The point of maximum curvature – usually just beyond the swell pressure – is then located. From this point, three lines are drawn: (1) horizontal, (2) tangent and (3) bisector of (1) and (2). Next, a line parallel to the rebound curve is drawn where it is tangent to the virgin compression curve. The

intersection of this line with the previously drawn bisector marks the corrected swell pressure corresponding to an undisturbed state of stress.

Another type of test has also been used in which the soil is allowed to swell and shrink while subjected to wetting and drying cycles. As the specimen is subjected to repeated drying and wetting cycles, it experiences volumetric shrinking and swelling. This essentially remolds the sample in a manner consistent with in-situ conditions while measuring the axial strains that occur throughout the successive cycles. In addition, the soil can be removed and weighed between cycles and periodically during drying cycles to track the moisture content throughout the test. After four or five cycles of wetting and drying, the soil ripens to a steady state of swell behavior, Figures 3 and 4.

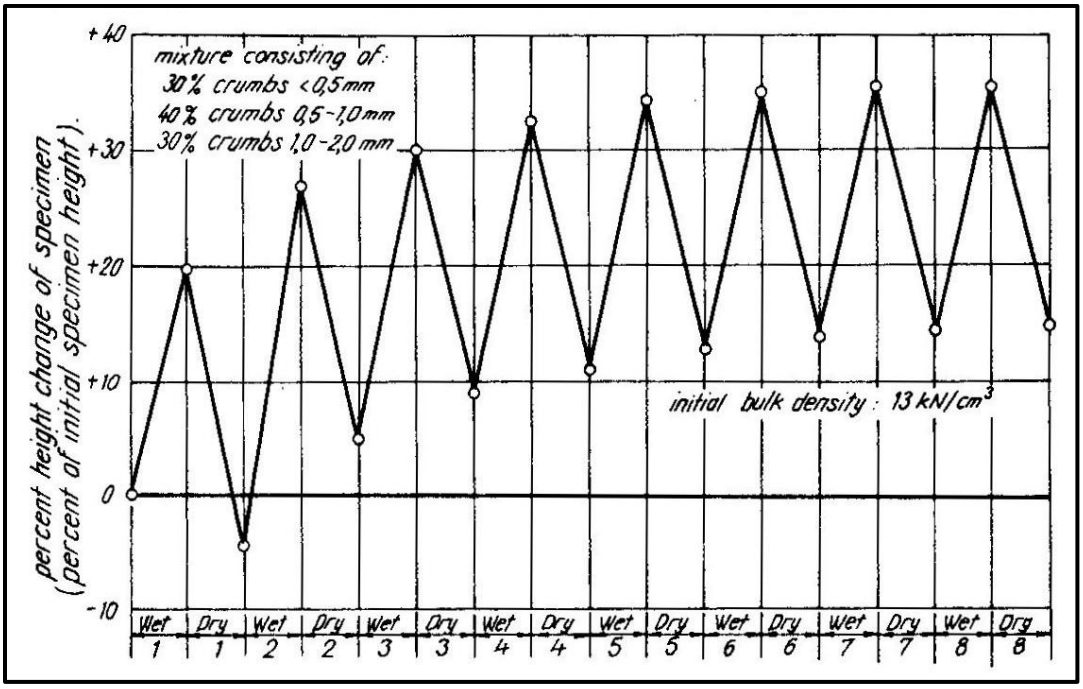

Figure 3. Cyclic Swell and Shrink Results from Popescu (1980)

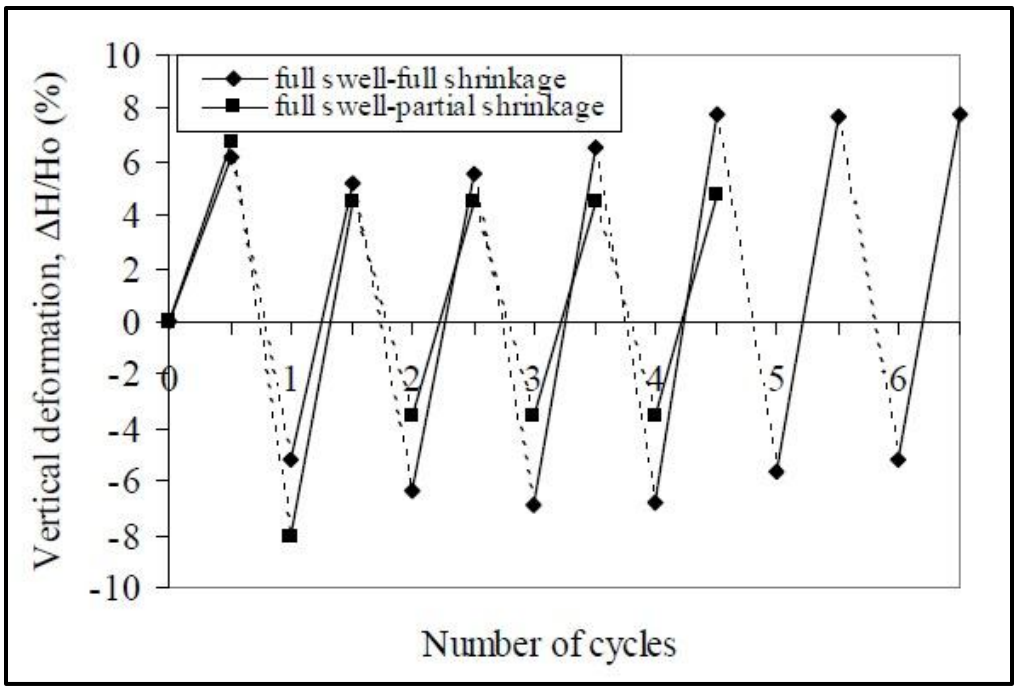

Figure 4. Cyclic Swell and Shrink Results from Tawfiq (2009)

Marr (2003) began developing a cyclic swell test method as a practical way to predict swell potential without resorting to more expensive procedures and complicated constitutive modeling. He used traditional, commonly available one-dimensional consolidation equipment during the study. Specimens were completely inundated in water and subject to a constant total stress during swelling stages. The consolidometer was removed from the frame and disassembled once swelling reached equilibrium. The specimen was then weighed and reassembled into the consolidometer.

During shrinking stages the consolidometer was again loaded into the frame and the same total stress was applied as for the swelling stage. During shrinking, however, water was not added to the cell. The soil was allowed to shrink as it air-dried until the

changes in height became negligible. Periodically, the specimen would be removed, weighed and reloaded to track the moisture content.

Shrinking by air-drying required approximately one month per shrink stage. In a later study, Allen (2005) developed a procedure for forced ventilation to accelerate the shrink stages. Allen modified a standard consolidometer so that air could be forced through the assembly at a pressure sufficiently large to shorten the drying time without damaging the soil specimen. A pressure of 5 psi was found to work well and shorten the drying time to just one or two days.

After each swell and shrink cycle, a plot is developed of height or axial strain versus moisture content. Marr originally tracked the specimen's void ratio, but as the soil shrinks three-dimensionally the total specimen volume becomes an unknown value. The void ratio may or may not be a meaningful description during shrinking stages, but the height or axial strain is certainly more straight-forward.

Additional cycles of swell and shrink stages are then performed until the relationship between height and moisture content reaches a steady state. For preliminary calculations, the initial moisture content of the specimen – prior to the first swell stage – may be assumed equal to the moisture content of high-quality samples obtained during trimming. The additional swell and shrink stages are performed exactly as described for the initial stages. Approximately four to five cycles of swell and shrink stages are typically required to reach the steady state. Figure 5 presents an example of the results from one full test.

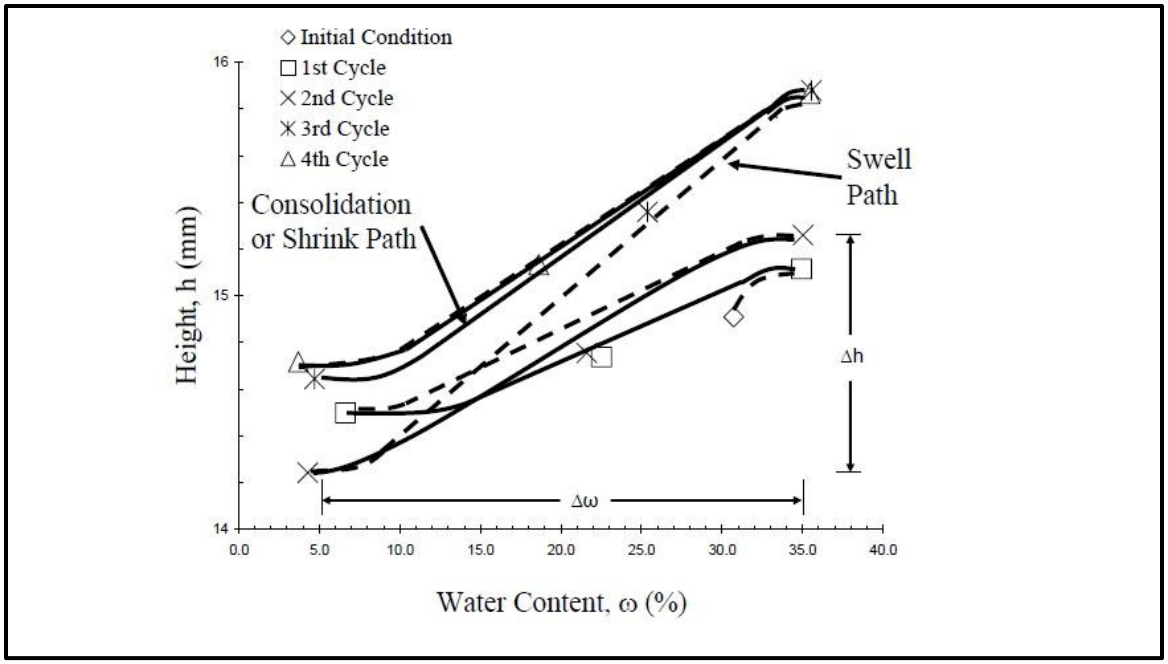

Figure 5. Example of Cyclic Swell-Shrink Behavior, Allen (2005)

The slope of the steady state line is the ultimate parameter gained from a cyclic swell test. It represents the rate at which swelling and shrinking strains may be expected to occur with changes in moisture content. The slope of each steady state line corresponds to a single constant value of total stress. Marr proposed combining multiple test results with different total stresses to define the constitutive surface in Figure 6. The range of moisture contents to be expected in the field is a detail that must be determined separately. One major benefit from this type of test is the remolding by shrinking and swelling that seems to recreate naturally occurring field conditions and results in a highly repeatable measurement.

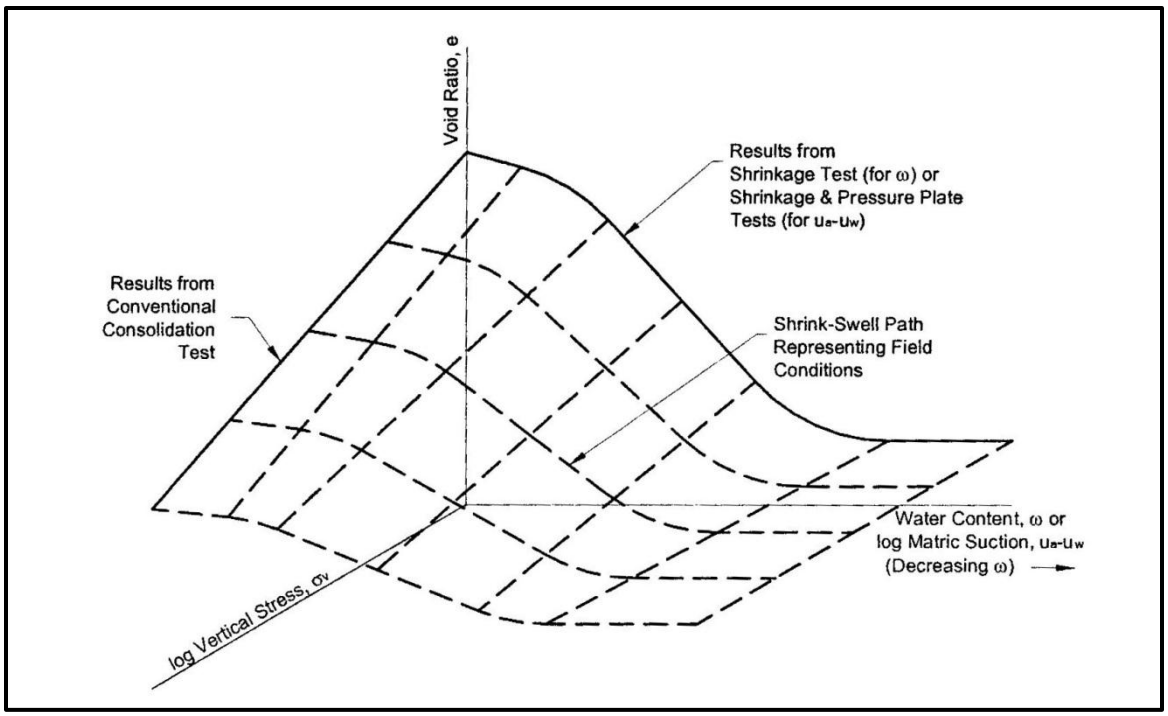

Figure 6. Constitutive Surface Measured with Cyclic Swell Tests, Marr (2003)

2. 2 Stiff Fissured Clays

2.2.1 Overview

The stiff fissured variety of expansive soils is particularly problematic in geotechnical design and remediation. The intact soil can be very strong and nearly impermeable. Problems arise because of their secondary structure of cracks and fissures, which form a chaotic network of relatively slick and permeable surfaces throughout the clay structure. The hydraulic conductivity and shear strength of these soils is a function of both the intact soil and the secondary structural boundaries.

2.2.2 Hydraulic Conductivity

It is well known that clays exhibit much lower hydraulic conductivities than sands and silts. Still, the measurement of moisture flow through clay is a well-established practice as long as the soil structure permits Darcian flow. Cracked and fissured clays may not abide this fundamental rule. Within the clay's structure, there may be at least three flow zones with significantly different flow properties. The intact clay is usually very nearly impermeable, but microcracks and fissures provide relatively preferential moisture pathways. Surface dessication cracks, on the other hand, provide a zone of completely uninhibited flow while they are open. Owing to the variability and incalculable spatial arrangement of flow zones, the overall hydraulic conductivity of fissured clays is quite difficult to predict or measure.

2.2.3 Shear Strength

Stiff fissured clays have several unique shear strength characteristics. Skempton and Larochelle (1965) summarized a number of important implications. First, laboratory and field tests that only utilize a small volume of soil are likely to be measuring strength of the intact soil alone. There may be very little if any shear resistance along open fissures, and this lowers the overall in-situ shear resistance. When loaded, pore water tends to migrate toward these fissures which lowers the effective stress and further reduces the shear resistance. As a consequence, laboratory tests are likely to overestimate shear strength if the specimens are too small and if the rate of loading is too fast to allow pore water to migrate as it would in-situ.

2.2.4 Crumb Structure and Cyclic Moisture Fluctuations

The upper portion of clay deposits, several processes work together to aggregate the individual clay particles (Popescu 1980). Cyclic moisture fluctuations, freezing and thawing, leaching, oxidation or reduction can all play a role in developing a crumb structure within a clay deposit. Crumbs refer to small clusters of clay minerals that become bound together with a binding agent such as calcium carbonate, iron oxide or colloidal silica. Crumbs are most volatile near the surface where the voids between crumbs may be open and permeable; inter-crumb voids are generally closed at greater depths, but may be opened by stress relief.

Well-developed crumb structures result in an overall secondary structure of the clay soil. The secondary structure undergoes changes as the individual crumbs are slaked and aggregated during cycles of wetting and drying. Shrinking generally encourages the soil to group into larger, denser crumbs. Subsequent wetting can break the larger crumbs apart, exposing additional surface areas of active clay minerals. After multiple cycles of wetting and drying, the crumbs tend to cluster and slake in a more stable, repeatable fashion.

3 Properties of Taylor Clay at the Lymon C. Reese Research Wall

3.1 Geology

The Taylor Group comprises several clay strata that were deposited in east-central Texas during the late Cretaceous period. Deposition of the Taylor and overlying Navarro Groups took place under a slowly receding shallow sea. The deposition began near the end of the Austin Chalk deposition. The dominant clay mineral in the Taylor group is montmorillonite (Beall, 1964). A number of studies throughout the twentieth century contributed to a more detailed understanding of the Taylor group.

Walcott (1901) described the Taylor formation as calcareous clay marls, locally known as "joint clays". The local terminology likely refers to Walcott's observation that the clay is jointed, laminated and friable throughout, having a crackled appearance when dry. Also noted was the presence of lime, in a chalky condition, as an accessory constituent. Fossils of Exogyra ponderosa (Figure 7) were reported to be frequent, but only in the lower portion of the formation. Finally, Walcott noted some difficulty in delineating the boundary between the Taylor and overlying Navarro formations.

Burford (1928) continued investigating the Taylor Group, and again encountered difficulty mapping the Taylor-Navarro contact. One contact was found 0.25 miles west of Kimbro, and was delineated as a straight line that intersected Old US Highway 20 approximately 2.5 miles east of Manor, TX, Figure 8. Burford described the contact as a 6-inch stratum of chalky, sandy clay.

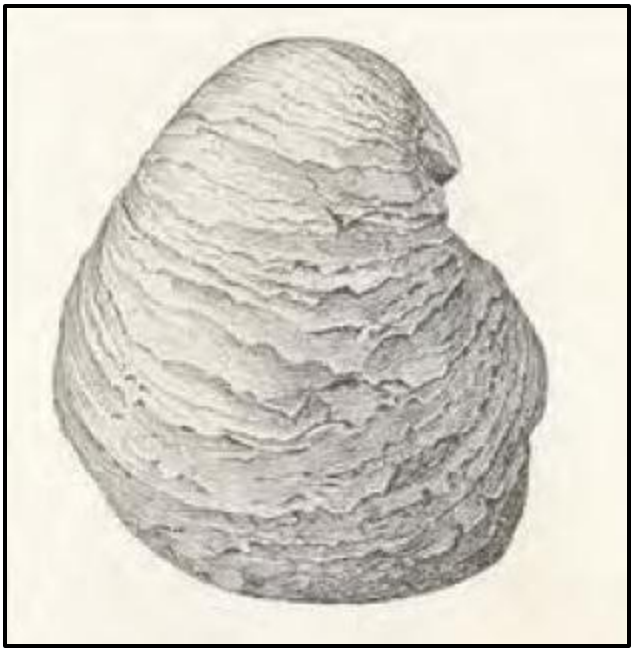

Figure 7. Example of Exogyra Ponderosa Fossil, Walcott (1901)

The upper portion of the Taylor Group is described as pure bentonite clay with common occurrences of Exogra ponderosa. The lower portion of the Navarro Group was characterized by a lack of Exogyra ponderosa and a 10-ft stratum of greenish-yellow clay. Faulting with an Eastern throw was present at and around the contact. West of the fault, fossils indicate the clay is of the Taylor Group; east of the fault, fossils and sediments were typical of the middle Navarro. The throw of the fault was approximated as at least 200 feet.

Beall (1964) summarized the historical efforts to classify strata within and surrounding the Taylor Group, Figure 9. Ambiguous contacts had led to a general confusion regarding the Taylor-Navarro contact. Beall suggested combining the

contact's two adjacent members – the Upper Taylor Marl Member and the Neylandville Marl – to a single, mappable member of the Taylor Group.

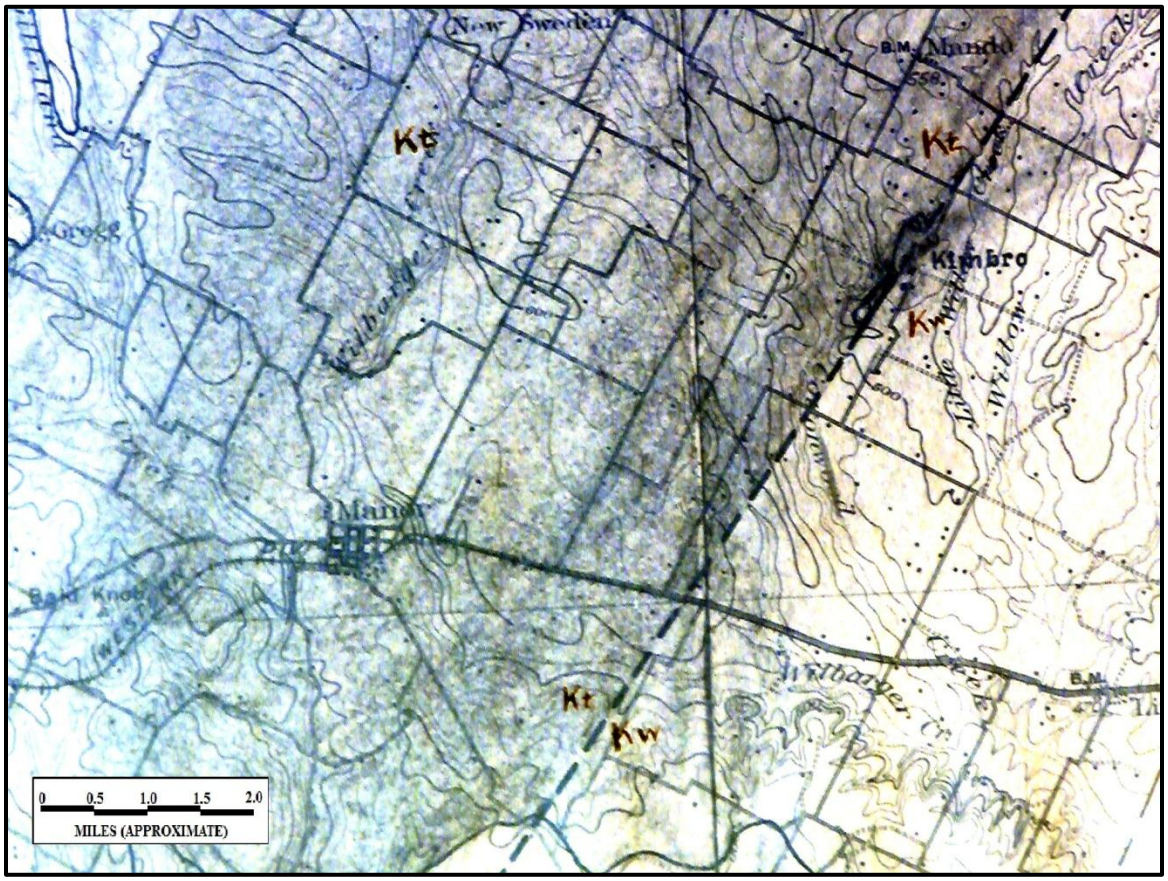

Figure 8. Delineation of Taylor-Navarro Contact, Burford (1928)

In addition, Beall presented the measured chemical contents of 46 samples from the Taylor Formation, Figure 10. Chemical contents were obtained by X-ray diffraction. The results confirm that montmorillonite is the formation's primary clay mineral. Sodium, calcium and magnesium were the montmorillonite's primary cations.

Young (1965) later proposed renaming the Upper Taylor member to the Bergstrom Formation, Figure 11. In doing so, he presented a summary of what would come to be called the Bergstrom Formation. It was described as a greenish-gray to brownish-gray, unctuous, montmorillonitic claystone, more calcareous toward the base. The Taylor-Navarro contact was described as a 6-inch thick calcareous siltstone bed.

Tipple (1975) conducted a series of tests on samples from a well that was dug through the Taylor Group in the vicinity of Manor, TX. Figure 12 shows a geologic map of the region. The results from his tests are presented in Figure 13. The well encountered the Bergstrom Formation from the surface to a depth of approximately 85 feet, followed by approximately 20 feet of Pecan Gap and 70 feet of Sprinkle. Montmorillonite was the dominant clay mineral throughout the profile.

Tipple used the method of Jonas and Brown (1959) to identify the interlayer ion population for all of the samples obtained from the Manor Well. The results indicate that calcium is nearly the exclusive interlayer ion for the montmorillonite at the well. This is compatible with Tipple's calcium carbonate measurements. Throughout the Taylor Group, calcium carbonate contents are typically around 40 percent.

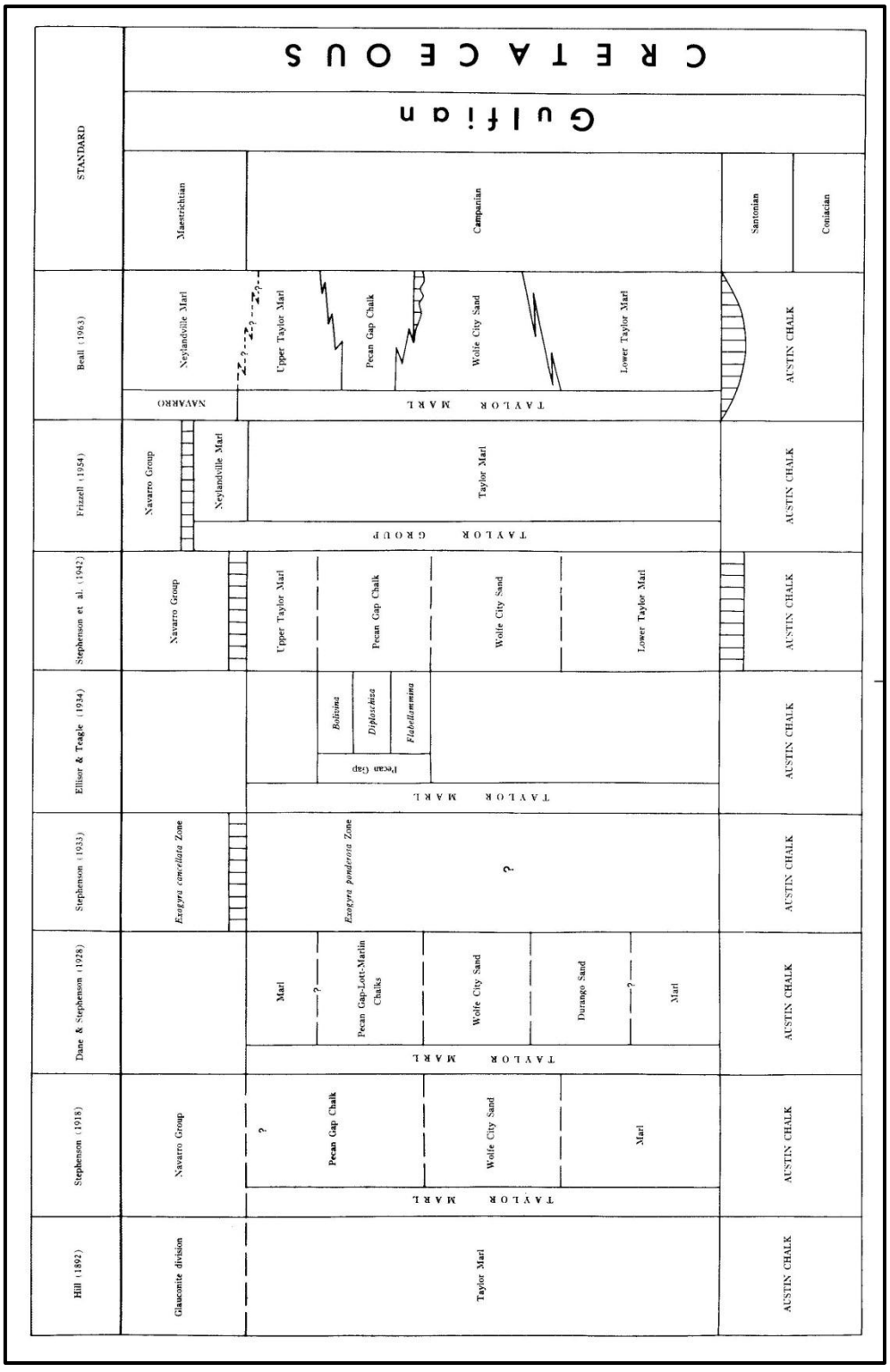

Figure 9. Historical Classifications of Strata within the Taylor Group, Beall (1964)

2/Sample No.	Locality No.	Montmorillonite Na:CaMg	Montmorillonite %	Kaolinite %	Illite %	Quartz %	Calcite %	Diffraction Peak: Montmorillonite (001)
1	172	100:0	55	10	3—	20+	10—	broad
2	172	95:5	55	10	3—	20	10	broad
3	146	20:80	65	--	3—	10	20+	broad
4	109	30:70	60	5	5	20+	10	broad
5	137	50:50	50	10	tr.	20	20+	broad
6	161	40:60	60	--	tr.	20	20+	broad
7	111	40:60	60	8	tr.	20+	10	
8	171	40:60	60	10	--	20+	10	
9	157	50:50	55	15	--	20+	10	sharp
10	112	50:50	55	15	--	20	10	
11	136	50:50	50	8	8	20	10	broad
12	125	50:50	60	--	3—	30+	5	sharp
13	142	100:0	40	15	5	30	10—	broad
14	176	45:55	70	--	--	20+	10	sharp
15	176	45:55	70	--	tr.	20+	10	
18	158	60:40	65	3—	--	20	10	sharp
19	163	50:50	60	3—	3—	20	10+	
20	155	60:40	50	10	3—	30	5—	
21	113	50:50	60	5	5	20—	10	
22	3/99	100:0	60	5	5	20+	10	sharp
23	99	100:0	55	5	3—	30	5+	sharp
24	165	50:50	60	3—	--	5	30+	diffuse
25	159	10:90	60	3—	--	5	30+	broad
26	159	50:50	55	3	?	5—	35+	broad
27	159	50:50	55	--	--	5—	35+	broad
29	108	35:65	60	5	5	20+	10—	sharp
30	108	40:60	90	--	--	3	3—	very sharp
31	104	50:50	90	--	--	3	3—	very sharp
32	168	20:80	45	3	10	5	35+	broad
37	168	10:90	55	--	--	--	45+	diffuse
39	114	40:60	65	10	tr.	15	10	sharp
40	114	50:50	60	10	tr.	20	10—	sharp
41	170	5:95	60	--	--	?	40	diffuse
42	99	95:5	65	3—	3—	20	5—	broad
43	99	95:5	65	5	5	20+	5—	broad
44	99	50:50	60	10	5	20	5	
45	99	95:5	60	5	5	20+	10—	broad
46	99	95:5	60	5	10	20	5—	broad

[1]These clay data are estimates based on comparison of diffraction intensities of Taylor Formation samples with mixtures of pure minerals (weight percentages). The ratio of sodium (Na) montmorillonite to calcium-magnesium (CaMg) montmorillonite is given in parts per hundred. All percentages are based on the total sample and are correct within approximately 5 percent. Note the following symbols: slightly less than (—); slightly greater than (+).

[2]Refer to Figure 12 for position of sample in facies of Taylor Formation.

[3]Lytle, Holloway and Phillips, No. 1 Atlantic Refining Company, located north and slightly east of area.

Figure 10. Chemical Analysis of Samples from Taylor Group, Beall (1964)

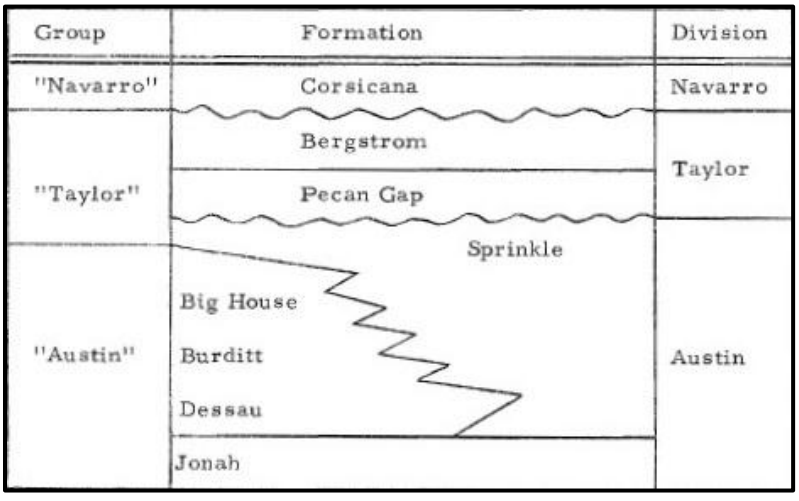

Figure 11. Revised Nomenclature for Upper Taylor Member, Young (1965)

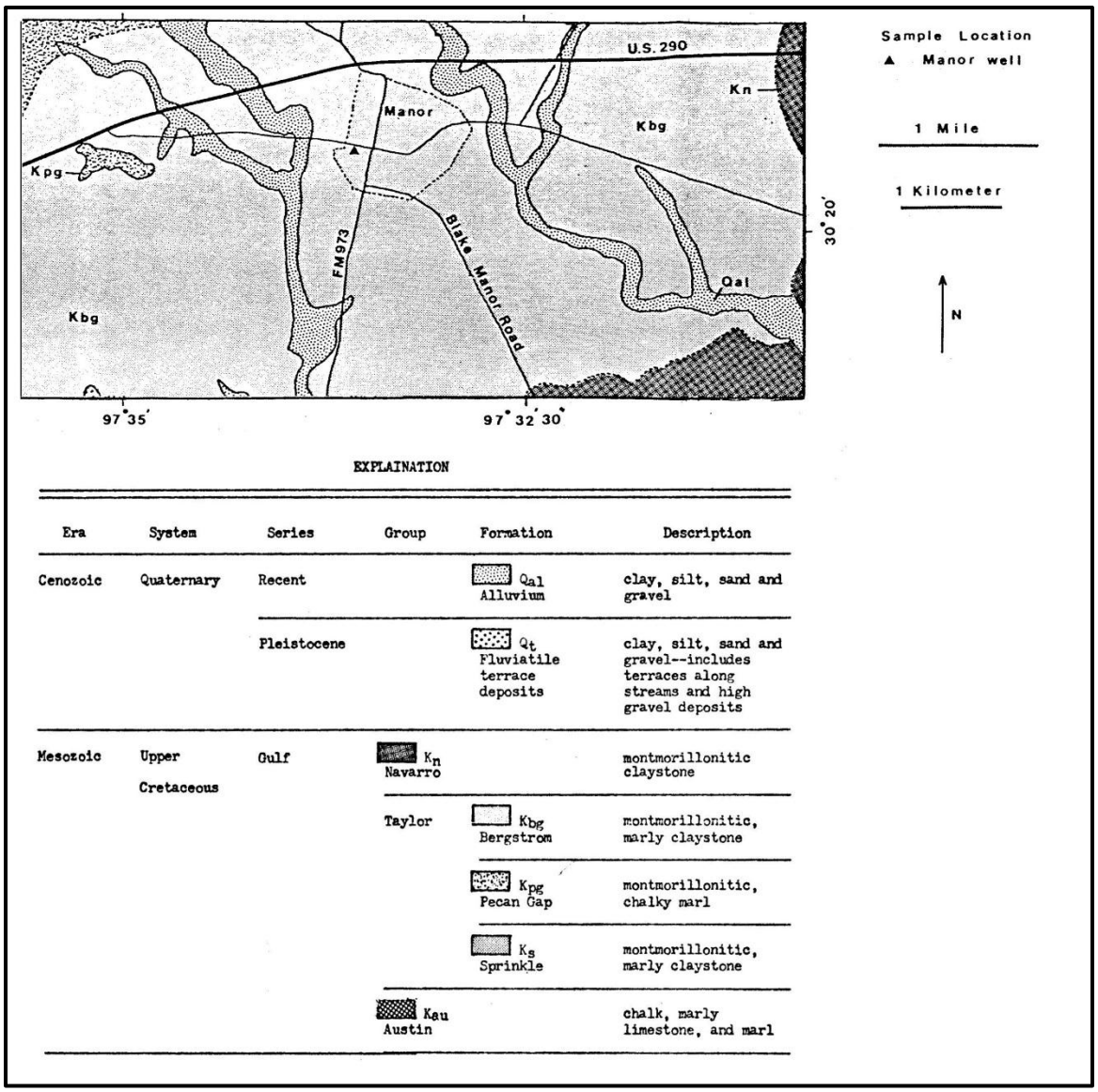

EXPLAINATION

Era	System	Series	Group	Formation	Description
Cenozoic	Quaternary	Recent		Q_{al} Alluvium	clay, silt, sand and gravel
		Pleistocene		Q_t Fluviatile terrace deposits	clay, silt, sand and gravel--includes terraces along streams and high gravel deposits
Mesozoic	Upper Cretaceous	Gulf	K_n Navarro		montmorillonitic claystone
			Taylor	K_{bg} Bergstrom	montmorillonitic, marly claystone
				K_{pg} Pecan Gap	montmorillonitic, chalky marl
				K_s Sprinkle	montmorillonitic, marly claystone
			K_{au} Austin		chalk, marly limestone, and marl

Figure 12. Geologic Map of the Vicinity of Manor, TX, Tipple (1975)

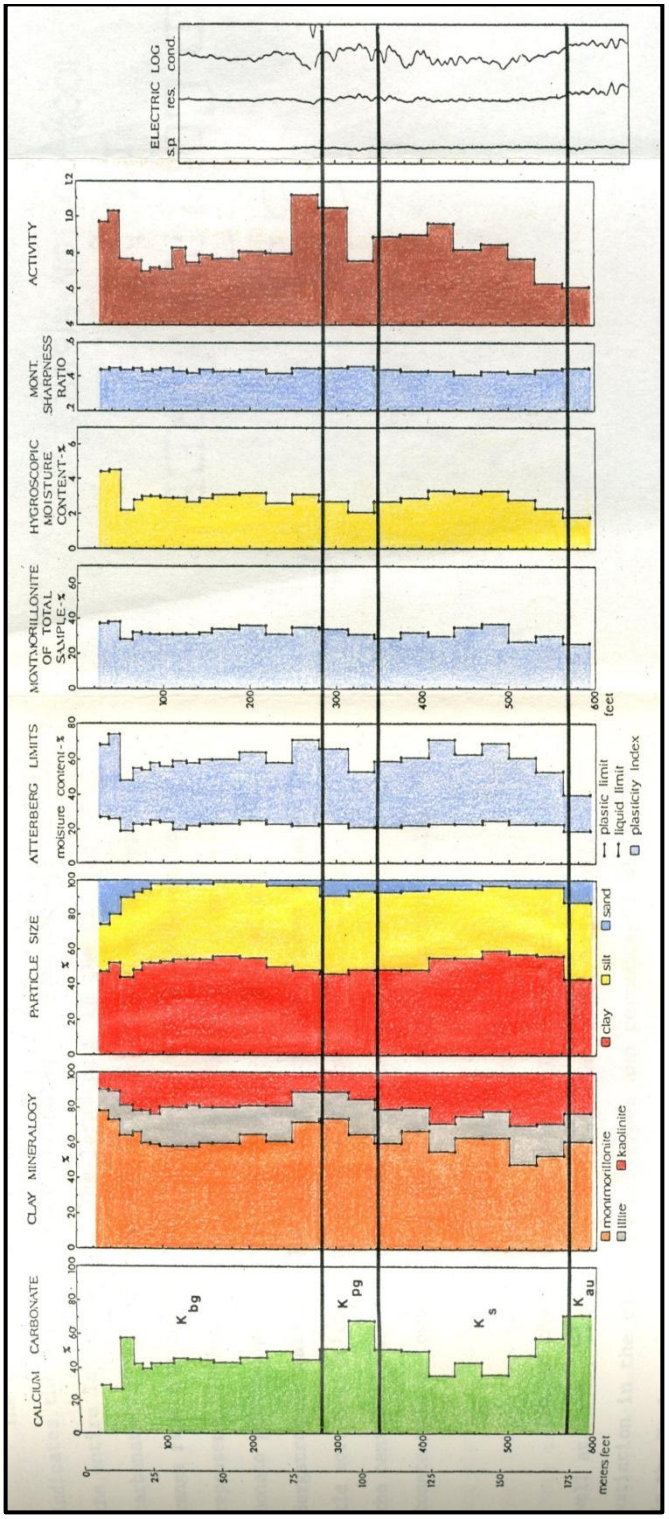

Figure 13. Test Results from Samples Retrieved from Manor Well, Tipple (1975)

3.2 Laboratory and Field Investigations

The engineering characteristics of clays from the Taylor Group have been repeatedly studied and reported in the literature. The clay is known to be quite stiff and overconsolidated with a pronounced secondary structure (Long, 1983). Garner and Young (1976) presented a profile of the engineering properties that are typical within the Taylor Group, Figure 14. Most notable in their summary is the interplay between calcium carbonate content and liquid limits. Just as Tipple (1975) observed, the liquid limits are inversely proportional to the calcium carbonate contents.

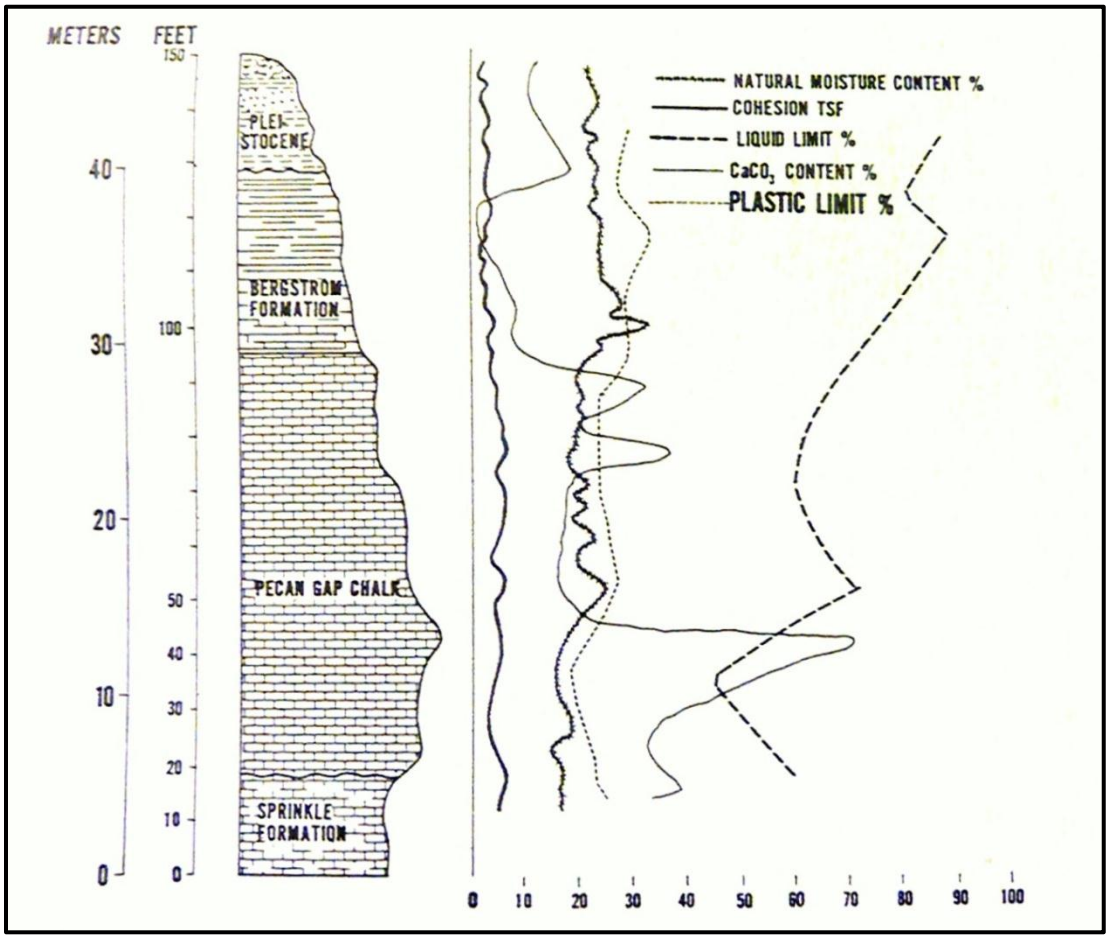

Figure 14. Typical Properties of the Taylor Group, Garner and Young (1976)

Long (1983) reported the engineering properties of soils from the Taylor Group at the site of his lateral load tests in Manor, TX. The test site was located along US Highway 290 at Station 319.5. The site was originally investigated in 1966 after a 6-foot deep rectangular test pit was excavated. Figure 15 summarizes the measured soil profile and shear strengths, which were measured by unconfined compression, unconsolidated undrained triaxial and pocket penetrometer tests. Note that the vertical scale represents depth below the base of the test pit, which was six feet below the ground surface.

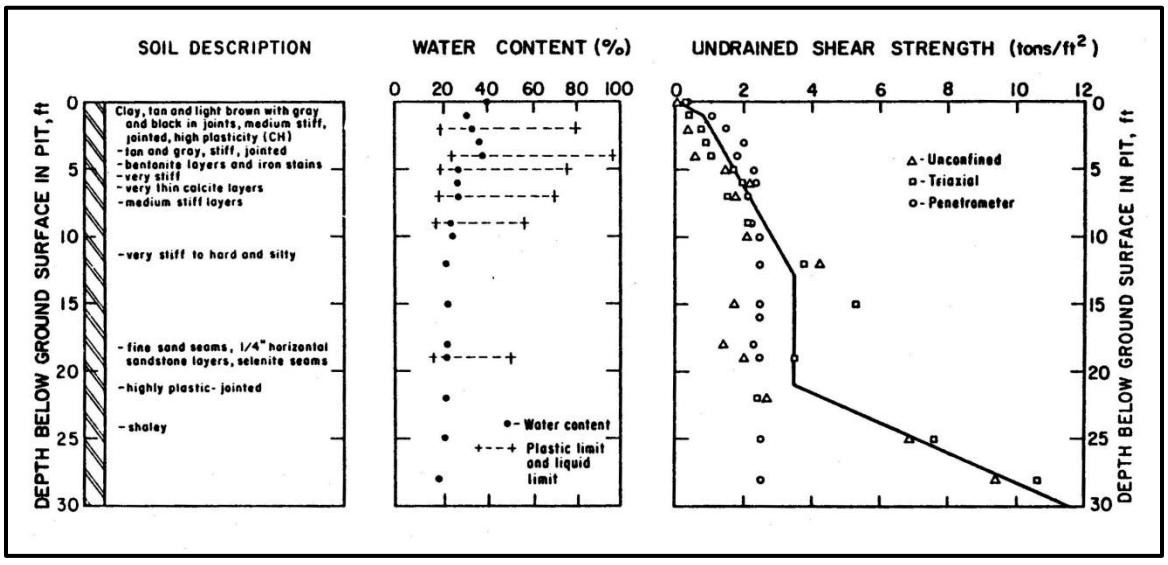

Figure 15. Soil Profile and Shear Strengths from 1966 Manor Tests, Long (1983)

The same test site was revisited in 1981 for additional research activities. Additional borings were drilled to obtain undisturbed samples for testing. While logging the soil, depths were correlated to the original 1966 investigation based on the depths of easily distinguishable layering.

One-dimensional consolidation tests were conducted on 2.5-inch diameter, 0.5-inch thick specimens. During testing, the specimens were initially loaded with 125 psf. If swelling occurred, additional pressure was applied until no swelling was apparent. From that point on, the tests used load increment ratios of one for loading, and one-half for unloading. A summary plot of vertical strain versus log of effective vertical pressure is shown in Figure 16. Long described the curves as typical of heavily overconsolidated clay. Namely, there is no clear indication of any point which might represent the transition from over- to normally-consolidated behavior. The recompression indices (R_r) were not included in the original report. They were calculated by the present author for this thesis.

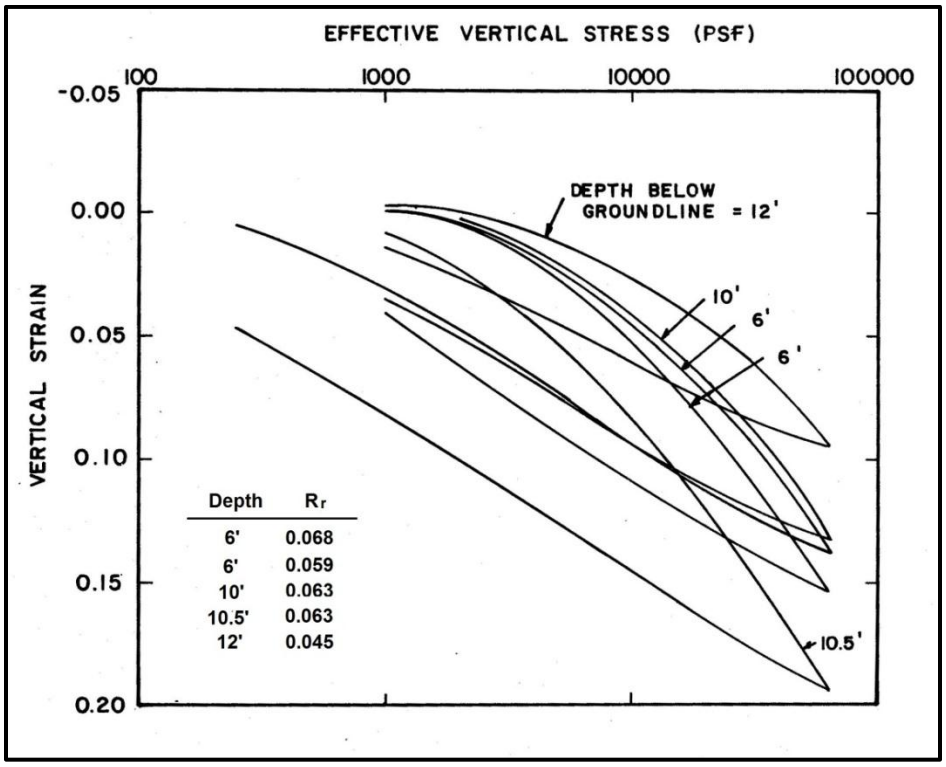

Figure 16. Consolidation Test Results from 1981 Manor Tests, Long (1983)

Long (1983) also reported the results from a series of isotropically consolidated, undrained triaxial compression tests with pore water pressure measurements. He presented the data as a collection of effective stress paths in P'-q space, Figure 17. Tests were conducted on specimens from depths between 8 and 17 feet. The linear trend, effective friction angle and effective cohesion intercept were not included in the original report. They were added separately by the present author for this thesis.

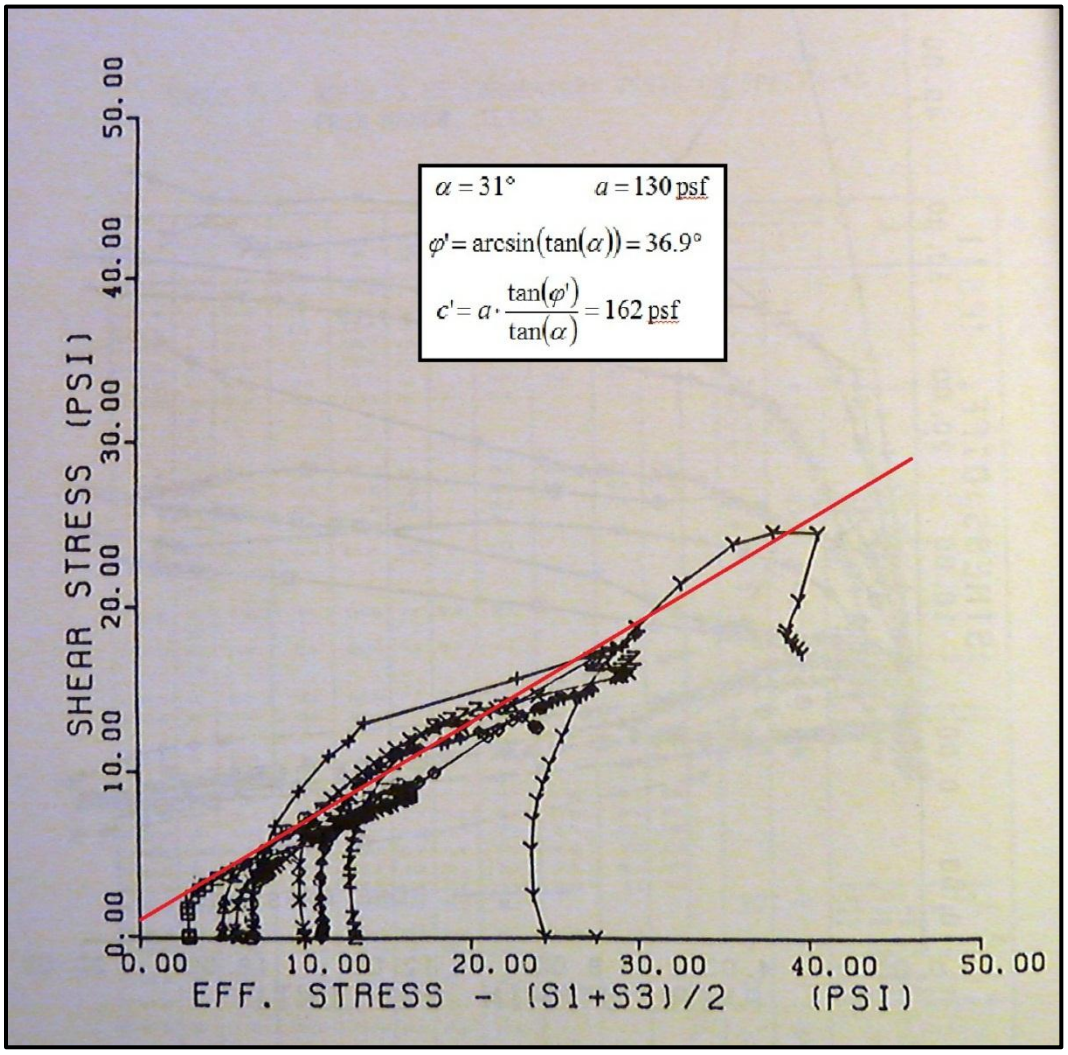

Figure 17. Effective Stress Paths from 1981 Manor Tests, Long (1983)

Compression tests from soils at the Manor site exhibited several different types of failure. The soil's secondary structure caused the behavior to vary based on the arrangement of joints and fissures within the test specimens. Figure 18 summarizes the types of shear failure that were observed.

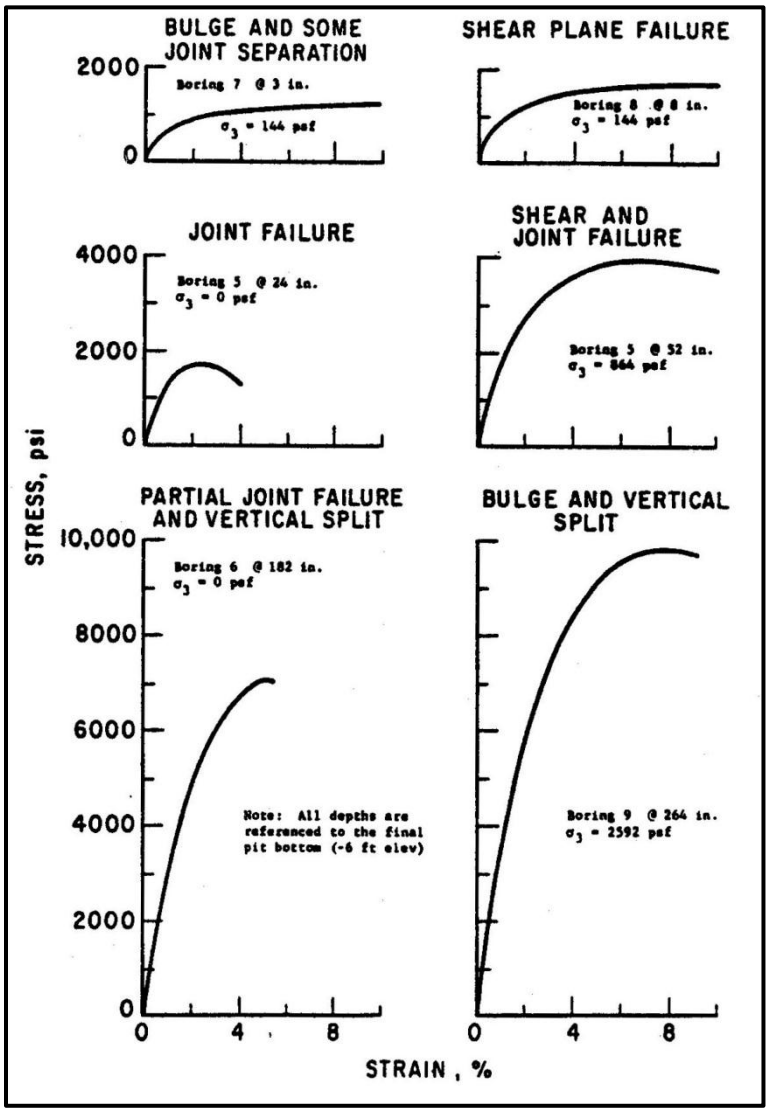

Figure 18. Typical Stress-Strain Curves from 1981 Manor Tests, Long (1983)

Funk (1975) and Tipple (1975) conducted extensive tests on Taylor soils from around the vicinity of Austin and Manor. Their focus was aimed at correlating the clay chemical contents with Atterberg limits. On average, they found soils in the Taylor Group to have relatively constant plastic limits, ranging mostly between 20 and 30. The various changes in chemical contents had much greater effects on the liquid limits. Liquid limits tended to increase with higher montmorillonite – and particularly sodium montmorillonite – contents and decrease with higher calcium carbonate contents. Liquid limits varied mostly between 55 and 80, but reached values as high as 100.

Tipple drew several additional conclusions about the soils' behavior around the contact between oxidized and unoxidzed zones. In general, the Atterberg limits and colloidal activity increased just above the contact going up into the weathered zone. Simultaneously, the calcium carbonate content and clay fraction tended to decrease. These observations are generally consistent with the laboratory results presented by both Tipple and Funk. Figure 19 shows the observed relationship between montmorillonite content and plasticity, Tipple (1975). The effect of carbonate content on the plasticity index is illustrated in Figure 20, Tipple (1975).

The only major difference in the two studies was sodium montmorillonite content of the samples. Tipple suggested a testing error that probably caused Funk to measure erroneously high sodium contents. Nevertheless, there exists a large variation in Atterberg limits throughout the Taylor Group. Geotechnical researchers in the Austin area have reported liquid limits for the Taylor clays ranging from 50 (Van-Hue, 1966) to 110 (Kayyal, 1986).

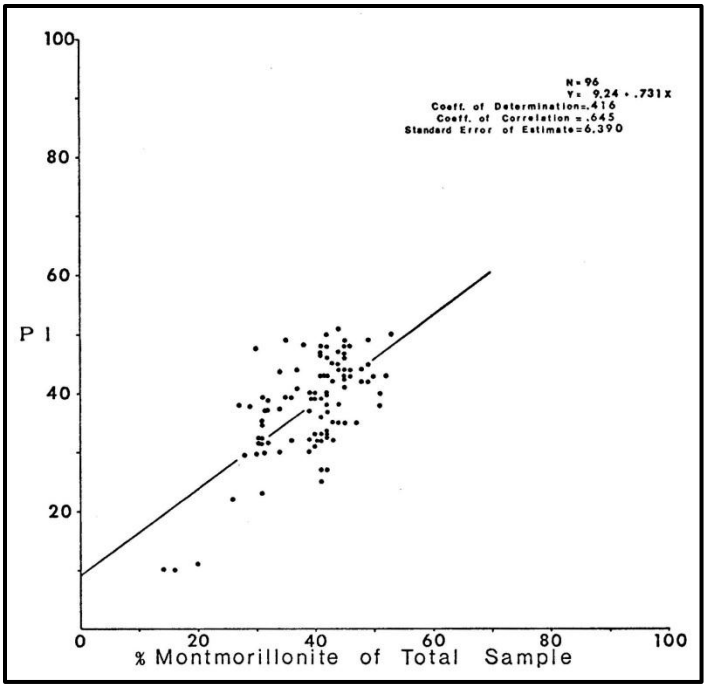

Figure 19. Montmorillonite Content vs. PI for Taylor Clays, Tipple (1975)

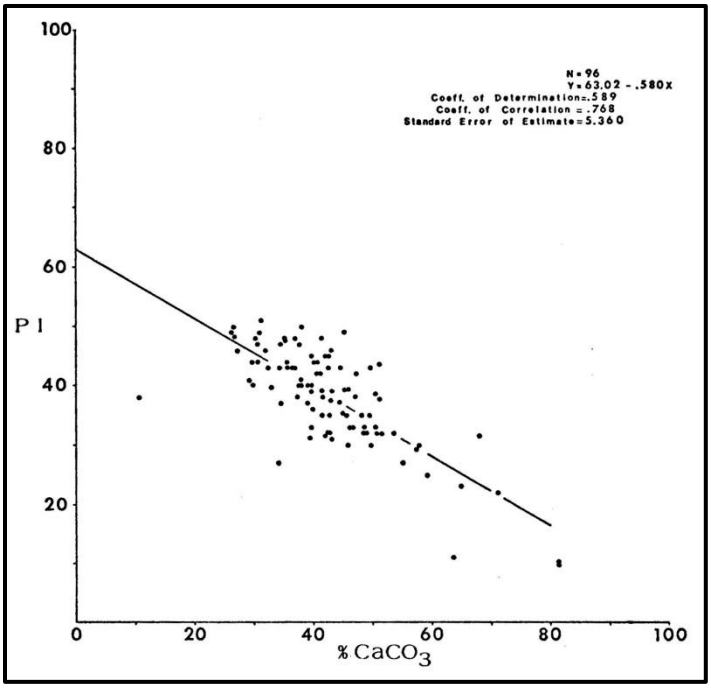

Figure 20. Calcium Carbonate Content vs. PI for Taylor Clays, Tipple (1975)

Marr (2003) ran a number of tests on clay from the Taylor group while developing the cyclic swell test described in Section 2.1.4. The soil was sampled in Austin, TX near the intersection of US Highway 183 and 51st Street. The sampled depths were between 10 and 20 ft. The soil's plastic and liquid limits ranged from 24 – 27 and 77 – 85, respectively. The soil's swell pressure was determined to be approximately 4200 psf during a one-dimensional consolidation test. The e-log-P' curve was too rounded to distinguish between over- and normally-consolidated stress ranges, Figure 21. The results of Marr's cyclic swell tests indicate that for a given change in moisture content, smaller vertical swelling strains occur under higher total stresses.

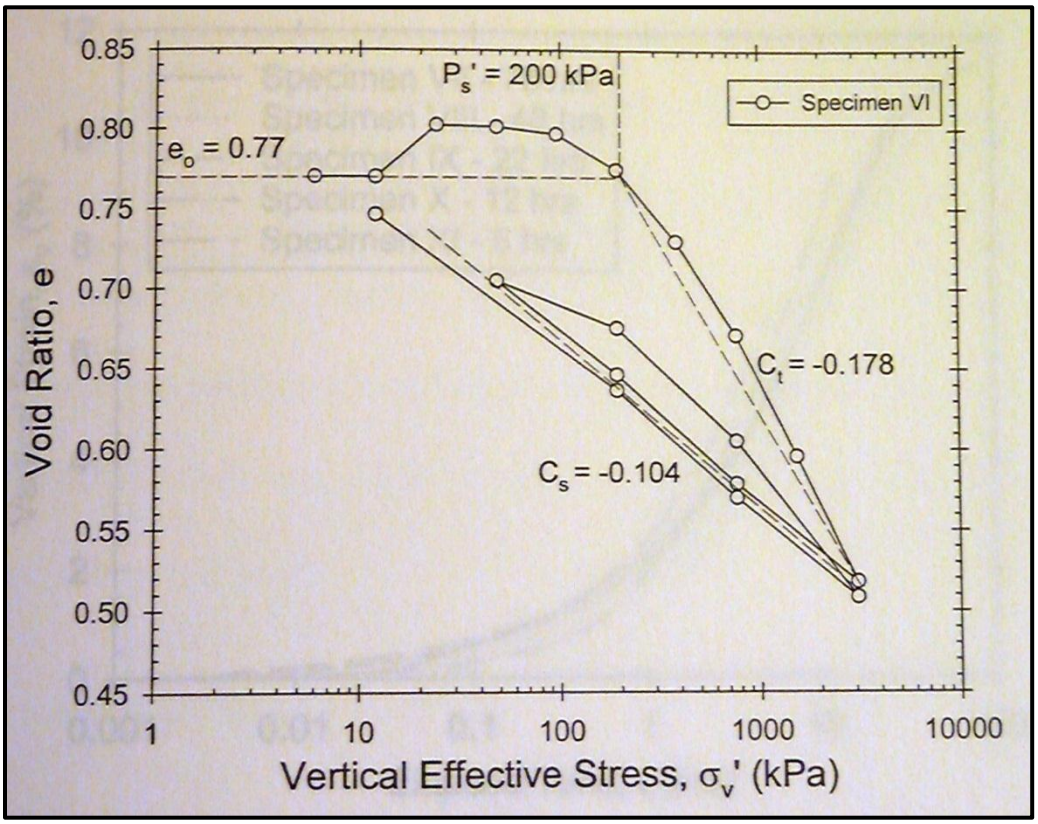

Figure 21. Consolidation Results from Taylor Clay from Austin, TX, Marr (2003)

4 Field Investigation at the Lymon C. Reese Research Wall

4.1 Overview

4.1.1 Site Location and Subsurface Investigation

The field and laboratory tests described in Chapters 3 and 4 were conducted on soils from the Lymon C. Reese Research Wall test site. The address is 13806 Old Highway 20, Manor, Texas 78653, Figure 22. Fugro Consultants, Inc. drilled three exploratory borings at the site on January 12 and 13, 2010. A piezometer was installed in boring B-1 to monitor groundwater. McKinney Drilling Company installed a drilled shaft retaining wall at the site during the spring of 2010. The cut side of the wall was excavated by the owner during August and September of 2010. Locations of the borings, drilled shafts and excavation are shown schematically in Figure 23. Boring logs from the exploratory borings are provided in Appendix A.

Figure 22. Location of Lymon C. Reese Research Wall in Manor, TX

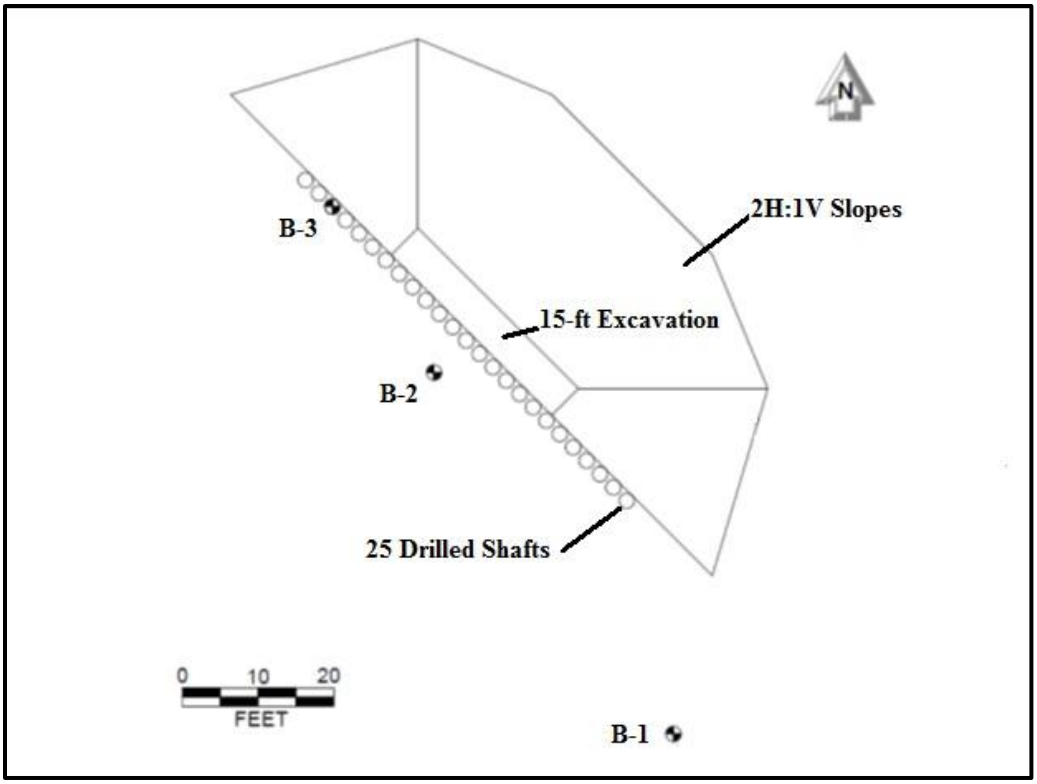

Figure 23. Site Schematic with Boring Locations

4.1.2 Geologic Setting

Exploratory borings revealed a shallow layer of dark, weathered clay that became a dull yellowish brown color and much stiffer with depth. The weathered zone extends from the surface to a depth of approximately 8 feet. The soil was closely fissured and blocky throughout the profile, but particularly so below the weathered zone. None of the borings detected sandy strata, but selenite seams were observed. Figure 24 shows the thickest band of selenite that was encountered, approximately 0.2 inches thick. This seam was intersected in boring B-2 at a depth of 38 feet.

Figure 24. Large Selenite Seam Intersected by B-2 at a Depth of 38 ft

Excavation of the cut side of the wall provided a clearer picture of the subsurface. Figure 25 illustrates the transition from dark brownish gray to dull yellow clay that was observed during excavation at depths of approximately 8 – 10 feet. Figure 26 is a close-up picture that provides better detail on the colors and transition. Numerous Exogyra ponderosa fossils were discovered in the excavated soil, Figure 27. The exact depths the fossils were discovered could not be recorded, but the depths of most frequent occurrence seem to have been between 5 and 10 feet.

Figure 25. Transition from Dark Gray to Dull Yellow Clay

Figure 26. Close-Up View of Transition from Dark Gray to Dull Yellow Clay

Figure 27. Exogyra Ponderosa Fossils Unearthed during Excavation

4.1.3 Climactic Setting

The site investigation and was conducted after several months of frequent precipitation. That precipitation, however, was only a temporary break from an ongoing drought in central Texas. Figure 28 illustrates when important sampling and construction activities occurred during this weather event.

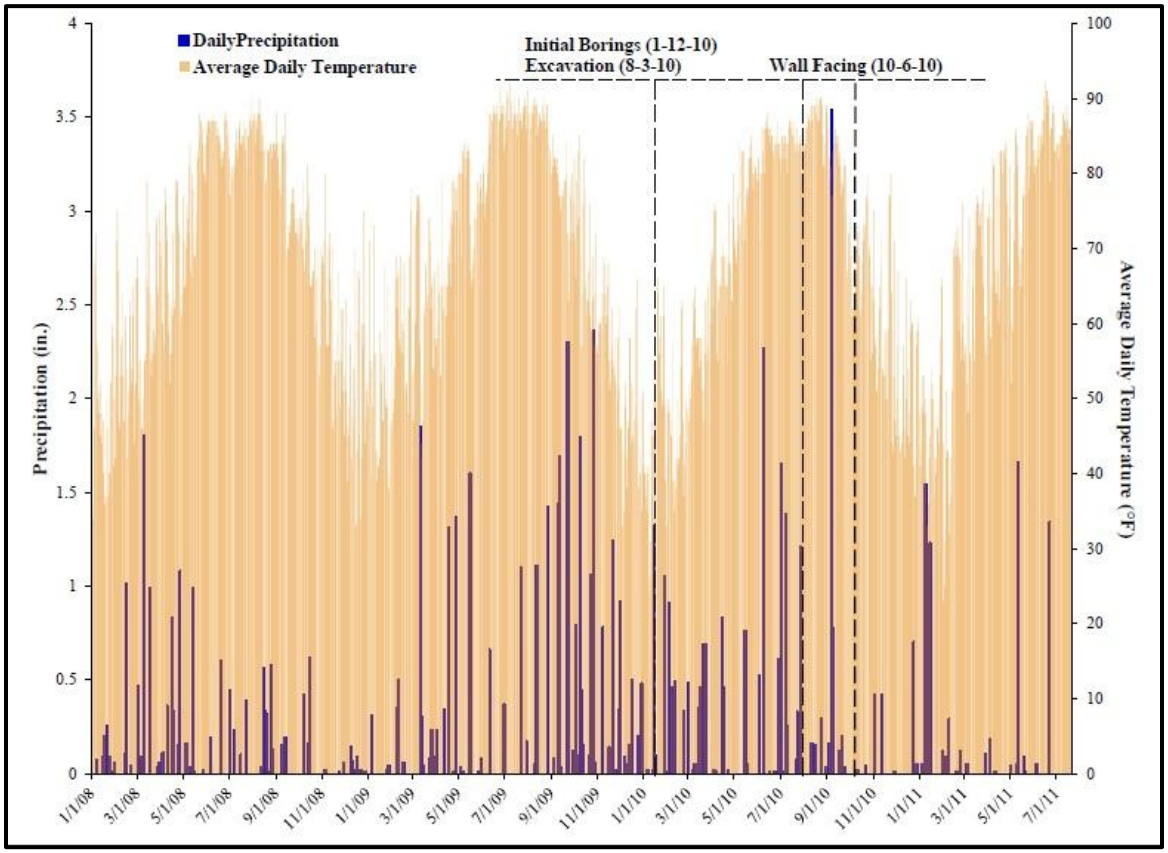

Figure 28. Weather Records During Central Texas Drought

4.2 In-Situ Tests

4.2.1 Pocket Penetrometer

Pocket penetrometer measurements were recorded throughout sampling. After extruding a sample from the seamless push tube and cutting one end squarely with a knife, the pocket penetrometer was pushed into the cut surface, Figure 29. Although this technique produces only the most approximate of measurements, Figure 30 illustrates that the predicted soil strengths are consistently high. Nearly half of the pocket penetrometer tests met refusal and are plotted as the maximum possible reading, 9000 psf.

Figure 29. Pocket Penetrometer Testing

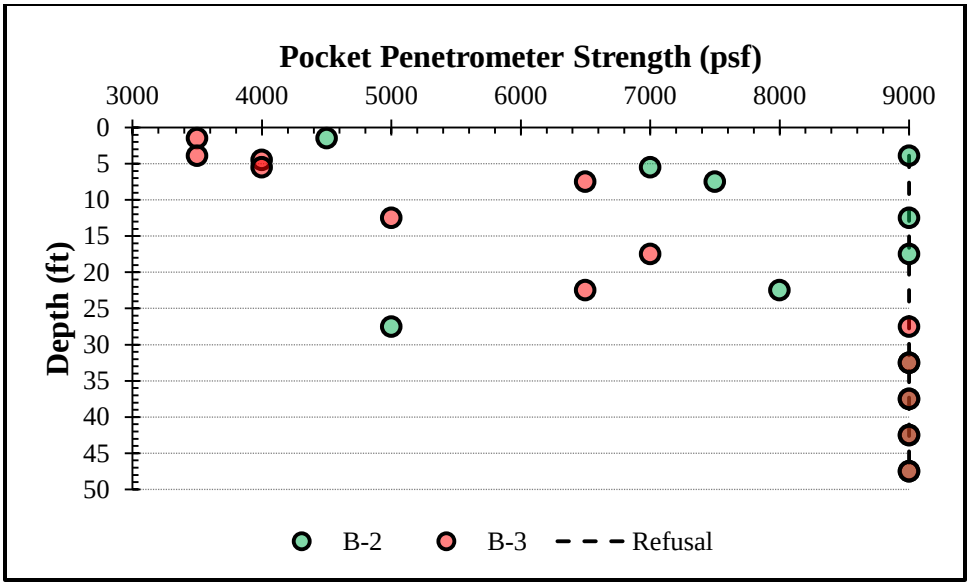

Figure 30. Results from Pocket Penetrometer Tests

4.2.2 Standard Penetration Test (SPT)

Standard penetration tests (SPT) were conducted in boring B-1 at 5-ft intervals while retrieving split-spoon samples for index tests. These tests were conducted in accordance with ASTM D1586 with the exceptions of hammer weight and drop height. The standard test calls for a hammer weight of 140-lb and drop height of 30 inches. These tests were conducted with a 170-lb hammer and 24-inch drop height. A simple energy correction was used to standardize the blow count, Equation 2. The energy-corrected blow counts (N') are plotted in Figure 31. SPT blow counts are not typically correlated to undrained strengths or other properties for clays (Reese et al. 2006).

$$N' = N \cdot \frac{W_{hammer} \cdot H_{drop}}{140lb \cdot 30in.} \qquad \text{.....Eq. 2}$$

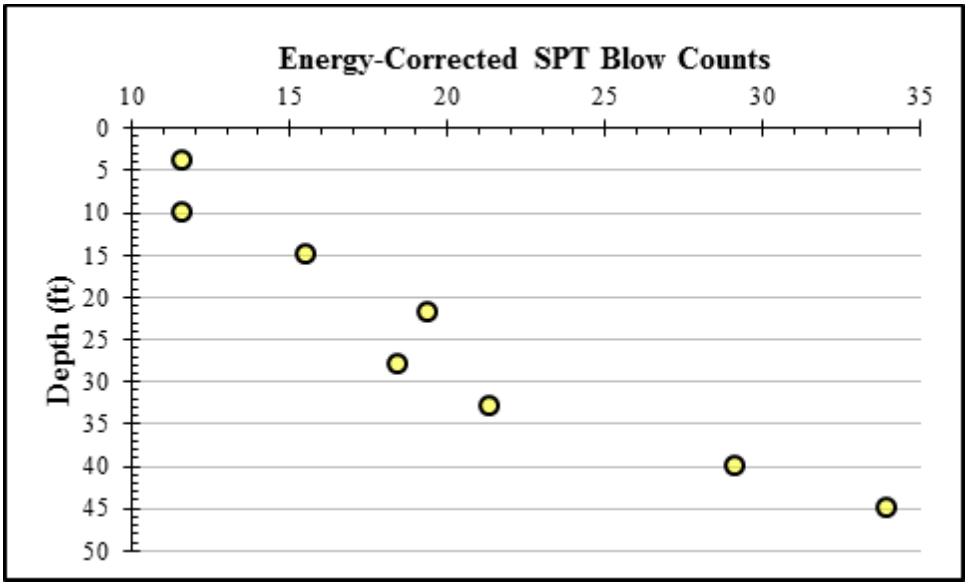

Figure 31. Energy-Corrected SPT Blow Counts

4.2.3 Texas Cone Penetration Test

Texas cone penetration (TCP) tests were conducted at 5-ft intervals in boreholes B-1 and B-3 in accordance with TxDOT test procedure Tex-132-E. The number of blows required to drive the cone twelve inches (N_{TCP}) was converted to undrained shear strength (S_u) using Equation 3 (2000 TxDOT Geotechnical Manual). Note that Equation 3 returns S_u in units of tons/ft^2. The resulting S_u profiles are plotted in Figure 32. The final four tests in B-3 met refusal and are signified by a vertical dashed line at the maximum TCP-generated undrained shear strength, 8000 psf.

$$S_u = \frac{N_{TCP}}{25} \quad \text{..... Eq. 3}$$

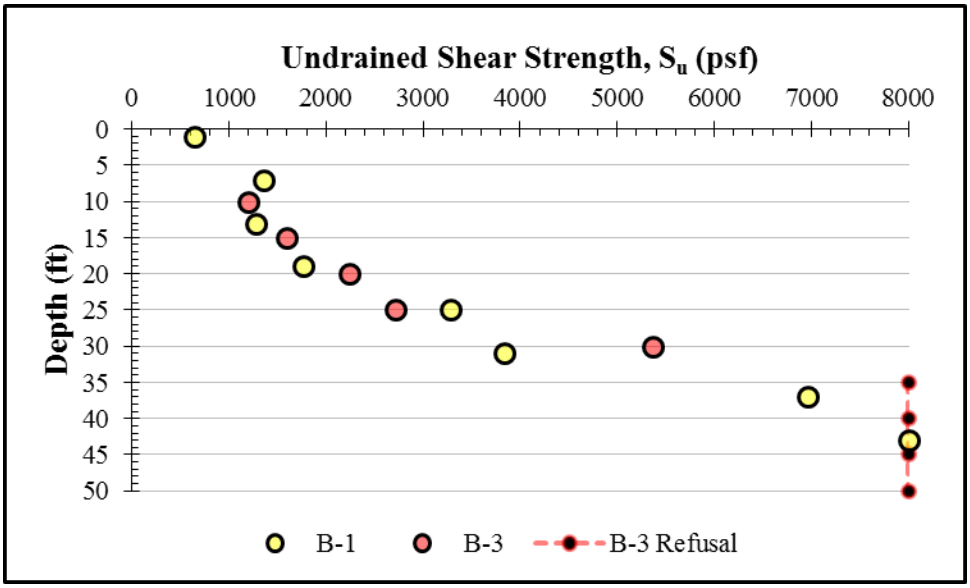

Figure 32. Undrained Strength Profile from TCP Correlations

4.2.4 Spectral Analysis of Surface Waves (SASW)

The spectral analysis of surface waves (SASW) test method was performed at the test site on June 15 and July 26, 2010. As a reference, the retaining wall's drilled shafts were installed on the week of March 30, 2010 and excavation of the cut side of the retaining wall began July 29, 2010. Each test was conducted with two different sensor arrays as illustrated in Figure 33. Sensory array #3 is also pictured in Figure 34.

The tests from each date are summarized in Tables 4 and 5. Equation 4 was used to convert shear wave velocities (v_s) to shear moduli (G). The soil's unit weight was idealized as constant with depth at a value of 125 lb/ft^3. P-wave velocities identified the groundwater table at a depth of 7.5 ft.

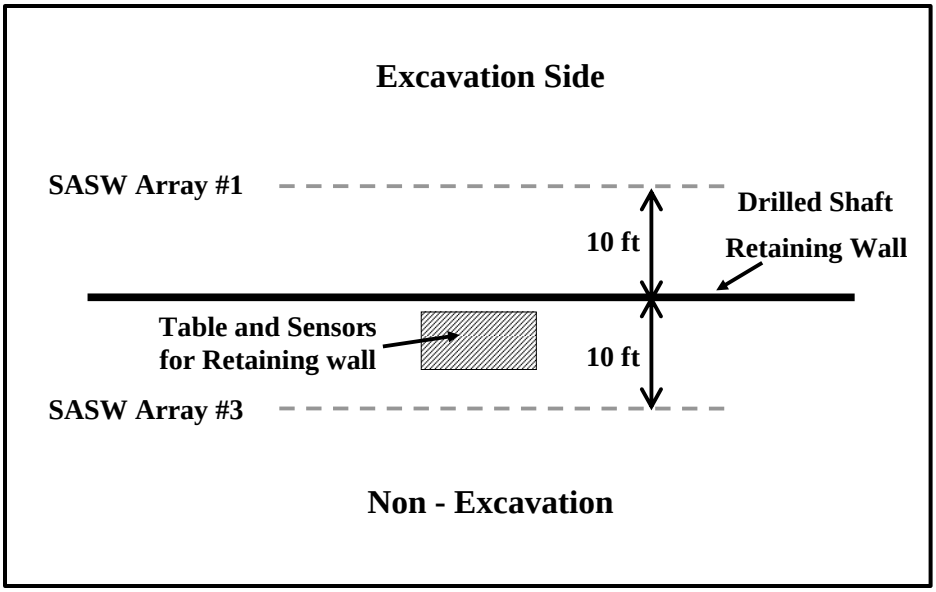

Figure 33. Sensor Arrays for SASW Tests Two Days Before Excavation

Figure 34. SASW Sensor Array #3

Table 4. SASW Results from 6-15-2011

	Depth (ft)	Shear Wave Velocity, v_s (ft/s)	Shear Modulus, G (k/ft^2)
Sensor Array #1	0 – 0.1	200	149
	0.1 – 1.0	250	233
	1.0 – 2.9	359	480
	2.9 – 7.5	379	535
	7.5 – 22.5	421	688
	22.5 – 32.5	550	1174
	32.5 – 40	950	3503
Sensor Array #3	0 – 0.6	109	44
	0.6 – 1.4	181	122
	1.4 – 2.9	250	233
	2.9 – 7.4	319	379
	7.4 – 19.6	382	566
	19.6 – 29.4	550	1174
	29.4 – 37	950	3503

$$G = v_s^2 \cdot \frac{\gamma}{g} \qquad \text{..... Eq. 4}$$

Table 5. SASW Results from 7-26-2011

	Depth (ft)	Shear Wave Velocity, v_s (ft/s)	Shear Modulus, G (k/ft^2)
Sensor Array #1	0 – 3.0	310	358
	3 – 7.5	360	483
	7.5 – 22.5	420	685
	22.5 – 32.5	550	1174
	32.5 - 144	850	2805
Sensor Array #3	0 – 2.9	320	382
	2.9 – 7.5	320	382
	7.5 – 20.5	410	653
	20.5 – 30.5	570	1261
	30.5 - 77	820	2610

Shear modulus profiles for the excavation and non-excavation sides of the retaining wall are shown in Figures 35 and 36, respectively. Only slight differences were observed between the two array positions and testing dates, Figure 37.

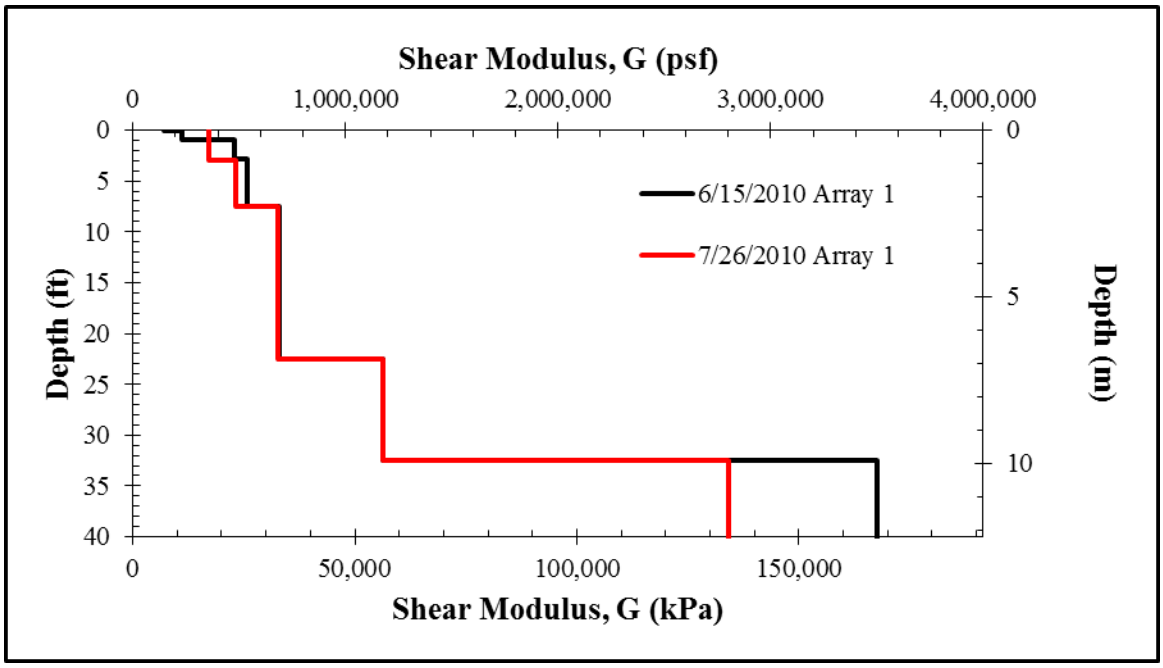

Figure 35. Shear Modulus Profiles from Excavation Side of Wall

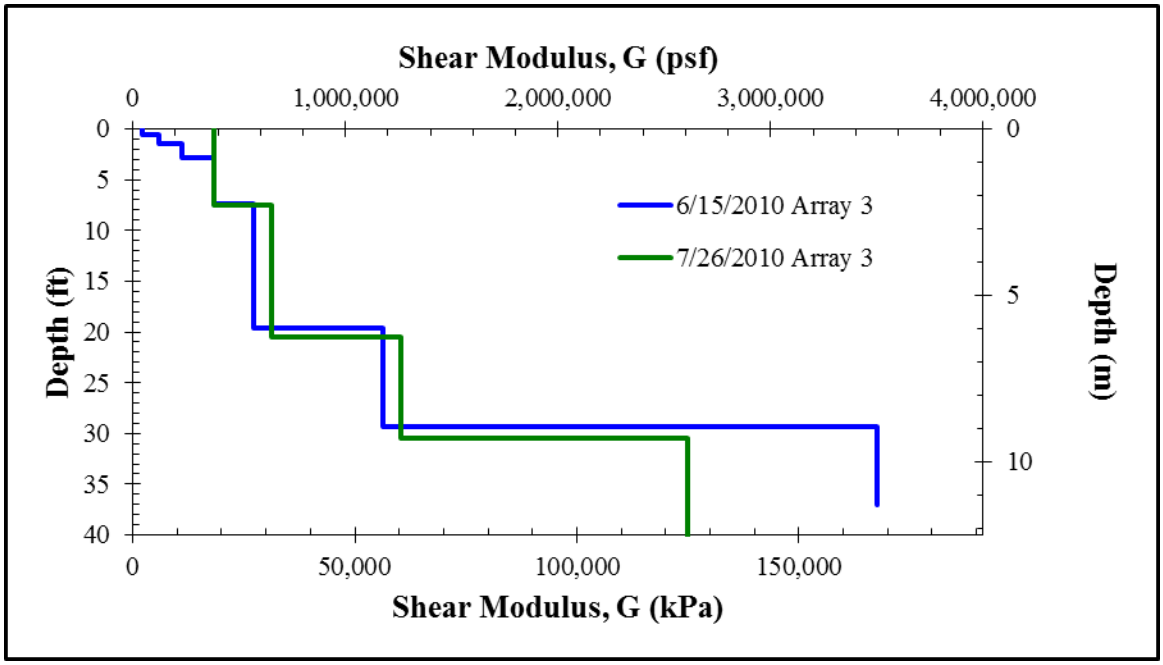

Figure 36. Shear Modulus Profiles from Non-Excavation Side of Wall

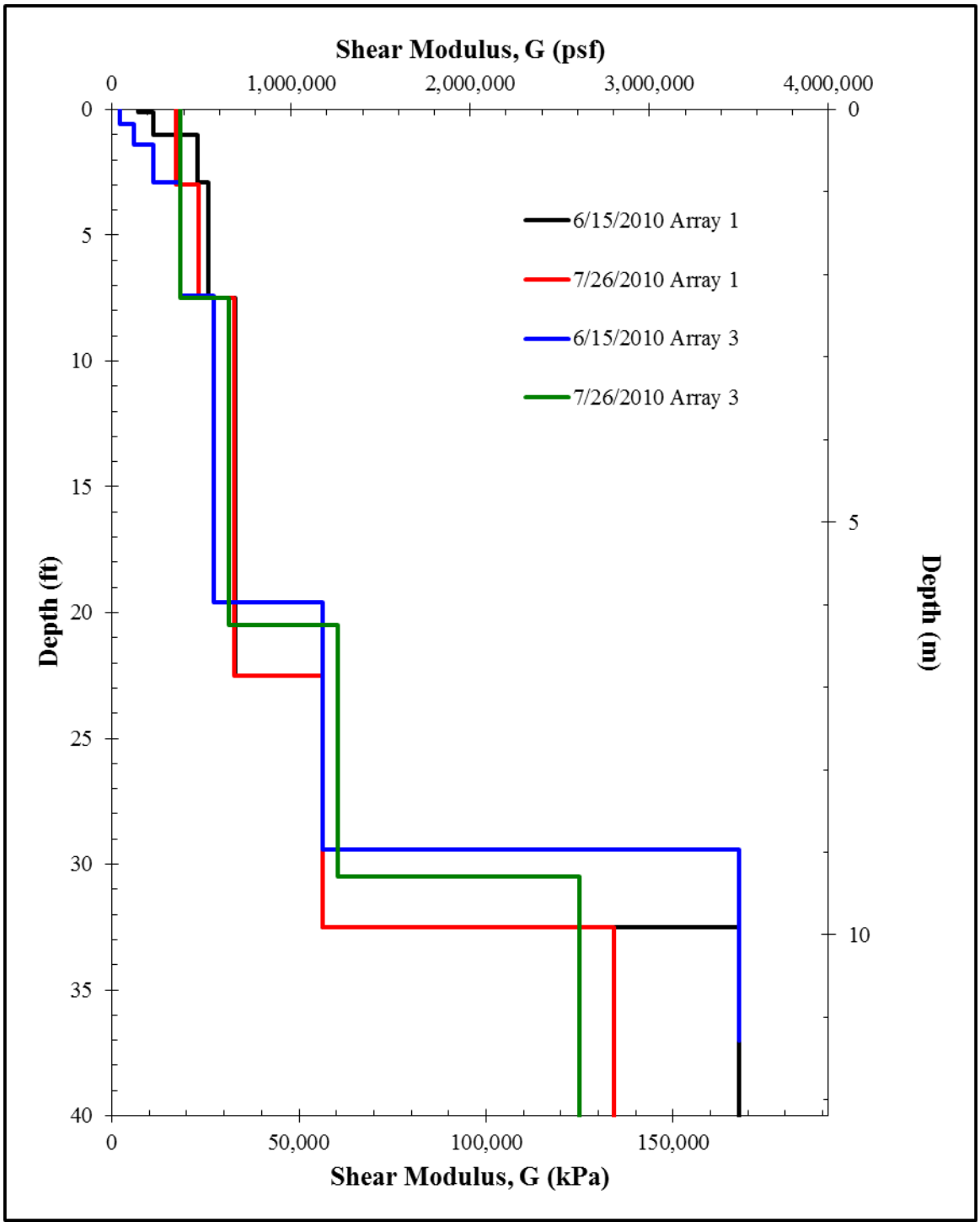

Figure 37. Summary of Measured Shear Modulus Profiles

5 Laboratory Investigation

5.1 Index Properties

5.1.1 Moisture Content

Moisture contents were directly measured in accordance with ASTM D2216. The moisture profile was first determined on samples retrieved during the initial subsurface investigation. Samples also were retrieved and tested when the soil was exposed during subsequent construction activities. Additional samples – none deeper than 5 feet – were sampled using a 1.5-inch hand auger. All of the samples were taken from within 50 feet of the Lymon C. Reese Research Wall and within two years of the initial subsurface investigation. The groundwater table was monitored with a piezometer that was installed in borehole B-1 (Dellinger, 2011).

The results, shown in Figure 38, reflect the extreme drought that plagued central Texas both before and during the course of this research. The top several feet of soil often dried to moisture contents between 18 and 23 percent. Periodic precipitation wetted the same depths to moisture contents near 30 percent, and sustained ponding raised moisture contents above 30 percent. The observed fluctuations tapered to a smaller magnitude with depth, but insufficient samples were obtained at depths below 5 ft to determine the depth at which moisture fluctuations ceased to occur. The depth to water increased steadily with time as the region's drought continued. Construction activities, mainly excavation, may have had significant effects on the measured groundwater level.

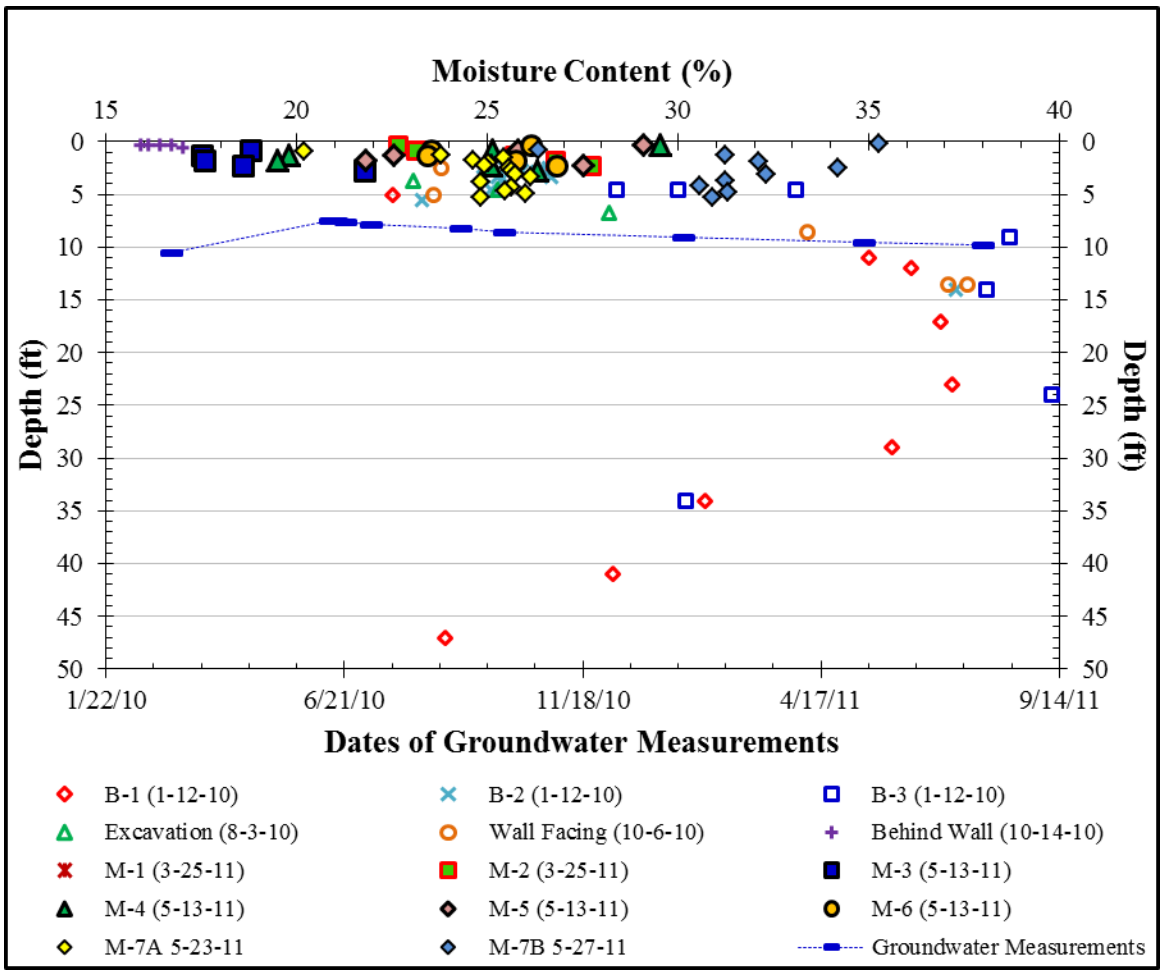

Figure 38. Summary of Moisture Content Measurements

5.1.2 Atterberg Limits

The liquid and plastic limits were measured on samples obtained from the initial subsurface investigation. The plasticity indices are in excess of 50 – and as high as 79 – throughout the soil profile.

Several testing parameters were varied to ensure that these large values were not relics of poor soil preparation or user error. The first round of tests was conducted at the

University of Texas soil mechanics laboratory. The soil was broken down and soaked in distilled water until it softened, and then it was blended in a high-speed shear mixer. Coffee filters were used to contain the soil while the moisture content dropped to a level near the liquid limit. The same drying process was used to prepare the soil for the plastic limit tests. The procedural aspects of each test were conducted in accordance with ASTM D4318.

A second round of Atterberg Limit tests at the University of Texas used a similar procedure. The soil was again soaked in distilled water, but the curing time was allowed to extend between two and three weeks. After the extended curing period, small portions of the wet soil were mixed with an equal portion of additional distilled water and blended in the high-speed shear mixer. Tiny clumps of clay that could not be broken down in the mixer were removed from the sample prior to testing. Only liquid limit tests were conducted on these samples.

A second party (Fugro Consultants Inc.) ran a third set of Atterberg Limits tests. This round was prepared in accordance with the TxDOT dry preparation method TEX-101-E. Although this method of preparation is significantly different than the wet preparation method that was used during the first two rounds of tests, and despite the fact that the tests were conducted in a different lab and by a different technician, all three rounds of tests showed close agreement.

Figure 39 summarizes the three rounds of tests. The highest plasticity indices occur between 15 and 20 feet. The Atterberg limit and moisture profiles are combined in

Figure 40. Moisture contents are slightly higher than the plastic limits throughout the profile.

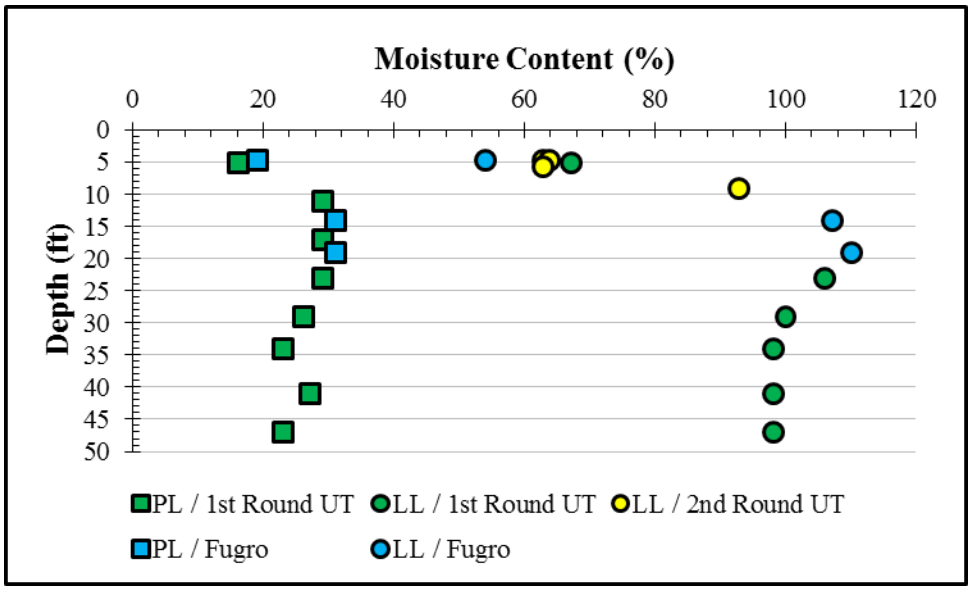

Figure 39. Summary of Atterberg Limit Measurements

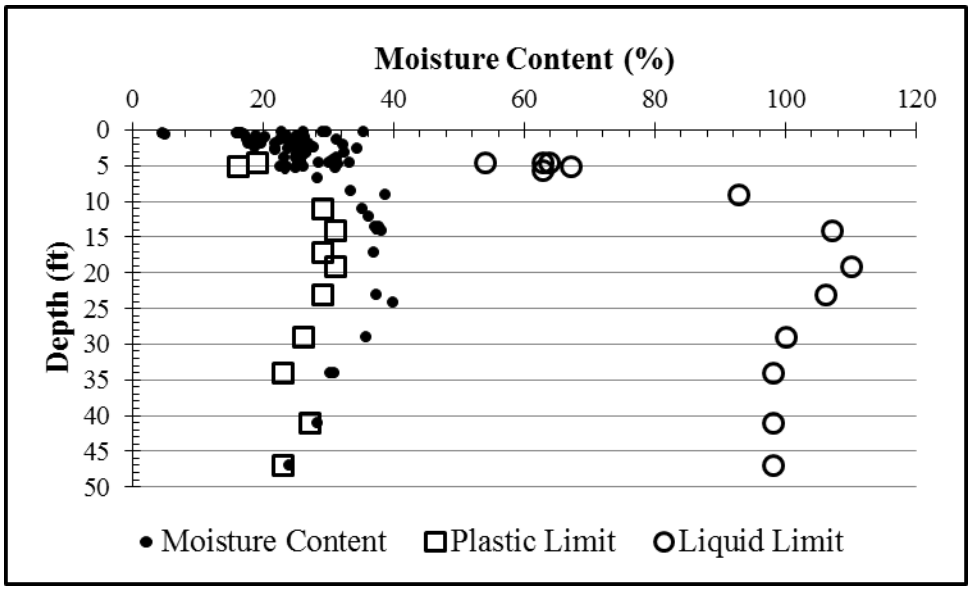

Figure 40. Summary of Atterberg Limits and In-Situ Moisture Contents

5.1.3 Unit Weight

Unit weights were measured from undisturbed samples that were trimmed to specific dimensions for laboratory testing. Trimming was a tedious procedure that usually required two to three hours per specimen. The soil's stiff and blocky structure necessitated sharp, rigid cutting tools to remove very thin slices of soil without disengaging larger blocks from the secondary mosaic structure. Figure 41 shows the tools that proved most useful for trimming: wire saw, Hyde safety knife, razor blades, open-type miter box and trimming guide.

The first step in trimming a specimen was cutting an appropriate length of soil off of the 8-inch long undisturbed sample that had previously been extruded from the seamless push-tube, Figure 42. This involved laying the undisturbed sample in the miter box and using a wire saw to cut the sample to length. The wire saw commonly encountered a small stone or pre-sheared surface, either of which resulted in a very rough cut. In these cases, the rough surface was carefully trimmed flush using a razor blade. Finally, a Hyde safety knife or other rigid metal straightedge would be used with the miter box to ensure a perfectly square and flush trim.

Next, the specimen would be loaded into the trimming guide. The specimen was seated on the surface that was already trimmed to ensure a square seating during trimming. Once the specimen was properly positioned, the trimming ring was pressed firmly down onto the top of the specimen, enough to penetrate roughly 0.1 inches. A razor blade was then used to remove very thin slices of soil in the close vicinity of the trimming ring, uniformly around the circumference of the specimen. Once the soil was

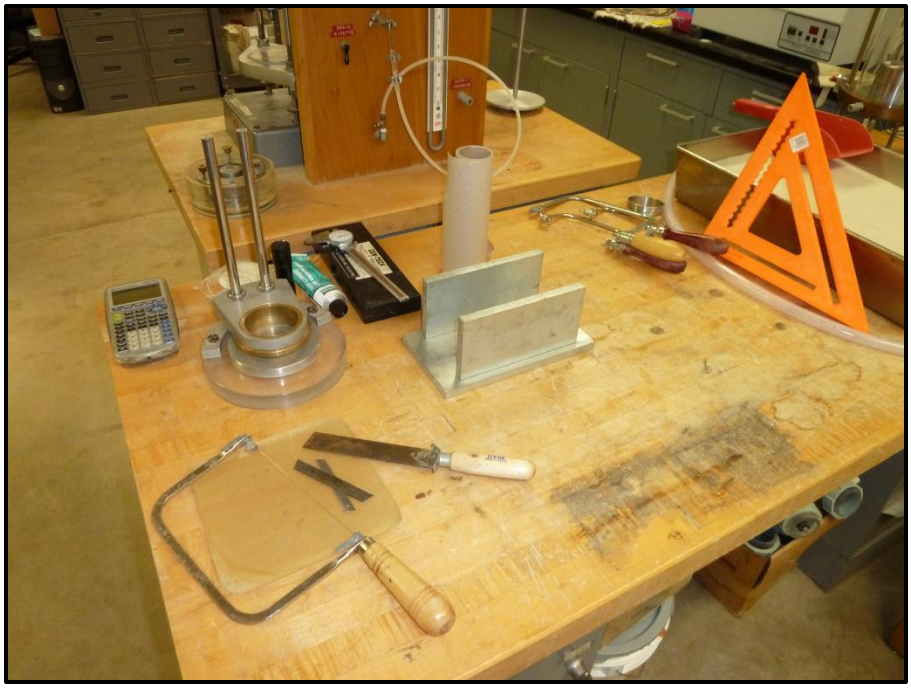

Figure 41. Trimming Tools

Figure 42. Rough Cutting Surface Associated with Wire Saw

trimmed nearly flush with the diameter of the ring, the ring was pushed further down and trimming was continued. This process was repeated until the specimen had been trimmed completely into the ring.

Isolating trimming to the vicinity of the ring was beneficial for preserving the in-situ moisture content, but it was also favorable to taper the trim downward (Figure 43) to avoid stress concentrations that tended to cause a blocky disintegration of the specimen. Whenever small pieces of rock were encountered, they were removed and replaced with fresh cuttings.

Once the soil was trimmed into the ring, the two ends were trimmed flush with the top and bottom edges of the ring. In some cases, a spacer was used for trimmed to a height slightly less than that of the ring. After removing the ring and soil from the trimming guide, a razor blade was used to trim the soil very close to the edges of the ring. Finally, a Hyde safety knife or other stiffer metal straightedge was used to ensure that the soil was flush with the ring's edge. If any rock material was encountered at the edge, it was removed and replaced with soil cuttings, Figure 44.

Because all of the density specimens were 2.5-inch diameter cylinders with thicknesses no larger than 1 inch, even small trimming imperfections could have caused a considerable underestimation of density. Specifically, the removal and replacement of small stones and the presence of chalky regions seemed to cause an underestimation of unit weights. These problems occurred at all depths, but proved most common below the weathered zone.

Figure 43. Tapered Trimming Surface

Figure 44. Rock Particle Requiring Removal and Replacement

The higher quality measurements from the weathered zone reveal an average total unit weight of approximately 123 lb/ft^3, Figure 45. Other measurements, including several that were taken by a second party, suggest that the unit weight decreases with depth. It seems more likely that these measurements are the relic of trimming problems. A more realistic profile of total unit weights has been interpreted from the more reasonable data, Table 6.

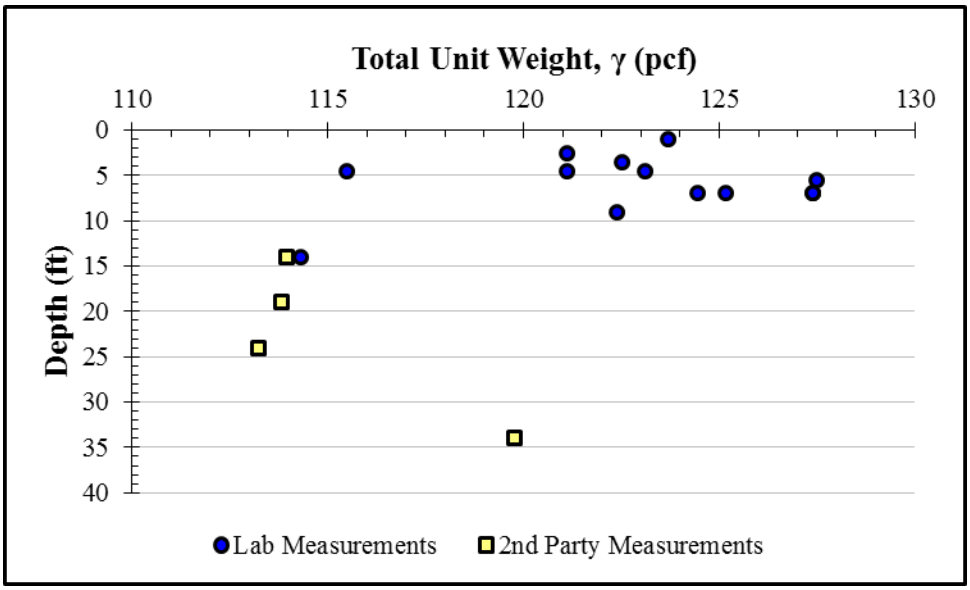

Figure 45. Profile of Total Unit Weights

Table 6. Interpreted Profile of Total Unit Weight

Depth (ft)	Total Unit Weight, γ (lb/ft^3)
0 – 5	120
5 – 10	123
Below 10	126

5.1.4 Grain-Size Analysis

The grain size distribution was determined by running hydrometer tests in accordance with ASTM D422. The soil was prepared by soaking in distilled water treated with sodium hexametaphosphate. After several days of particle dispersement and softening, a high-speed shear mixer was used to further mix the soil-water solution. The results are presented in Figure 46. The clay fractions – the percent finer than 0.002 mm – are summarized in Table 7. The variability may be explained by isolated patches of chalky material.

Table 7. Summary of Clay Fractions

Borehole	Depth (ft)	Clay Fraction, CF (%)
B-3	6 - 8	51.5
B-1	10.5 - 12	80
B-1	16.5 - 18	65
B-1	28.5 - 30	72

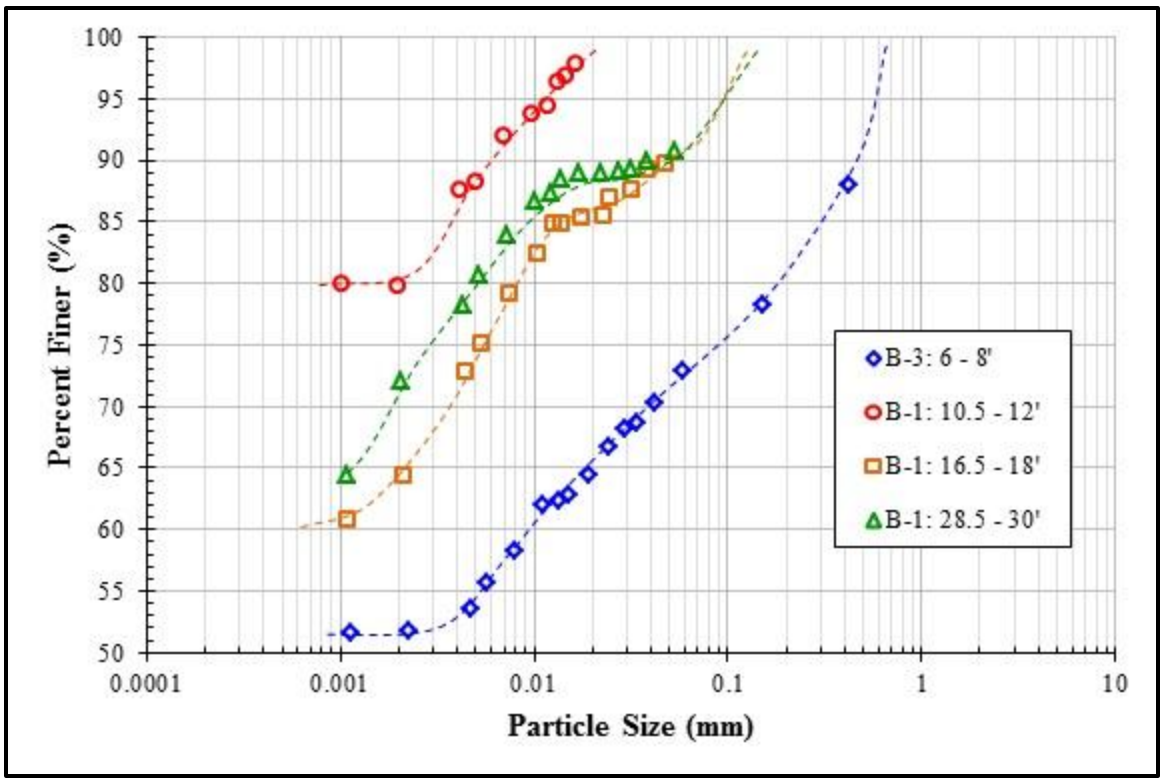

Figure 46. Summary of Grain Size Distributions

5.2 Consolidation

5.2.1 Test Procedures

Five one-dimensional consolidation tests were conducted to assess the soil's compressibility and stress history. The test specimens were all carefully trimmed from seamless push-tube samples and subject to at least two load-rebound cycles. The specific loading and wetting sequences had a significant effect on the measurements. The magnitude and duration of the initial dry seating load were particularly controlling factors.

The time-settlement data was very scattered and sometimes downright chaotic for each of the five consolidation tests. It was often difficult to define a load increment's settlement, making it impossible to differentiate between primary and secondary strains. The heterogeneity and anisotropy of this type of soil is significantly different than the idealized material upon which Terzaghi's theory of consolidated is derived. Nevertheless, Terzaghi's theory provides a useful framework for characterization in terms of total observed settlement, Olson (2009).

Theoretical time-settlement curves were fitted to the raw data using a forward modeling approach that involved fitting a theoretical time-settlement curve to match the raw data. The formulation for the theoretical curve is simply Terzaghi's theory of consolidation. The forward model allows the user to adjust several input values until the theoretical data matches the raw data.

The user-defined values of S_0, S_{100}, H_{dr} and c_v generate a theoretical consolidation curve spanning degrees of consolidation from zero through 99. The theoretical curve stretches through excessive time values for degrees of consolidation larger than 99. The drainage distance (H_{dr}) was calculated separately for each load increment as half of the specimen's height at the beginning of that increment. Initial values of S_0 and S_{100} are then entered to match the raw data. Next, the coefficient of consolidation (c_v) is adjusted within reasonable bounds until the theoretical curve begins to match the raw data. Finally, S_0, S_{100} and c_v are finely tuned to achieve the best fit.

The forward model was set up as an array in a spreadsheet so that it would automatically plot on the same graph as the raw data. The first column of the array

contains degrees of consolidation (U) ranging from zero to 99. This column essentially provides the model's independent variable. The next column calculates the time factor (T) using Equation 5. The next column calculates elapsed time (t) using Equation 6. The theoretical settlement is then calculated as a function of U, S_0 and S_{100}, Equation 7.

$$T = \begin{cases} \dfrac{\pi}{4} \cdot \left(\dfrac{U}{100} \right)^2 & U < 60\% \\ \sqrt[3]{\dfrac{\left(\dfrac{U}{100} \right)^6}{2 \cdot \left[1 - \left(\dfrac{U}{100} \right)^6 \right]}} & U \geq 60\% \end{cases} \quad \text{..... Eq. 5}$$

$$t = \frac{T \cdot H_{dr}^2}{c_v} \quad \text{..... Eq. 6}$$

$$S = S_0 - \left(\frac{U}{100} \right)(S_0 - S_{100}) \quad \text{..... Eq. 7}$$

Every load increment's raw time-settlement data is fitted with theoretical curves in Appendices B – F. Both square-root of time and log of time graphs are presented for each load increment. The square-root of time plots also contain horizontal dashed lines corresponding to S_{60}. This simply delineates the zone between S_0 and S_{60} through which S-√t should be linear. Non-Terzaghian effects often result in distorted time-settlement measurements in the first minute or so of a load increment. It was often beneficial to use the first 60% of settlement to define S_0 instead of the first 30 seconds. In every case, an effort was made to fit both plots. Many times it was impossible to fit a theoretical curve

on either time scale. In these cases judgment was used to achieve the best fit possible using reasonable input parameters.

Still using the theoretical consolidation framework, the soil's hydraulic conductivity was back-calculated for each load increment. The coefficient of compressibility was calculated using Equation 8. Again, S_0 and S_{100} refer to total observed settlement. The change in effective stress is equal to the increase or decrease in effective stress from the previous to the current load increment. The hydraulic conductivity (k) is then calculated using Equation 9.

$$a_v = -\frac{S_{100} - S_0}{H_s \Delta\sigma'} \qquad \text{..... Eq. 8}$$

$$k = \frac{c_v a_v \gamma_w}{1 + e_{50}} \qquad \text{..... Eq. 9}$$

Each test was run in accordance with ASTM D2435, but the individual loading and wetting sequences were not identical. Each load sequence used a load increment ratio of 1 and an unloading ratio of ½. Tests 1 and 2 were initially loaded with 125 psf and then inundated after a waiting period of several minutes. The data acquisition system failed during several load increments of Test 1. Tests 3 – 5 were initially loaded with weights approximating their in-situ vertical effective stresses, and they were loaded in the dry condition for precisely 30 minutes before inundation. Test 3 was allowed to swell under its in-situ vertical stress after inundation. Additional weights were applied to maintain constant volume after inundation for Tests 4 and 5.

5.2.2 Summary of Results

Figures 47 – 51 present the hydraulic conductivities, coefficients of consolidation and void ratios from the five tests. The back-calculated hydraulic conductivities are small, generally ranging from 2 x 10^{-7} down to 2 x 10^{-9} ft/day through the load cycles. Based on these results, the hydraulic conductivities at in-situ effective stresses are summarized in Table 8.

The e-log-P' plots verify that the soil is heavily overconsolidated. The virgin compression curves for Tests 1 and 2 are too rounded to define a compression index or a clear transition to normally consolidated compression. The higher dry seating loads for Tests 3 – 5 resulted in a clearer transition to normally consolidated compression and discernible compression indices. Overconsolidation ratios ranged from 9 – 14. The results from all five tests are summarized in Table 9. Figures 52 and 53 compare the initial load and rebound curves for each test in terms of strain and void ratio, respectively.

Table 8. Back-Calculated Hydraulic Conductivities (k) at In-Situ Stresses

Test ID	Depth (ft)	Hydraulic Conductivity, k (ft/day)	k (cm/sec)
1	6 – 8	3 x 10^{-9}	1 x 10^{-12}
2	8 – 10	8 x 10^{-9}	3 x 10^{-12}
3	4 – 5	4 x 10^{-9}	1 x 10^{-12}
4	4 – 5	4 x 10^{-9}	1 x 10^{-12}
5	13 - 15	4 x 10^{-9}	1 x 10^{-12}

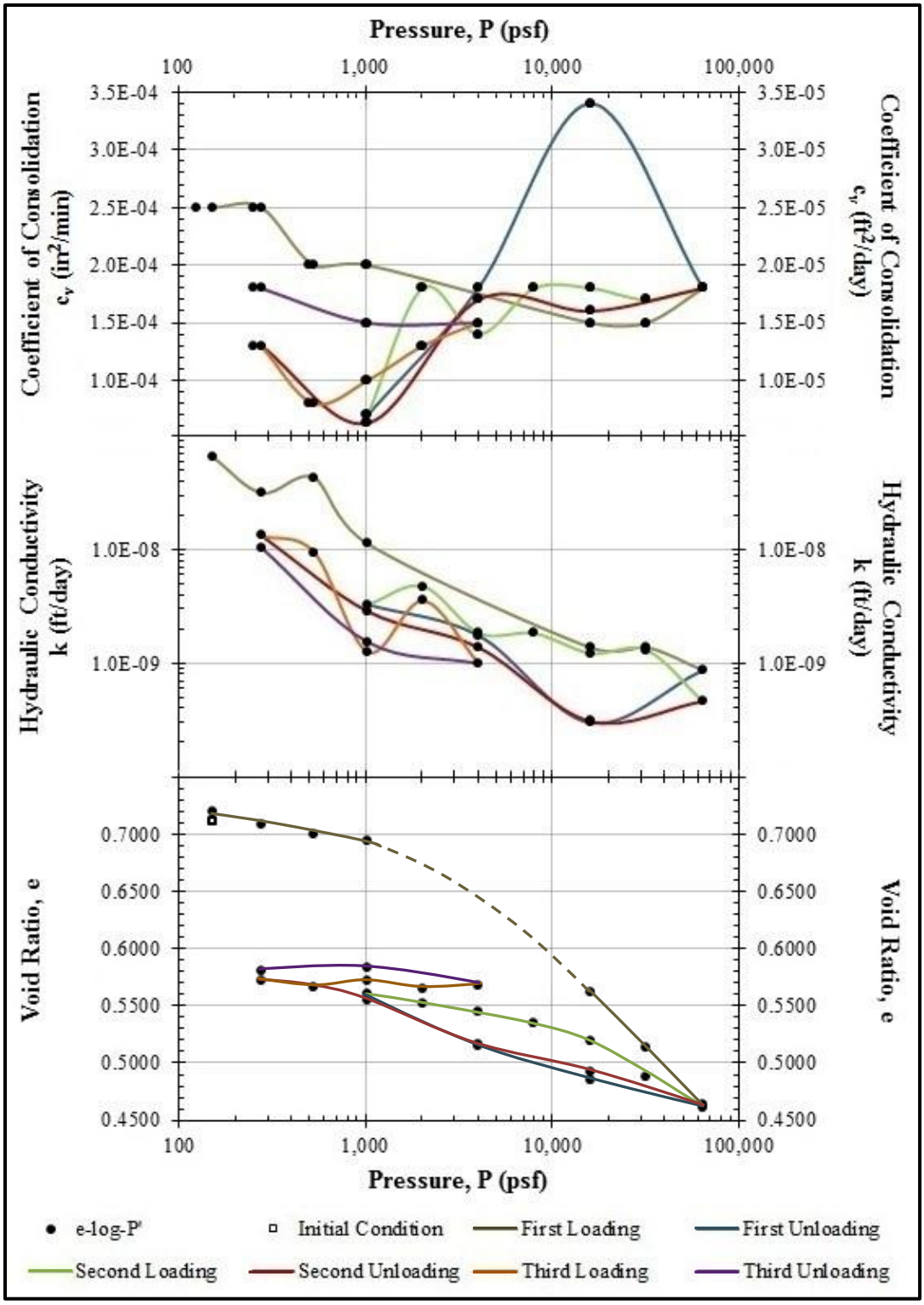

Figure 47. Consolidation Test #1: B-3, 6 – 8 ft

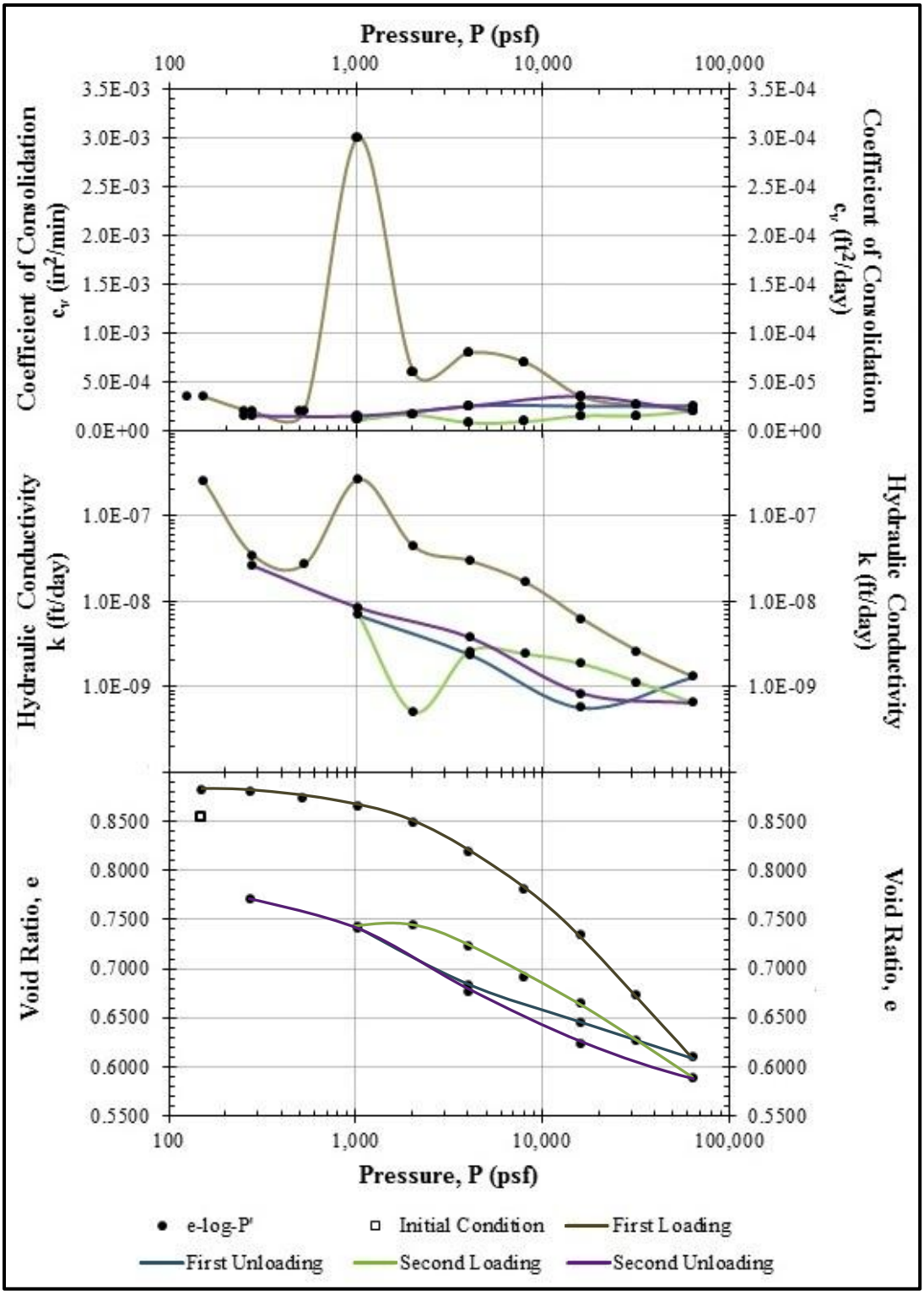

Figure 48. Consolidation Test #2: B-3, 8 – 10 ft

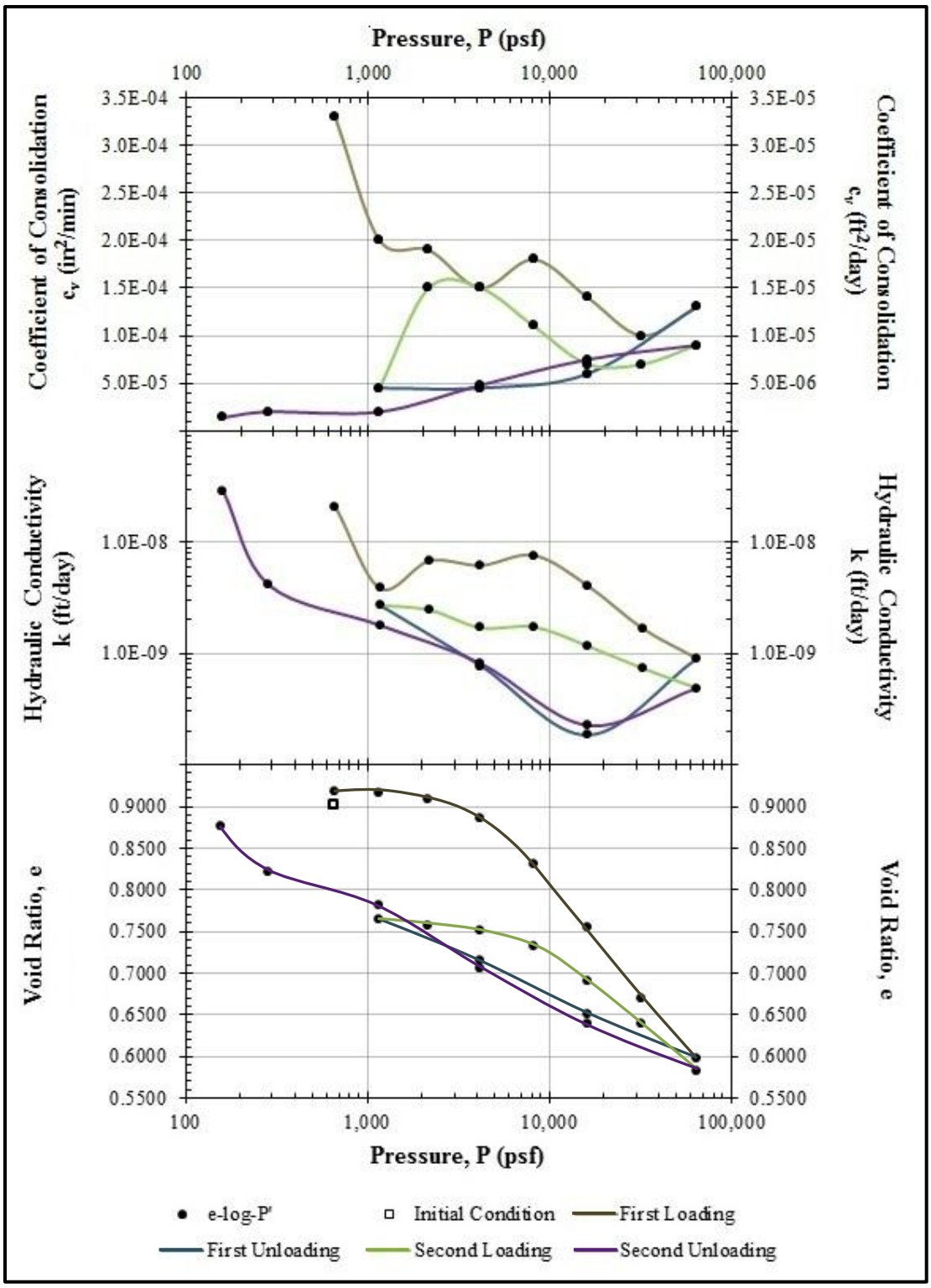

Figure 49. Consolidation Test #3: B-3, 4 – 5 ft

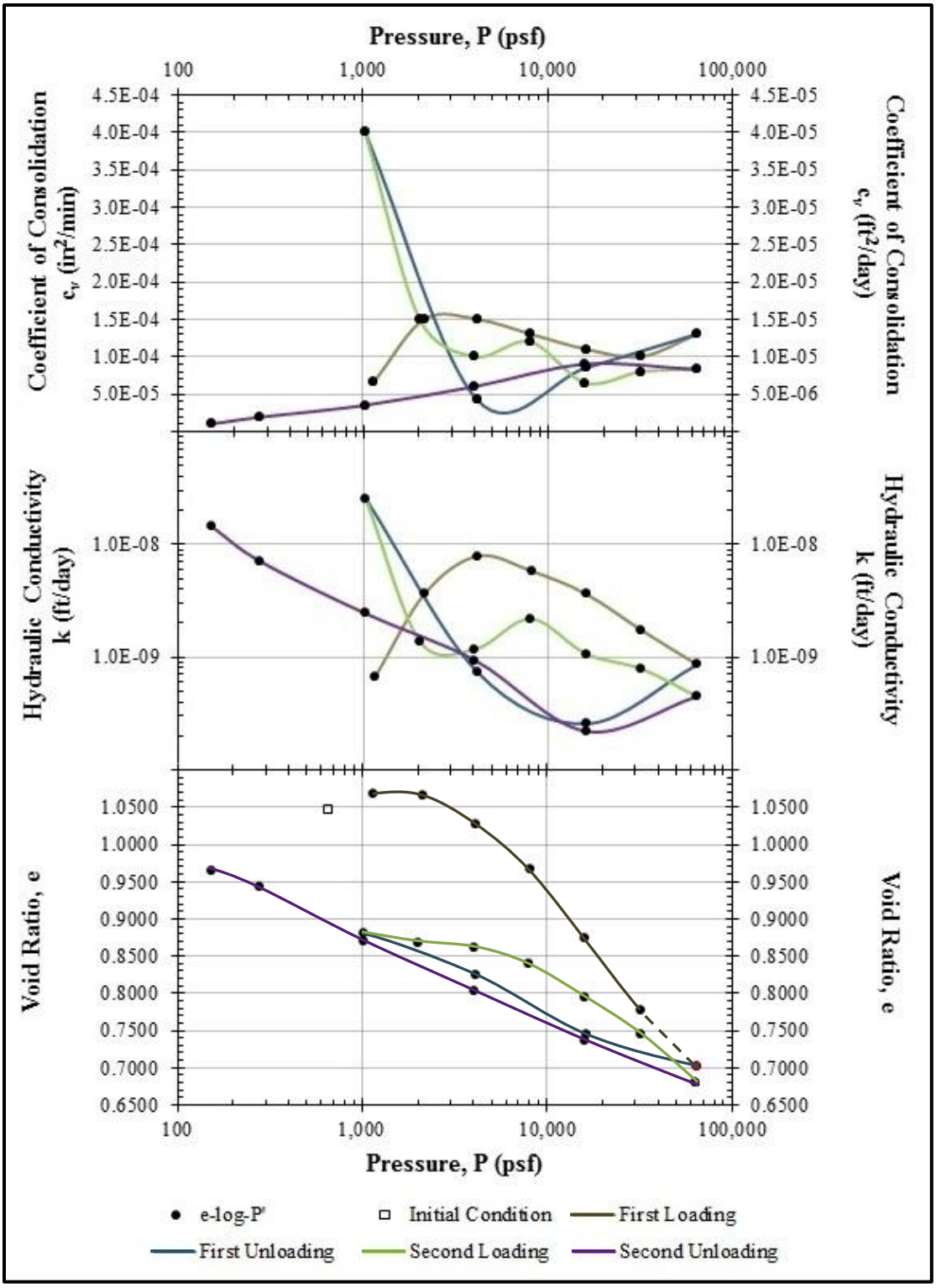

Figure 50. Consolidation Test #4: B-3, 4 – 5 ft

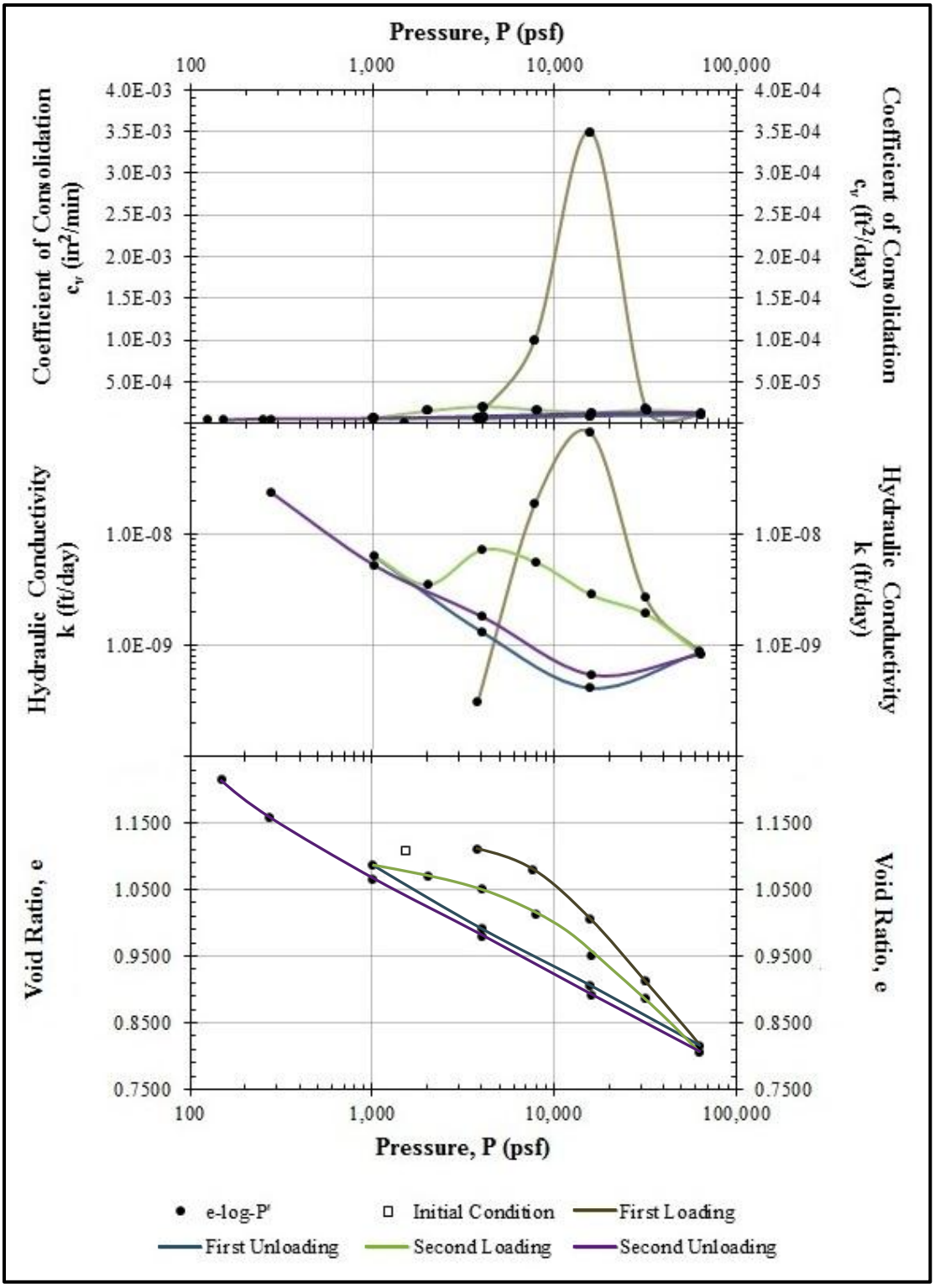

Figure 51. Consolidation Test #5: B-3, 13 – 15 ft

Table 9. Summary of Consolidation Tests

Test #	Boring	Depth (ft)	c_r	c_c	σ'_v (pcf)	OCR	PL	PI	e_0
1	B-3	6 - 8	0.033	-	750	-	23	55	0.7117
2	B-3	8 - 10	-	-	900	-	26	67	0.8541
3	B-3	4 - 5	0.103	0.288	500	14	19	44	0.9019
4	B-3	4 - 5	0.112	0.319	500	12	19	44	1.0454
5	B-2	13 - 15	0.150	0.313	1150	9	31	76	1.1076

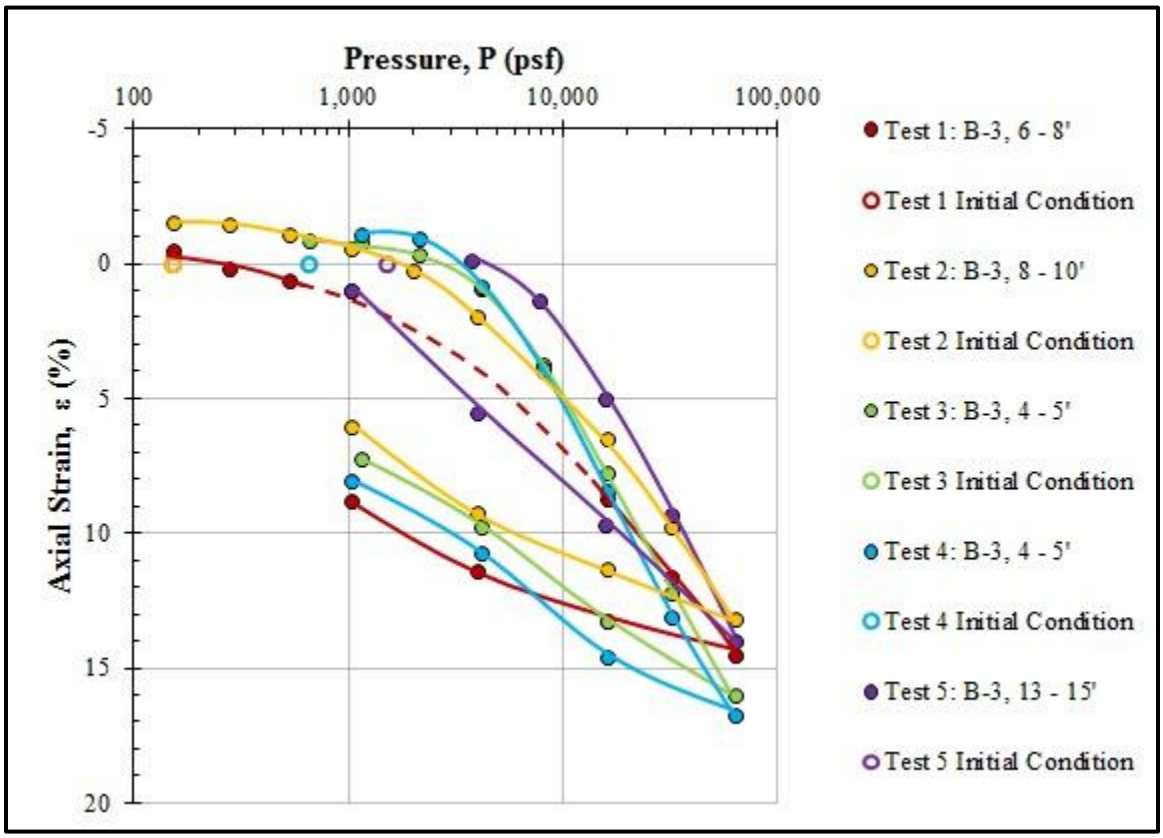

Figure 52. Summary of Load-Rebound ε-log-P Curves

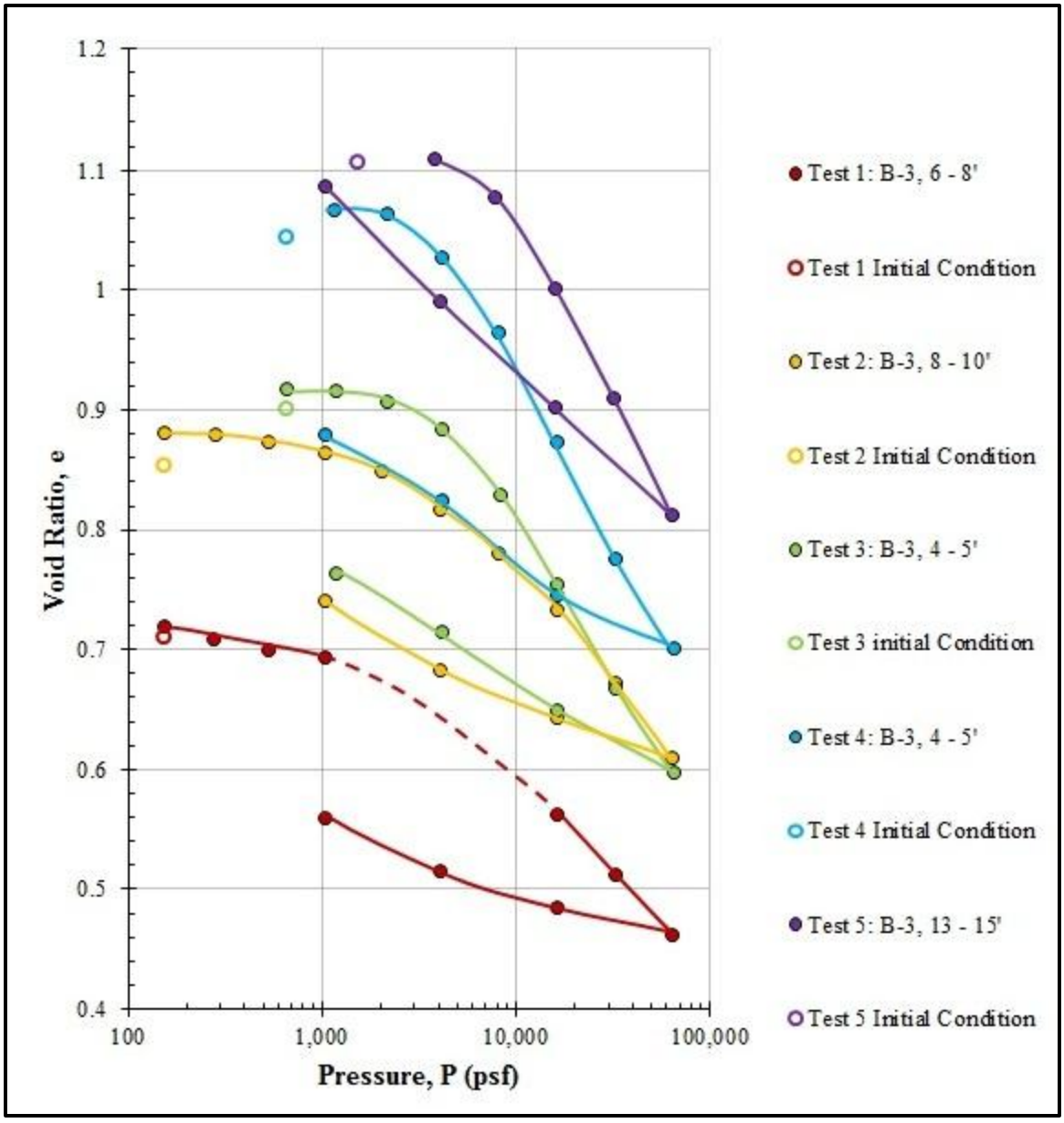

Figure 53. Summary of Load-Rebound e-log-P Curves

5.3 Cyclic Lateral Shrink and Swell

5.3.1 Overview of Test Method

A series of cyclic shrink-swell tests were conducted on horizontally trimmed specimens to estimate the soil's response to cyclic changes in moisture content. In these tests, the axial strain and moisture content are measured while the sample is repeatedly wetted and force-ventilated under a constant total normal stress. Because the samples were trimmed horizontally, the normal stress is analogous to the lateral restraint provided by a retaining wall. The test method was adapted from a similar test developed by Marr (2003) and Allen (2005).

5.3.2 Trimming Procedure

Specimens were trimmed from vertically sampled undisturbed seamless push tube samples. The specimens were trimmed transversely through the samples so that the specimens' longitudinal axes corresponded to a horizontal plane in the field. The first step in specimen preparation was cutting a 3-inch length of soil from the undisturbed sample. Because these tests were only conducted on the relatively soft weathered clay from the active zone, a wire saw was adequate for cutting through the undisturbed sample. A Hyde safety knife or other rigid metal straightedge was then used along with an open type miter box to square and flush one of the specimen's edges, Figure 54a.

The specimen would then be seated on its squared end inside the miter box. Holding the soil firmly against one of the miter box walls, a wire saw could be used to cut a roughly ½-inch secant through the specimen's diameter. This cut was continued across the specimen to form a plane parallel to the sample's original longitudinal axis.

Next, the specimen was rotated 180 degrees in the miter box and a second ½-inch secant plane was trimmed parallel to the first, Figure 54b.

Once both secant planes were trimmed square and flush, one was used to seat the specimen on a plastic trimming surface. The cutting edge of a lightly greased 2.5-inch diameter, 1-inch tall ring was then carefully centered and seated on specimen's exposed secant plane. Because of geometric limitations, this was a nontrivial step that required careful attention. After a light seating, a level was used to ensure the ring was plumb. At this point, it was convenient to trim away the specimen's four corners for high quality moisture samples, Figure 54c.

Finally, a razor blade was used to slowly trim soil away from the area just outside the cutting surface of the ring. Once the soil was nearly flush with the ring, the ring was pushed down further into the sample. This was done very slowly, and the level was constantly checked to ensure that the ring remained plumb as it was pushed down around the soil specimen, Figure 54d.

Once the maximum thickness of soil was trimmed into the ring, the specimen was trimmed squarely at the top and bottom of the ring. A spacer was then used to push and trim enough soil away from the top – cutting edge – of the ring to make room for a filter paper and porous stone. Whenever small pieces of rock material were encountered, they were removed and filled with compacted soil trimmings.

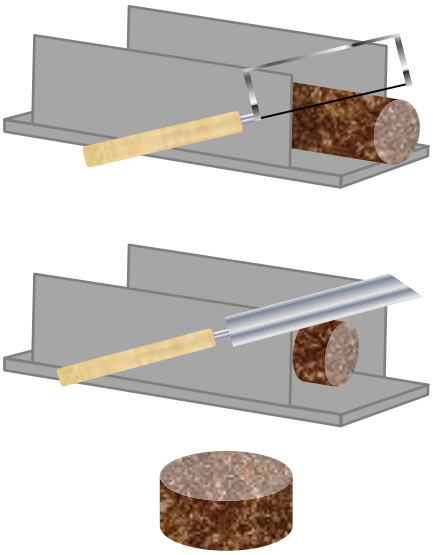

(A) Using wire saw and knife to separate specimen from sample.

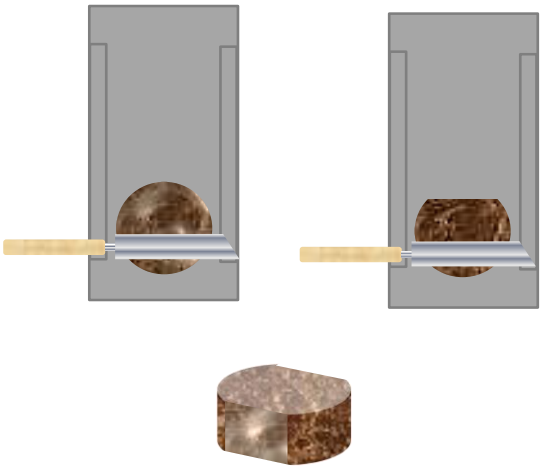

(B) Cutting two parallel secant planes into the specimen.

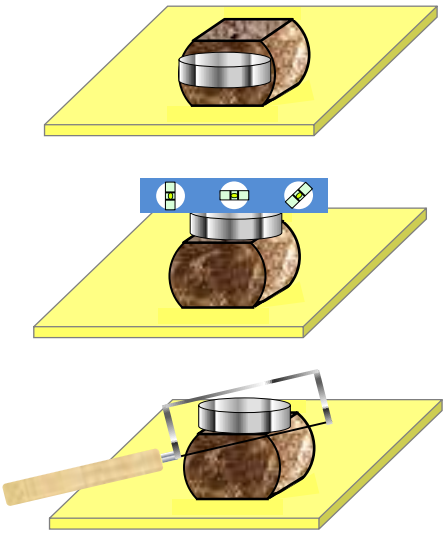

(C) Centering and seat the ring, then removing the corners.

(D) Trimming the soil outside the cutting edge of the ring with a razor blade.

Figure 54. Trimming Procedure for Lateral Cyclic Swell Tests

5.3.3 Equipment Setup

The cyclic swell tests were conducted using standard constant rate of strain (CRS) consolidation equipment. This includes a floating ring CRS consolidation cell, two columns of a pressure panel and a GeoJAC load frame from GEOTAC. GeoJAC software was used to control the load frame from a computer, and an integrated data acquisition system (DAS) was used to collect measurements of displacement, load and pressure. A schematic of the setup is shown in Figure 55.

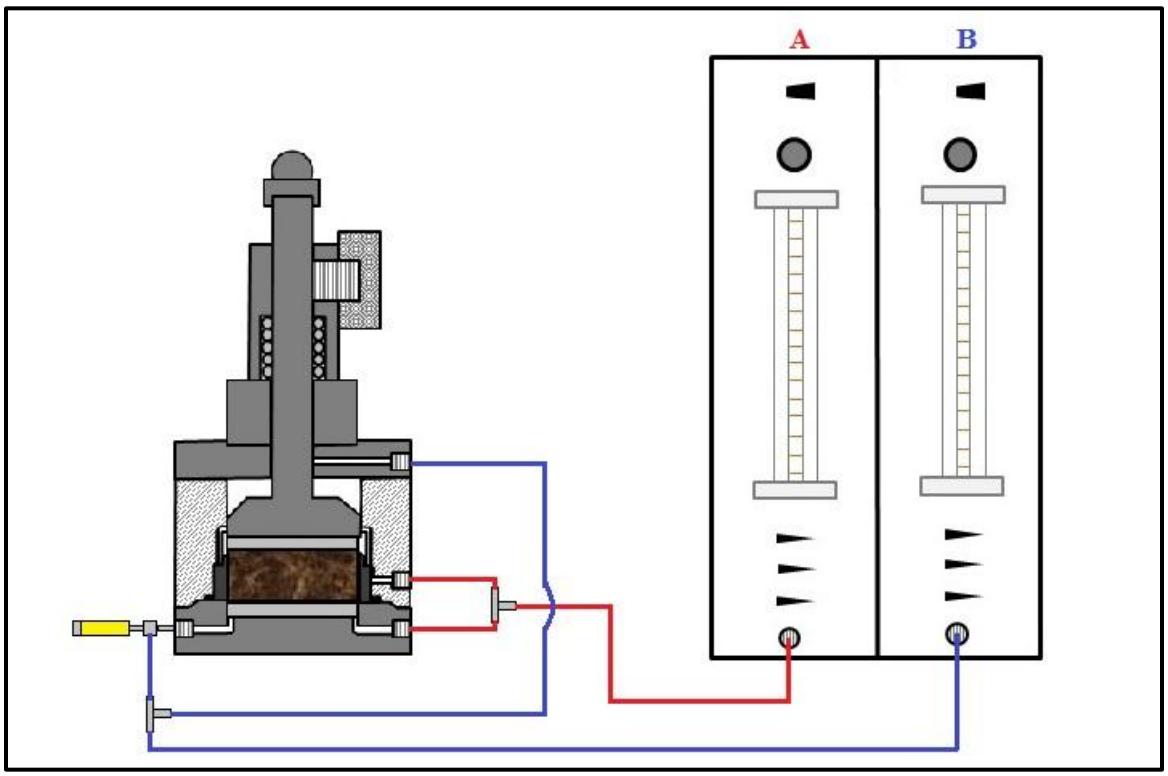

Figure 55. Equipment Setup for Cyclic Swell Tests

The top and bottom halves of the consolidation cell are isolated from one another, and each half has two available ports. Two columns of a pressure panel were utilized for each test. Each column was connected to both a top and bottom port of the consolidation cell, with one line being connected to the bottom half of the cell through a pressure transducer. Note that the column labels – "A" and "B" – from Figure 55 will be referenced in the discussion of test procedures in Section 5.3.4. An LVDT and a load cell were mounted on the GeoJAC. The top and bottom halves of the CRS cell were connected with three mounting screws and sealed water tight using a greased O-ring.

5.3.4 Test Method

The CRS cell and DAS are both readied prior to trimming the soil specimens. With their bottom valves closed, the burette and annulus of column A are filled with water and those of column B are drained. Masses are recorded for the ring, porous stones – both wet and dry – and filter papers. Throughout the test, these masses are occasionally required as tare weights to calculate intermediate specimen weights. The specimen diameter, height and mass are all measured immediately after trimming.

After recording the initial specimen measurements, the specimens are loaded into the CRS cell. One porous stone is laid into its recessed position and covered with a damp filter paper. The soil and ring are placed on top of the filter paper. Another filter paper and porous stone are placed on top of the soil, within the ring. The O-ring is then placed around the base of the ring. The top half of the CRS cell is clamped to the bottom half

and all of the fluid lines are connected to the CRS cell ports. The load piston is then firmly seated against the soil and locked into place.

Once assembled, the cell is loaded onto the GeoJAC load frame and the load cell is zeroed. Using the computer to control the GeoJAC in Displacement Control mode, the load ram is slowly lowered until it makes slight contact with the CRS load cap. The LVDT is then zeroed. Next, the software is changed to Load Control mode and the predetermined normal load for the test is applied. Immediately thereafter, the load cap piston is unlocked. The specimen should be loaded in this dry condition for a period of time between 10 and 30 minutes. Dry seating periods for the tests reported herein were typically between 5 and 10 minutes.

After the dry seating period, the CRS cell is filled with water while the normal load is held constant. The cell is filled by making the following adjustments to pressure panel columns A and B: turn the top valve to the vent position, enable both the pipette and annulus and open the bottom valve. Depending on the test setup, a pressure of 2 or 3 psi may need to be applied to the top of column A to force water through the CRS cell. At some point while filling the CRS cell, the pressure transducer should be flushed and zeroed. Note that column A will have to be closed and refilled with water at least once to finish filling the CRS with water. The CRS cell is sufficiently full when the water level in column A recedes at the same rate that water level in column B rises.

When the cell is filled, temporarily close the bottom valves of columns A and B and adjust the water levels. The annulus levels should be at a maximum so that the tick marks on the pipette are amplified. The water level in each pipette should be equal, at the

pipettes' middle reading. The enabling valves on each column should then be set to the pipette position. Finally, note the time and zero-readings for each pipette, and open the bottom valves. The soil is then allowed to swell until significant changes in height no longer occur.

After the first swell stage, the cell is drained and the specimen is removed and weighed. The first step in draining the cell is locking the load cap into place and closing the bottom valves of columns A and B. The annulus and pipette of each column are then drained. Leaving column A in the drain position, a pressure of 3 – 5 psi is applied to column B and each column's bottom valve is opened. When the cell is essentially dry, column B is turned back to the vent position and close the bottom valves of columns A and B.

At this point the specimen may be removed and weighed. The GeoJAC's load piston is raised by switching the software back to Displacement Mode and entering the command. The three clamping screws are then removed, and – depending on the length of the fluid lines – some of the fluid lines will have disconnected from cell ports so that the top half of the cell can be lifted off of the base. The weight of the specimen is quickly recorded, along with details of any tare weights. If possible, both filter papers are replaced with fresh, dry papers and the assembly is returned to the CRS cell for the first shrink stage.

The CRS cell is again assembled as it was for the swell stage, except that each column's pipette and annulus are drained and the inside of the CRS cell is wiped dry. Once the clamping screws and fluid lines are reconnected, the CRS cell is positioned on

the GeoJAC just as it was for the swell stage and the same predetermined total normal load is applied. A new zero for the LVDT is noted while the GeoJAC's load piston is seated, and a new DAS task is initiated to record the shrink stage measurements.

Air is now force ventilated through the CRS cell to accelerate the natural process of shrinkage. For this process, the top of column A is set to the vent position and pressure is applied to the top of column B. The bottom valves of both columns are opened, and the pressure is increased until the pressure transducer attached to the CRS cell reads approximately 5 psi.

Periodically during the shrink stage, the specimen is removed and weighed to obtain a measurement of moisture content. The forced ventilation pressure is removed prior to removing the specimen, and then the CRS cell is removed from the GeoJAC and opened. The specimen is removed and weighed, then returned to the CRS cell. As more time elapses during the shrink stage and the specimen develops large cracks (Figure 56), it becomes more difficult to remove and handle the specimen. Special care must be taken during these measurements to ensure that there is no loss of solid soil particles during weighing. The cracked specimens provide a valuable representation of desiccation that occurs near the surface in the field, Figure 57.

After each weighing, the specimen is returned to the CRS for continued forced ventilation. The shrink stage is continued until significant changes in height cease to occur. At the end of the shrink stage, the specimen is again removed and weighed. The test is concluded at the end of the final shrink stage. At that time, the specimen is removed, weighed and then oven dried. Unless significant solids are lost during the test,

the oven dry weight reveals the true weight of solids and should be used to backcalculate moisture contents from throughout the test.

Figure 56. Examples of Extreme Cracking from Shrink Stage of Cyclic Swell Test

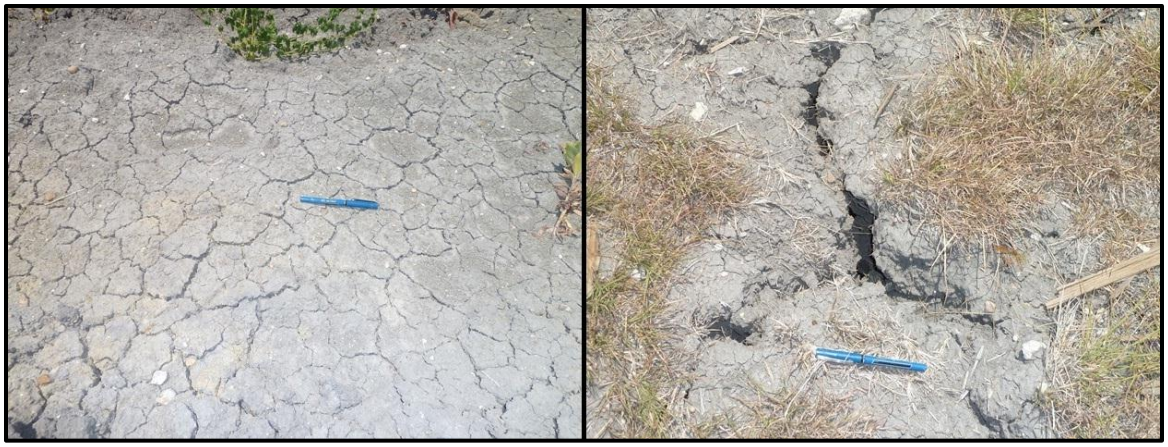

Figure 57. Examples of In-Situ Desiccation Cracking

The relationship between height or strain and moisture content is nearly linear. By assuming the relationship is linear, each swell-shrink cycle may be summarized by a single best-fit line with slope k_s. The steady state value of k_s, hereafter termed the cyclic swell coefficient, can either be taken from the final swell-shrink cycle or the average of several similar cycles. It is a dimensionless value, technically percent per percent. If multiple tests are run at different normal stresses, a constitutive surface can be constructed in terms of total stress, moisture content and height or strain, Figure 58. This constitutive surface can also be simplified by plotting values of k_s versus the log of total stress, Figure 59.

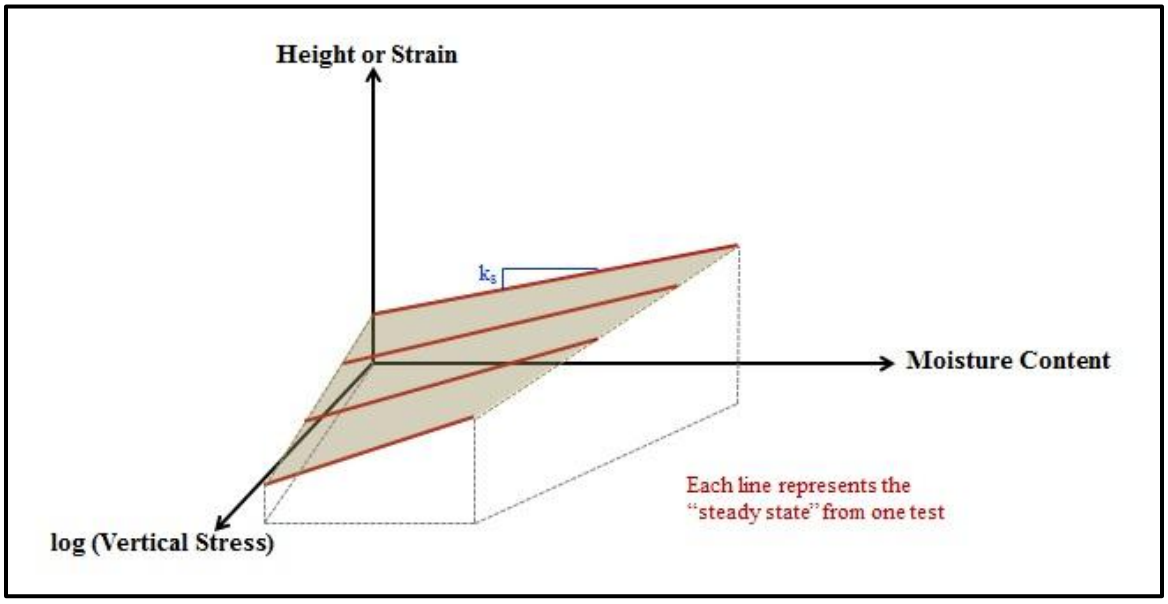

Figure 58. Constitutive Surface for Cyclic Swell Tests

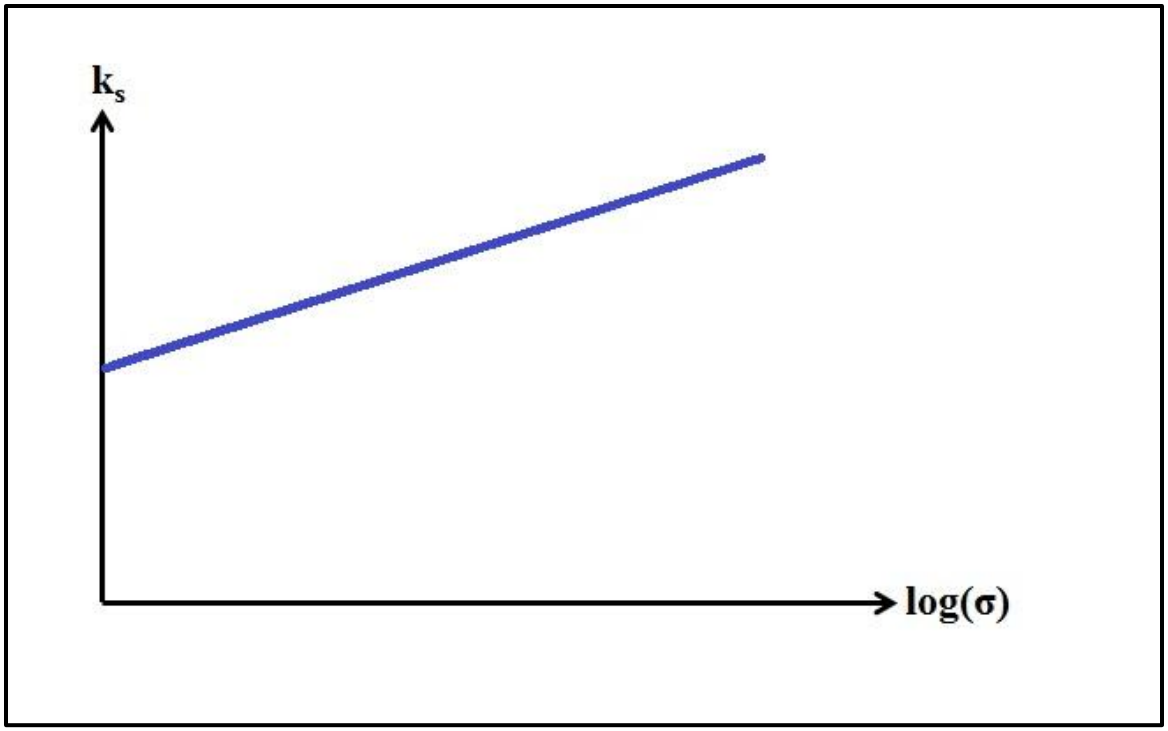

Figure 59. Practical Presentation of Constitutive Surface

5.3.5 Summary of Results

Four cyclic swell tests were conducted. The specimens were trimmed from dark, weathered clay sampled from depths ranging from 2 – 6 feet. The four tests' parameters are summarized below in Table 10. The total stress for each test was chosen to replicate lateral stresses in the field. Test 1 was loaded at less than in-situ conditions, while tests 3 – 4 were loaded at stresses that either approximated or overestimated in-situ pressures.

Table 10. Summary of Accelerated Swell-Shrink Tests

Test ID	Boring	Depth (ft)	σ_t (psf)	γ_t (pcf)	$w_{c,ini}$ (%)	$w_{c,min}$ (%)	$w_{c,max}$ (%)
1	B-2	3 – 4	150	122.4	25.4	4.3	31.3
2	B-2	2 – 3	500	121.1	26.6	3.3	28.7
3	B-2	4 – 5	1000	123.1	26.7	4.3	28.4
4	B-2	5 - 6	4050	127.5	23.3	3.3	24.6

The cumulative time-strain measurements from Test 1 are presented in Figure 60. The specimen achieved successively larger swelling strains after the first three shrink cycles and then reached its steady state. The moisture-strain measurements are shown in Figure 61. Least squares linear regressions were fitted to each cycle's data set to determine k_s values. The coefficients of consolidation from swell stages and the cyclic ranges of moisture content are illustrated in Figure 62. The k_s and c_v values are summarized in Table 11.

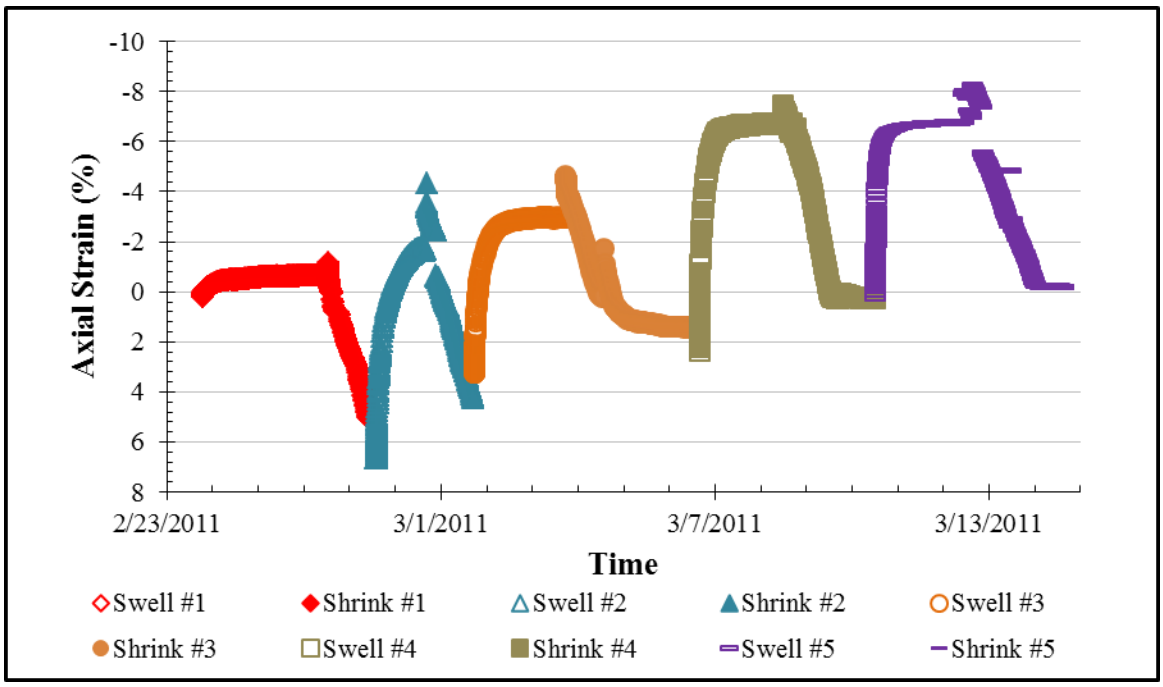

Figure 60. Cyclic Swell Test 1: Cumulative Time-Strain Measurements

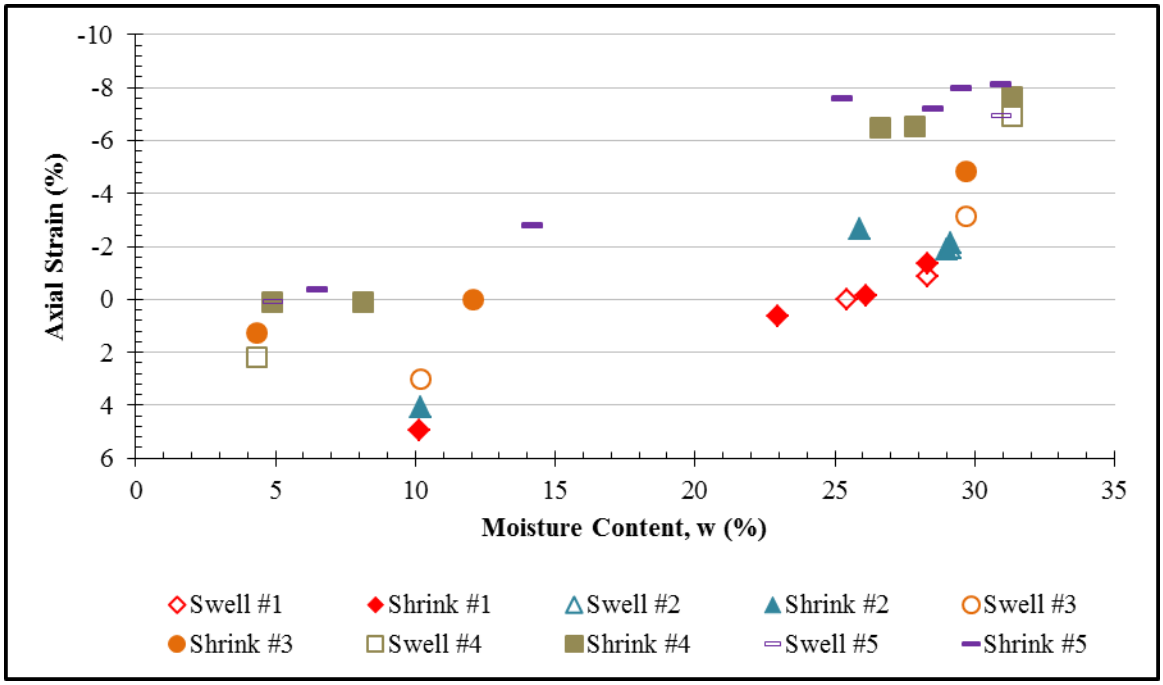

Figure 61. Cyclic Swell Test 1: Strain vs. Moisture Content

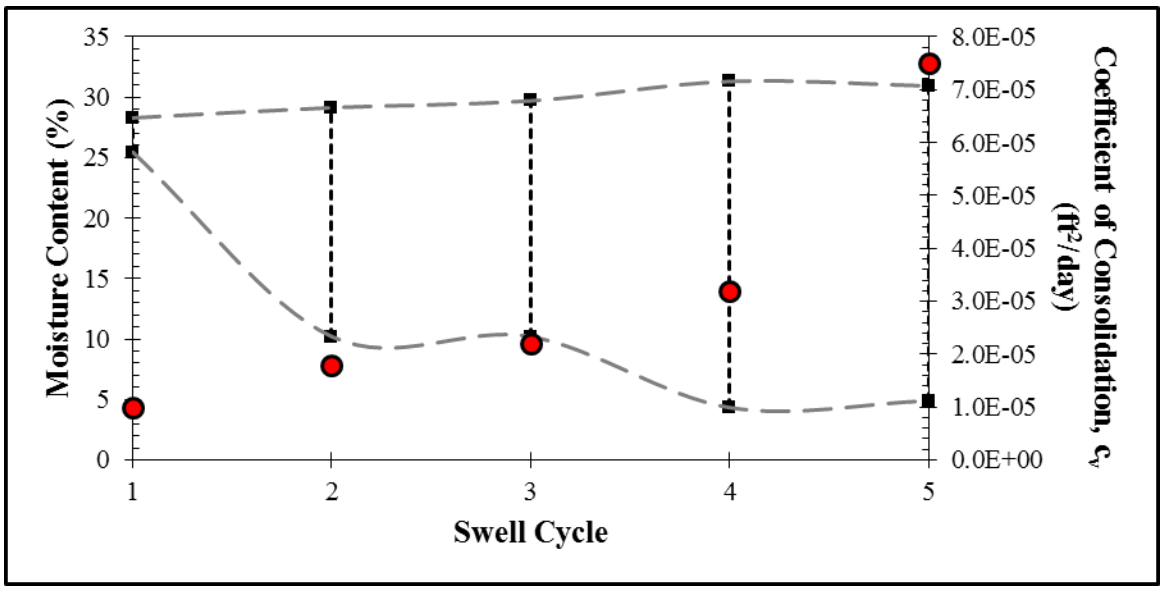

Figure 62. Cyclic Swell Test 1: Cyclic Moisture Variations

Table 11. Cyclic Swell Test 1: Summary of k_s and c_v Values

Cycle	1	2	3	4	5
c_v (ft^2/day)	1.0×10^{-5}	1.8×10^{-5}	2.2×10^{-5}	3.2×10^{-5}	7.5×10^{-5}
k_s	0.329	0.400	0.248	0.325	0.311

The cumulative time-strain measurements from Test 2 are presented in Figure 63. The specimen achieved successively larger swelling strains after the first three shrink cycles and then reached its steady state. The swelling strains appeared to reach a steady state by the end of the fifth cycle, but the cycle-to-cycle variations were somewhat chaotic. In addition, the specimen's height appears to have been altered during its removal for a moisture measurement during the third cycle. The moisture-strain measurements are shown in Figure 64. Least squares linear regressions were fitted to each cycle's data set to determine k_s values. The coefficients of consolidation from swell stages and the cyclic ranges of moisture content are illustrated in Figure 65. The k_s and c_v values are summarized in Table 12.

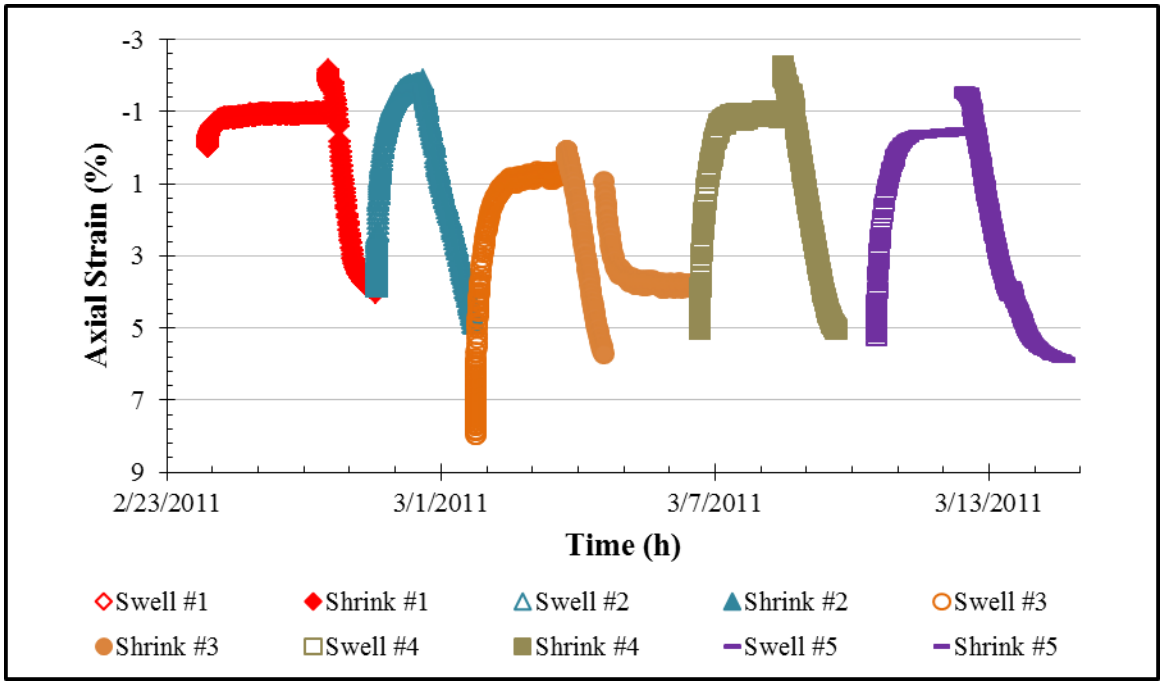

Figure 63. Cyclic Swell Test 2: Cumulative Time-Strain Measurements

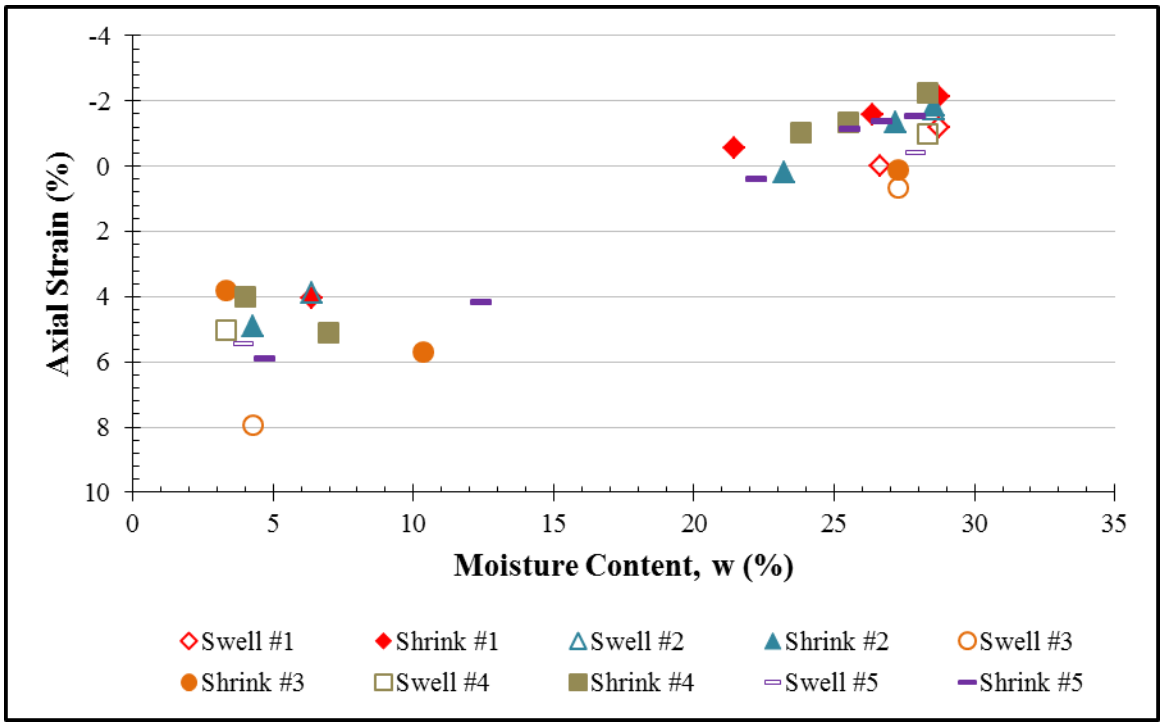

Figure 64. Cyclic Swell Test 2: Strain vs. Moisture Content

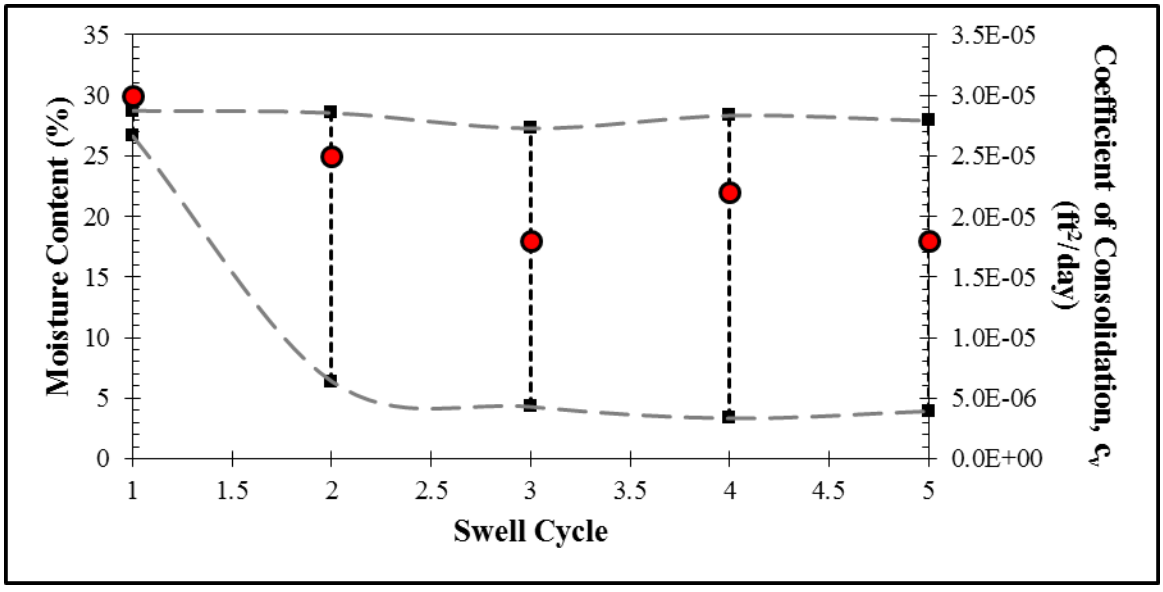

Figure 65. Cyclic Swell Test 2: Cyclic Moisture Variations

Table 12. Cyclic Swell Test 2: Summary of k_s and c_v Values

Cycle	1	2	3	4	5
c_v (ft^2/day)	3.0×10^{-5}	2.5×10^{-5}	1.8×10^{-5}	2.2×10^{-5}	1.8×10^{-5}
k_s	0.246	0.263	0.240	0.276	0.304

The cumulative time-strain measurements from Test 3 are presented in Figure 66. The specimen achieved successively smaller swelling strains after the first two shrink cycles and then began to level off toward its steady state. The moisture-strain measurements are shown in Figure 67. Least squares linear regressions were fitted to each cycle's data set to determine k_s values. The coefficients of consolidation from swell stages and the cyclic ranges of moisture content are illustrated in Figure 68. The k_s and c_v values are summarized in Table 13.

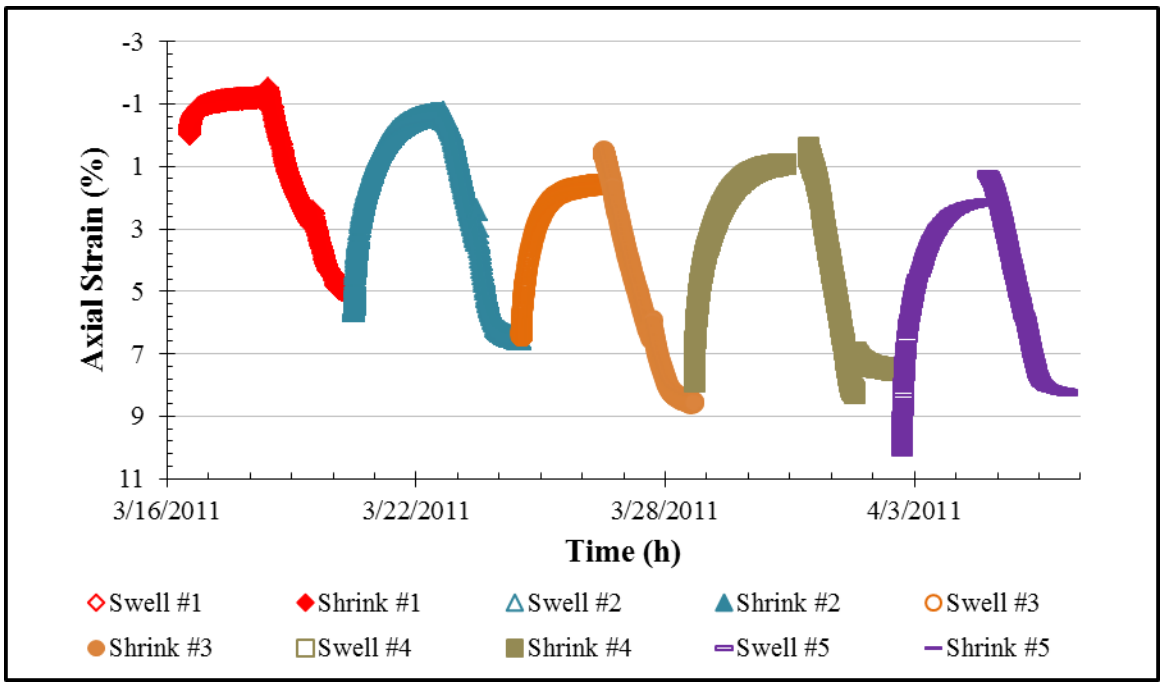

Figure 66. Cyclic Swell Test 3: Cumulative Time-Strain Measurements

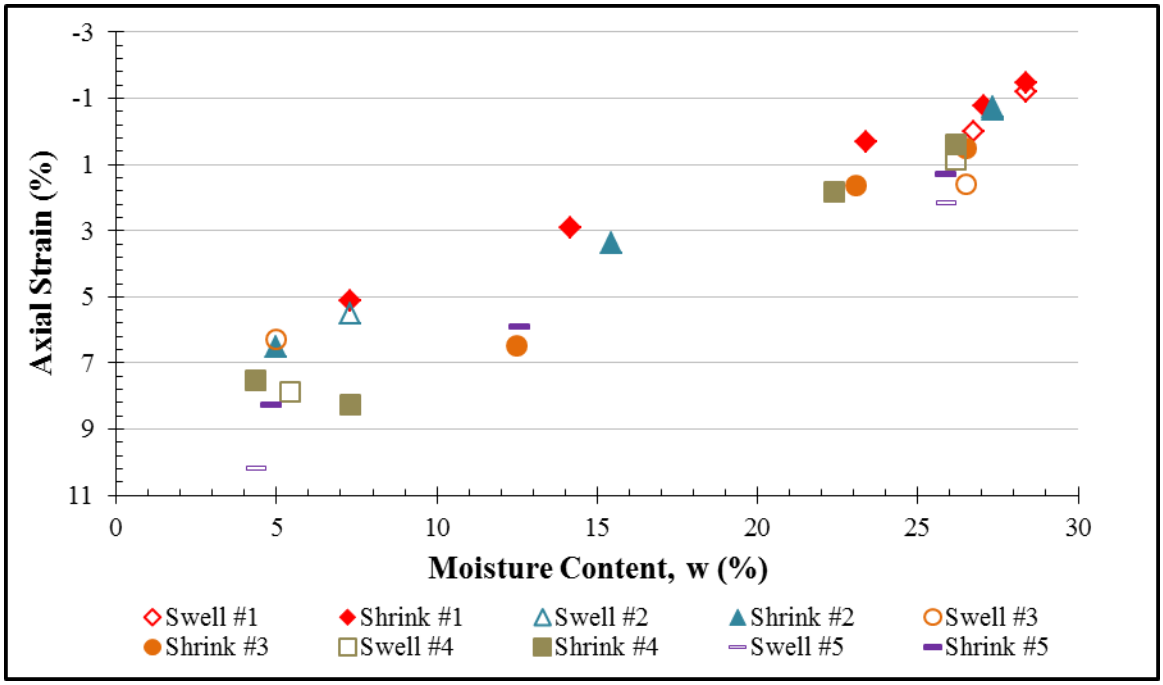

Figure 67. Cyclic Swell Test 3: Strain vs. Moisture Content

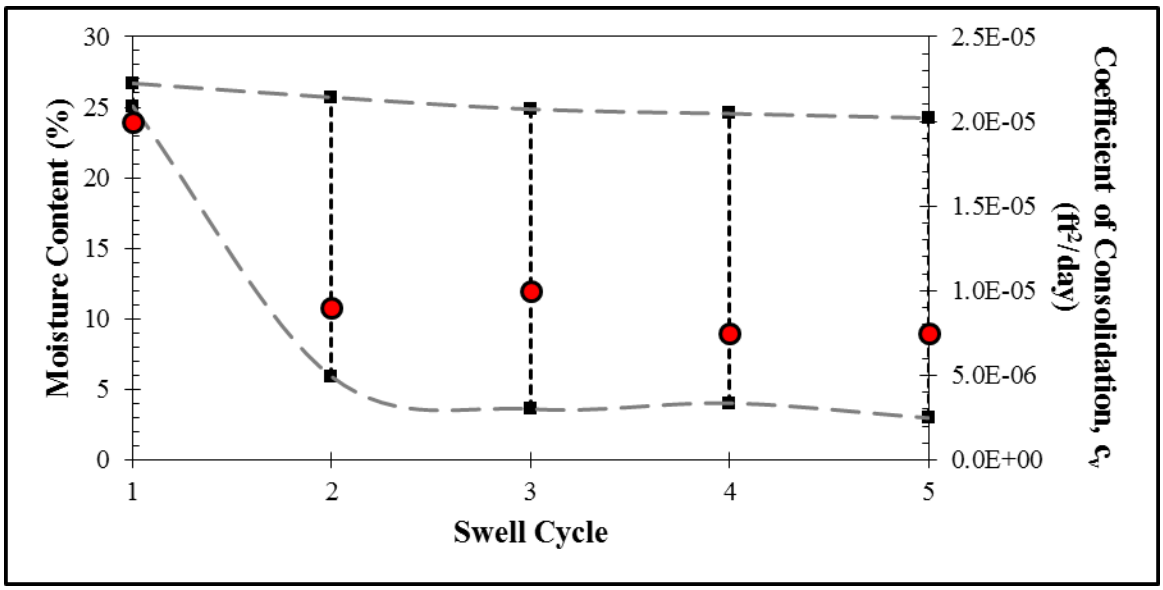

Figure 68. Cyclic Swell Test 3: Cyclic Moisture Variations

Table 13. Cyclic Swell Test 3: Summary of k_s and c_v Values

Cycle	1	2	3	4	5
c_v (ft^2/day)	2.0×10^{-5}	9.0×10^{-6}	1.0×10^{-5}	7.5×10^{-6}	7.5×10^{-6}
k_s	0.293	0.318	0.314	0.351	0.351

The cumulative time-strain measurements from Test 4 are presented in Figure 69. The specimen compressed through the successive cycles and began to reach its steady state by the fifth cycle. The moisture-strain measurements are shown in Figure 70. Least squares linear regressions were fitted to each cycle's data set to determine k_s values. The coefficients of consolidation from swell stages and the cyclic ranges of moisture content are illustrated in Figure 71. The k_s and c_v values are summarized in Table 14.

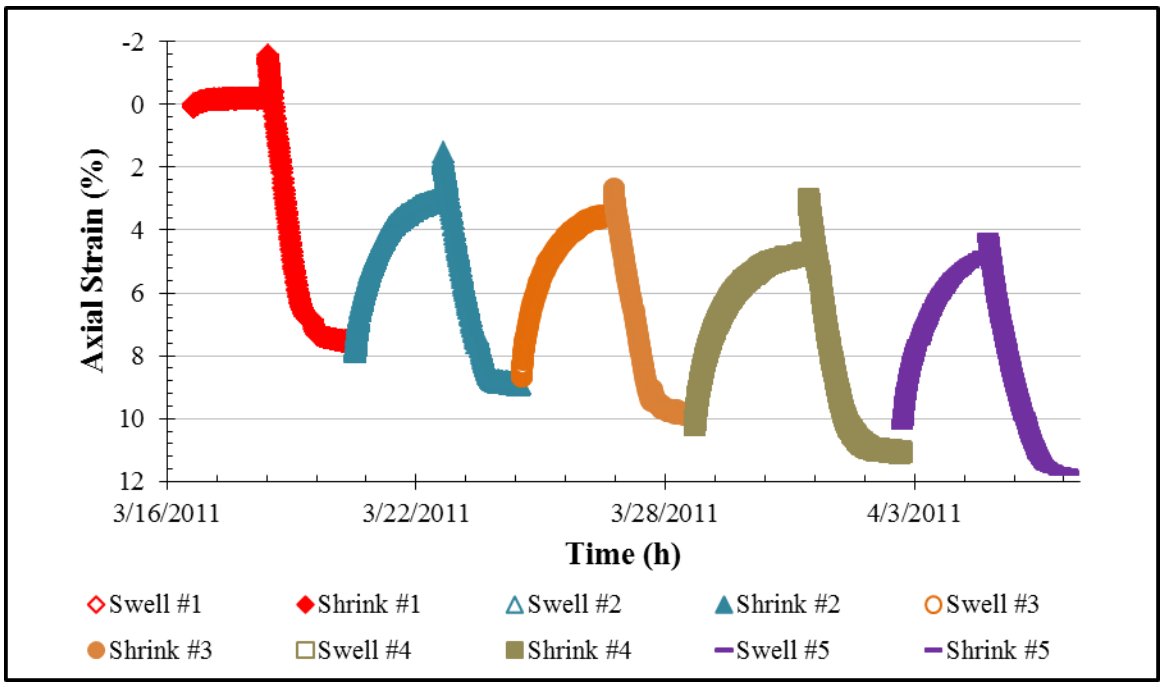

Figure 69. Cyclic Swell Test 4: Cumulative Time-Strain Measurements

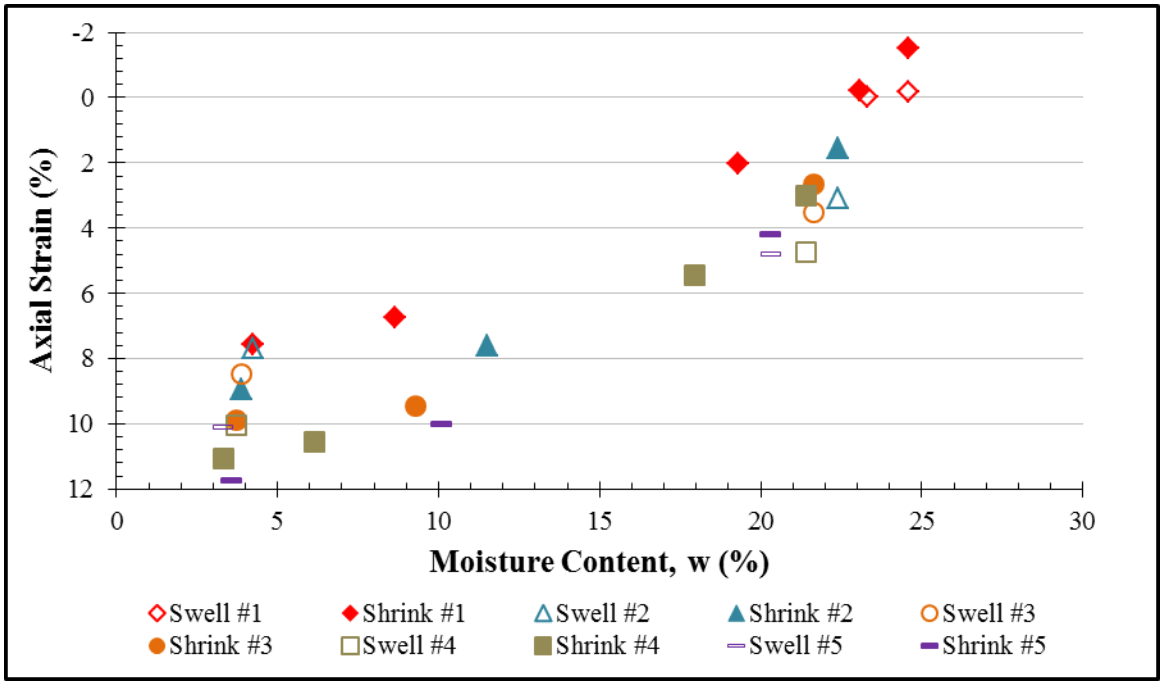

Figure 70. Cyclic Swell Test 4: Strain vs. Moisture Content

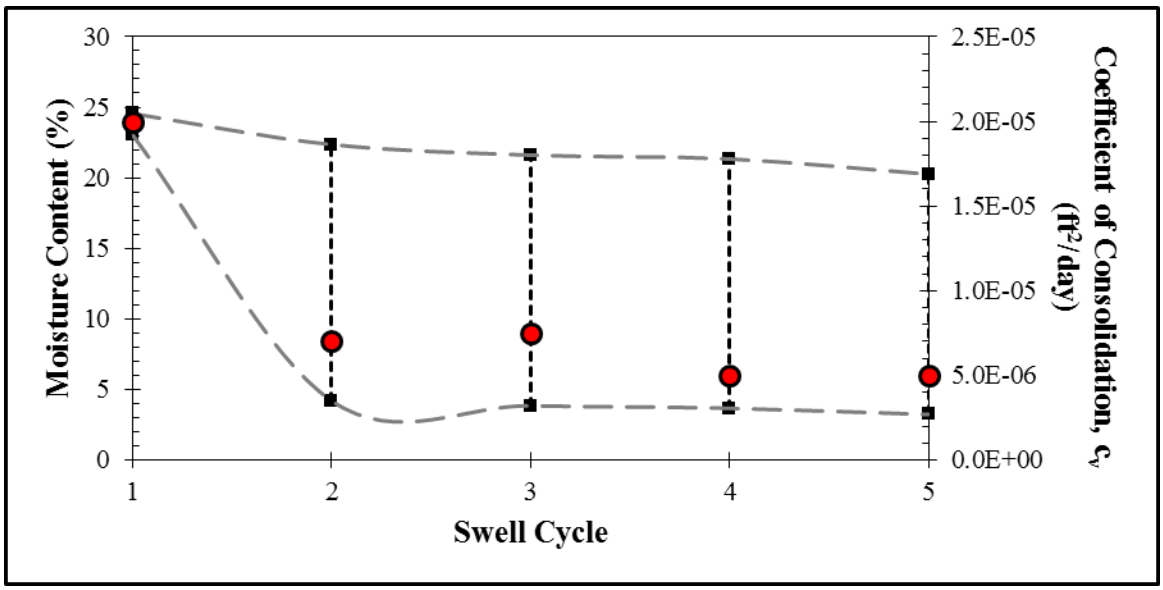

Figure 71. Cyclic Swell Test 4: Cyclic Moisture Variations

Table 14. Cyclic Swell Test 4: Summary of k_s and c_v Values

Cycle	1	2	3	4	5
c_v (ft^2/day)	2.0×10^{-5}	7.0×10^{-6}	7.5×10^{-6}	5.0×10^{-6}	5.0×10^{-6}
k_s	0.430	0.335	0.359	0.385	0.388

Each test's steady state cyclic swell coefficient was calculated as an average of the fourth and fifth cycle k_s values. The steady state values are given in Table 15. Figure 72 shows the steady state line from each test plotted over the range of moisture contents that were observed throughout each test. The constitutive surface is summarized by the plot of k_s versus total stress, Figure 73.

Table 15. Steady State Cyclic Swell Coefficients

Test	1	2	3	4
k_s	-0.319	-0.290	-0.351	-0.386

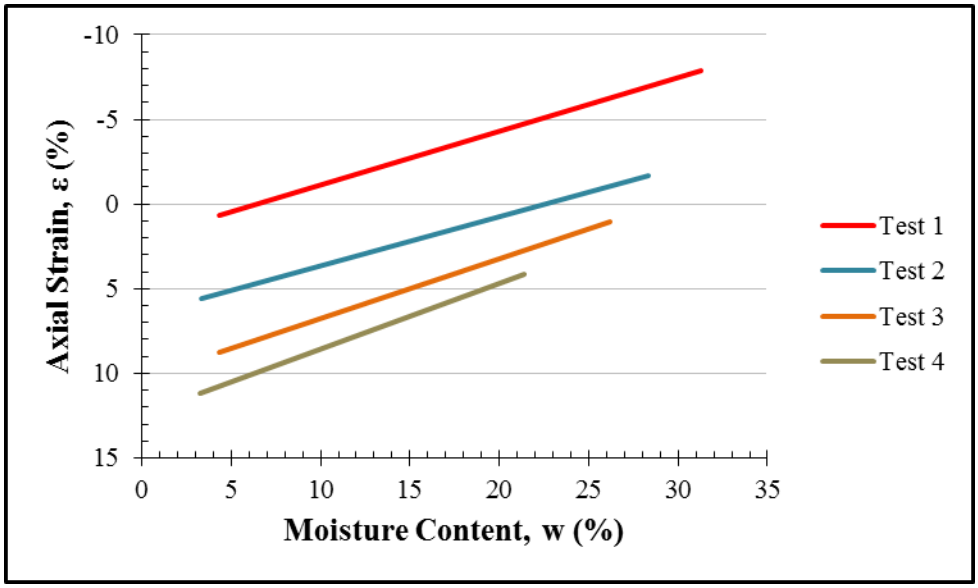

Figure 72. Summary of Steady State Shrink-Swell Behavior

Several observations were made from the results. First, the tedious trimming procedure may inflict varying degrees of disturbance on different samples. Figure 74 summarizes the first swell stage curves from each test. Although each specimen was trimmed from similar samples from the same borehole, there is no clear relationship between the initial swell and total normal stress. It must be noted, however, that the test site's profile of Atterberg limits – and thereby swell potential – is not constant, or even linear. Finally, any interpretation of Figure 74 must recognize that the normal stress applied for Test 1 was considerably lower than any likely in-situ condition.

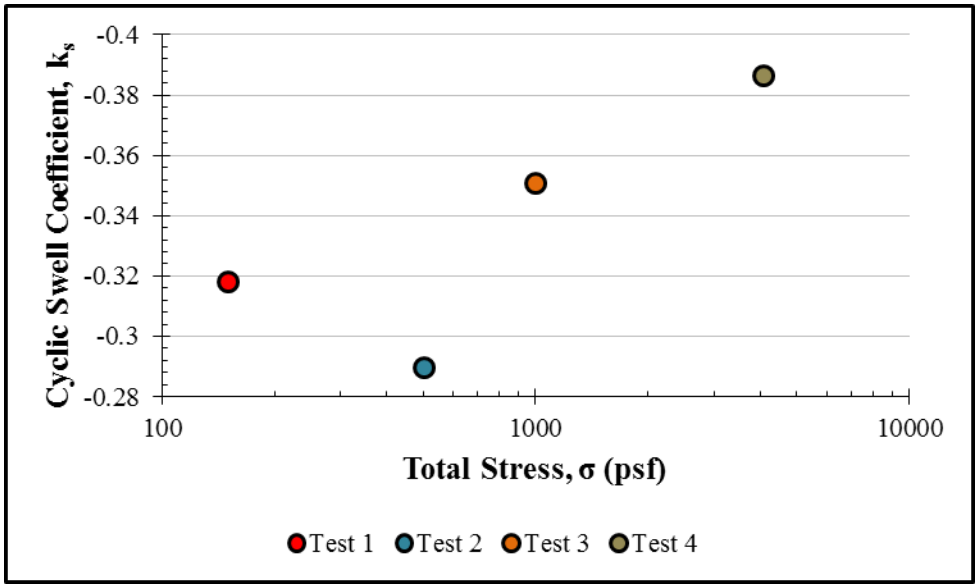

Figure 73. Simplified Constitutive Surface

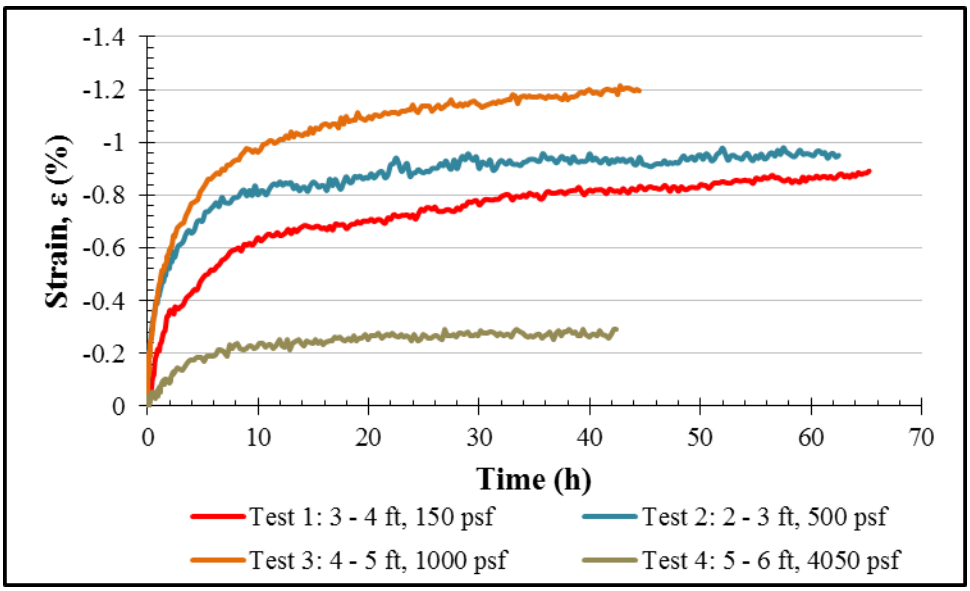

Figure 74. Summary of Initial Swell Stage Curves

The results generally became more reasonable after the first cycle, once the specimens had been remolded by drying and rewetting. In general, the specimens swelled to progressively higher magnitude strains through successive cycles. This seems to indicate that cycles of drying and rewetting break down the soil's crumb structure, unlocking more and more swell potential.

Each test's total normal stress also had a noticeable effect on the results. As the total stress is increased, the soil reaches a smaller range of moisture contents. The lower bound, analogous to the shrinkage limit, remained fairly constant through the different stress levels. The upper bound for moisture content was more strongly affected, with the relatively lightly loaded specimens reaching significantly higher moisture contents.

Although the range of moisture contents was lower for higher total stresses, the cyclic swell coefficient (k_s) was higher. That is, for a given change in moisture content at the steady state, larger swelling strains occurred under higher total stress conditions. The caveat to this observation is that the steady state coefficients of consolidation decrease with increasing total stress, Figure 75.

Ultimately, the total stress level did affect the maximum magnitude of steady state strains. Lightly loaded specimens achieved larger swelling strains through successive swell cycles, while the more heavily loaded specimens contracted from cycle to cycle. These cycle-to-cycle changes in strain appeared to have the most significant effect on steady state behavior.

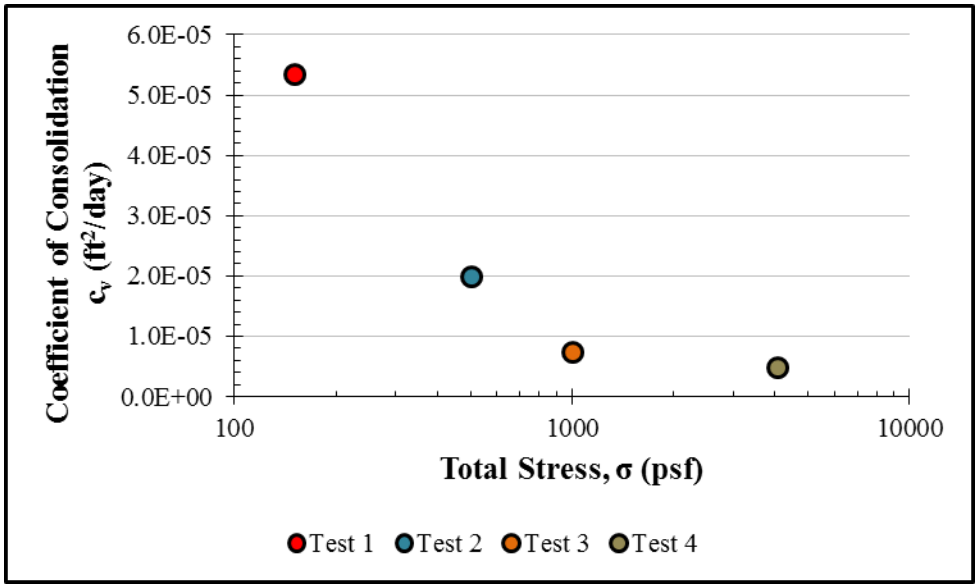

Figure 75. Cyclic Swell Steady State Coefficients of Consolidation

5.4 Undrained Shear Strength

The undrained shear strength was evaluated in the laboratory with unconsolidated undrained (UU) triaxial compression tests that were run in accordance with ASTM D2850. The UU triaxial tests were run in the University of Texas and the Fugro Consultants, Inc. laboratories. The tests indicate that the undrained shear strength increases with depth, but also that the soil's secondary structure facilitates the development of shear displacements before shear planes have developed in the intact soil. This characteristic manifested as abrupt decreases in the deviator stress during testing which caused the software to terminate the test.

The first two tests – illustrated with dashed lines in Figures 76 and 77 – were conducted on specimens trimmed to diameters of 1.4 inches at the University of Texas. The trimming was intended to remove soil that was disturbed during sampling, but instead appeared to cause visible structural damage to the final soil specimen. The other five tests were conducted on 2.8-inch diameter specimens at the Fugro Consultants, Inc. laboratory in Austin. The samples' ends were trimmed square and flush for this round of tests, but the diameters were not trimmed. Further details of each test are included in Appendix G.

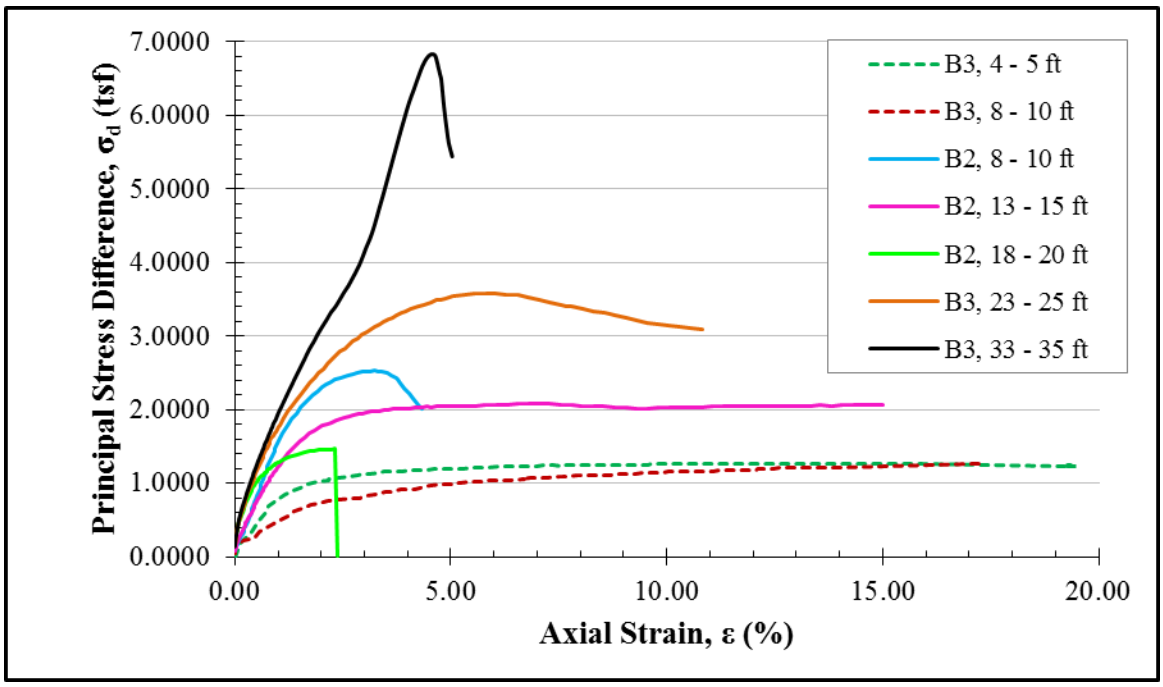

Figure 76. Summary of UU Triaxial Stress-Strain Measurements

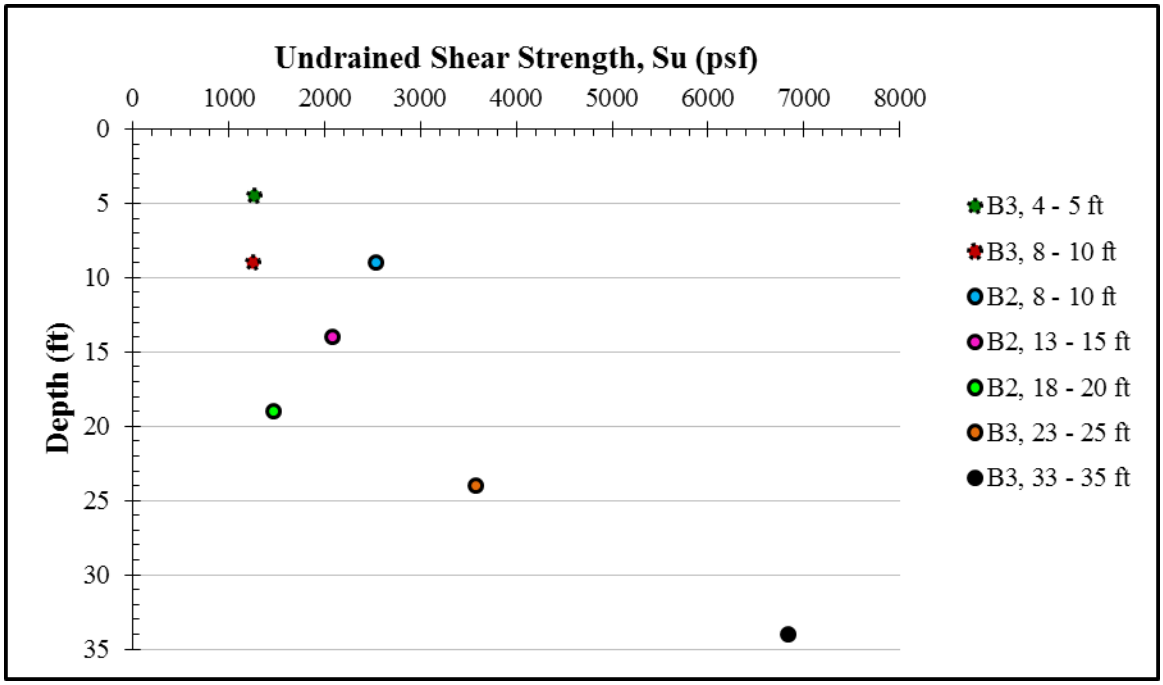

Figure 77. UU Triaxial Strength Profile

5.5 Drained Shear Strength

5.5.1 Testing Procedure

A series of consolidated drained direct shear tests were conducted to evaluate the peak and residual drained failure envelopes. The tests were performed in accordance with ASTM D 3080 at normal stresses equal to one, two and four times the estimated in-situ vertical effective stress. It was difficult to predict an appropriate shear rate due to the soil's ambiguous time-settlement characteristics. In an effort to both shear the soil slowly enough for pore pressures to dissipate and to conduct the tests over a practical and repeatable period of time, each test was set up to shear through a distance of 0.5 inches over a period of 4 days. The corresponding shear rate is 0.000087 in/min.

All three specimens were trimmed from a single undisturbed seamless push-tube sample. The specimens were trimmed into a 2.5-inch ring and then extruded directly into the top half of the shear box. The ends were then trimmed to flush 90-degree angles using the top half of the shear box as a guide. Once trimmed, the two halves of the shear box were connected with clamping screws, and the specimen was seated against the bottom porous stone.

Each test consisted of one peak shear stage and a series of residual shear stages. The soil was consolidated to the appropriate normal stress prior to each shear stage. Each consolidation stage comprised roughly 10 minutes of dry consolidation to close fissures and microcracks followed by one to two days of inundated consolidation under the same normal load. Clamping screws were always used to align the shear box during

consolidation and removed immediately prior to recording zero values for the subsequent shearing stage.

Each specimen's residual drained strength was measured under at least two different normal stresses. Two residual shear stages were performed at the same normal stress that was used for the initial peak shear, then additional residual shear stages were performed at two and/or four times that load. The weight of the specimen was measured immediately following each shear stage and after smoothing the shear surface. After the final shear stage, the specimens were removed from the shear box and oven dried.

The shear surface was smoothed with a putty knife prior to each residual strength measurement. If large lumps or other discontinuities formed during the peak shear stage, they were preserved when smoothing the shear surface for the first residual shear stage, Figure 78. Then, for all subsequent shear stages, the shear surface was both flattened and smoothed, Figure 79. Note that only Test 1 developed a pronounced lump during the peak shear stage.

Figure 78. Lumped Shear Surface Smoothed for Residual Shear

Figure 79. Flattened Shear Surface Smoothed for Residual Shear

5.5.2 Summary of Results

Peak and residual drained strength envelopes were defined from the test data and are presented in Figure 80. The envelope for drained peak strength is curved, but at least one additional data point would be needed at a lower normal stress to define the curve with confidence. The friction angle and cohesion intercept values for both envelopes are reported in Table 16.

The parameters for peak strength are only applicable to the normal stresses – one, two and four times the in-situ vertical effective stress – that were tested. The residual envelope, though it contains some scatter, is more linear and may be more readily extrapolated. The stress-displacement curves for each test are presented in Figures 81 - 83. Photographs and moisture contents from each shear stage are given in Appendix H.

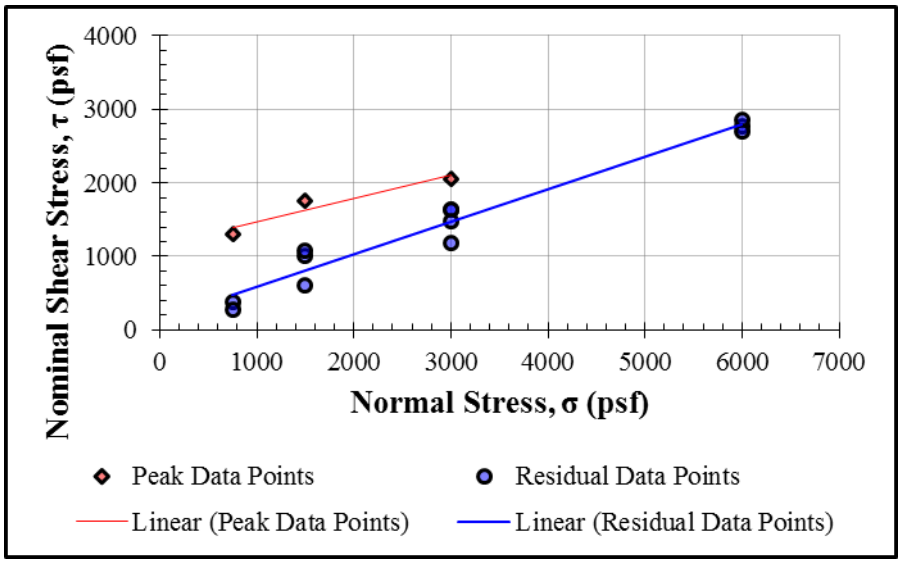

Figure 80. Drained Failure Envelopes from Direct Shear Tests

Table 16. Summary of Drained Failure Envelope Parameters

Envelope	Friction Angle, Φ' (°)	Cohesion Intercept, c' (psf)	Stress Range (psf)
Peak	17.7	1150	750 - 3000
Residual	24.0	135	750 - 6000

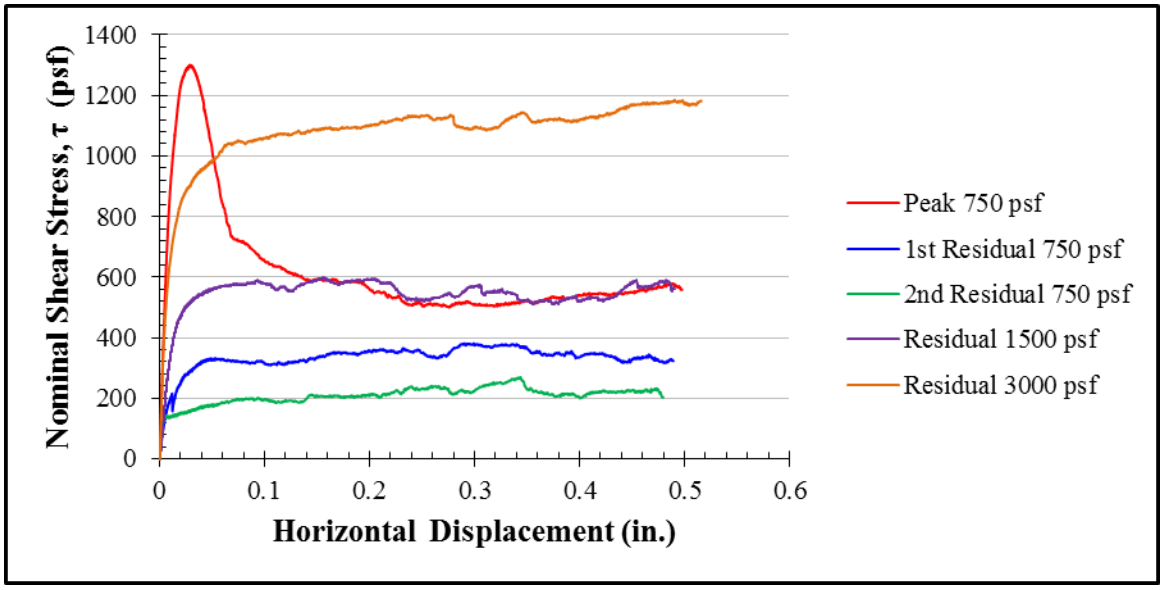

Figure 81. Stress-Displacement Curves from Direct Shear Test #1

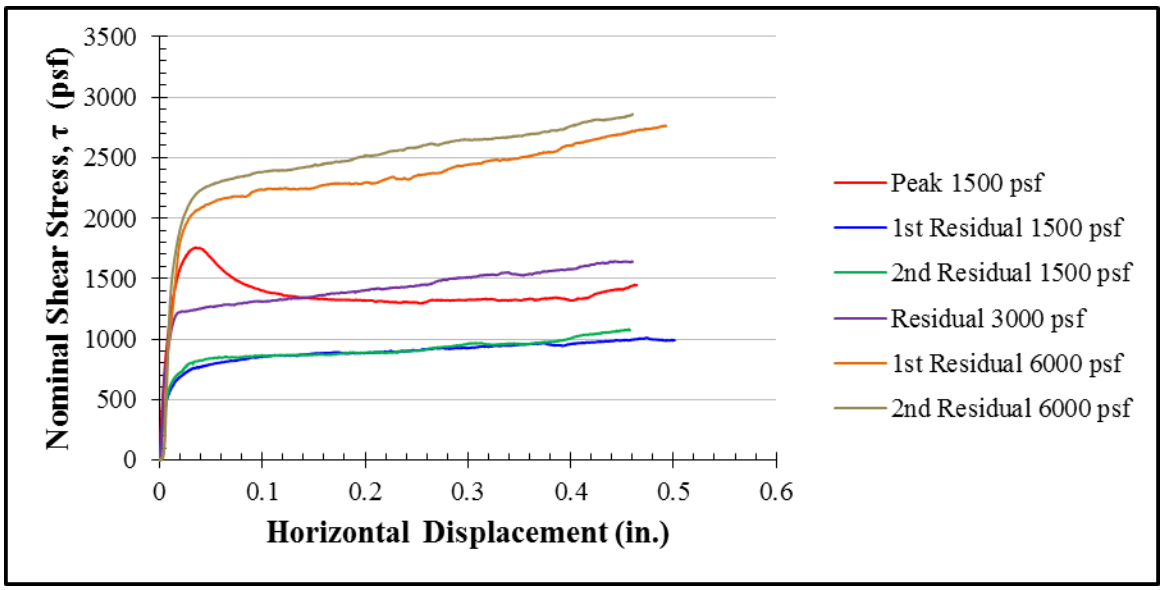

Figure 82. Stress-Displacement Curves from Direct Shear Test #2

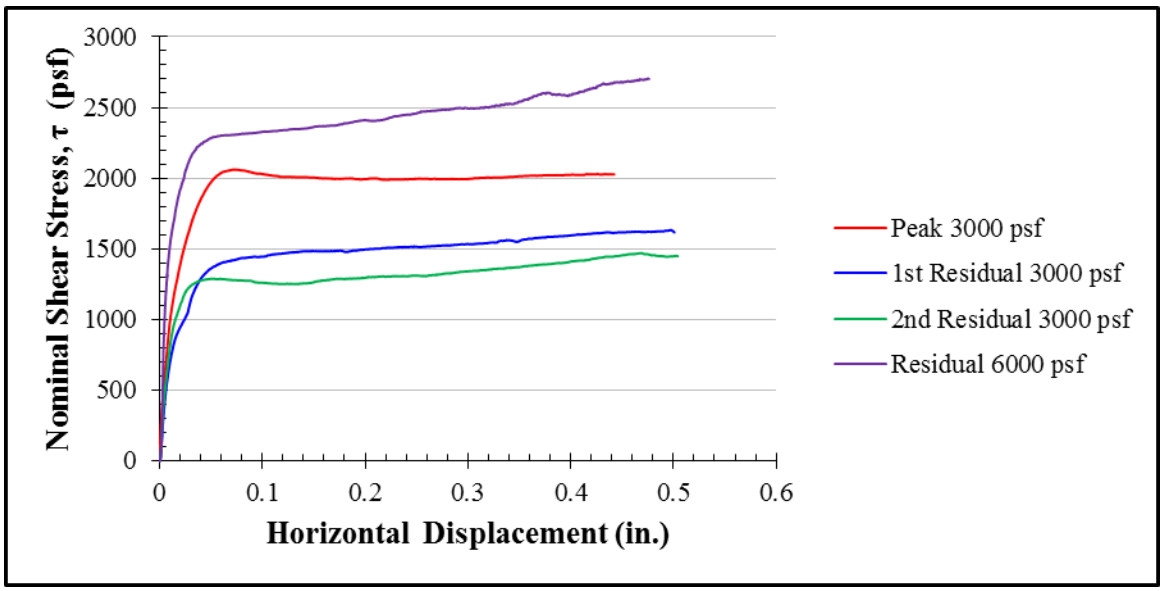

Figure 83. Stress-Displacement Curves from Direct Shear Test #3

6 Comprehensive Analysis of the Taylor Clay

6.1 Soil Classification

The soil is classified in the United Soil Classification System (USCS) in accordance with ASTM D 2487. Figure 84 shows that the Atterberg limits plot well above the A-line, indicating substantial plasticity. For every depth that clay fractions were measured, the soil classifies as fat clay (CH).

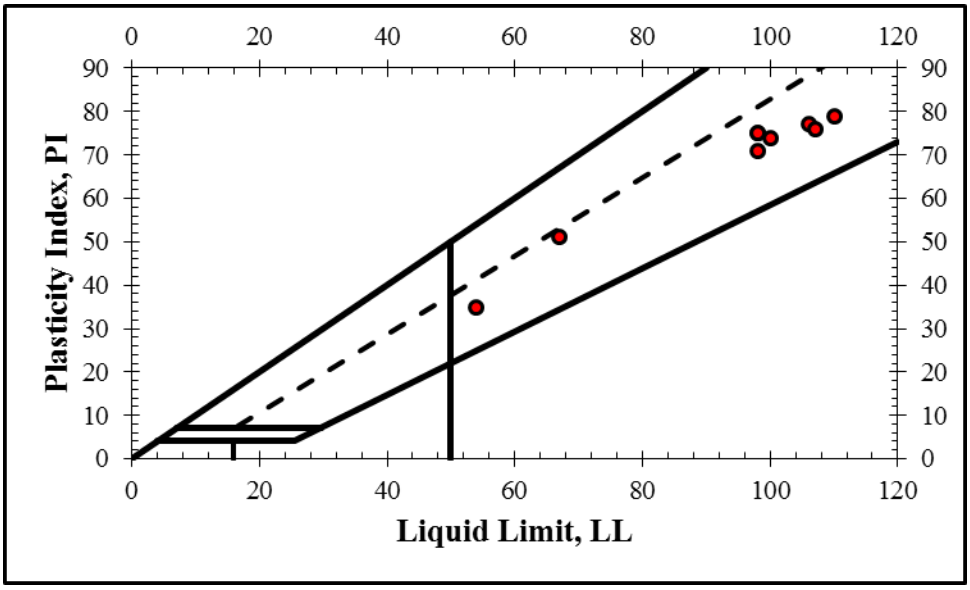

Figure 84. USCS Plasticity Chart

Geologic maps from Burford (1928) and Tipple (1975) suggest that the site is very near the Taylor-Navarro contact. The presence of Exogyra ponderosa at shallow depths suggests that the site is on the Taylor side of the contact. The lack of an observed

contact – one that, according to Young (1965), would be conspicuous – confirms that the soils for this study are indeed from the Taylor group. More specifically, they are from the top of the Bergstrom Formation. Burford described this specific zone of soil as highly bentonitic, indicating very high montmorillonite content.

6.2 Identifying the Active Zone

The active zone is the depth through which seasonal moisture fluctuations are observed (Nelson and Miller, 1992). Multiple measurements confirmed substantial changes in moisture content through the first five feet, but very limited samples were available for deeper moisture measurements. The moisture contents from two sets of samples that were retrieved 9 months apart from each other appear to converge between depths of 8.5 and 13.5 feet. Based on the observation, the active zone may only be cautiously estimated as approximately 10 feet deep.

6.3 Delineation of Strata

The subsurface conditions are best described as two dominant strata separated by a thin transitional zone. The top stratum is an 8-foot thick layer of dark brownish gray, highly weathered clay. This top layer proved sticky and unworkable when wet, but quickly dried upon exposure to become a dusty rock-like material.

At a depth of roughly 8 feet, the top layer begins to lighten to a tannish yellow color. Specimens trimmed from this depth contained small pockets of a white chalky material. As the color became more yellow, the soil structure also became stiffer and

more rock-like. The secondary structure became more pronounced around this depth. This transition stratum is difficult to delineate, but is approximately two feet thick. This zone more than likely marks the historical range of groundwater level. The yellow color still indicates that iron within the clay has been oxidized.

Below a depth of 10 feet, the soil becomes very stiff and the color remains tannish, eventually transitioning to a darker brown. Chalky deposits become less frequent with depth. Upon exposure and drying, the soil from this layer breaks down into small gravel-size crumbs. The primary structure of this layer is very strong and resistant to shear. In handling the soil, it was clear that shear displacements could only be achieved along existing fissures and micro-cracks.

6.4 Compressibility

This particular soil's compressibility is a relatively elusive parameter to characterize. The results from one-dimensional consolidation tests, which were presented in Section 5.2, did not always indicate a clear transition from over- to normally-consolidated behavior. More often, as Long (1983) reported, the e-log-P curves are too rounded to identify a maximum previous vertical effective stress. Even with load increments applied up to 64,000 psf, some of the e-log-P' curves only appear to approach linear virgin compression. The application of large, approximately in-situ, dry seating loads resulted in a clearer transition to normally consolidated compression in Tests 3 – 5.

Although the e-log-P' curves for tests 3 – 5 appear to reveal a transition to normally consolidated behavior, the resulting compressibility parameters are not

consistent with historical trends. Terzaghi and Peck (1948) reported that liquid limits correlate well with compression indices (c_c) with a relationship defined by Equation 10. The results from Tests 3 – 5 are plotted against this relationship in Figure 85, showing no agreement at all. Although the correlation was developed for normally consolidated soils, some general agreement would have been expected. Furthermore, the ratio of compression to recompression indices (c_c/c_r) usually falls between 5 and 10. The measured ratios vary outside of this range, rather consistently, between 2 and 3. It is worth noting that the measured recompression indices from Tests 3 – 5 are in agreement with those reported by Long (1983).

$$c_c = 0.009 \cdot (LL - 10) \quad \text{..... Eq. 10}$$

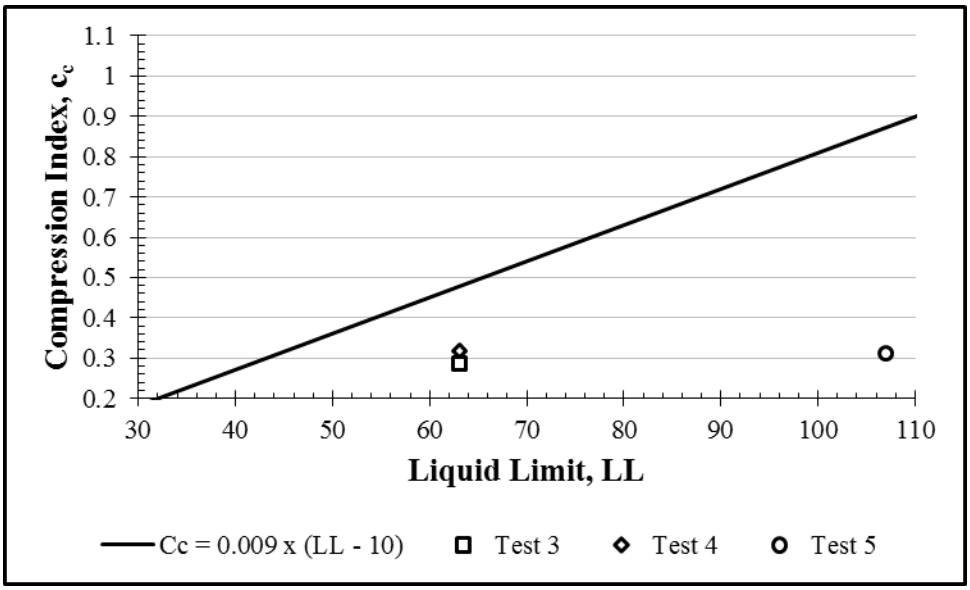

Figure 85. Measured vs. Expected c_c vs. LL Values

The disparity between measured and expected compression characteristics may be explained by several factors. The soil could be so heavily overconsolidated that higher loads would be required to actually observe normally consolidated behavior. Carbonates are known to be present throughout the Taylor clays, and some degree of cementation could have taken place within the clay. Finally, although the specimens were carefully trimmed for each test, sampling by seamless push tube could have caused a significant amount of disturbance. Any or all of these factors could explain the erratic compressibilities that were observed in the laboratory.

6.5 Shear Strength

The soil's undrained shear strength was evaluated in the lab and the field. Results from the different tests agree well, but the undrained shear strength does not exhibit a typical linear increase with depth. Instead, the increase is nearly bilinear, as illustrated by the heavy dashed curve in Figure 86. The undrained shear strength at the surface is approximately 1200 psf. The c/P' ratios for the shallow ($\psi_{shallow}$) and deep (ψ_{deep}) linear segments are 0.23 and 4.34, respectively. Oddly enough, the values for $\psi_{shallow}$ and ψ_{deep} are exact inverses of one another. The bilinear undrained shear strength profile is very similar to that reported by Long (1983).

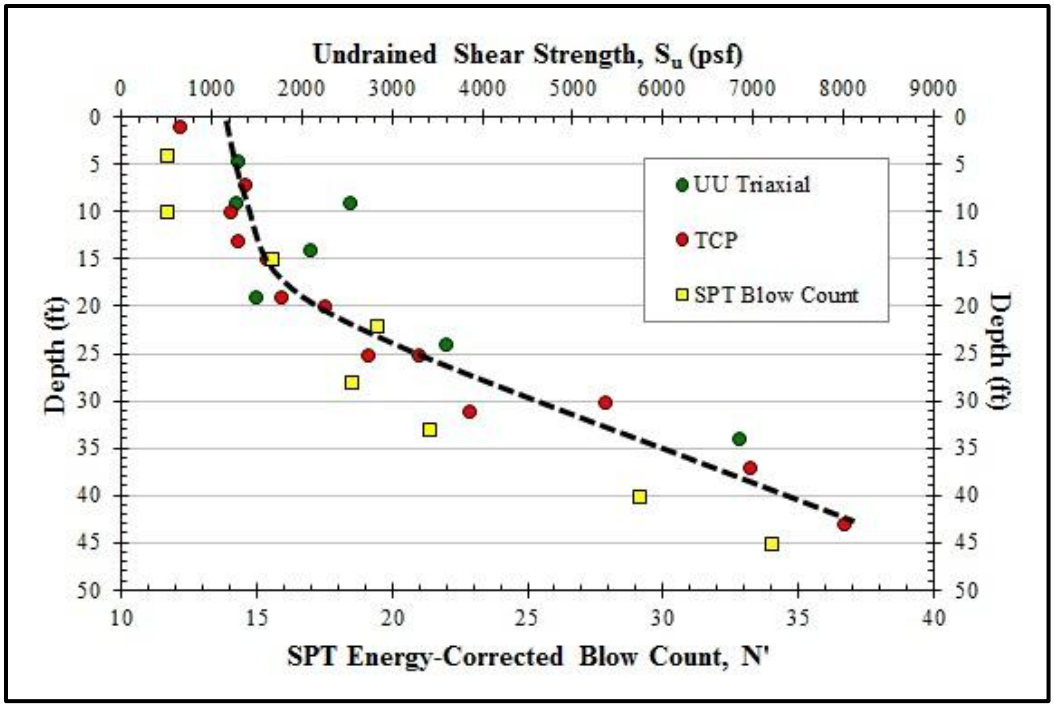

Figure 86. Combined Test Results for Undrained Shear Strength

Both peak and residual drained failure envelopes were constructed from the results of direct shear tests. The soil's peak envelope is curved concave downwards, and its cohesion intercept is not readily discernible from the limited number of measured data points. The secant friction angles for each data point on the peak envelope are shown in Figure 87. The secant friction angles are also illustrated for the stress levels that were tested for residual shear in Figure 88, although there is much less variation for the secant friction angles for the residual envelope. Figure 88 shows the range of secant friction angles corresponding to the range in residual strength data points at each normal stress. In each case, the secant friction angles are much higher than usual.

Stark and Eid (1994, 1997) presented design charts to help characterize the curved failure envelopes that are common for drained conditions with stiff fissured clays. The authors essentially provided a set of curves that relate liquid limit and clay fraction to a soil's secant friction angle at various normal stresses. By interpolating between curves that pertain to specific normal stresses, a soil's curved failure envelope can be predicted in terms of its liquid limit and clay fraction. One chart was developed for fully softened peak envelopes (Figure 89) and another for residual envelopes (Figure 90).

The measured secant angles do not fit the expected range for either peak or residual data points. It is not immediately clear why the data deviates so much from the trend, but there are several possibilities. Stark's range was generated with normally consolidated specimens. The soil being tested in this study is heavily overconsolidated. In addition, it could be cemented. The individual test results – that is, stress-displacement curves – are reasonable, but the soil itself appears stronger than typical clays.

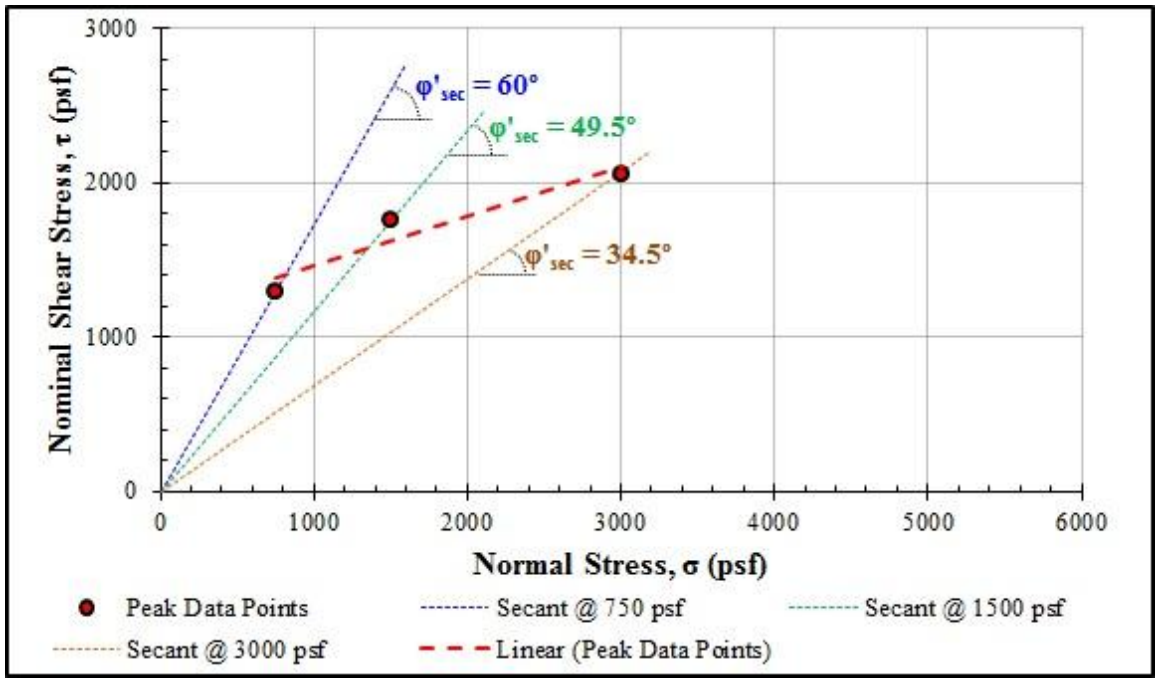

Figure 87. Secant Friction Angles for Peak Drained Strengths

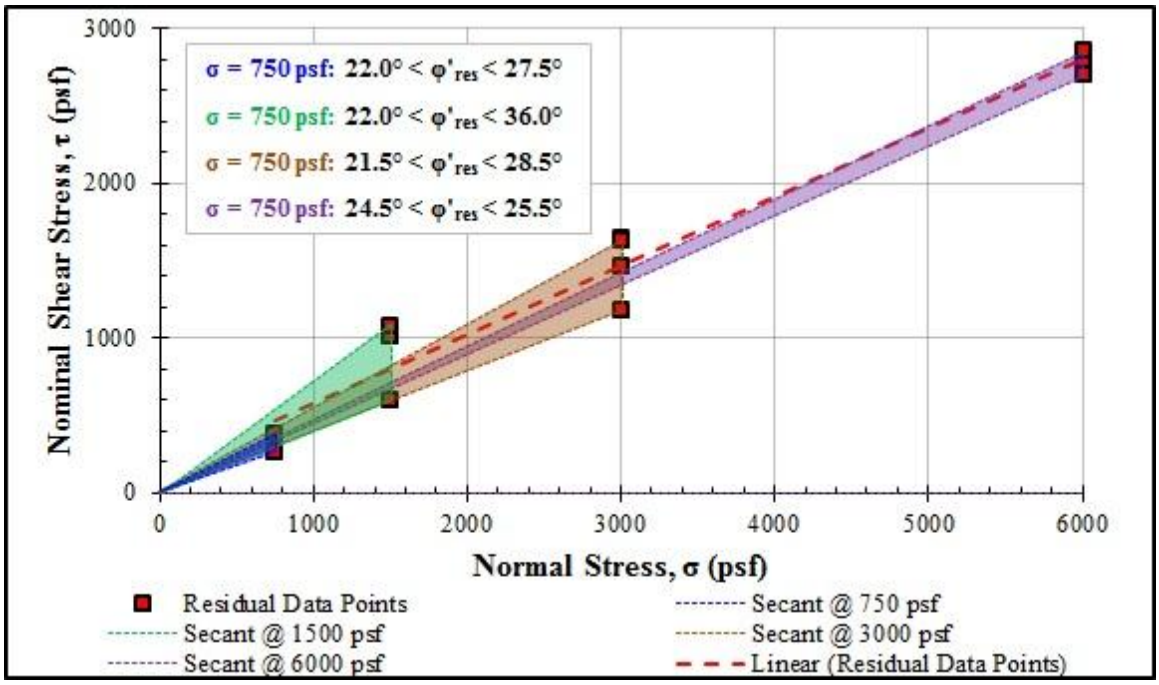

Figure 88. Secant Friction Angles for Residual Drained Strengths

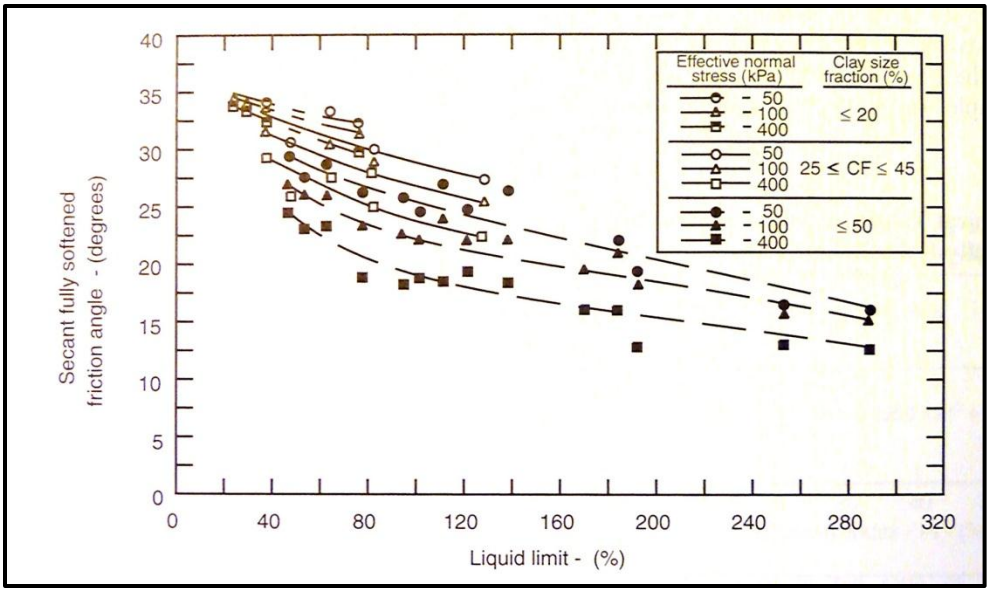

Figure 89. Correlation between Liquid Limit, Clay Fraction and Secant Peak Friction Angle, Stark & Eid (1997)

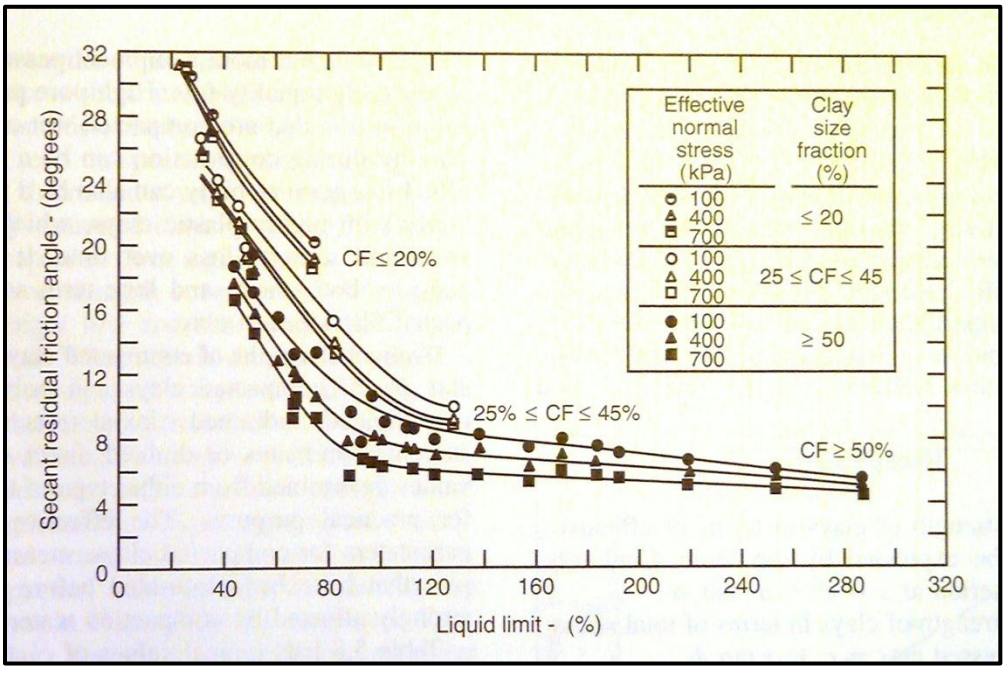

Figure 90. Correlation between Liquid Limit, Clay Fraction and Secant Residual Friction Angle, Stark & Eid (1994)

6.6 Hydraulic Conductivity

Time-settlement curves from consolidation and swell tests provided a means to back out the soil's hydraulic conductivity using a modified application of the theory of consolidation in which total settlements were considered. The method is described in Section 5.2.1. Results from all tests indicate the soil's hydraulic conductivity is approximately 5×10^{-9} ft/day. These results are indicative of the soil's primary, dense clay structure.

The soil contains a complicated network of fissures and microcracks that may act as preferential moisture pathways. In addition, wide dessication cracks form when the soil dries. These cracks play a significant role in the transport of water, as shown in Figure 91. The figure shows five moisture profiles that were measured in the same area. M-2 was measured after a long period of dry weather, and the other four profiles were measured 24 hours after the first major precipitation that interrupted that dry period. The inflections of the four profiles that were measured after the rainfall estimate the points of the water's downward progress after 24 hours, and thereby estimate the hydraulic conductivity.

The two sets of measurements are drastically different. The observational tests suggest hydraulic conductivities between 1 and 2 ft/day. The two estimates of hydraulic conductivity vary by 10 orders of magnitude. The two different types of tests may represent bounding parameters for the soil's actual hydraulic conductivity. The lab tests failed to model the presence of preferential moisture pathways, while the observational field tests exploited such pathways.

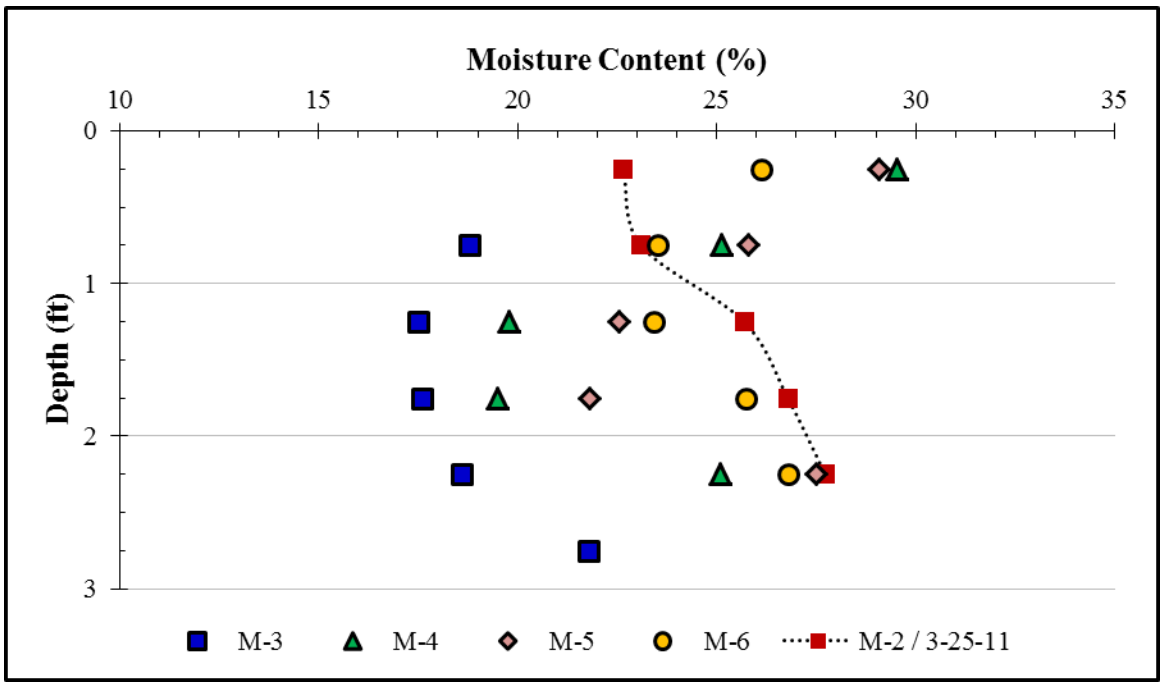

Figure 91. Observational Field Measurements for Hydraulic Conductivity

6.7 Swell Potential

According to index properties, the soil's swell potential is "very high". Table 17 summarizes a profile of representative soil properties for the empirical swell guidelines. The plasticity indices are much larger than necessary for a very high swelling potential classification. The soil's colloidal activity (A_c) values average around 1.1, which is considered normal and indicative of calcium montmorillonite. According to Seed's chart that relates swell potential to activity and clay content, the soil exhibits very high swell potential, Figure 92. The chart by Daksanamurthy and Raman, relating swell potential to LL and PI, gives the same designation, Figure 93. Overall, the soil's characteristics meet or exceed the empirical guidelines for a "very high swell potential" classification.

Table 17. Representative Index Properties

Depth	Liquid Limit, LL	Plasticity Index, PI	Clay Fraction, CF (%)	Activity, A_c
7	78	55	51.5	1.1
11	96	80	80	1.0
17	108	79	65	1.2
29	100	72	72	1.0

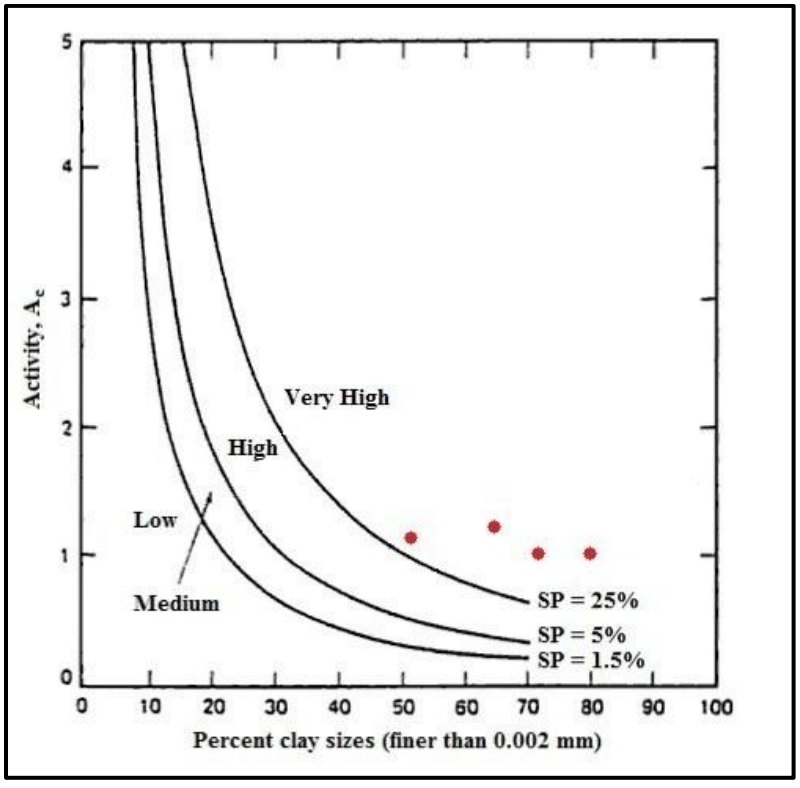

Figure 92. Qualitative Swell Potential, Seed (1962)

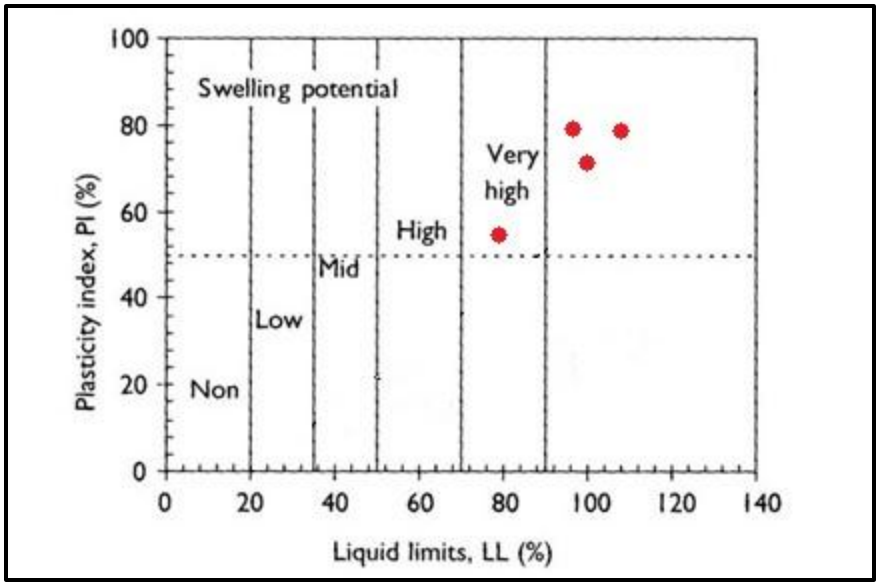

Figure 93. Qualitative Swell Potential, Daksanamurthy and Raman, 1973

Laboratory tests focused on measuring the cyclic swell potential in the lateral direction. Initial swelling from in-situ moisture under a constant total stress generally resulted in approximately 1% axial swelling strains. Under the same total stresses, but through the soil's full range of potential moisture contents, the swelling strains increased to the range of 6 – 8%. It seems that the cycles of wetting and drying progressively unlocked additional surface area from within relatively active crumbs of the soil structure. The magnitudes of swelling strains are similar to those measured by Marr (2003), but the overall behavior is different. The current study found that k_s increased with increasing total stress. That is, for a given change in moisture content, larger strains occurred under larger total stresses. Marr's study showed the opposite trend; that, for a given change in moisture content, higher total stresses resulted in smaller vertical strains.

Vertical swell potential was also inferred from some of the consolidation results. In particular, Tests 4 and 5 were inundated under constant volume conditions to measure the swell pressure. The tests revealed swell pressures of approximately 1200 and 3800 psf at depths of 5 and 15 feet, respectively. This is in agreement with Marr's (2003) measurement of 4200 psf at approximately the same depth in a similar deposit.

7 Conclusions and Recommendations

The Lymon C. Reese Research Wall was installed in the very top portion of the Bergstrom Formation, the upper member of the Taylor Group. The soil profile consists chiefly of three dominant zones:

- The top stratum is approximately 8 feet thick. The soil is dark brownish gray and highly weathered. The primary clay mineral is montmorillonite, and the swell potential is very high. The soil is stiff, fissured and very sticky when wet.
- A transitional zone occurs between depths of approximately 8 and 10 feet. The soil lightens to a dull yellow color, and small patches of chalk are present. The soil's secondary structure becomes more pronounced.
- Below 10 feet, the dull yellow color begins to turn a darker brown with depth. The soil becomes very stiff, much like claystone. The secondary structure becomes a dominant feature.

All soils tested in the study were heavily overconsolidated, with overconsolidation ratios no smaller than 9. In some cases it was impossible to distinguish a transition between over- and normally-consolidated stress ranges. The more discernible test results still didn't conform to typical behavior. The soil's undrained strength increases with depth in a typical manner until a depth of approximately 15 feet. Beyond this depth, the strength increases much faster than would be expected for typical soils.

Trimming the soil for laboratory tests was a tedious procedure, and sampling with seamless push tubes may have disturbed the soil to an extent that trimming could not erase. The most repeatable and reasonable test results were obtained from specimens that were subjected to repeated loading or wetting/drying. That is, the residual drained strengths from direct shear tests and the steady state swell condition. It seems that the repeated loading conditions acclimate the soil to its trimmed condition and restore some sense of in-situ conditions.

The cyclic swell tests provided an indication of the upper stratum's lateral swell potential. Swelling from in-situ moisture contents and approximately in-situ stresses resulted in swelling strains in the range of 0.8 – 1.0 percent. A stress smaller than in-situ resulted in 1.2% strain; larger than in-situ resulted in 0.2%. After reaching steady state and swelling from their driest to wettest conditions, the swelling strains for all tests increased to the range of 7 – 8%.

The standard CRS consolidation equipment proved very useful for the cyclic swell tests. The computer-operated load frame may provide an opportunity to automate the test to some degree. One major challenge remains the unloading and reloading of the specimen throughout the test to obtain intermediate moisture contents. Great care is required to keep the soil intact and maintain a continuous set of measurements.

The hydraulic conductivity varied drastically between back-calculated lab measurements and field observations, which corresponded to two very different flow paths. The in-situ hydraulic conductivity probably varies within those bounds, its value depending on depth or confinement and moisture content.

Appendix A: Boring Logs

TERMS AND SYMBOLS USED ON TxDOT BORING LOGS

SOIL TYPES

- CH, Fat Clay
- CL, Lean Clay
- ML, Silt
- Sand
- Gravel
- Fill/Other

ROCK TYPES

- Limestone
- Shale

SOIL GRAIN SIZE

U.S.STANDARD SIEVE

6"	3"	3/4"	4	10	40	200	
BOULDERS	COBBLES	GRAVEL		SAND			SILT / CLAY
		COARSE	FINE	COARSE	MEDIUM	FINE	
152	76.2	19.1	4.76	2.00	0.420	0.074	0.002

SOIL GRAIN SIZE IN MILLIMETERS

STRENGTH OF GRANULAR SOILS (1)

CONSISTENCY	THD Penetrometer (blows/ft or blows/300mm)
Very Loose	0 to 8
Loose	8 to 20
Slightly Compact	20 to 40
Compact	40 to 80
Dense	80 to 5"/100 (125mm/100)
Very Dense	5"/100 to 0"/100 (125mm/100 to 0mm/100)

STRENGTH OF COHESIVE SOILS (1)

DENSITY	THD Penetrometer (blows/ft or blows/300mm)
Very Soft	0 to 8
Soft	8 to 20
Stiff	20 to 40
Very Stiff	40 to 80
Hard	80 to 5"/100 (125mm/100)
Very Hard	5"/100 to 0"/100 (125mm/100 to 0mm/100)

BEDROCK HARDNESS (1)

HARDNESS	THD Penetrometer (blows/ft or blows/300mm)
Very Hard	0" - 2"/100 (0 - 50mm/100)
Hard	1" - 5"/100 (25 - 125mm/100)
Soft	4" - 6"/100 (100 - 150mm/100)

1) TxDOT Geotechnical Manual, Chapter 3 - Soil and Bedrock Classification & Logging (3-15)

ASTM D 2488 TABLE 7 Criteria for Describing Structure

Description	Criteria
Stratified	Alternating layers of varying material or color with layers at least 6 mm thick; note thickness
Laminated	Alternating layers of varying material or color with the layers less than 6mm thick; note thickness
Fissured	Breaks along definite planes of fracture with little resistance to fracturing
Slickensided	Fracture planes appear polished or glossy, sometimes striated
Blocky	Cohesive soil that can be broken down into small angular lumps which resist further breakdown
Lensed	Inclusion of small pockets of different soils, such as small lenses of sand scattered through a mass of clay; note thickness
Homogeneous	Same color and appearance throughout

Criteria for Describing Inclusions

Description	Criteria
Parting	Inclusion <1/8" thick extending through sample
Seam	Inclusion 1/8" to 3" thick extending through sample
Layer	Inclusion >3" thick extending through sample

Terms used in Addtional Remarks on Wincore Logs

Description	Criteria
PP	Pocket Penetration Test (tsf)
SPT	Modified Standard Penetration Test (bpf)
REC	Rock Core Recovery (%)
RQD	Rock Quality Designation, ASTM (D 6032)
Q	Unconsolidated Undrained Triaxial Test (tsf)
U	Unconfined Compression Test (tsf)

DRILLING LOG

	County	Travis	Hole	B-1	District		
WinCore	Highway		Structure	Retaining Wall	Date	1/12/10	
Version 3.1	CSJ	UT Manor Wall Project	Station		Grnd. Elev.	0.00 ft	
			Offset		GW Elev.	-45.70 ft	

Elev. (ft)	LOG	Texas Cone Penetrometer	Strata Description	Triaxial Test: Lateral Press. (psi)	Triaxial Test: Deviator Stress (psi)	Properties: MC	Properties: LL	Properties: PI	Properties: Wet Den. (pcf)	Additional Remarks
		4 (6) 4 (6)	CLAY, soft, dark brown, w/scattered sand and fine gravel. (Residual Soil) (CH)							
-5.5		9 (6) 8 (6)	CLAY, soft to hard, tan and light gray, blocky, calcareous, w/ferrous staining and selenite seams. (Taylor) (CH)							SPT = 12
		8 (6) 8 (6)								SPT = 12
		10 (6) 12 (6)								SPT = 16 w/increasing selenite seams
		19 (6) 22 (6)								SPT = 20
		24 (6) 24 (6)								SPT = 19
		37 (6) 50 (6)								SPT = 22
-39.		50 (6) 50 (6)	CLAYSHALE, low to moderate hardness, dark gray, slightly fissile, w/occasional pyritic seams and nodules. (Taylor)							w/occasional tan seams SPT = 30
										SPT = 35
-47.										

Remarks: Boring was drilled to the 47.0-ft depth using dry drilling techniques. Upon completion of the bor ehole, groundwater recorded at 45.7 ft after a 1.5 hour waiting period. A 2-inch diameter piezometer was set in the borehole with a screened interval of 5.0 to 20.0 ft below ground surface. Standard Penetration Test (SPT) blowcounts were performed using a 170-lb hammer with a 24-inch hammer drop.

Any ground water elevation information provided on this boring log is representative of conditions existing on the day and for the specific location where this information was collected. The actual groundwater elevation may fluctuate due to time, climatic conditions, and/or construction activity.

Driller: Fugro Consultants, Inc. Logger: Fugro Consultants, Inc. Organization: Fugro Consultants, Inc.

M:\GEO\REPORTS\2009\04.30091079 UT Manor Wall Project\UT Manor Wall logs 1-28-10.clg

DRILLING LOG

	County	Travis	Hole	B-2	District		
WinCore	Highway		Structure	Retaining Wall	Date	1/12/10	
Version 3.1	CSJ	UT Manor Wall Project	Station		Grnd. Elev.	0.00 ft	
			Offset		GW Elev.	-29.10 ft	

Elev. (ft)	LOG	Texas Cone Penetrometer	Strata Description	Triaxial Test: Lateral Press. (psi)	Triaxial Test: Deviator Stress (psi)	Properties: MC	LL	PI	Wet Den. (pcf)	Additional Remarks
			CLAY, very stiff to hard, dark gray, w/scattered shell fragments, roots, and fine rounded gravel. (Residual Soil) (CH)							PP = 2.25 PP = 4.5+ PP = 3.5 PP = 3.75
-6.			CLAY, very stiff to hard, tan and light gray, blocky, calcareous, w/ferrous staining and selenite seams. (Taylor) (CH)							PP = 4.5+ PP = 4.5+ PP = 4.0 PP = 2.5 w/increasing selenite seams PP = 4.5+ PP = 4.5+ w/selenite-coated joints at 38 ft
-39.5			CLAYSHALE, low to moderate hardness, dark gray, slightly fissile, w/occasional pyritic seams and nodules. (Taylor)							PP = 4.5+ w/occasional tan seams PP = 4.5+
-50.										

5 10 15 20 25 30 35 40 45 50 55 60

Remarks: Boring was drilled to the 50.0-ft depth using dry drilling techniques and groundwater was recorded at 29.1 ft after a 15 minute waiting period. Upon completion of the borehole, groundwater was recorded at 41.0 ft. A slope inclinometer casing was set in the borehole.

Any ground water elevation information provided on this boring log is representative of conditions existing on the day and for the specific location where this information was collected. The actual groundwater elevation may fluctuate due to time, climatic conditions, and/or construction activity.

Driller: Fugro Consultants, Inc. Logger: Fugro Consultants, Inc. Organization: Fugro Consultants, Inc.

M:\GEO\REPORTS\2009\04.30091079 UT Manor Wall Project\UT Manor Wall logs 1-28-10.clg

DRILLING LOG

	County	Travis	Hole	B-3	District		
WinCore	Highway		Structure	Retaining Wall	Date	1/13/10	
Version 3.1	CSJ	UT Manor Wall Project	Station		Grnd. Elev.	0.00 ft	
			Offset		GW Elev.	-42.50 ft	

Elev. (ft)	LOG	Texas Cone Penetrometer	Strata Description	Triaxial Test: Lateral Press. (psi)	Triaxial Test: Deviator Stress (psi)	Properties: MC LL PI Wet Den. (pcf)	Additional Remarks
0			CLAY, stiff to very stiff, dark gray, w/scattered shell fragments, roots, and fine rounded gravel. (Residual Soil) (CH)				PP = 1.75
5							PP = 1.75 PP = 2.0 PP = 2.0
-6.			CLAY, very stiff to hard, tan and light gray, blocky, calcareous, w/ferrous staining and selenite seams. (Taylor) (CH)				
10		7 (6) 8 (6)					PP = 3.25
15		9 (6) 11 (6)					PP = 2.5
20		13 (6) 15 (6)					PP = 3.5
25		14 (6) 20 (6)					PP = 3.25 w/increasing selenite seams
30		34 (6) 33 (6)					PP = 4.5+
35		50 (6) 50 (4)					PP = 4.5+
40		30 (6) 50 (4.25)					PP = 4.5+
-43.3		50 (2.25) 50 (1.25)	CLAYSHALE, low to moderate hardness, dark gray, slightly fissile, w/occasional pyritic seams and nodules. (Taylor)				PP = 4.5+ w/occasional tan seams
45							PP = 4.5+
-50.3		50 (0.75) 50 (3)					
50							
55							
60							

Remarks: Boring was drilled to the 50.3-ft depth using dry drilling techniques and groundwater was recorded at 42.5 ft after a 15 minute waiting period. Upon completion of the borehole, the boring was backfilled with soil cuttings.

Any ground water elevation information provided on this boring log is representative of conditions existing on the day and for the specific location where this information was collected. The actual groundwater elevation may fluctuate due to time, climatic conditions, and/or construction activity.

Driller: Fugro Consultants, Inc. Logger: Fugro Consultants, Inc. Organization: Fugro Consultants, Inc.

M:\GEO\REPORTS\2009\04.30091079 UT Manor Wall Project\UT Manor Wall logs 1-28-10.clg

Appendix B: Consolidation Test 1

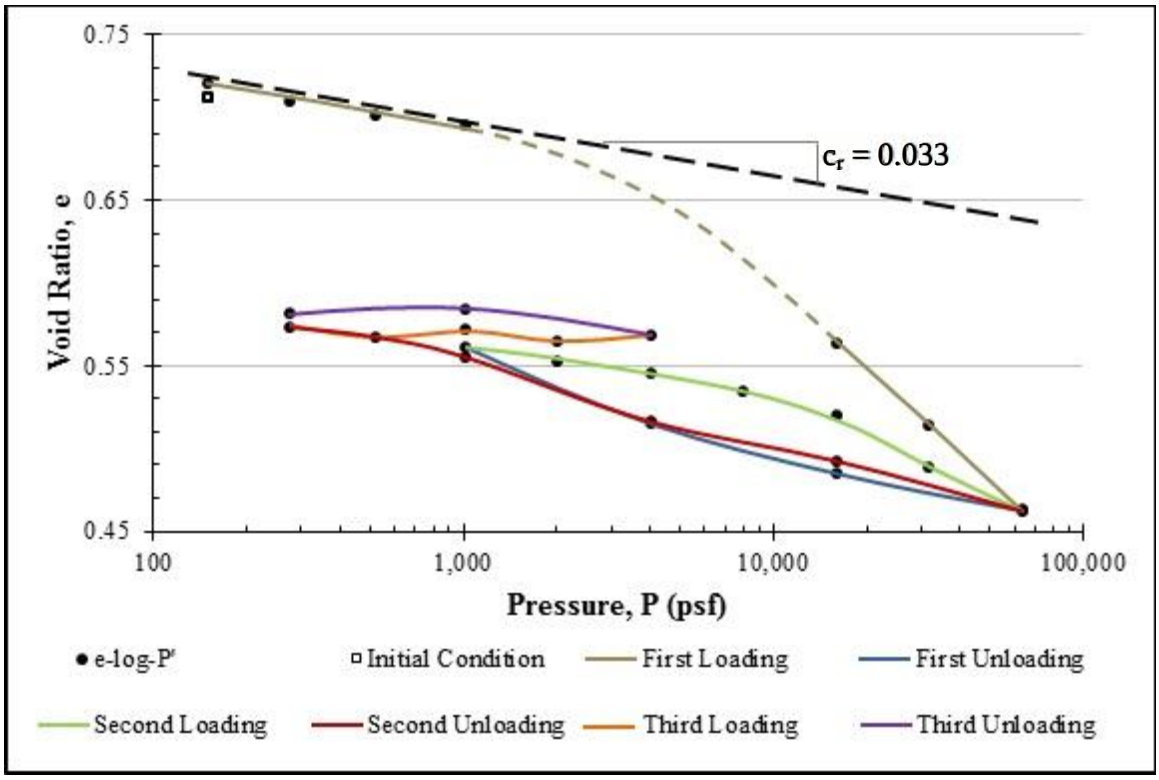

$$c_r = -\frac{e_2 - e_1}{\log(\sigma_2 / \sigma_1)} = -\frac{0.645 - 0.720}{\log(40000/200)} = 0.033$$

$$R_r = \frac{c_r}{1 + e_0} = \frac{0.033}{1 + 0.7117} = 0.019$$

Inundation:125 psf				
S_0 (in.)	S_{100} (in.)	c_v (in^2/min)	k (ft/day)	t_{50} (min)
0.0002	-0.0037	0.00025	6.5 x 10^{-8}	110

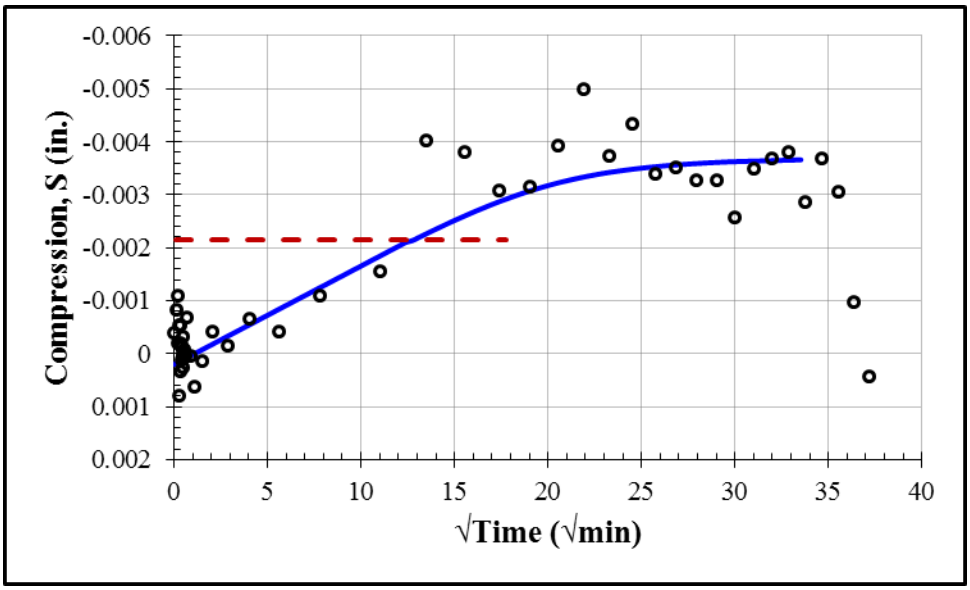

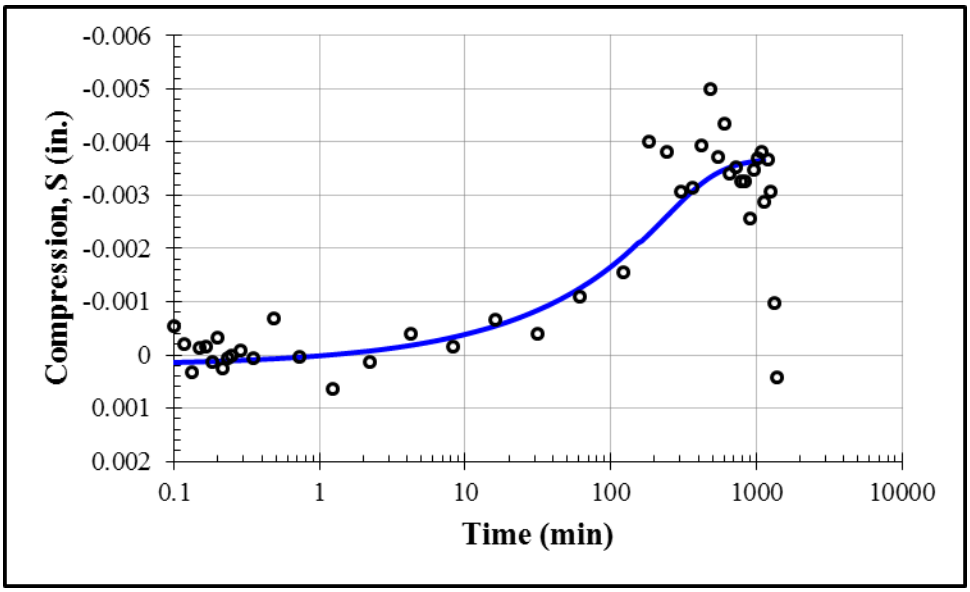

First Loading: 250 psf				
S_0 (in.)	S_{100} (in.)	c_v (in^2/min)	k (ft/day)	t_{50} (min)
0.0003	0.0022	0.00025	3.2 x 10^{-8}	110

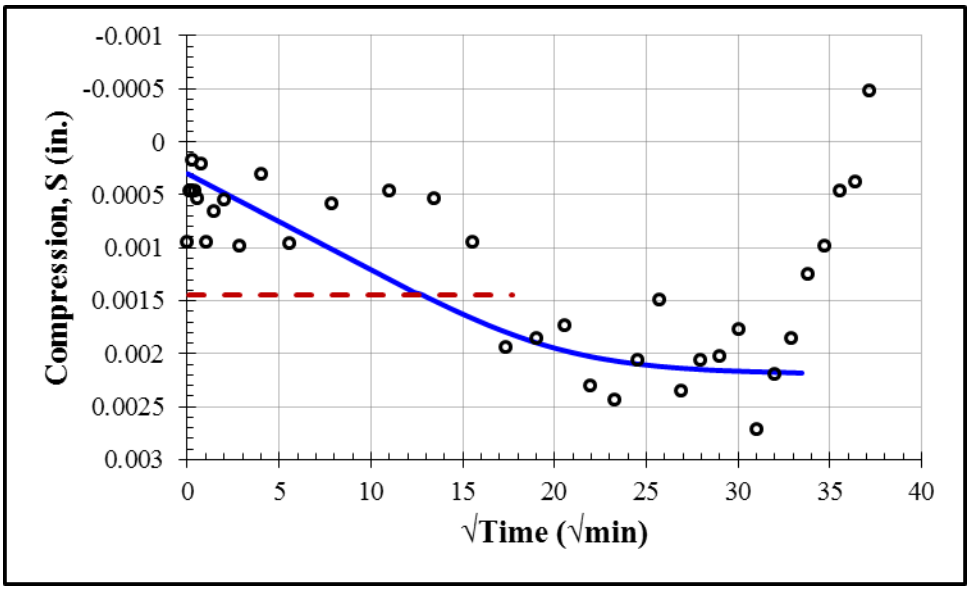

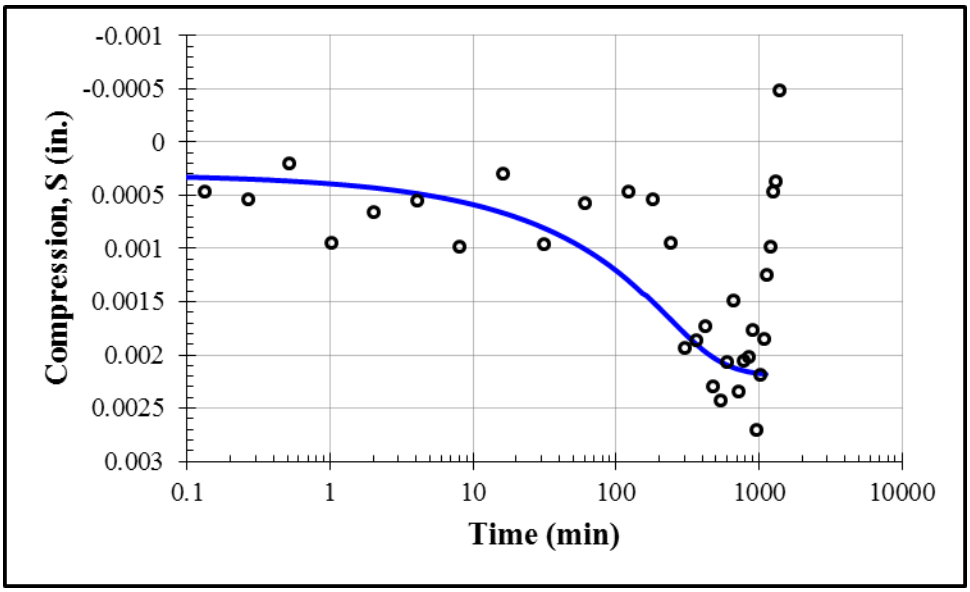

First Loading: 500 psf				
S_0 (in.)	S_{100} (in.)	c_v (in^2/min)	k (ft/day)	t_{50} (min)
0.0000	0.0065	0.0002	4.3×10^{-8}	138

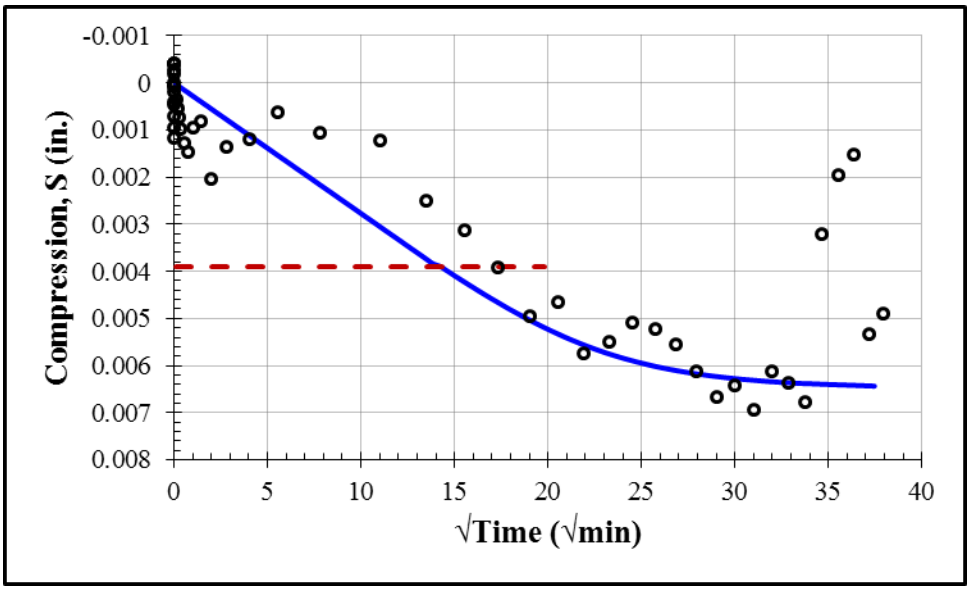

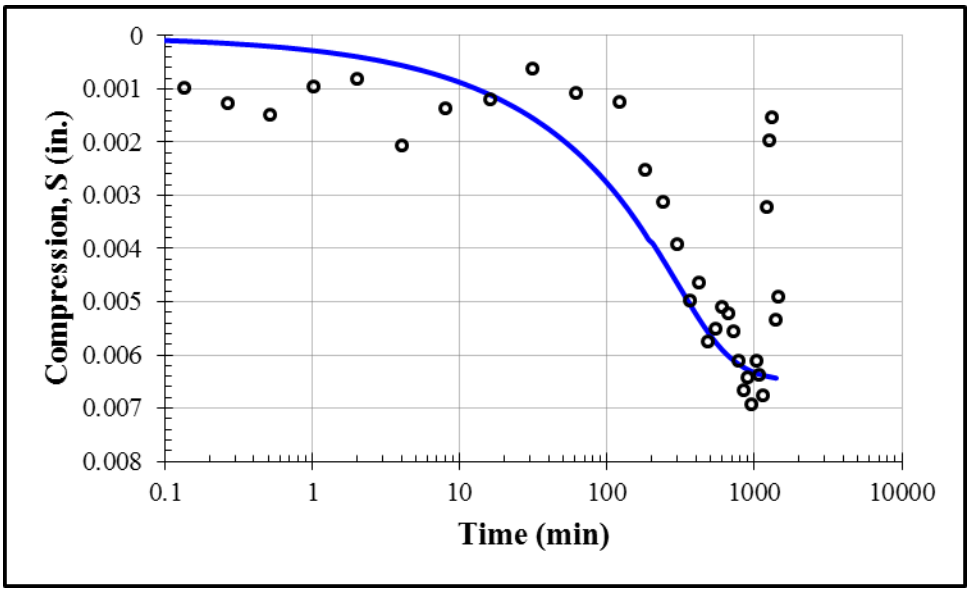

First Loading: 1000 psf				
S_0 (in.)	S_{100} (in.)	c_v (in^2/min)	k (ft/day)	t_{50} (min)
0.0075	0.0109	0.0002	1.1 x 10^{-8}	135

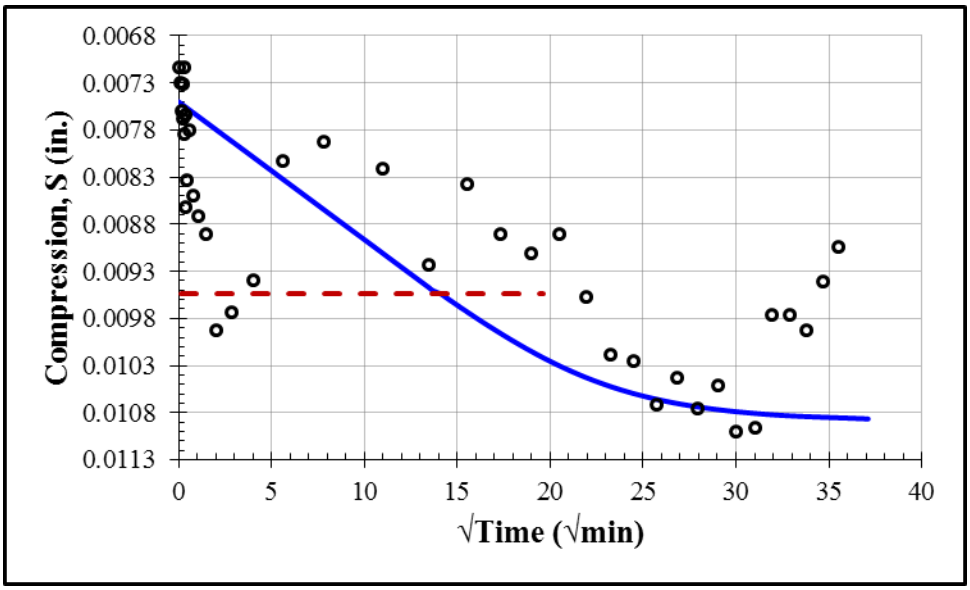

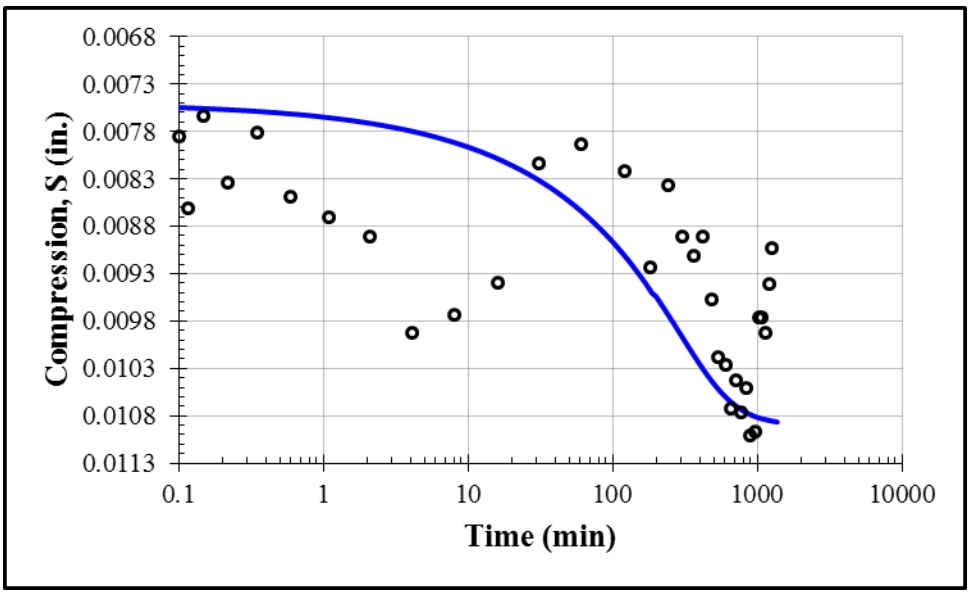

First Loading: 16000 psf				
S_0 (in.)	S_{100} (in.)	c_v (in^2/min)	k (ft/day)	t_{50} (min)
0.0555	0.0730	0.00015	1.4×10^{-9}	159

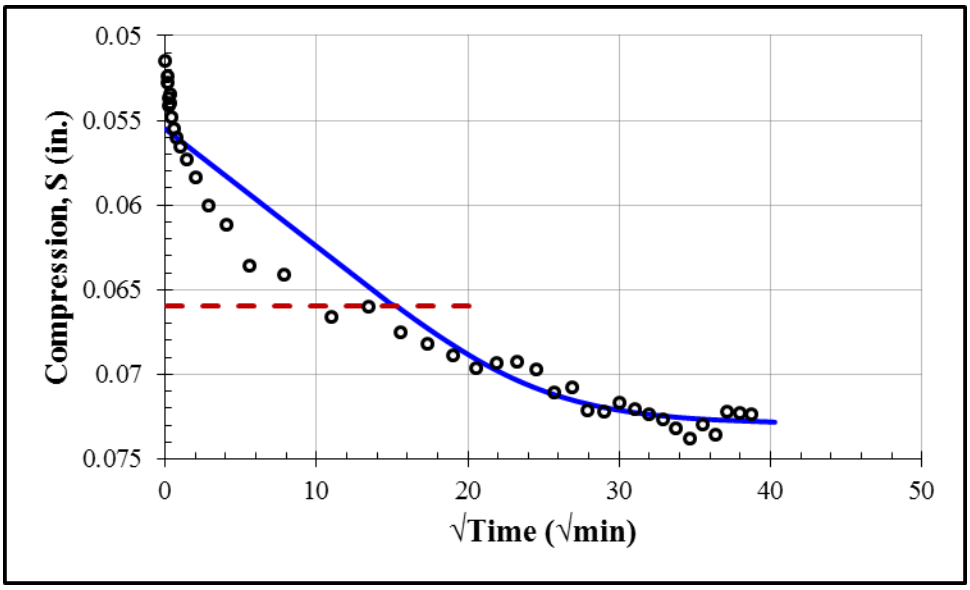

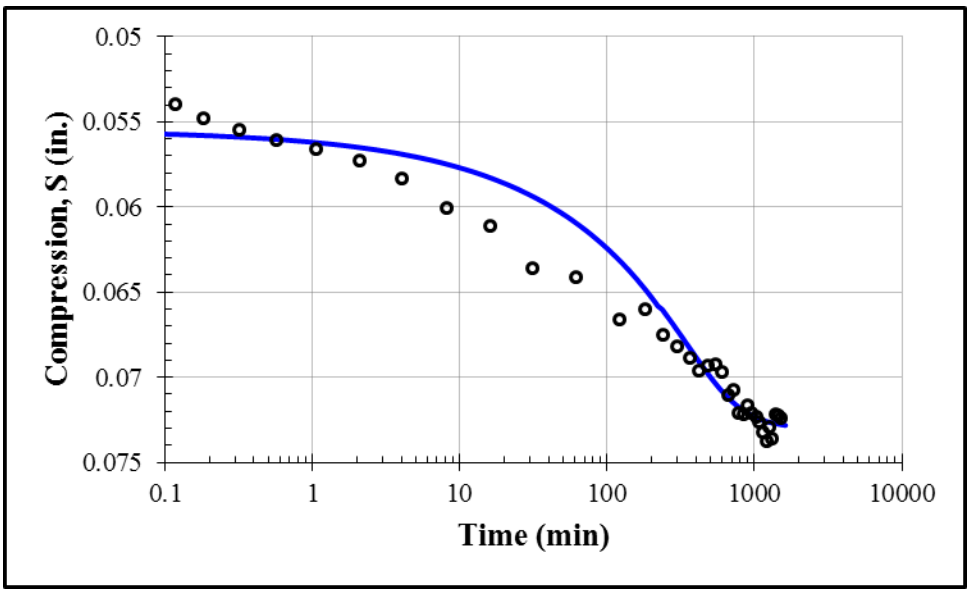

First Loading: 32000 psf				
S_0 (in.)	S_{100} (in.)	c_v (in^2/min)	k (ft/day)	t_{50} (min)
0.0785	0.0977	0.00015	1.4×10^{-9}	148

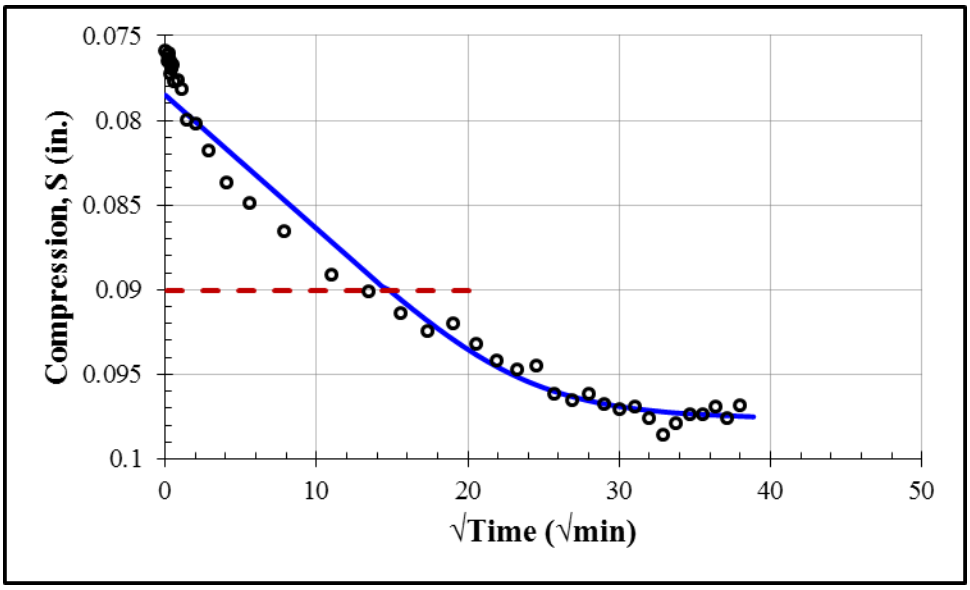

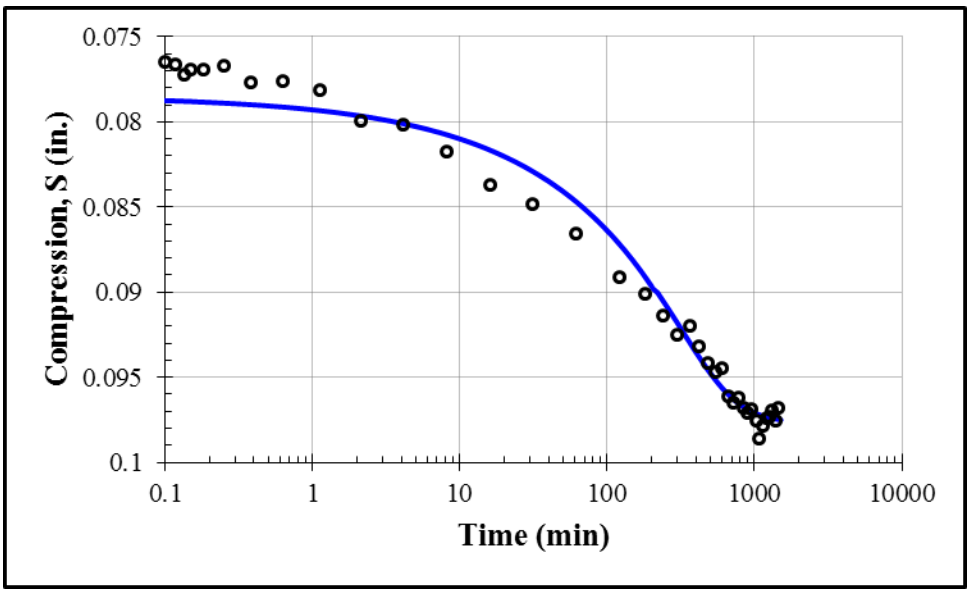

First Loading: 64000 psf				
S_0 (in.)	S_{100} (in.)	c_v (in^2/min)	k (ft/day)	t_{50} (min)
0.1030	0.1236	0.00018	8.7×10^{-10}	114

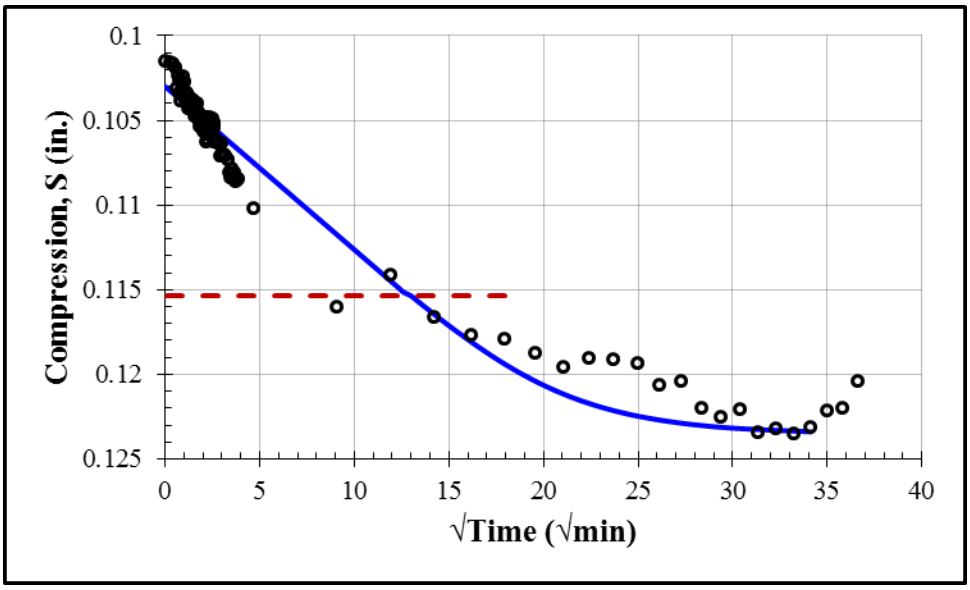

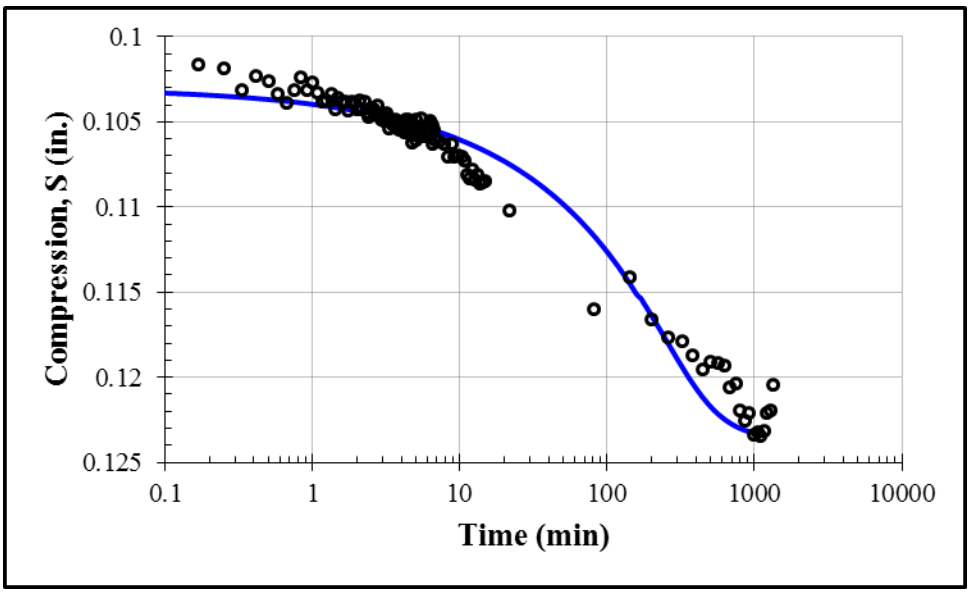

First Unloading: 16000 psf				
S_0 (in.)	S_{100} (in.)	c_v (in^2/min)	k (ft/day)	t_{50} (min)
0.1145	0.1089	0.00034	3.0×10^{-10}	58

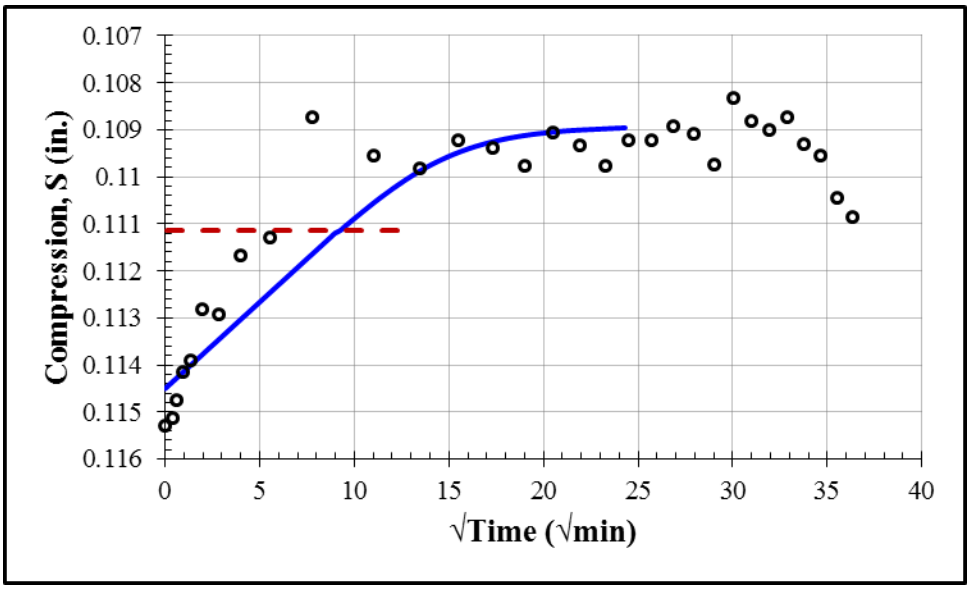

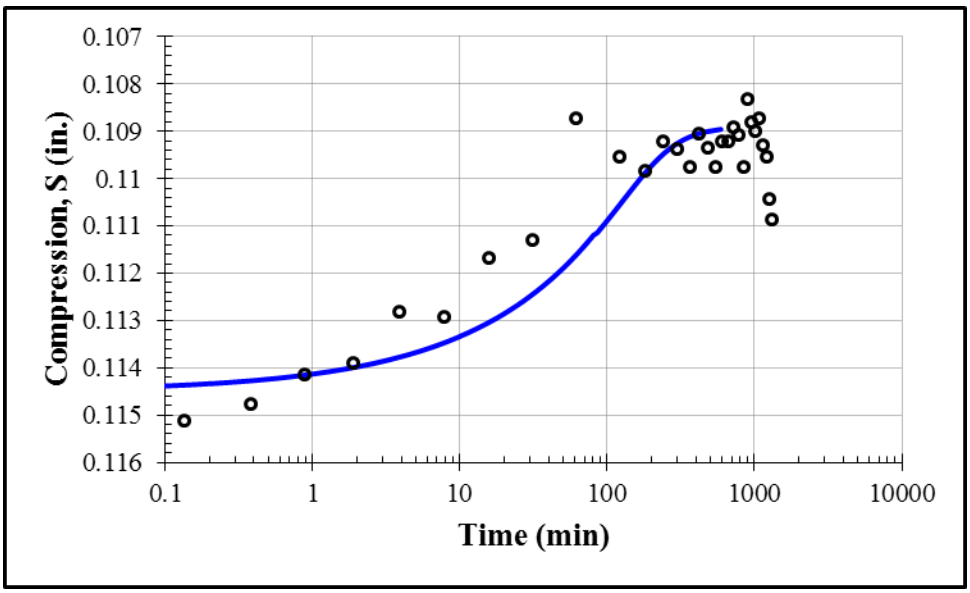

First Unloading: 4000 psf				
S_0 (in.)	S_{100} (in.)	c_v (in^2/min)	k (ft/day)	t_{50} (min)
0.1075	0.0921	0.00018	1.8×10^{-9}	112

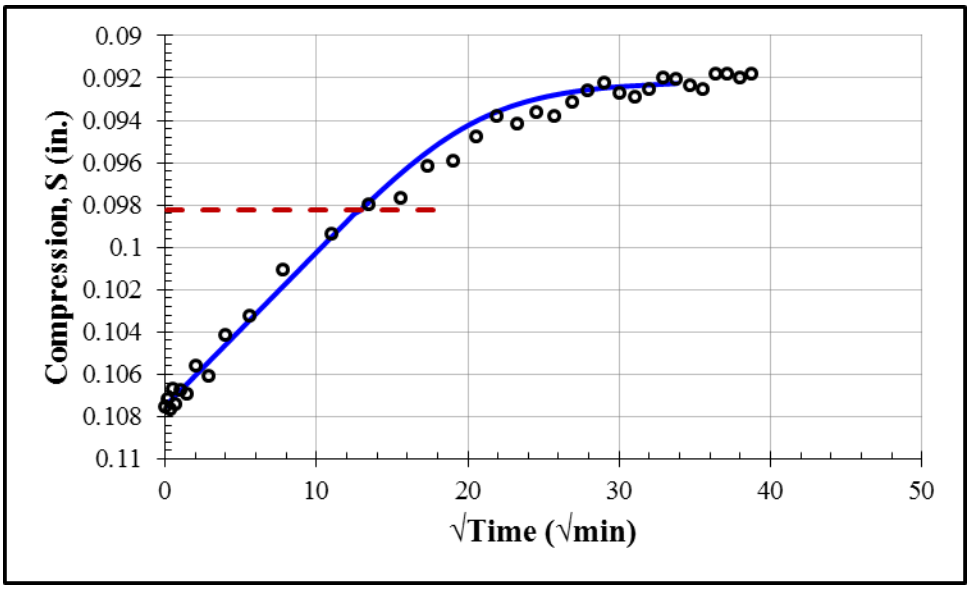

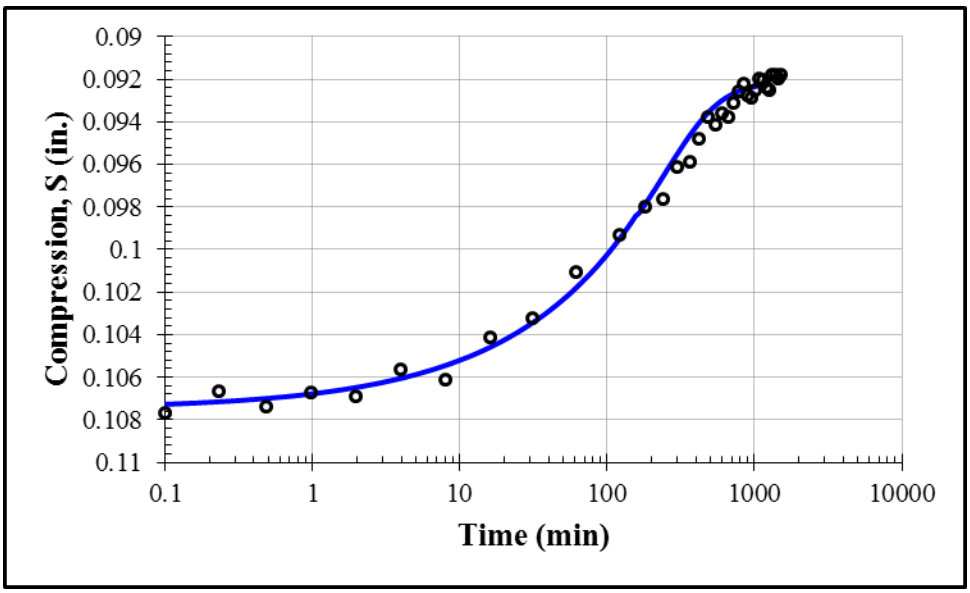

First Unloading: 1000 psf				
S_0 (in.)	S_{100} (in.)	c_v (in^2/min)	k (ft/day)	t_{50} (min)
0.0882	0.0700	0.00007	3.3 x 10^{-9}	306

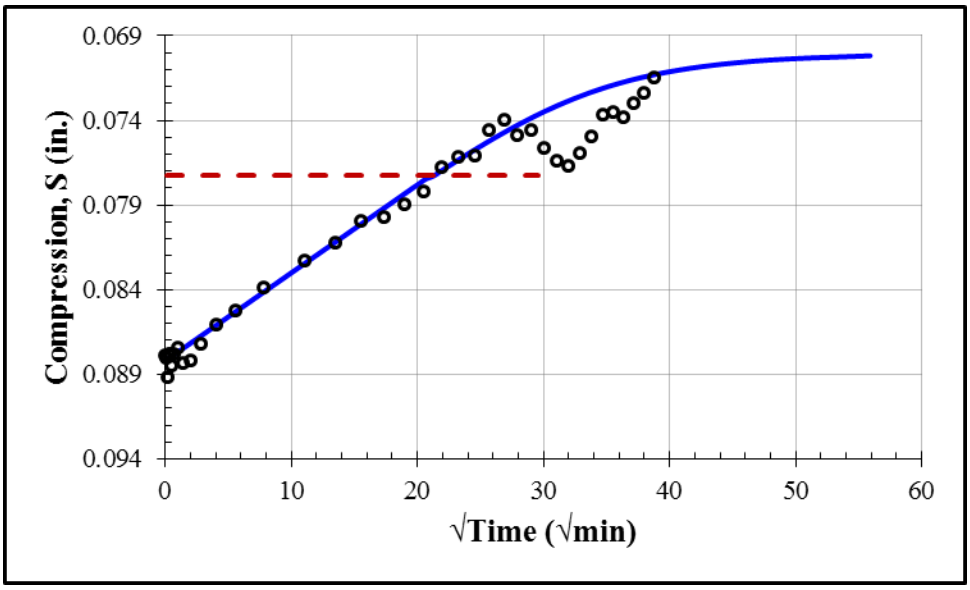

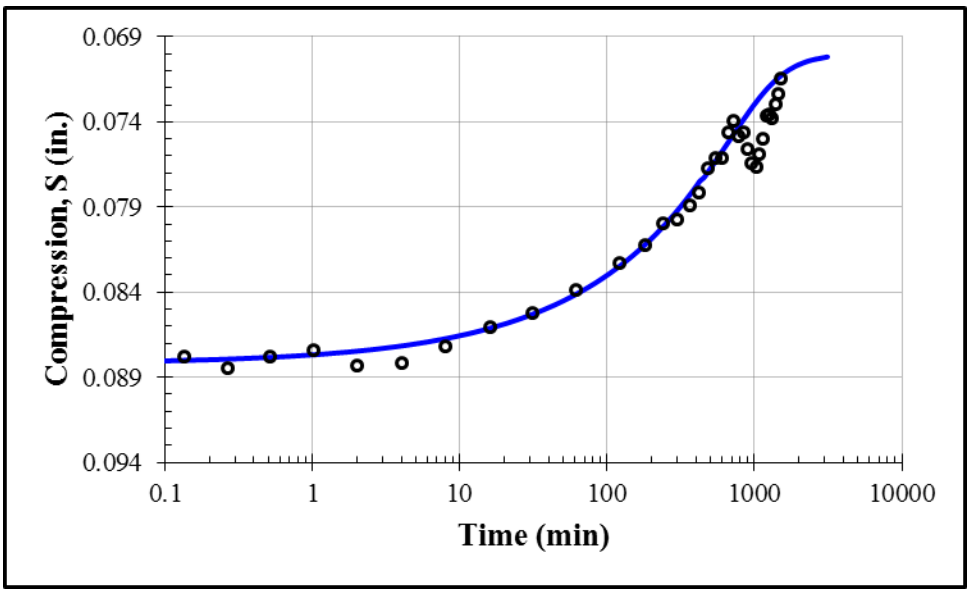

Second Loading: 2000 psf				
S_0 (in.)	S_{100} (in.)	c_v (in^2/min)	k (ft/day)	t_{50} (min)
0.0709	0.0743	0.00018	4.6×10^{-9}	125

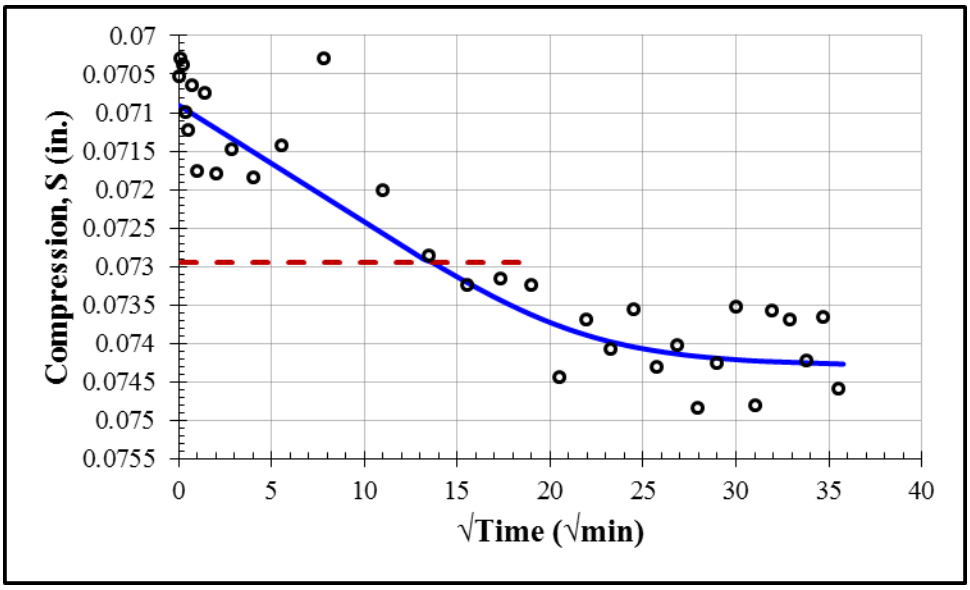

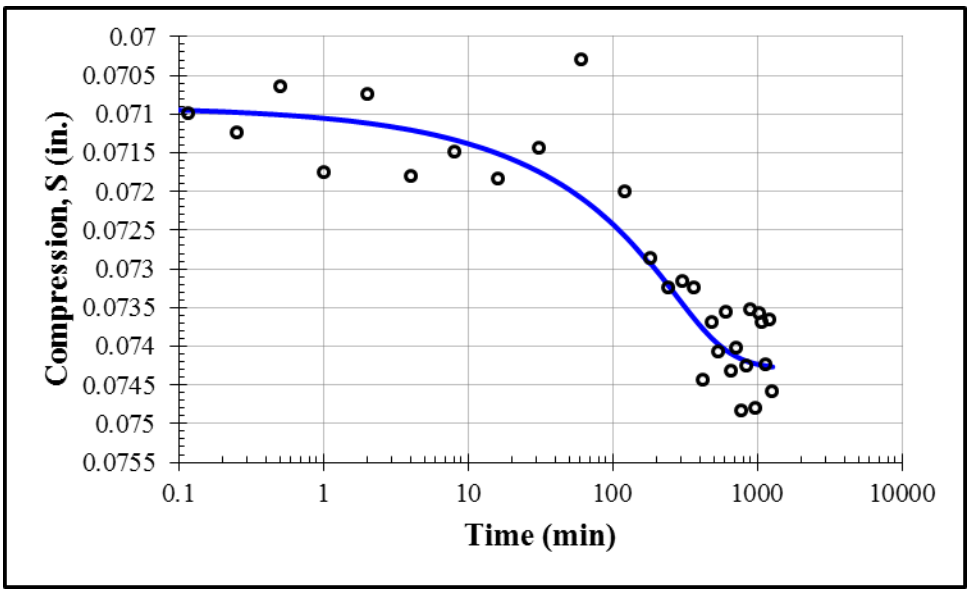

Second Loading: 4000 psf				
S_0 (in.)	S_{100} (in.)	c_v (in^2/min)	k (ft/day)	t_{50} (min)
0.0755	0.0789	0.00014	1.8×10^{-9}	159

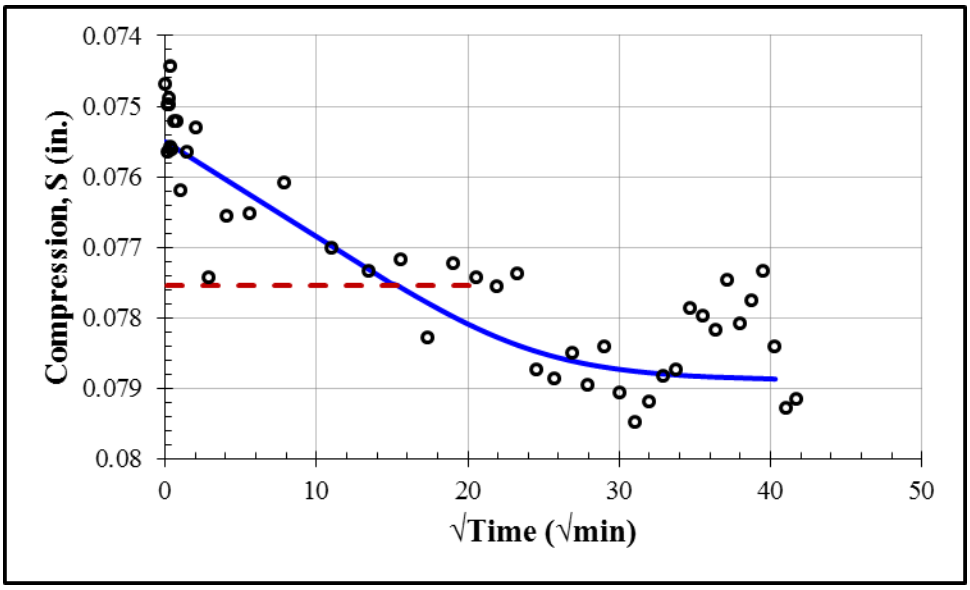

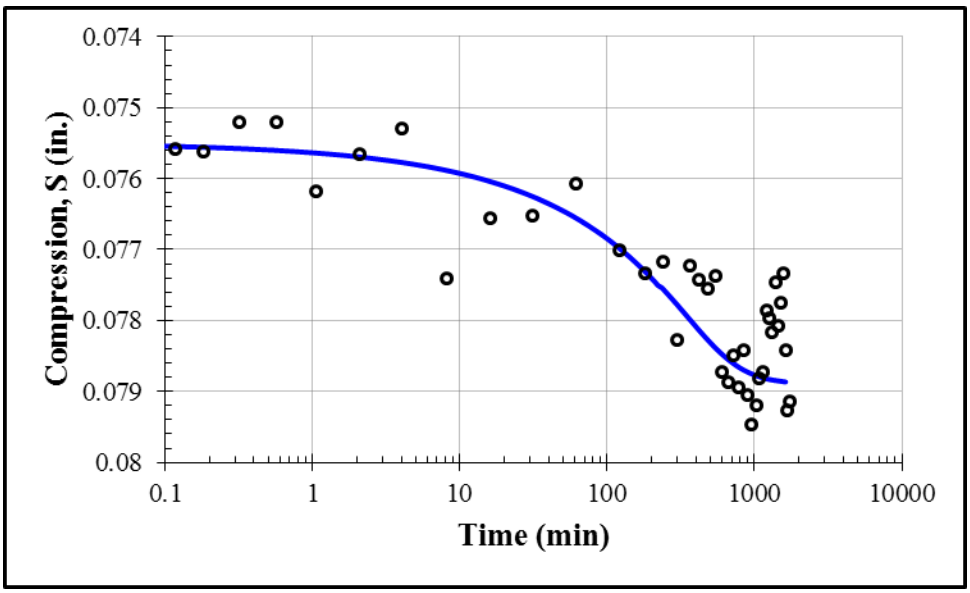

Second Loading: 8000 psf				
S_0 (in.)	S_{100} (in.)	c_v (in^2/min)	k (ft/day)	t_{50} (min)
0.0798	0.0851	0.00018	1.8×10^{-9}	122

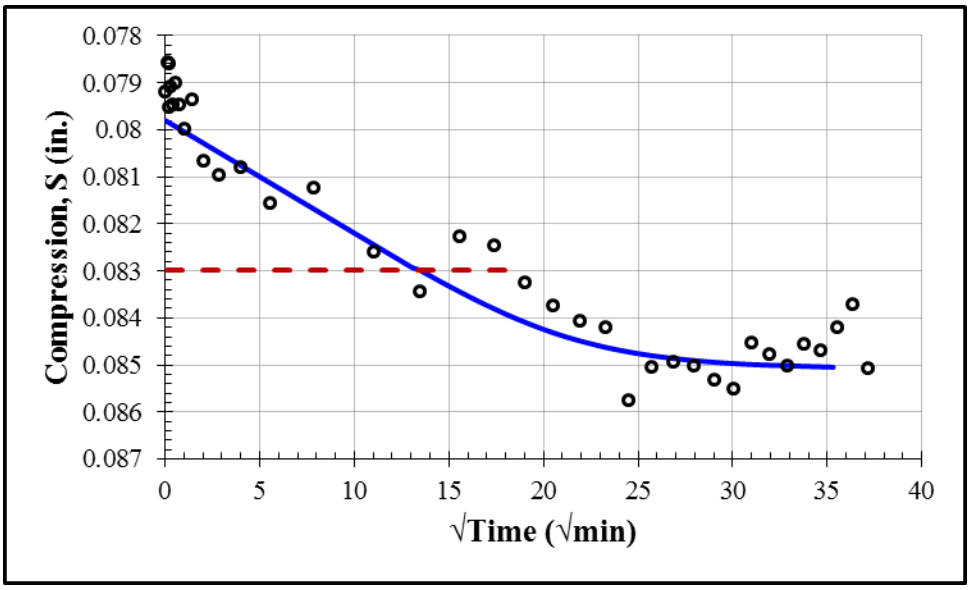

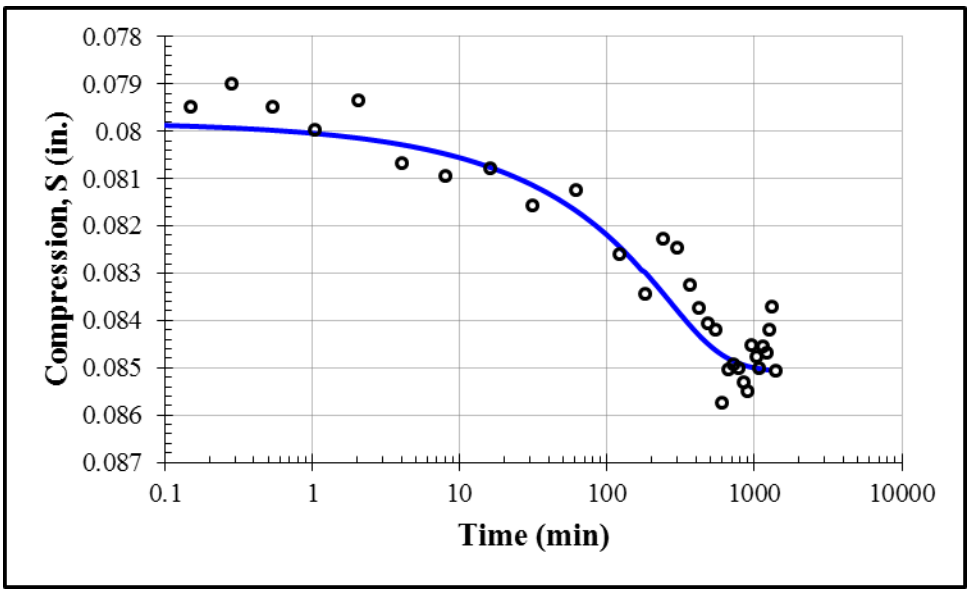

Second Loading: 16000 psf				
S_0 (in.)	S_{100} (in.)	c_v (in^2/min)	k (ft/day)	t_{50} (min)
0.0857	0.0928	0.00018	1.2×10^{-9}	120

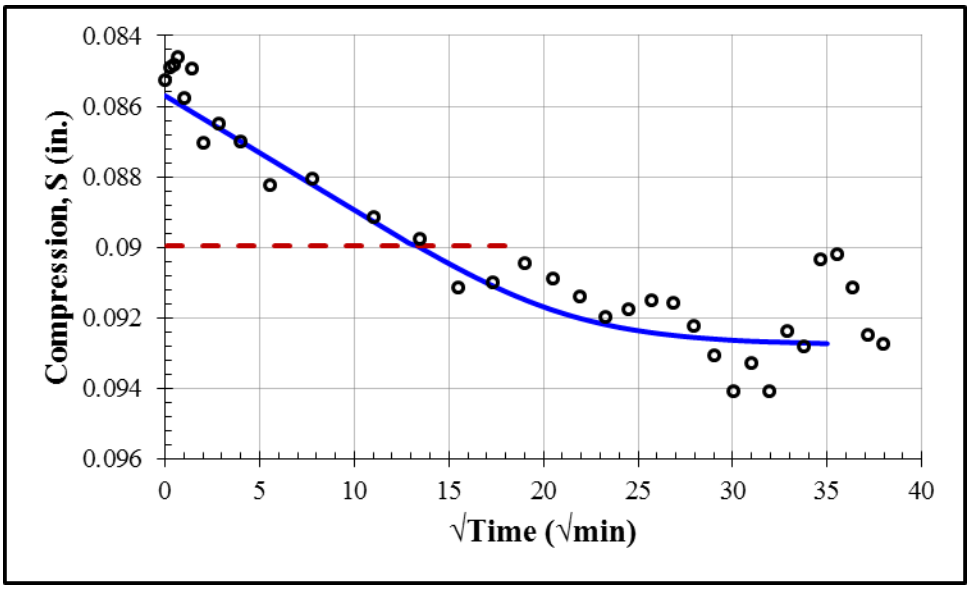

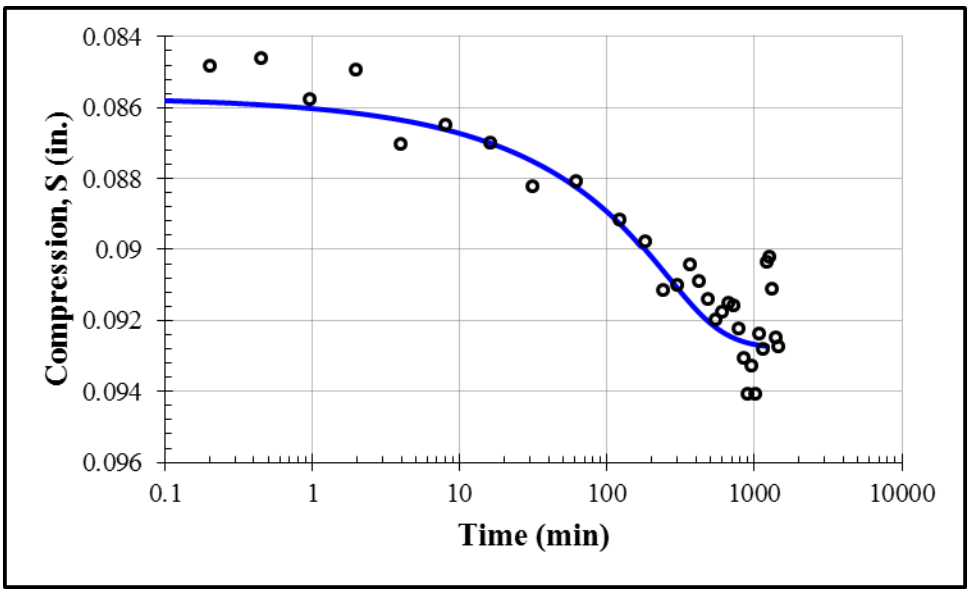

Second Loading: 32000 psf				
S_0 (in.)	S_{100} (in.)	c_v (in^2/min)	k (ft/day)	t_{50} (min)
0.0930	0.1092	0.00017	1.3×10^{-9}	124

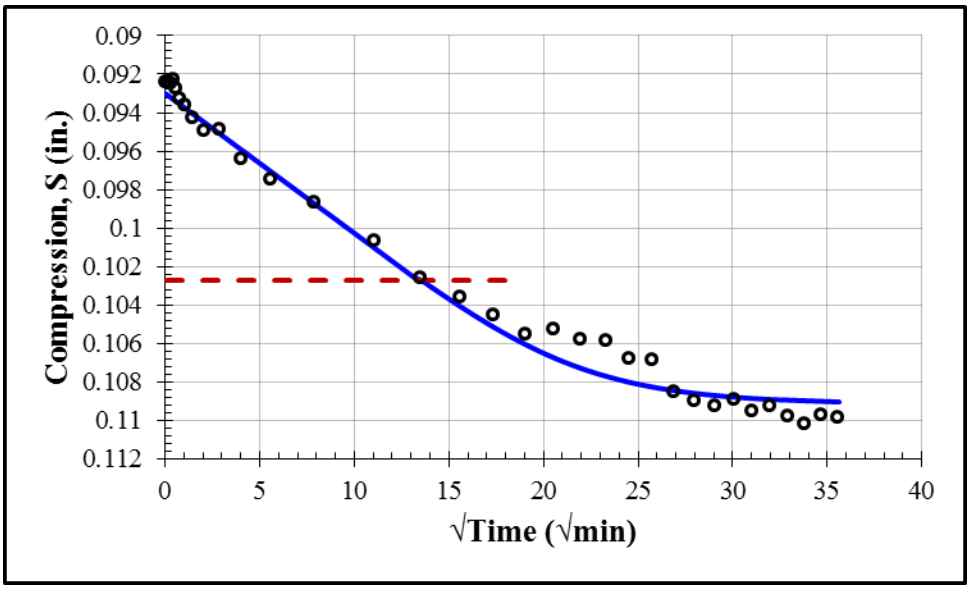

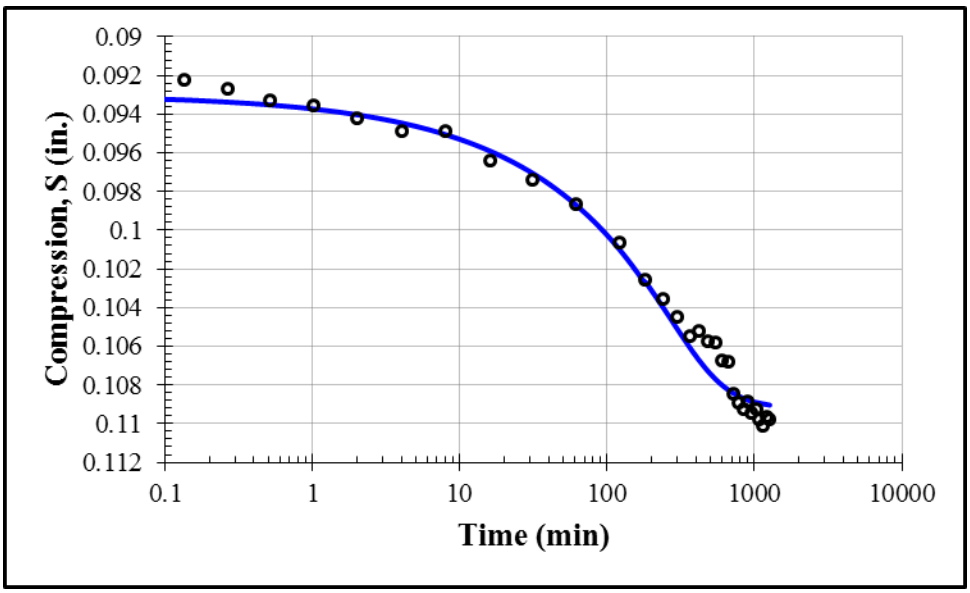

Second Loading: 64000 psf				
S_0 (in.)	S_{100} (in.)	c_v (in^2/min)	k (ft/day)	t_{50} (min)
0.1135	0.1245	0.00018	4.6 x 10^{-10}	110

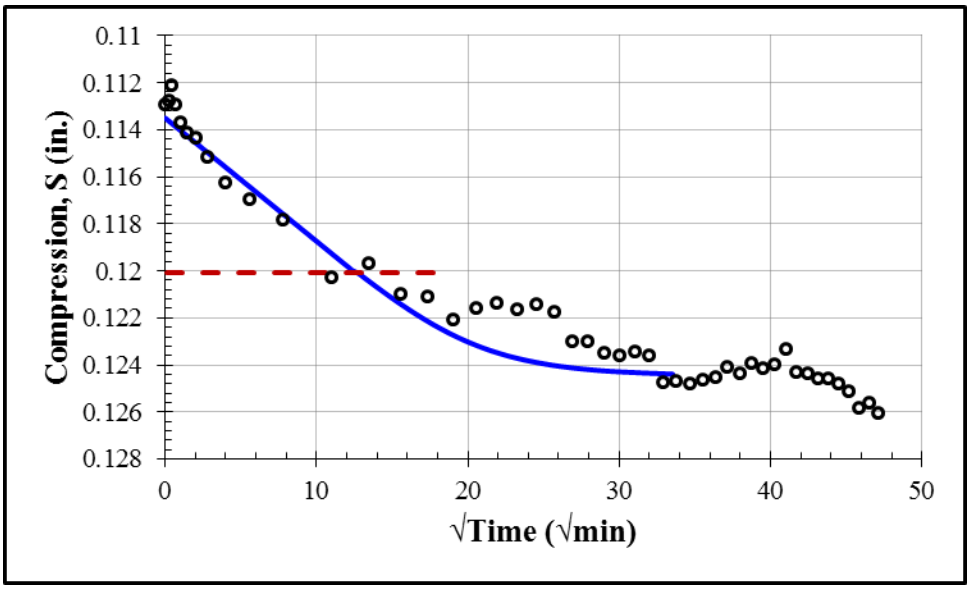

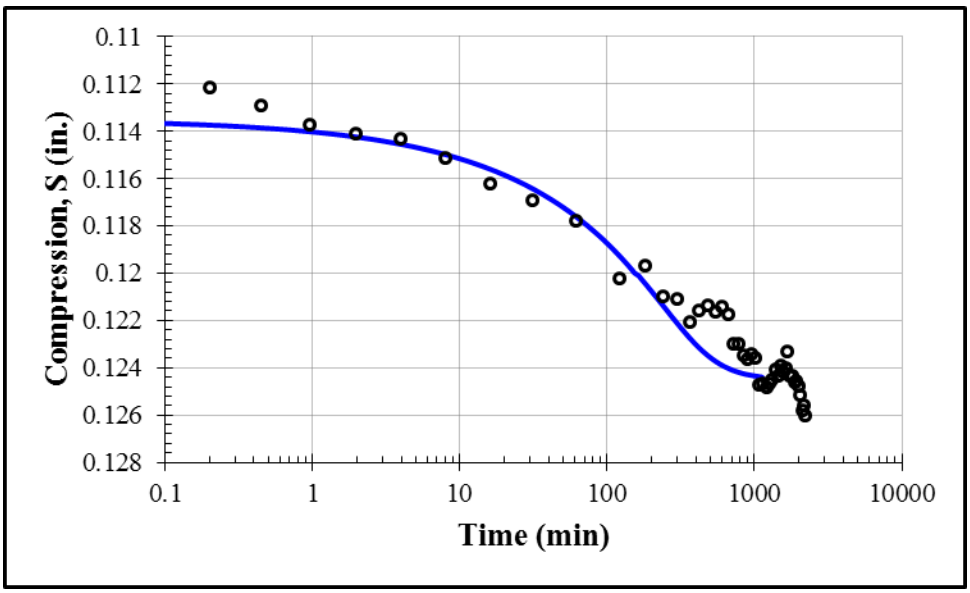

Second Unloading: 16000 psf				
S_0 (in.)	S_{100} (in.)	c_v (in^2/min)	k (ft/day)	t_{50} (min)
0.1185	0.1062	0.00016	3.1 x 10^{-10}	121

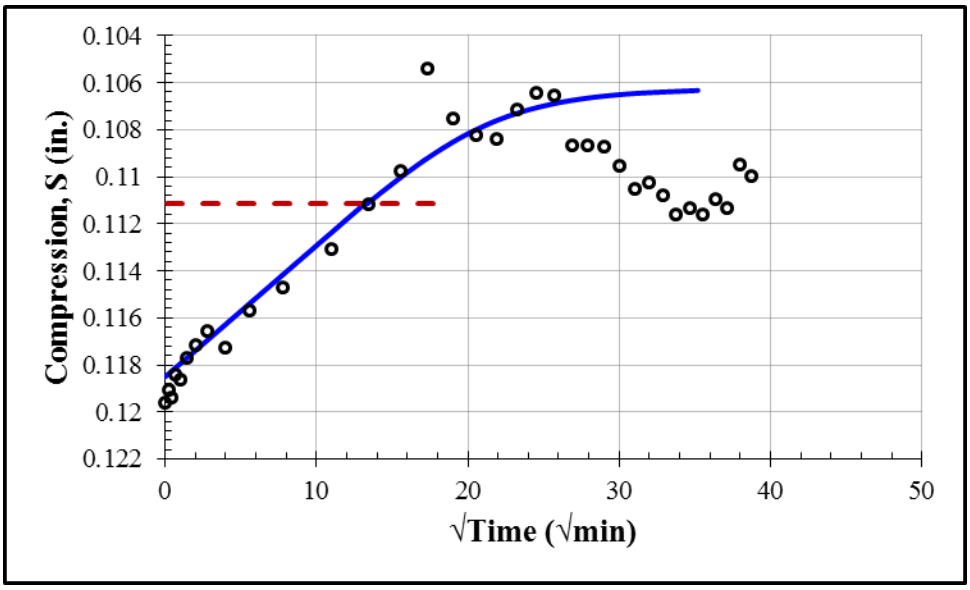

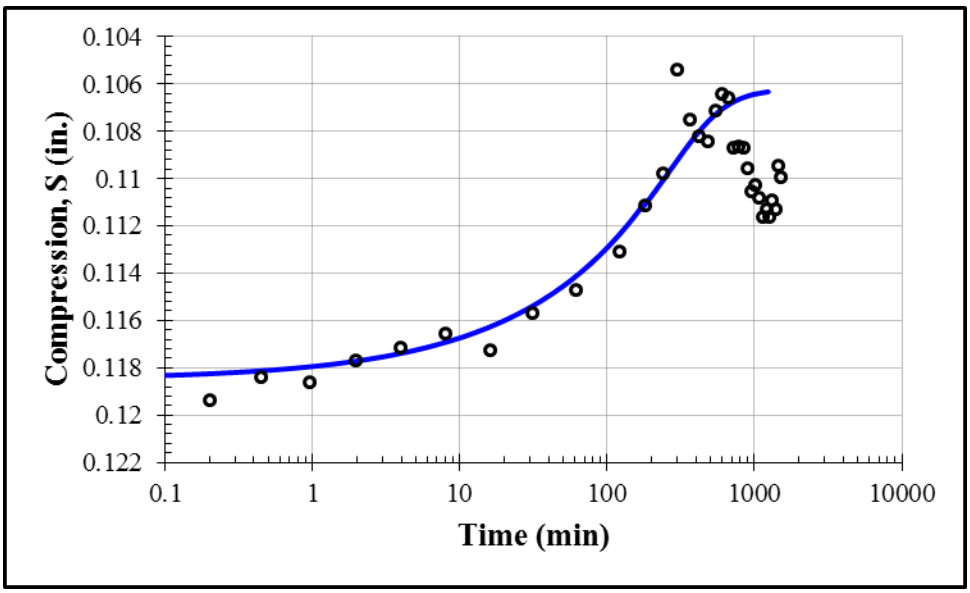

Second Unloading: 4000 psf				
S_0 (in.)	S_{100} (in.)	c_v (in^2/min)	k (ft/day)	t_{50} (min)
0.1057	0.0929	000017	1.4×10^{-9}	119

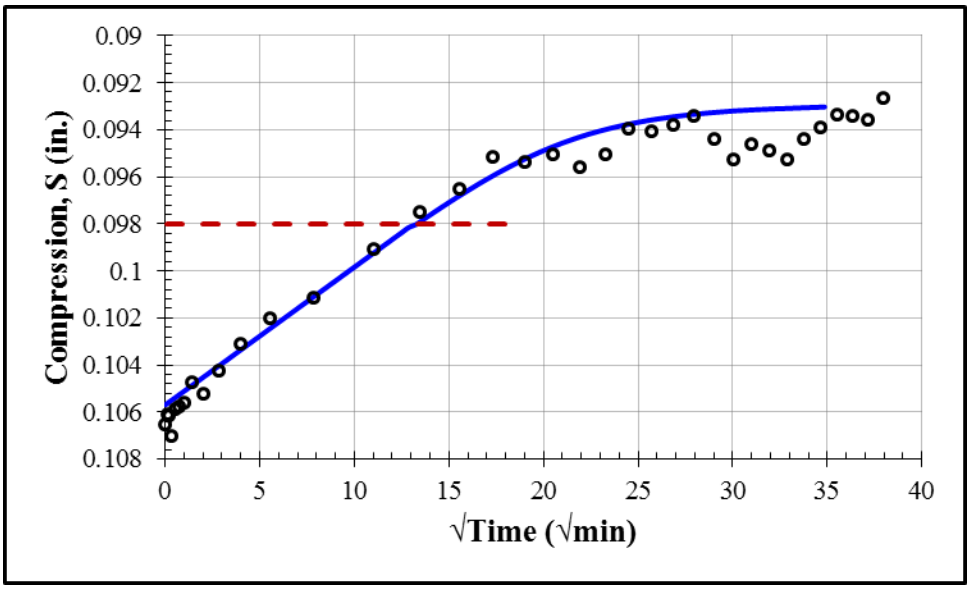

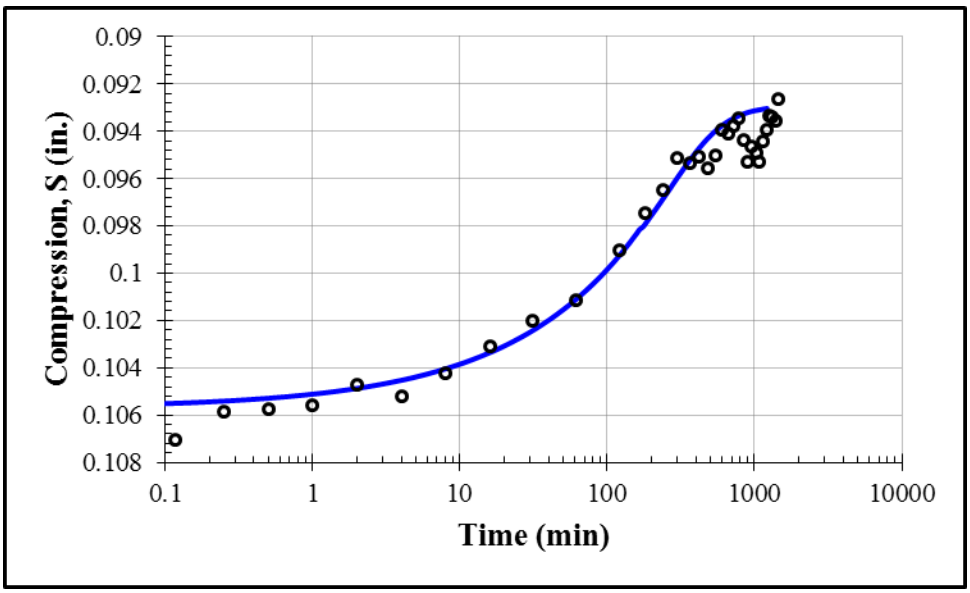

Second Unloading: 1000 psf				
S_0 (in.)	S_{100} (in.)	c_v (in^2/min)	k (ft/day)	t_{50} (min)
0.0904	0.0728	0.000063	2.8×10^{-9}	338

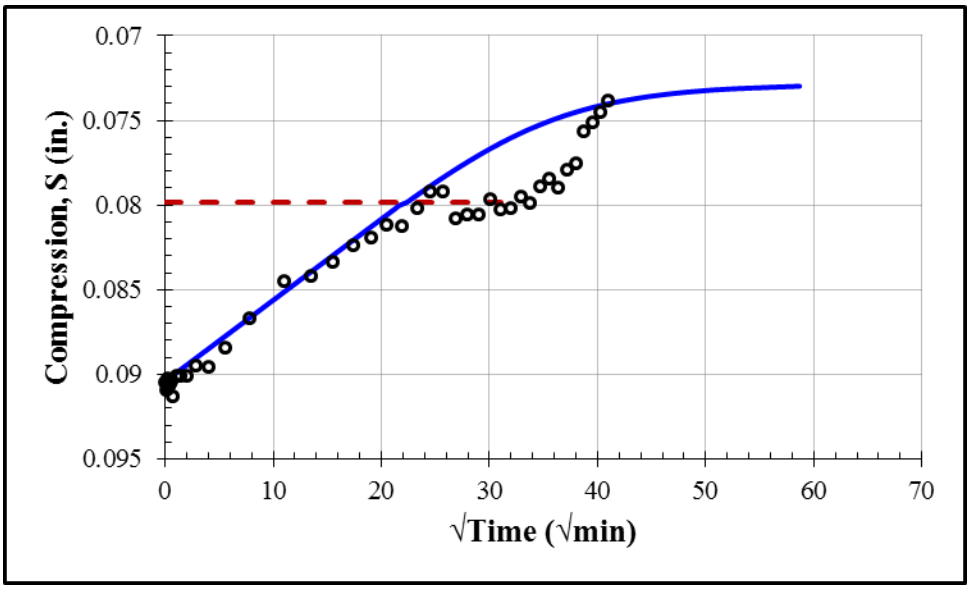

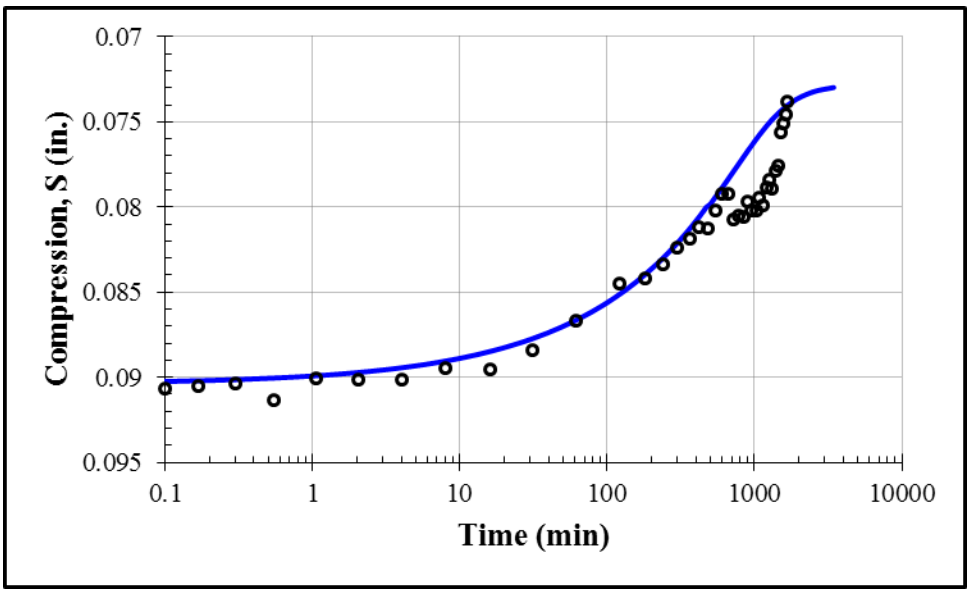

Second Unloading: 250 psf				
S_0 (in.)	S_{100} (in.)	c_v (in^2/min)	k (ft/day)	t_{50} (min)
0.0736	0.0638	0.00013	1.3×10^{-8}	172

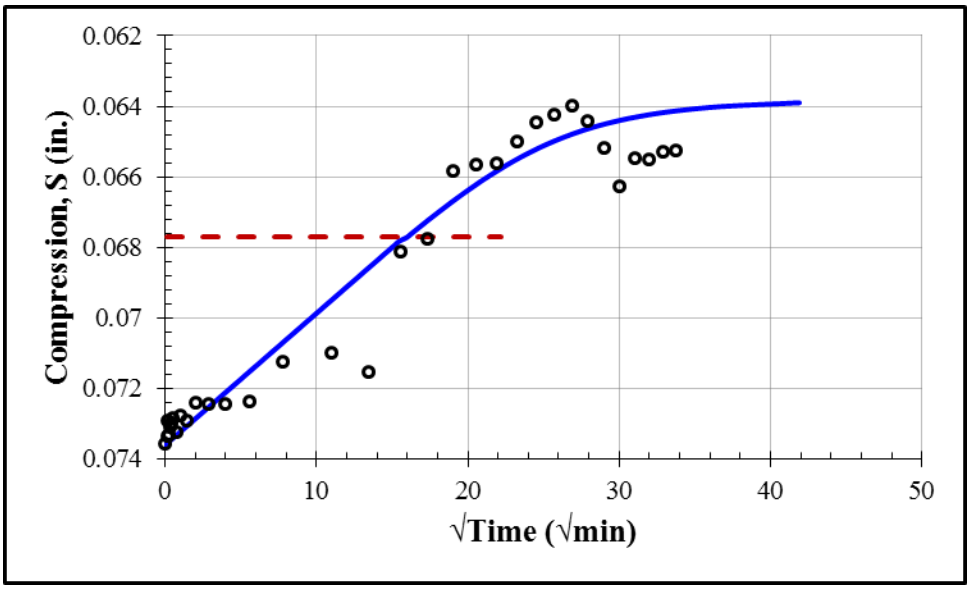

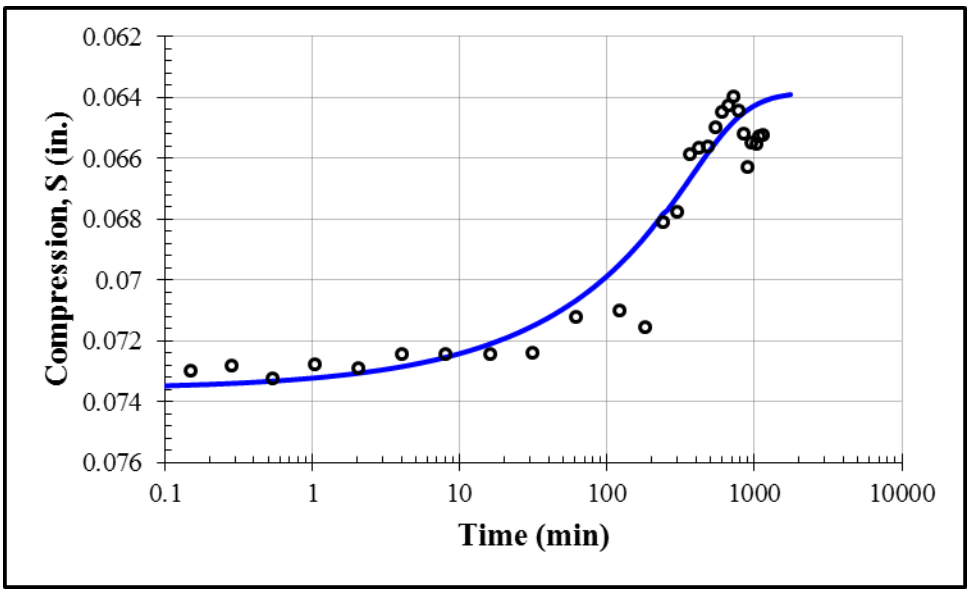

Third Loading: 500 psf				
S_0 (in.)	S_{100} (in.)	c_v (in^2/min)	k (ft/day)	t_{50} (min)
0.0637	0.0675	0.00008	9.5 x 10^{-9}	288

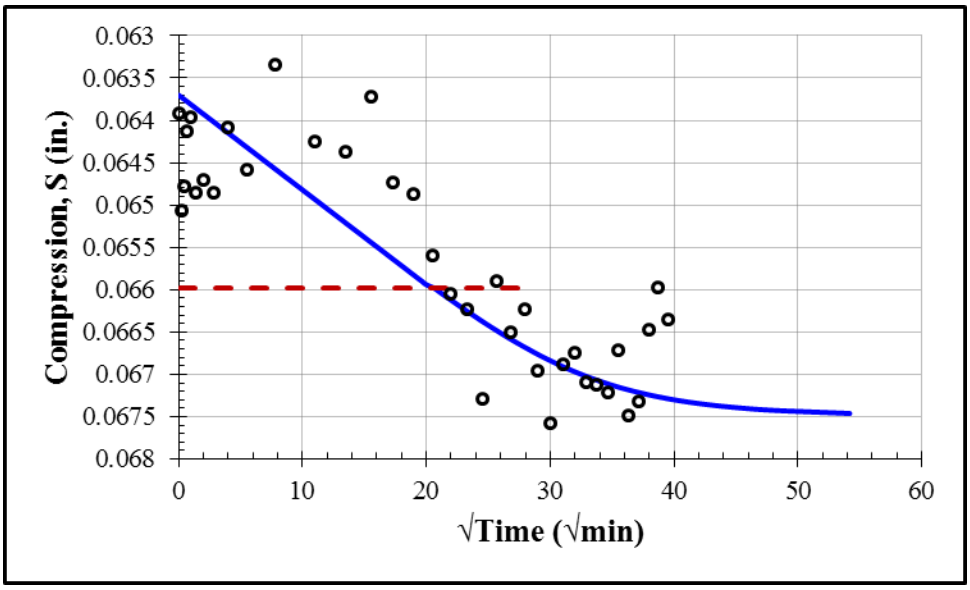

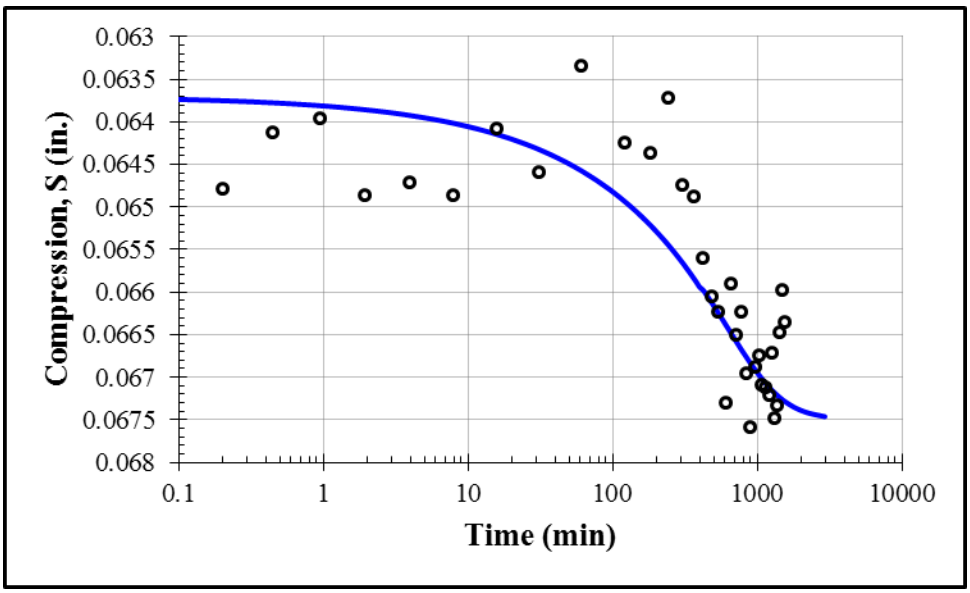

Third Loading: 1000 psf				
S_0 (in.)	S_{100} (in.)	c_v (in^2/min)	k (ft/day)	t_{50} (min)
0.0665	0.0657	0.0001	1.3 x 10^{-9}	229

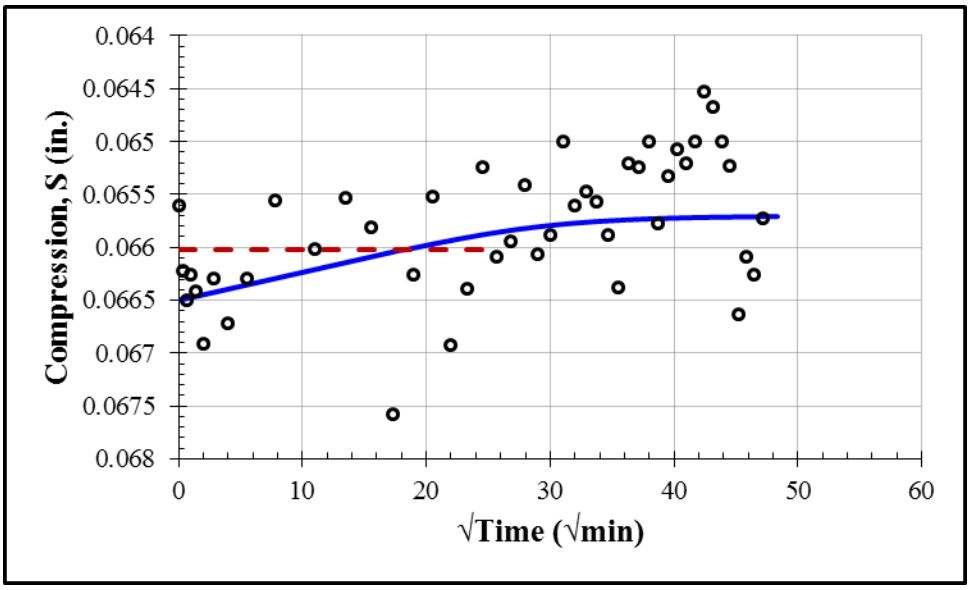

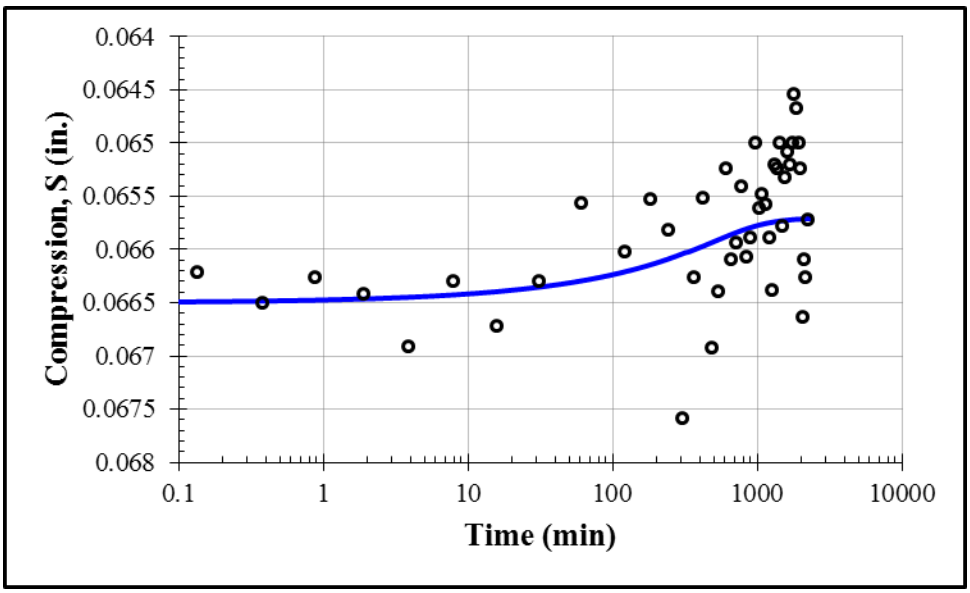

Third Loading: 2000 psf				
S_0 (in.)	S_{100} (in.)	c_v (in^2/min)	k (ft/day)	t_{50} (min)
0.0665	0.0700	0.00013	3.6×10^{-9}	176

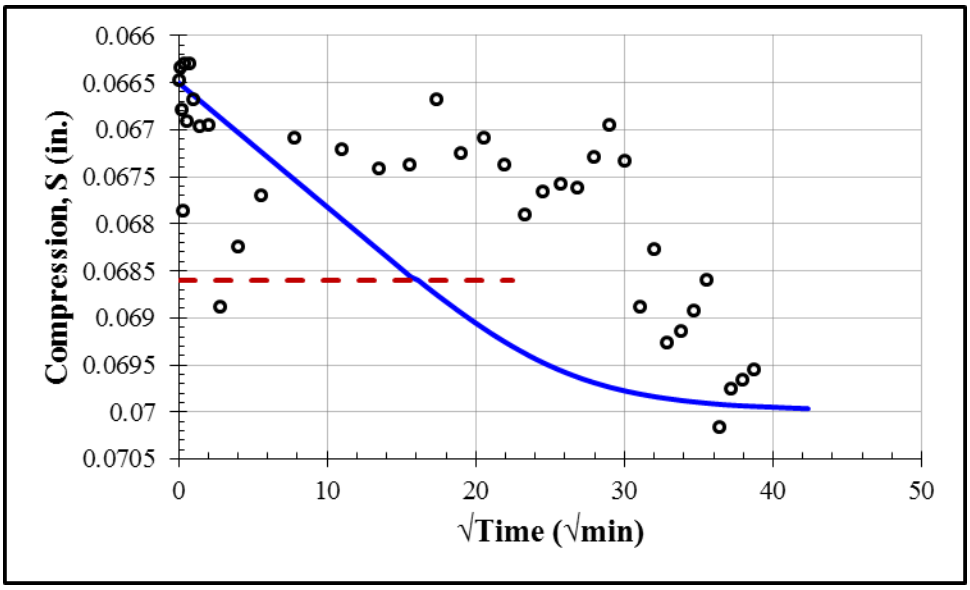

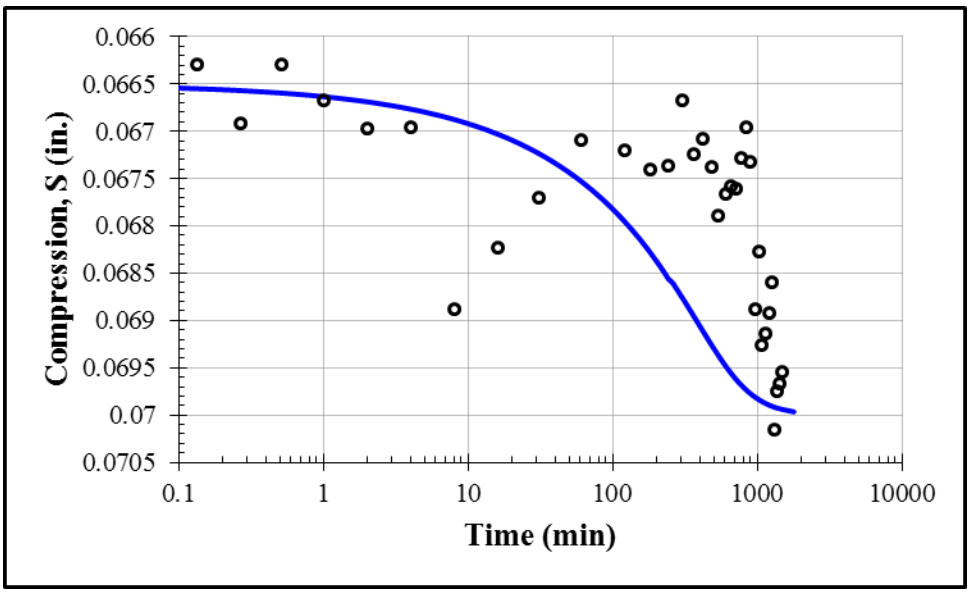

Third Loading: 4000 psf				
S_0 (in.)	S_{100} (in.)	c_v (in^2/min)	k (ft/day)	t_{50} (min)
0.0712	0.0695	0.00015	9.9×10^{-10}	150

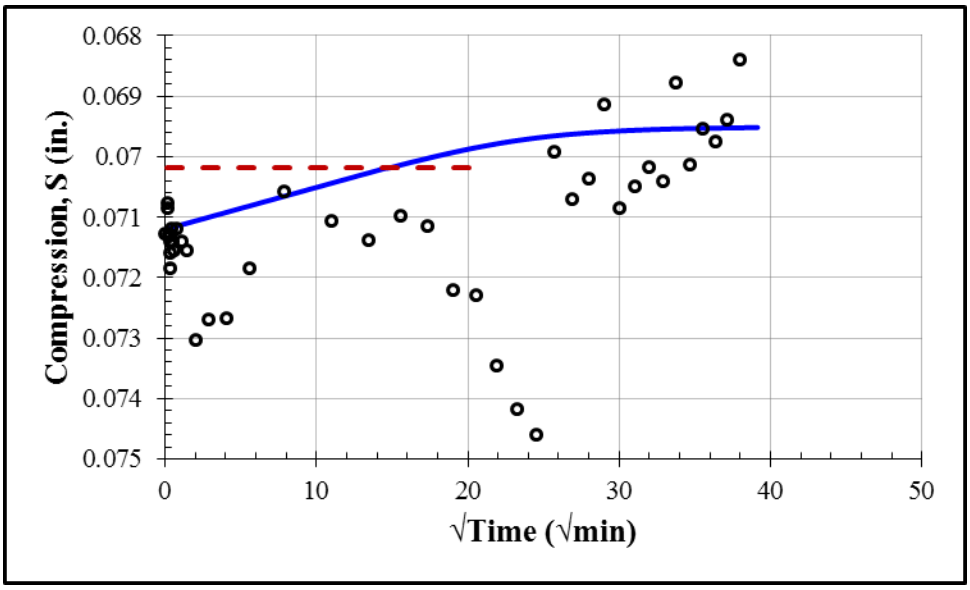

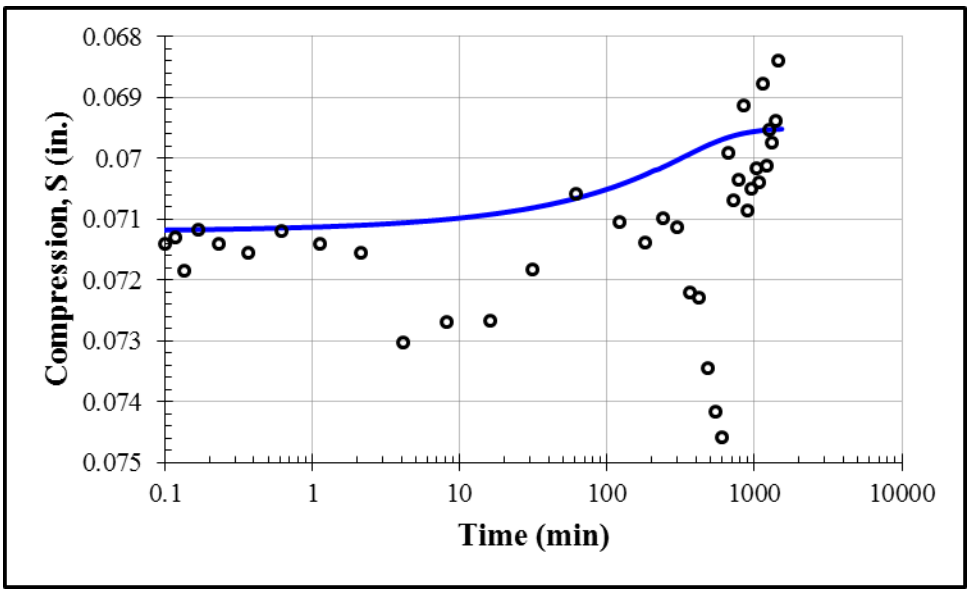

Third Unloading: 1000 psf				
S_0 (in.)	S_{100} (in.)	c_v (in^2/min)	k (ft/day)	t_{50} (min)
0.0653	0.0614	0.00015	1.5 x 10^{-9}	153

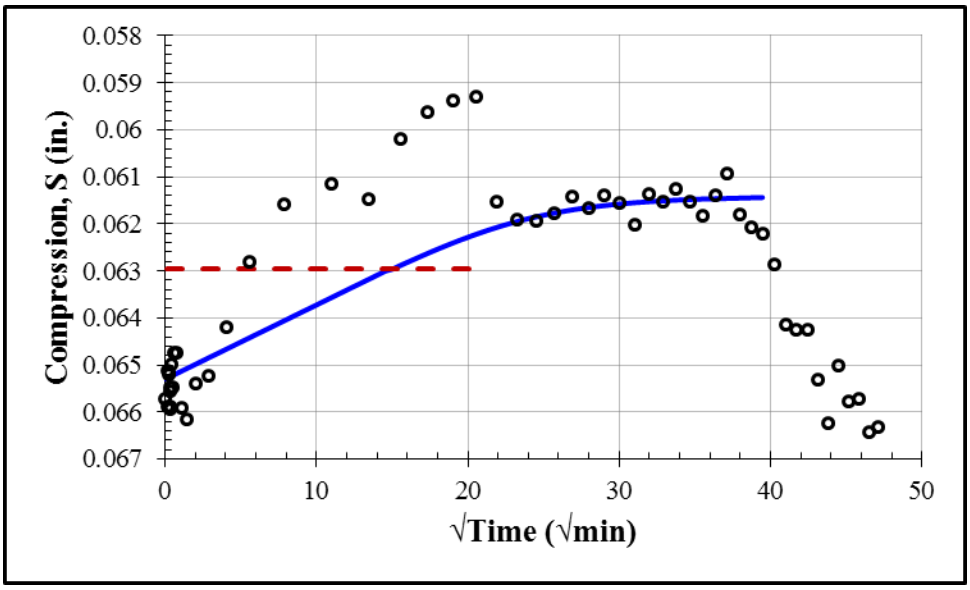

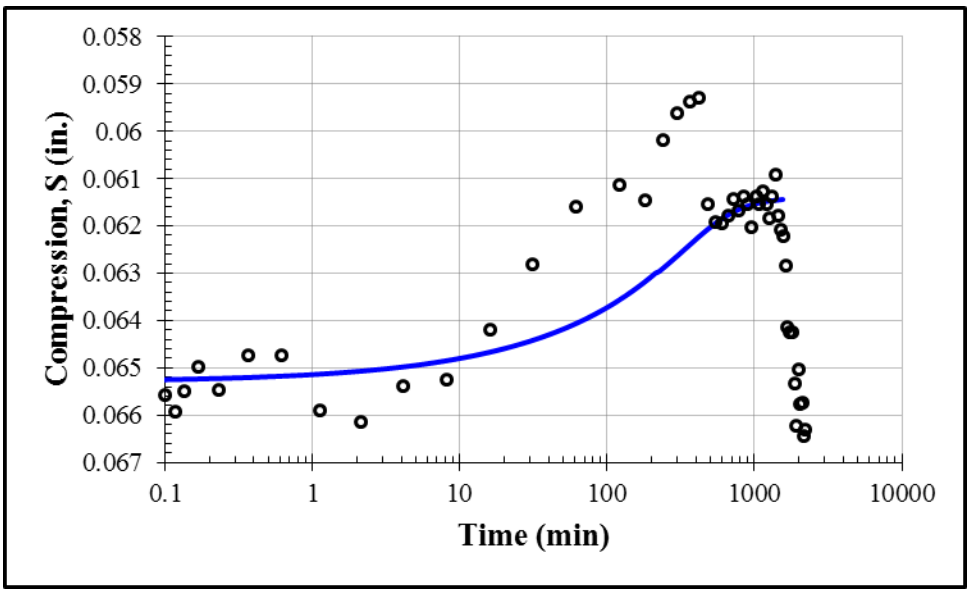

Third Unloading: 250 psf				
S_0 (in.)	S_{100} (in.)	c_v (in^2/min)	k (ft/day)	t_{50} (min)
0.0663	0.0608	0.00018	1.0 x 10^{-8}	127

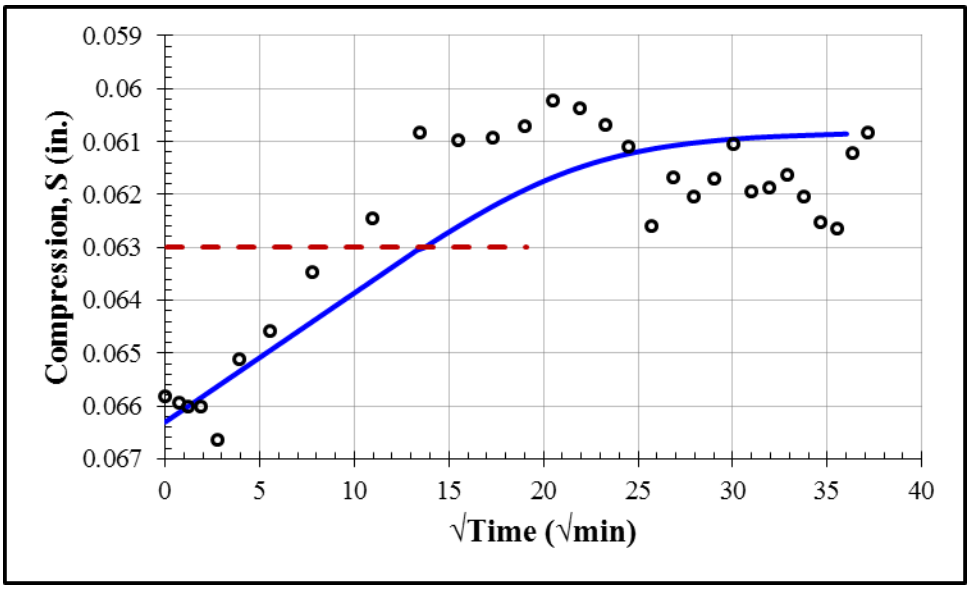

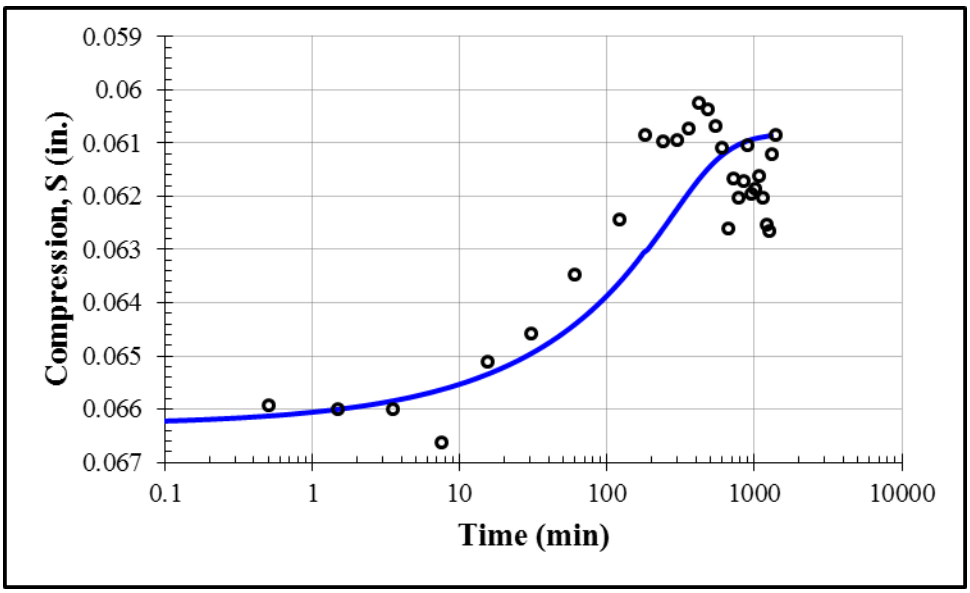

Appendix C: Consolidation Test 2

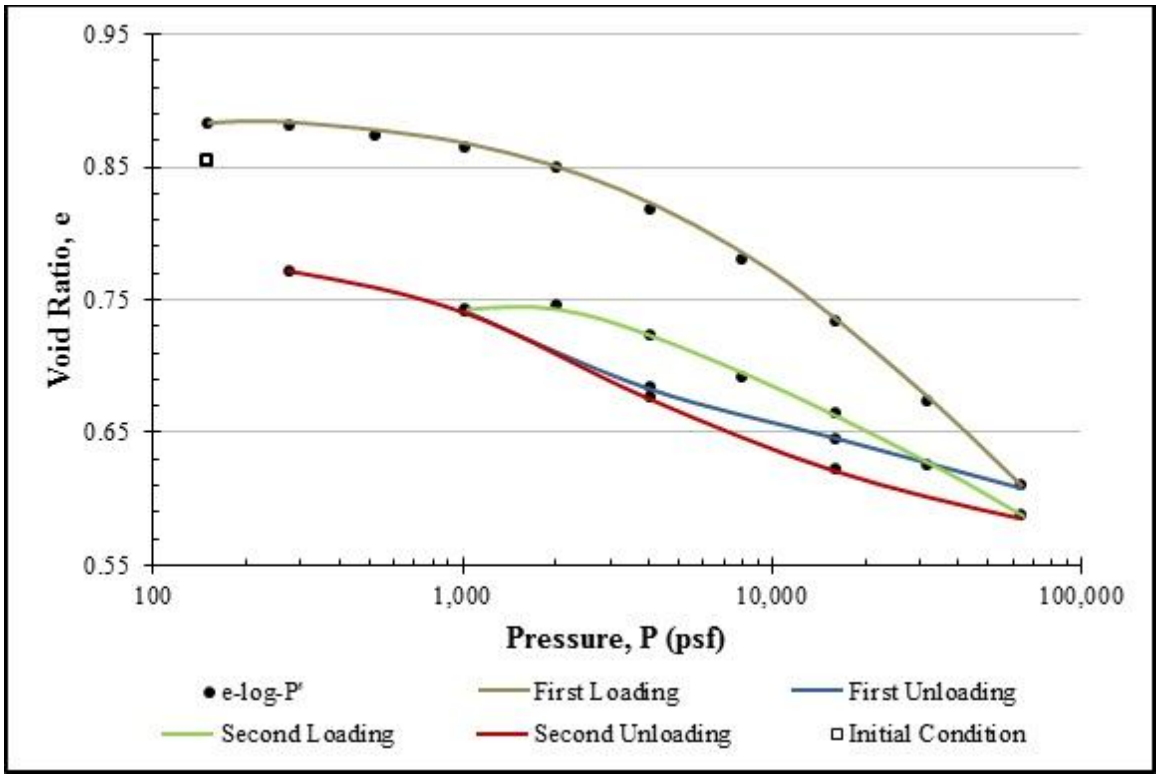
0.95
0.85
0.75
0.65
0.55
Void Ratio, e
100
1,000
10,000
100,000
Pressure, P (psf)
e-log-P'
First Loading
First Unloading
Second Loading
Second Unloading
Initial Condition

Inundation: 125 psf				
S_0 (in.)	S_{100} (in.)	c_v (in^2/min)	k (ft/day)	t_{50} (min)
0.0008	-0.0100	0.00035	2.5 x 10^{-7}	79

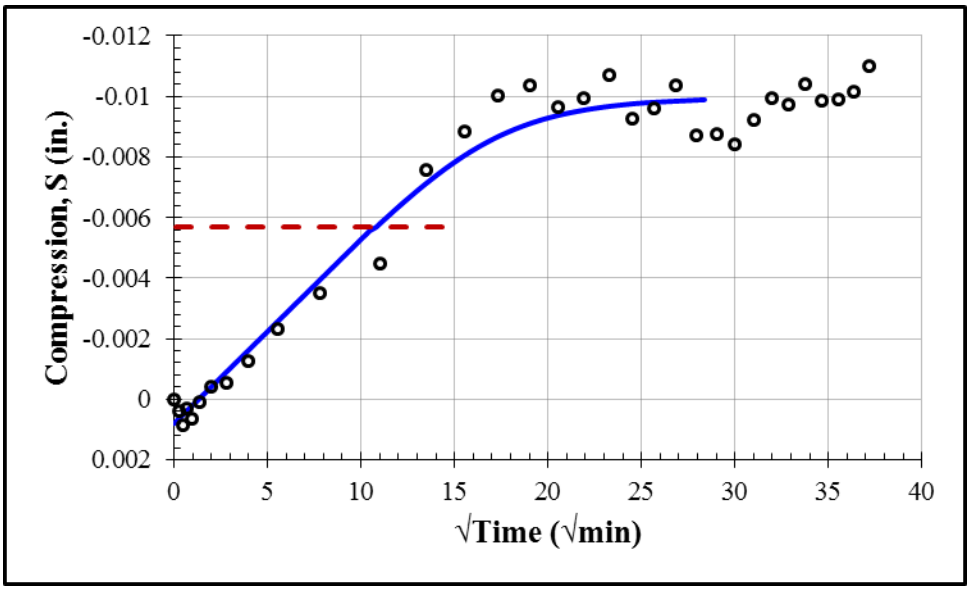

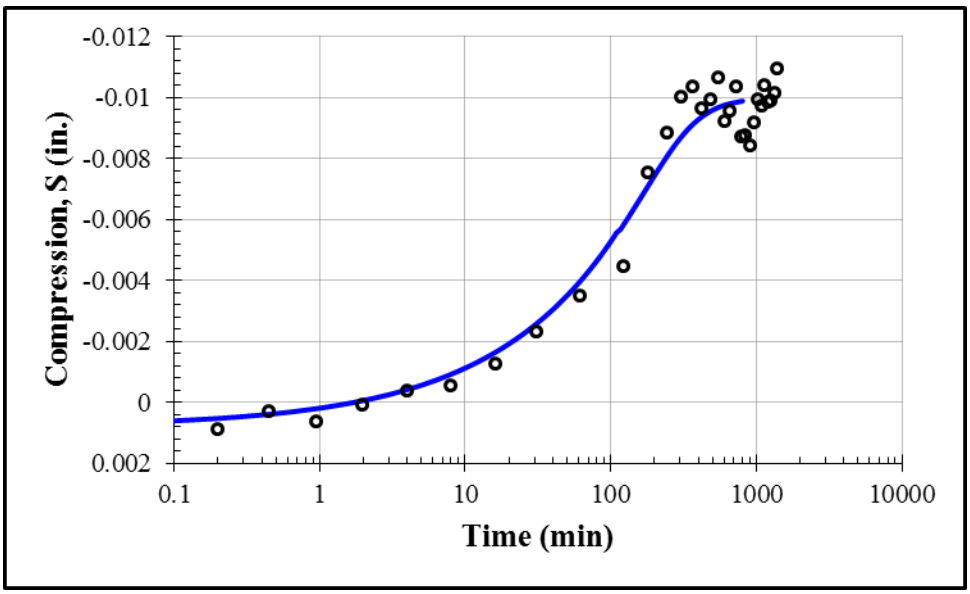

First Loading: 250 psf				
S_0 (in.)	S_{100} (in.)	c_v (in^2/min)	k (ft/day)	t_{50} (min)
-0.0101	-0.0075	0.0002	3.5 x 10^{-8}	142

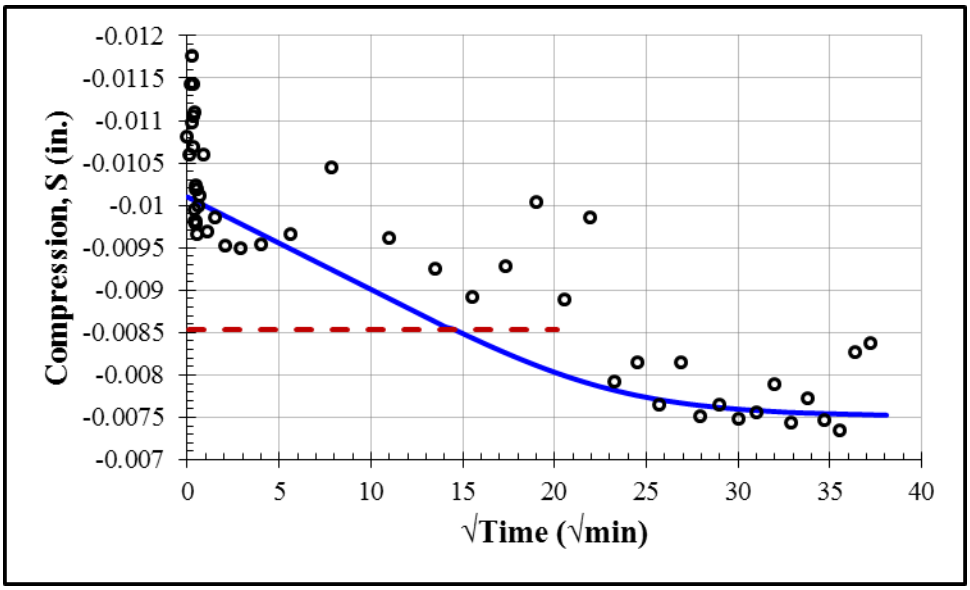

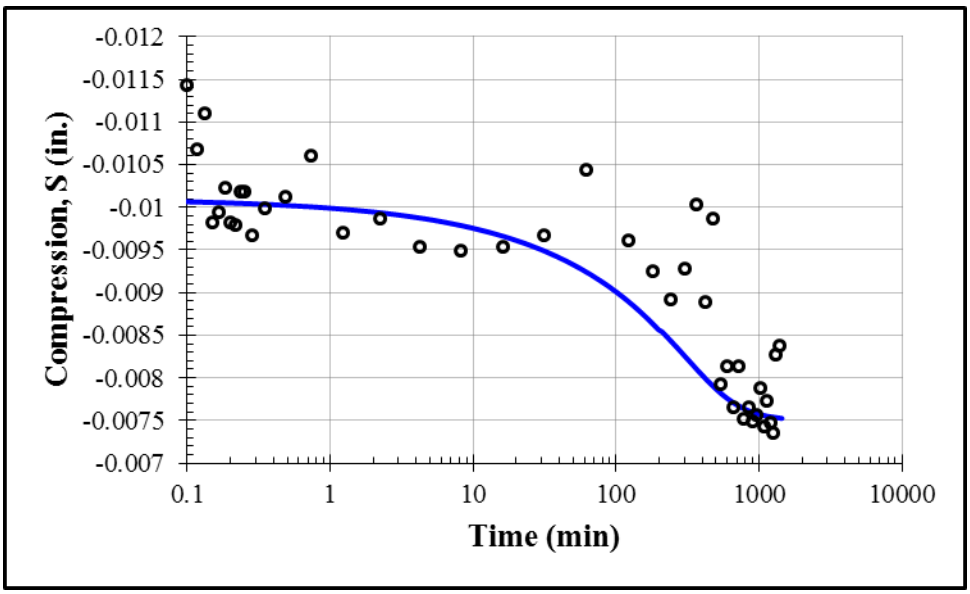

First Loading: 500 psf				
S_0 (in.)	S_{100} (in.)	c_v (in^2/min)	k (ft/day)	t_{50} (min)
-0.0065	-0.0024	0.0002	2.7 x 10^{-8}	141

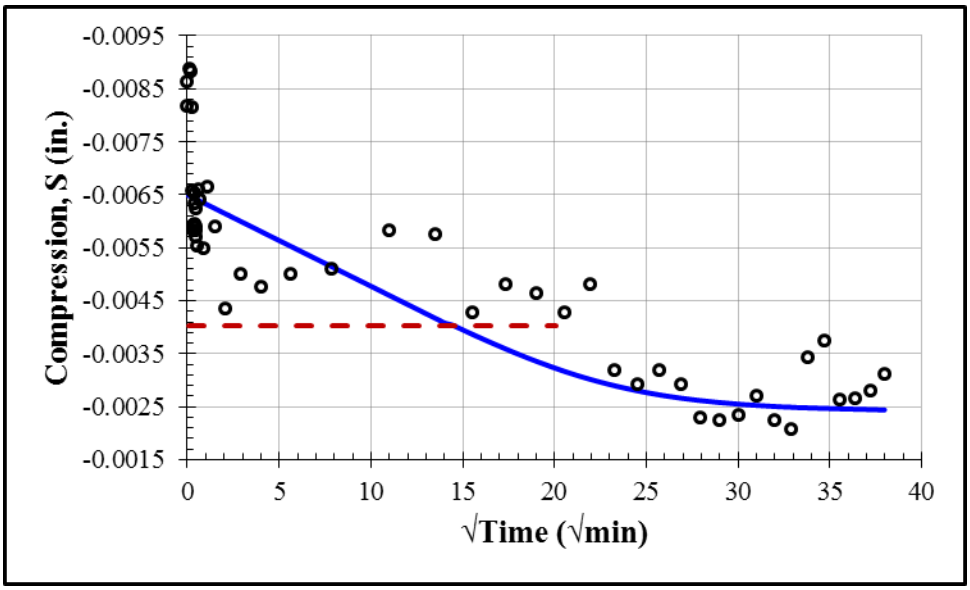

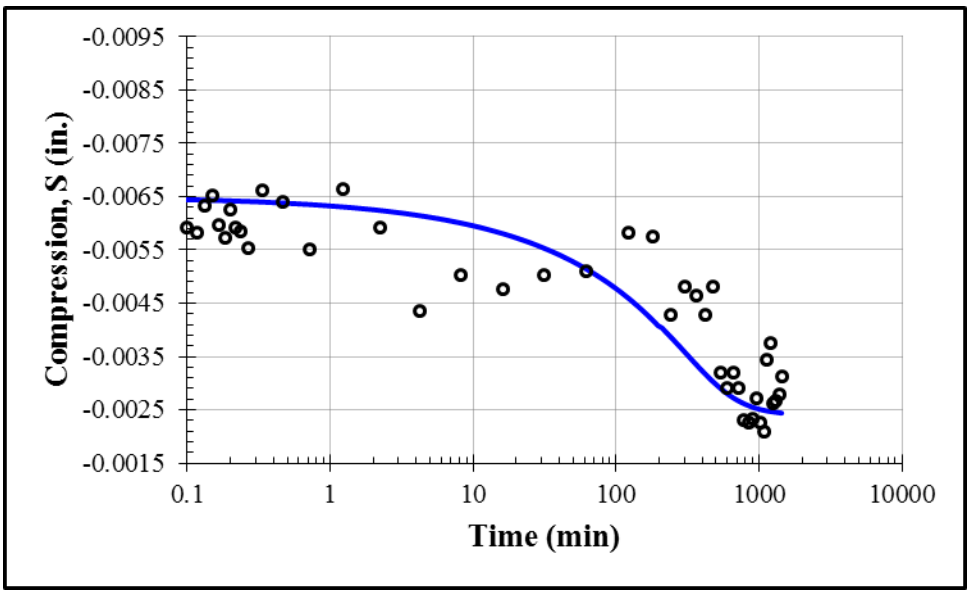

First Loading: 1000 psf				
S_0 (in.)	S_{100} (in.)	c_v (in^2/min)	k (ft/day)	t_{50} (min)
-0.0019	0.0035	0.003	2.7 x 10^{-7}	9.3

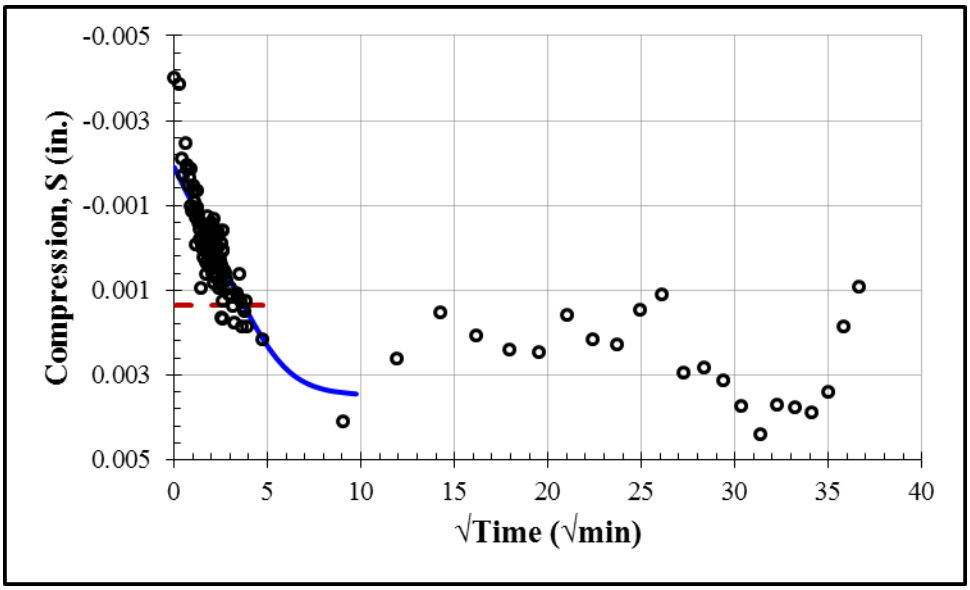

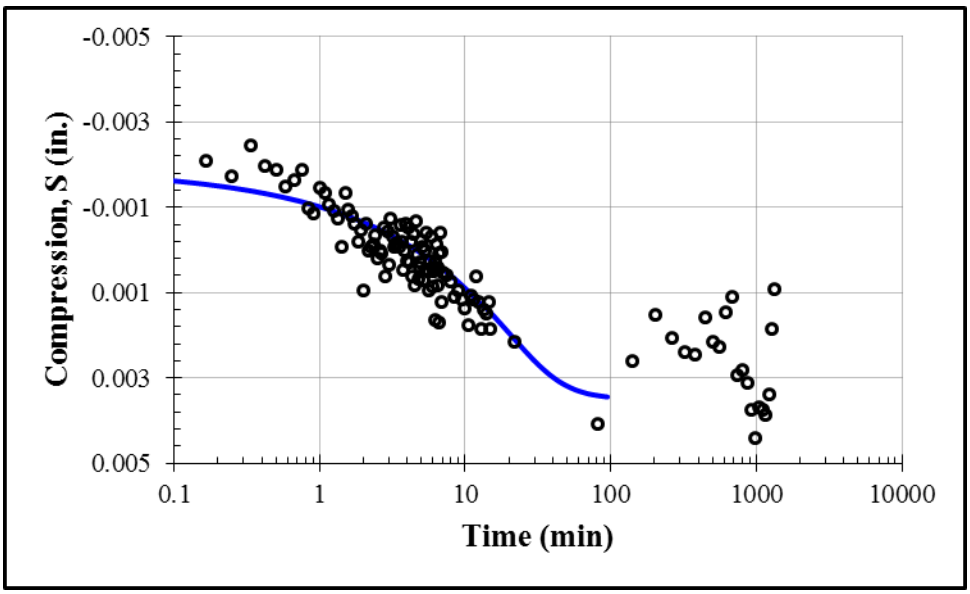

First Loading: 2000 psf				
S_0 (in.)	S_{100} (in.)	c_v (in^2/min)	k (ft/day)	t_{50} (min)
0.0032	0.0120	0.0006	4.4 x 10^{-8}	46

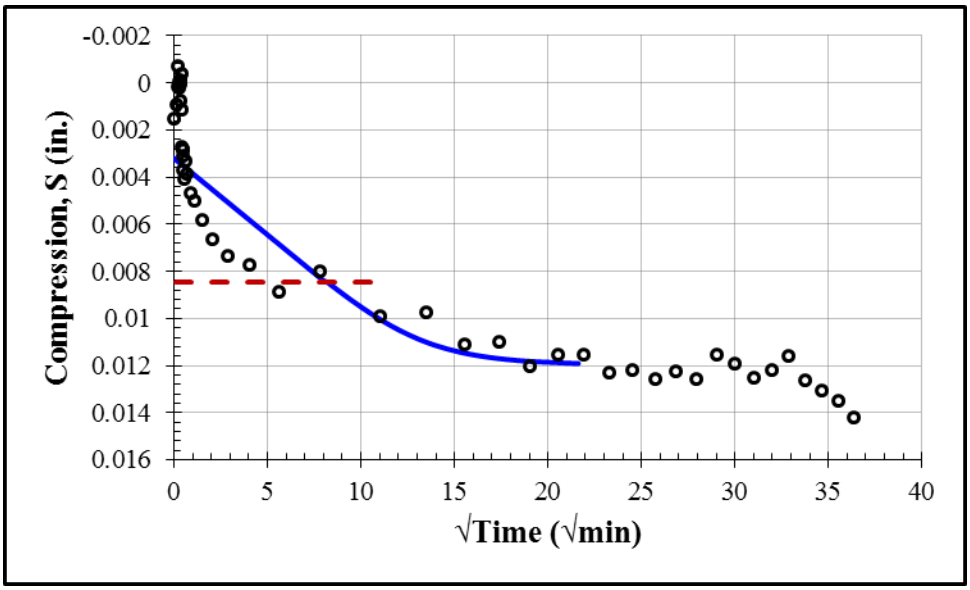

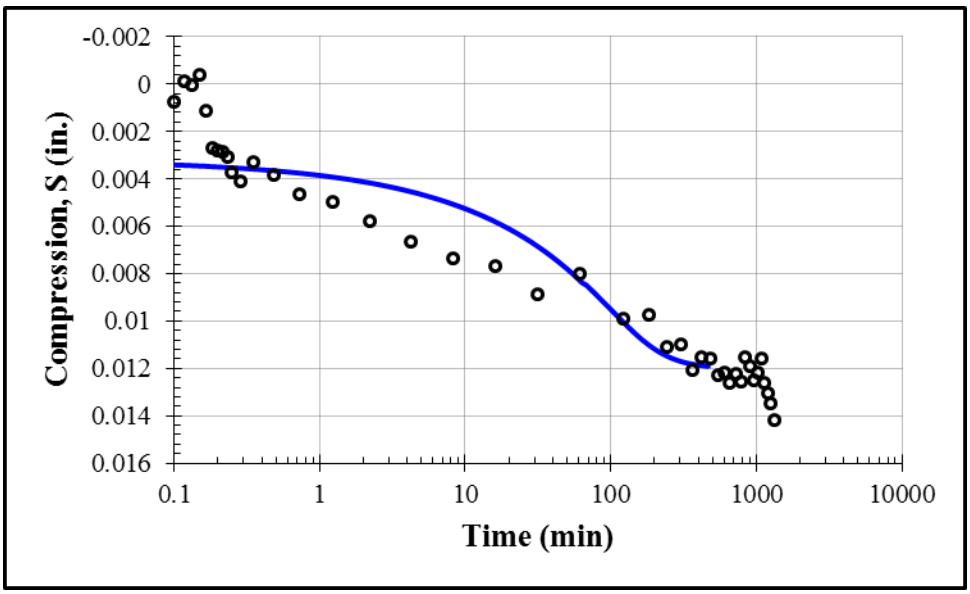

First Loading: 4000 psf				
S_0 (in.)	S_{100} (in.)	c_v (in^2/min)	k (ft/day)	t_{50} (min)
0.0178	0.0270	0.0008	3.0×10^{-8}	33

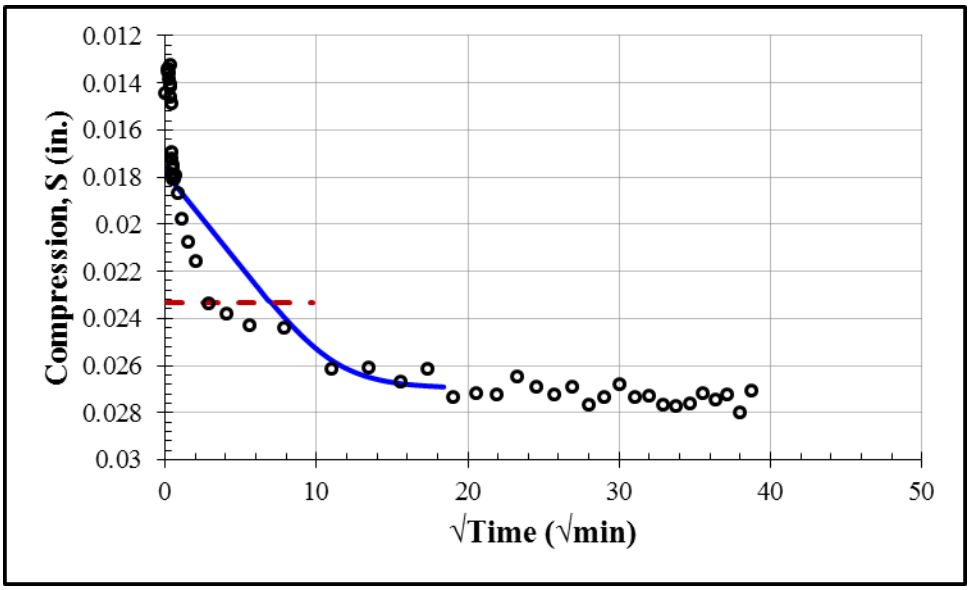

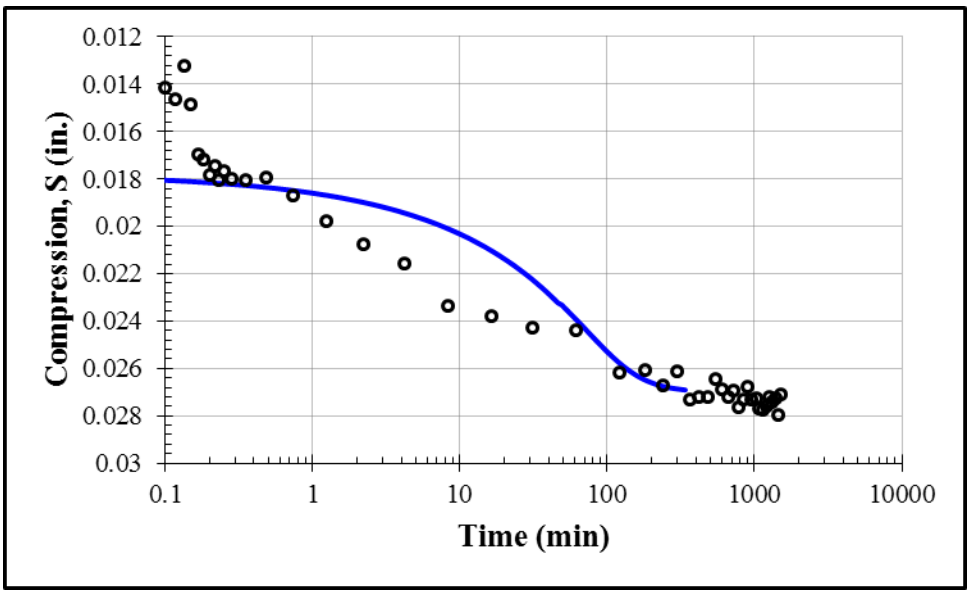

First Loading: 8000 psf				
S_0 (in.)	S_{100} (in.)	c_v (in^2/min)	k (ft/day)	t_{50} (min)
0.0328	0.0448	0.0007	1.7 x 10^{-8}	37

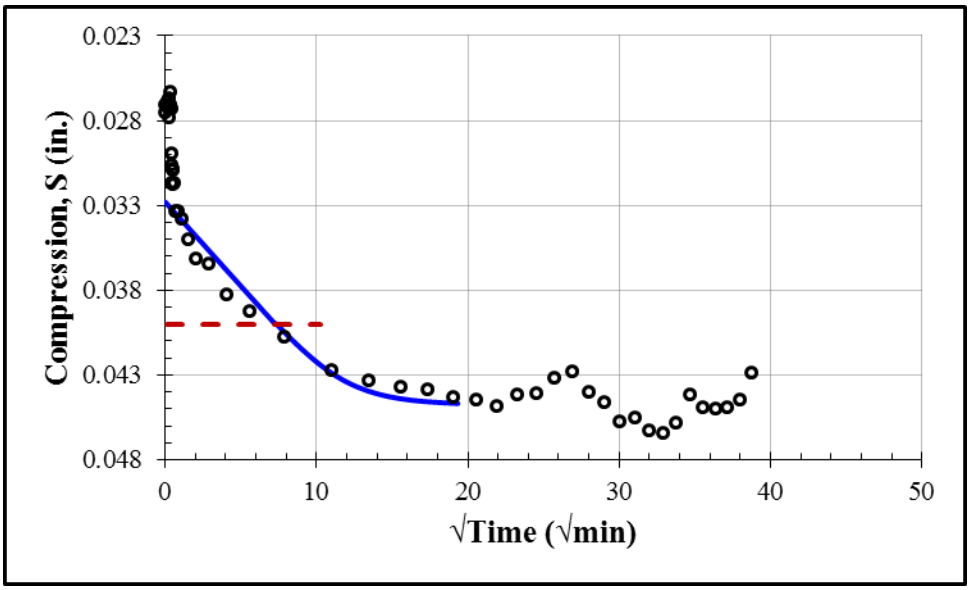

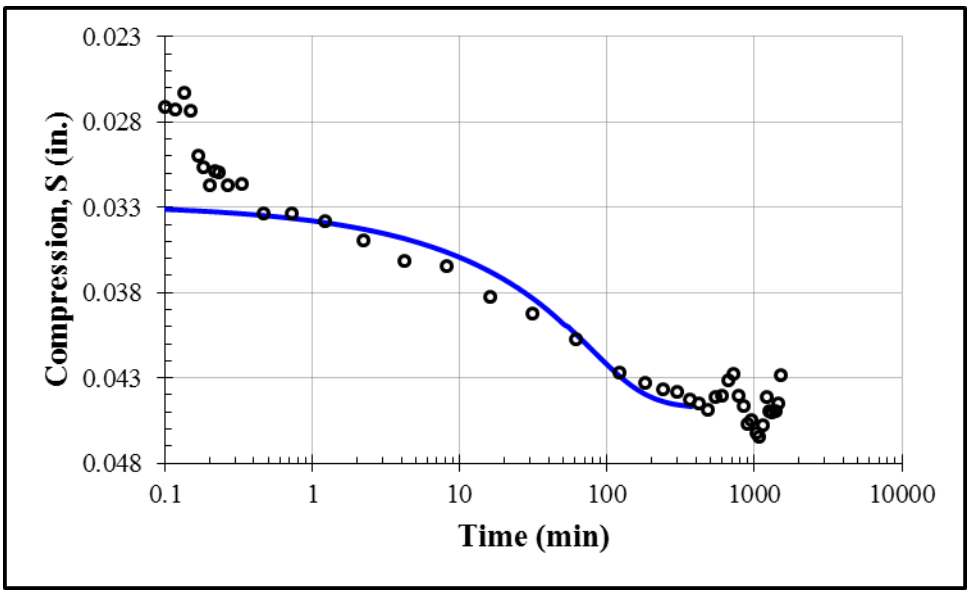

First Loading: 16000 psf				
S_0 (in.)	S_{100} (in.)	c_v (in^2/min)	k (ft/day)	t_{50} (min)
0.0485	0.0668	0.00035	6.3 x 10^{-9}	70

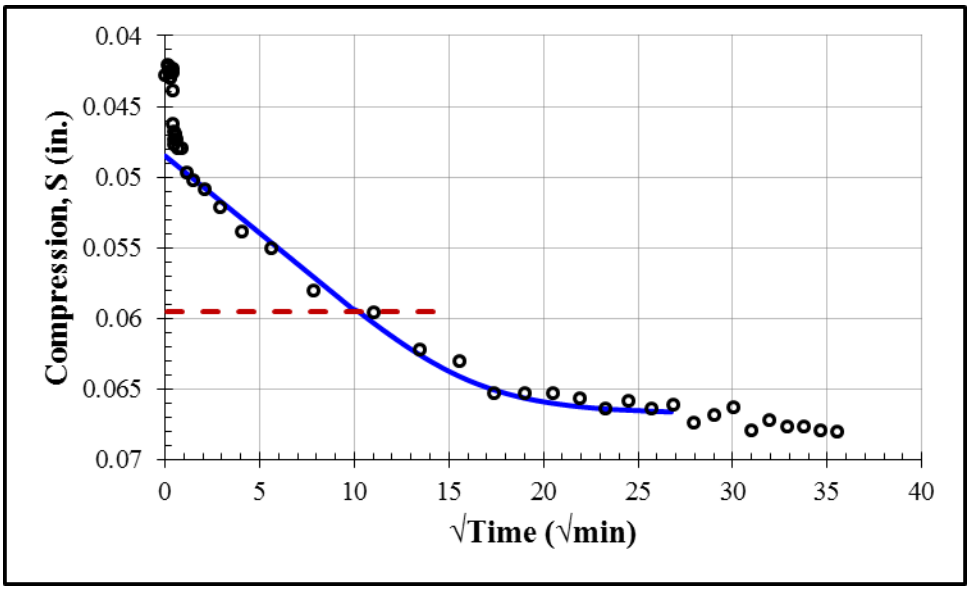

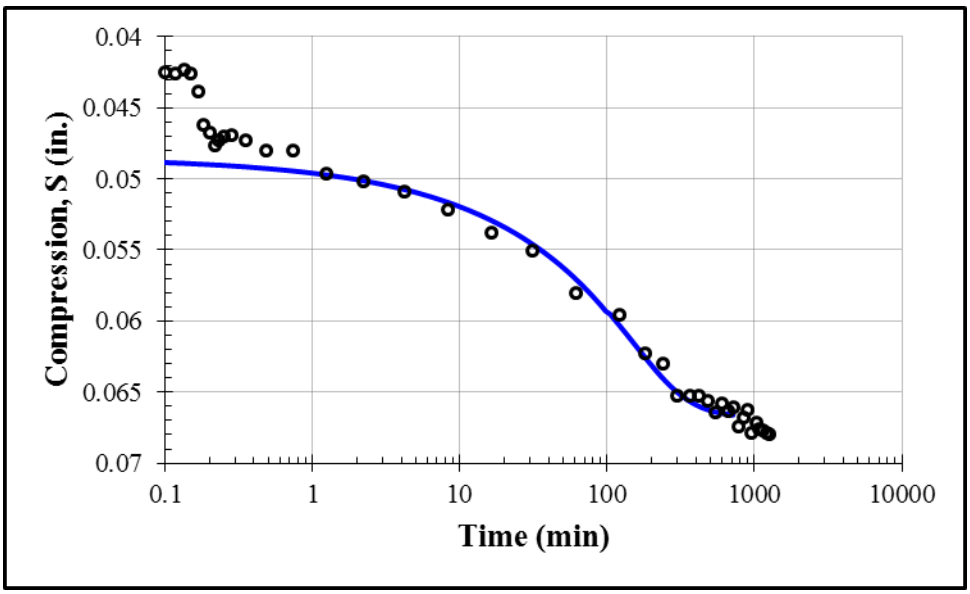

First Loading: 32000 psf				
S_0 (in.)	S_{100} (in.)	c_v (in^2/min)	k (ft/day)	t_{50} (min)
0.0738	0.0948	0.00026	2.6 x 10^{-9}	88

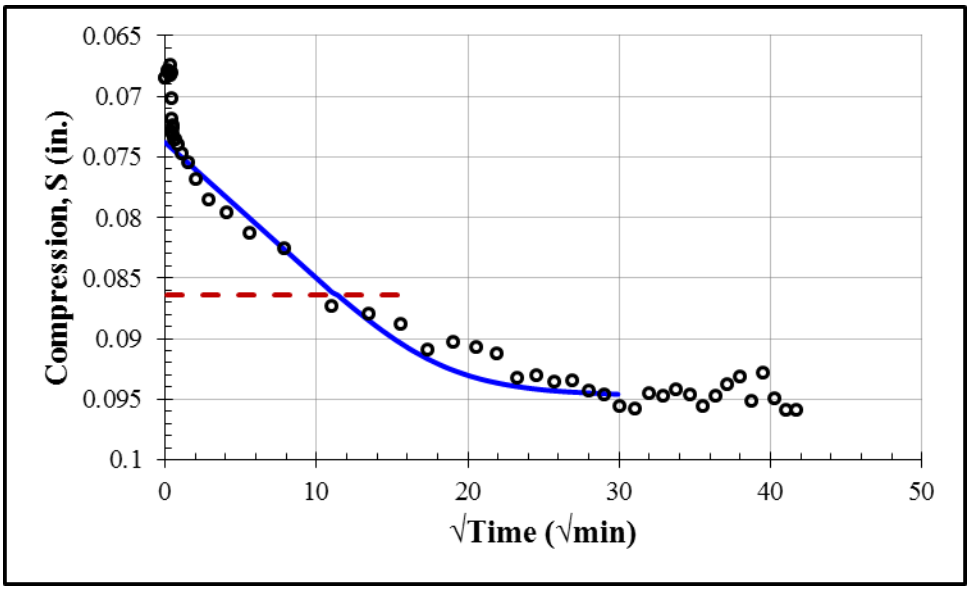

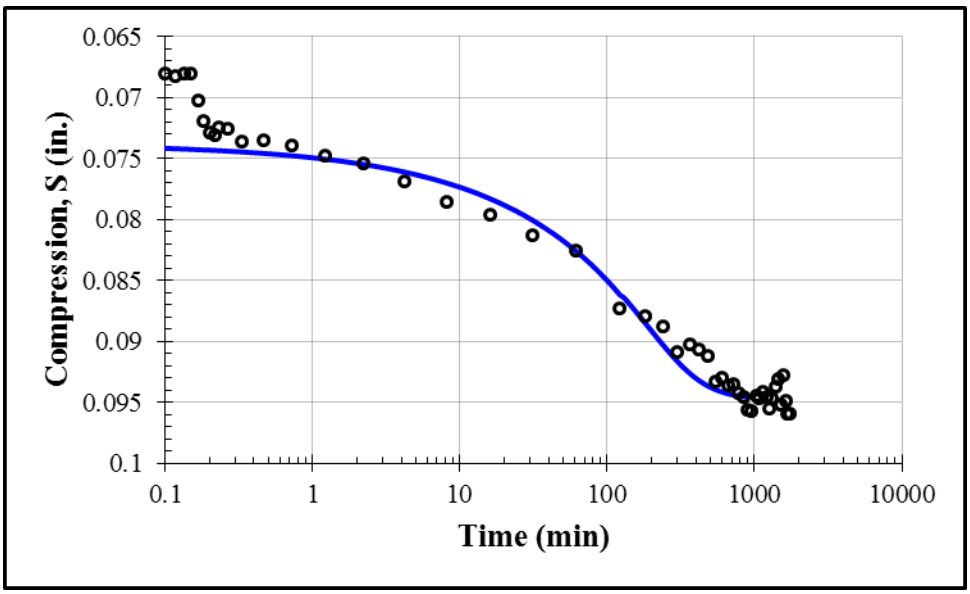

First Loading: 64000 psf				
S_0 (in.)	S_{100} (in.)	c_v (in^2/min)	k (ft/day)	t_{50} (min)
0.1025	0.1248	0.00025	1.3×10^{-9}	84

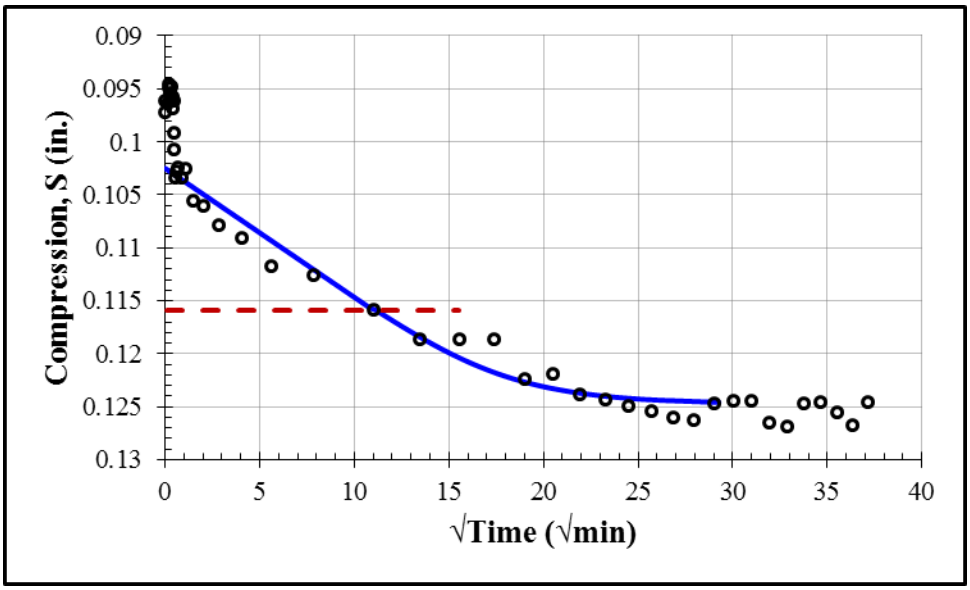

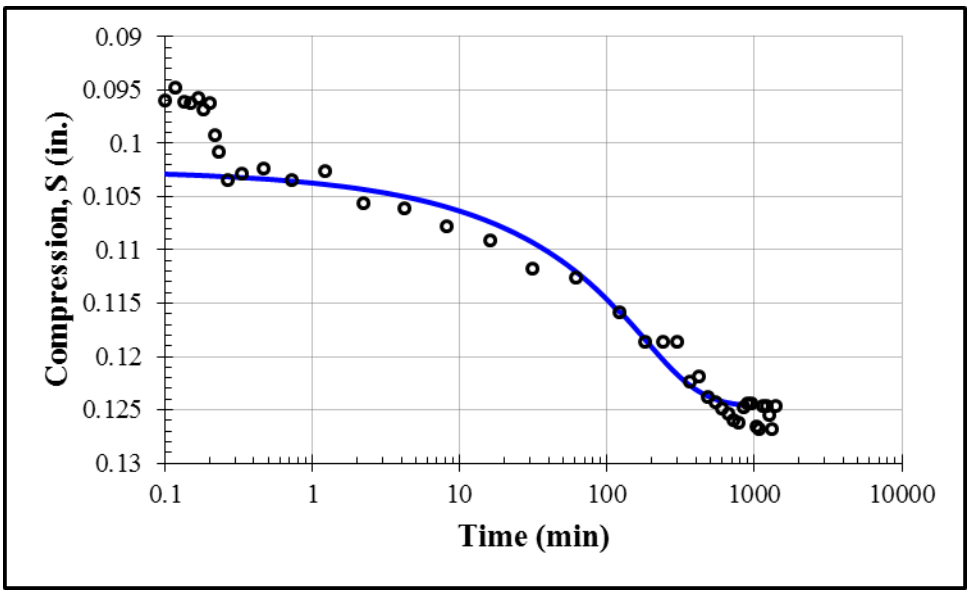

First Unloading: 16000 psf				
S_0 (in.)	S_{100} (in.)	c_v (in^2/min)	k (ft/day)	t_{50} (min)
0.1195	0.1050	0.00025	5.6 x 10^{-10}	76

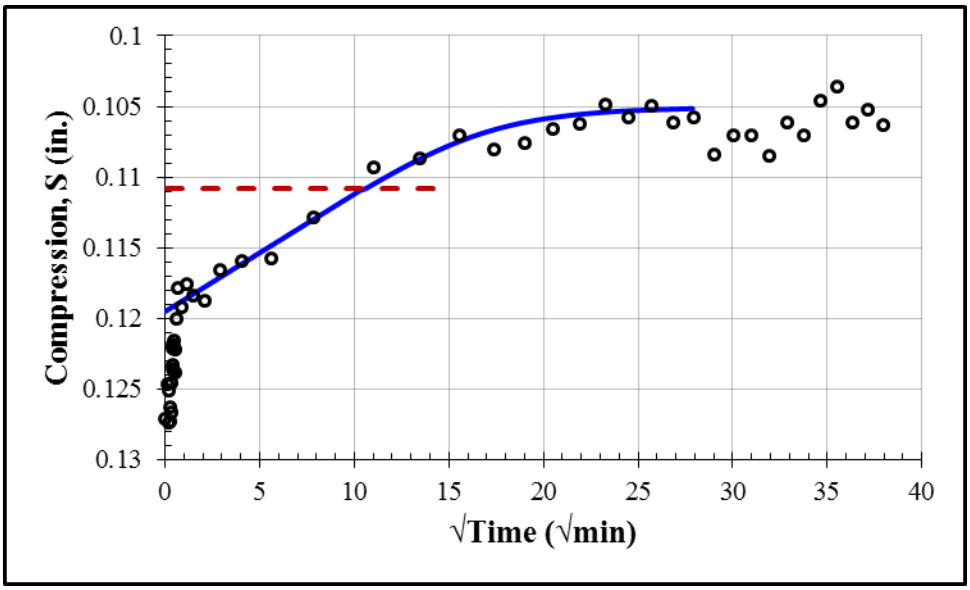

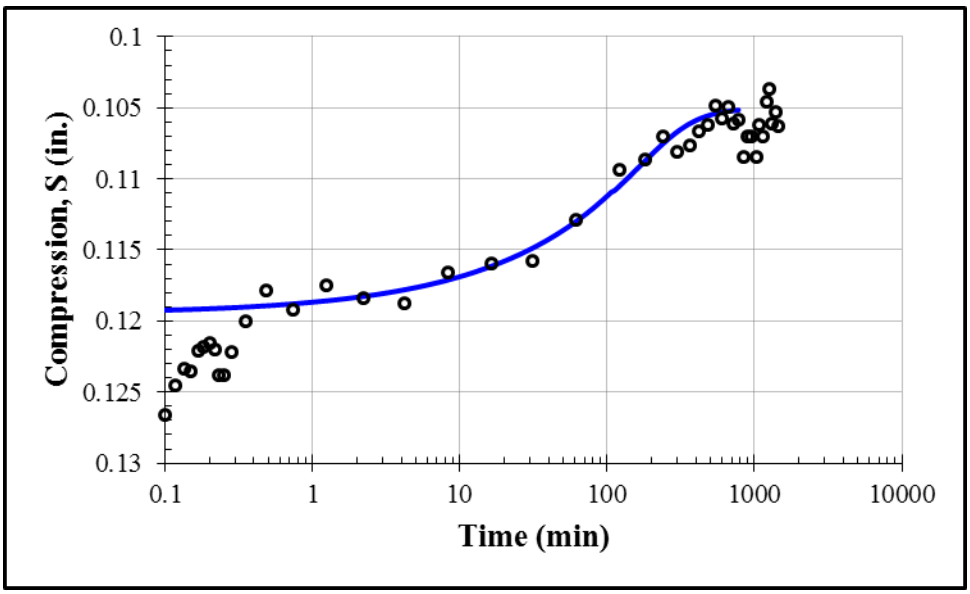

First Unloading: 4000 psf				
S_0 (in.)	S_{100} (in.)	c_v (in^2/min)	k (ft/day)	t_{50} (min)
0.1015	0.0865	0.00025	2.4 x 10^{-9}	81

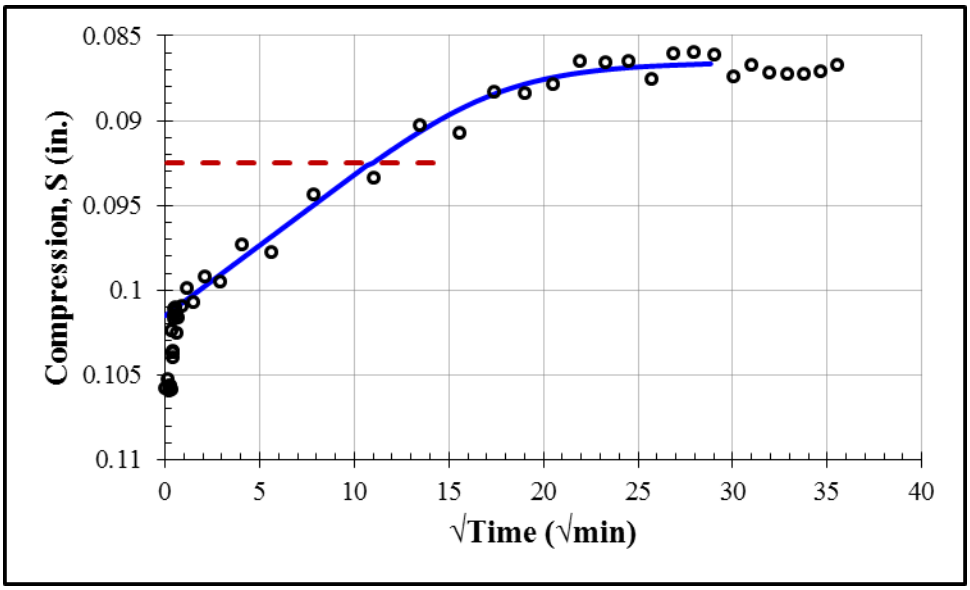

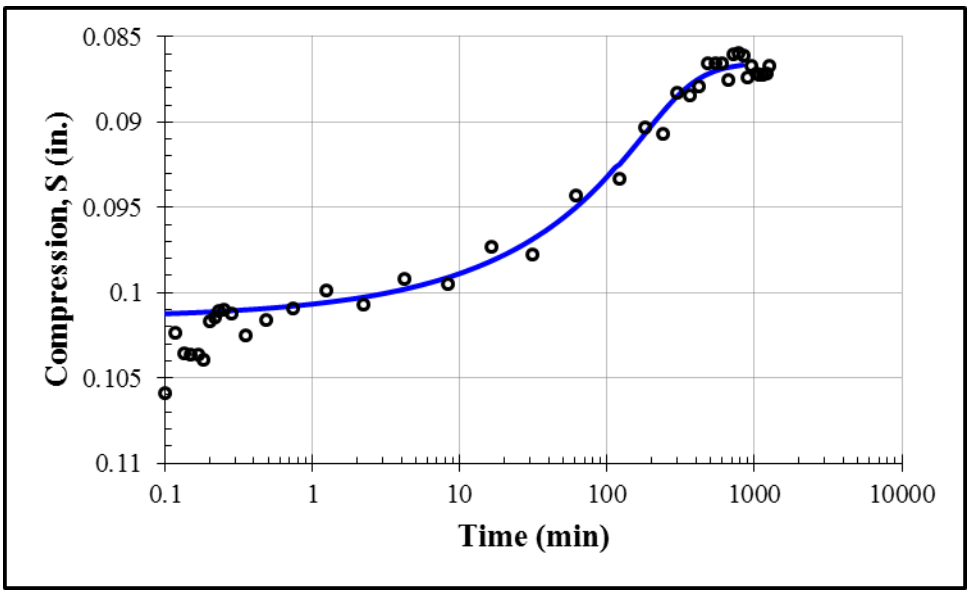

First Unloading: 1000 psf				
S_0 (in.)	S_{100} (in.)	c_v (in^2/min)	k (ft/day)	t_{50} (min)
0.0848	0.0608	0.00011	6.8 x 10^{-9}	197

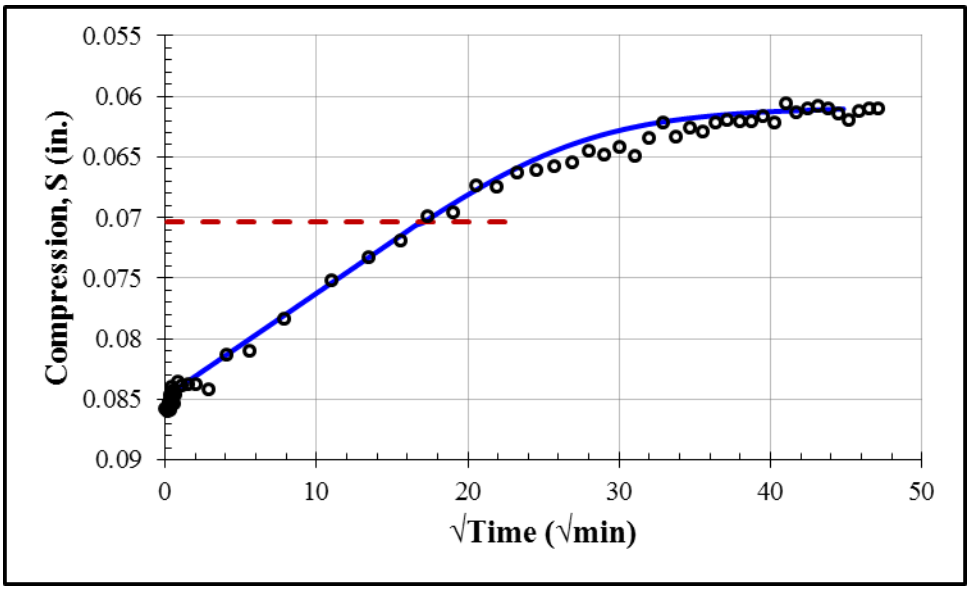

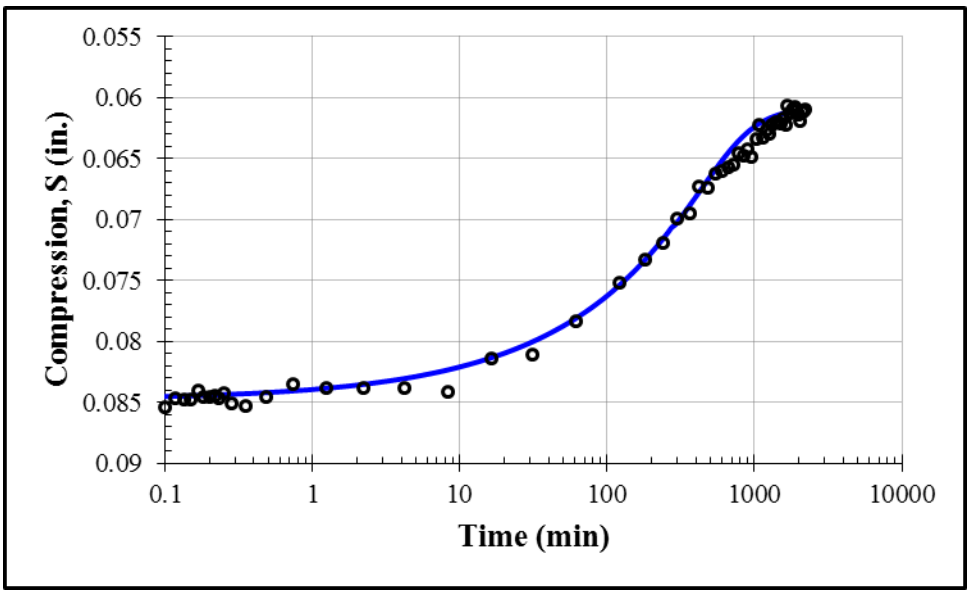

Second Loading: 2000 psf				
S_0 (in.)	S_{100} (in.)	c_v (in^2/min)	k (ft/day)	t_{50} (min)
0.0596	0.0600	0.00016	5.0×10^{-10}	146

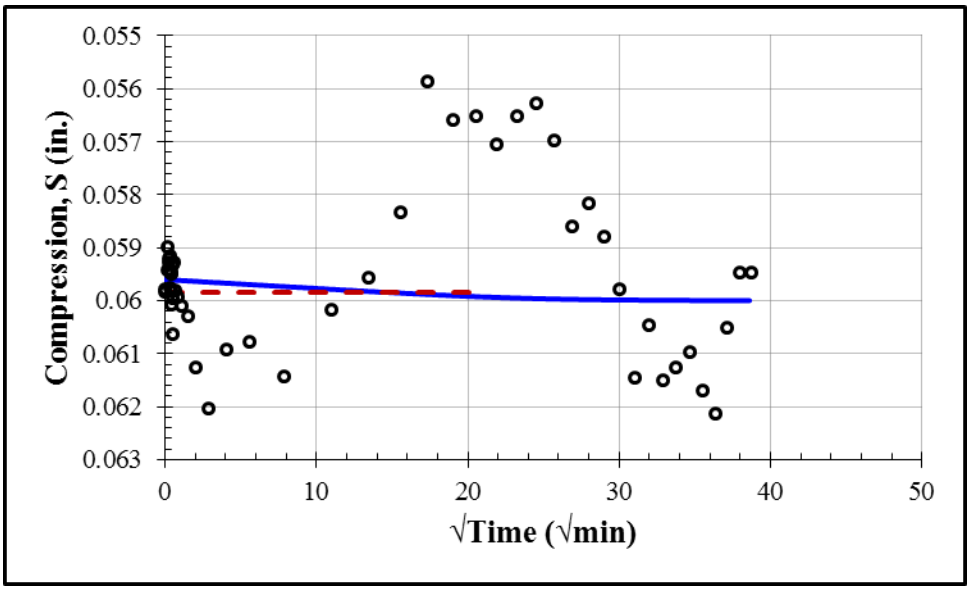

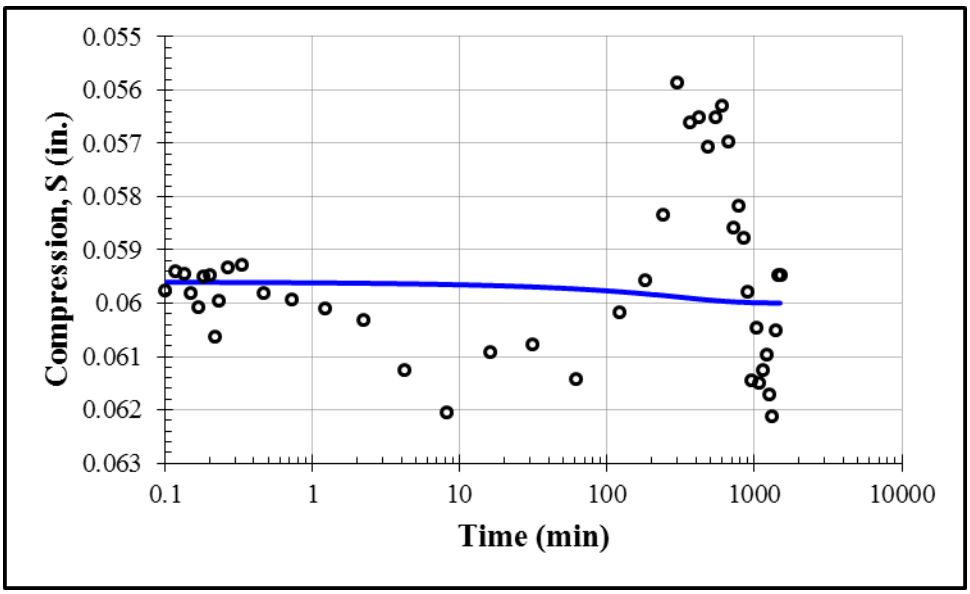

Second Loading: 4000 psf				
S_0 (in.)	S_{100} (in.)	c_v (in^2/min)	k (ft/day)	t_{50} (min)
0.0610	0.0693	0.00008	2.6 x 10^{-9}	293

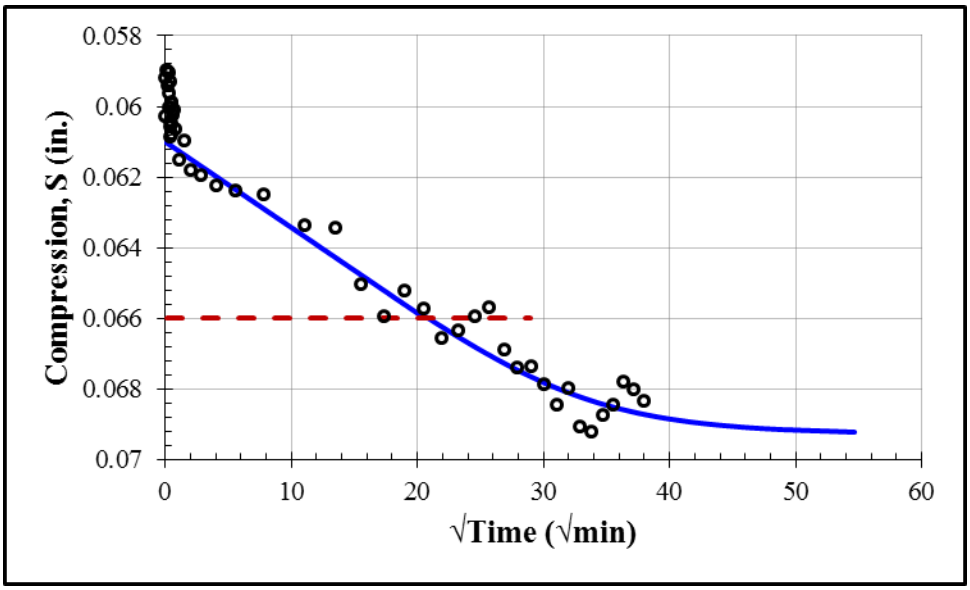

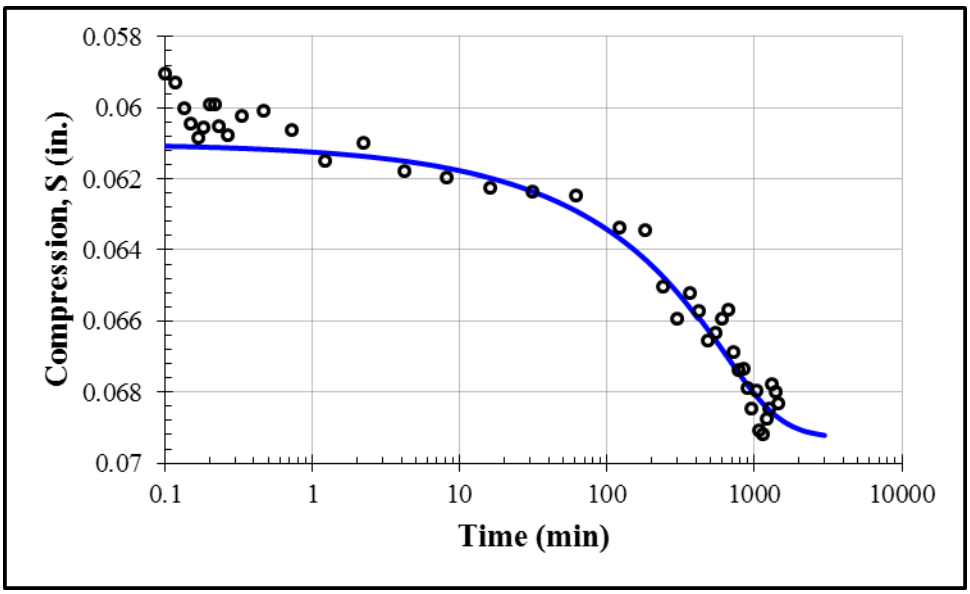

Second Loading: 8000 psf				
S_0 (in.)	S_{100} (in.)	c_v (in^2/min)	k (ft/day)	t_{50} (min)
0.0696	0.0835	0.00009	2.4 x 10^{-9}	254

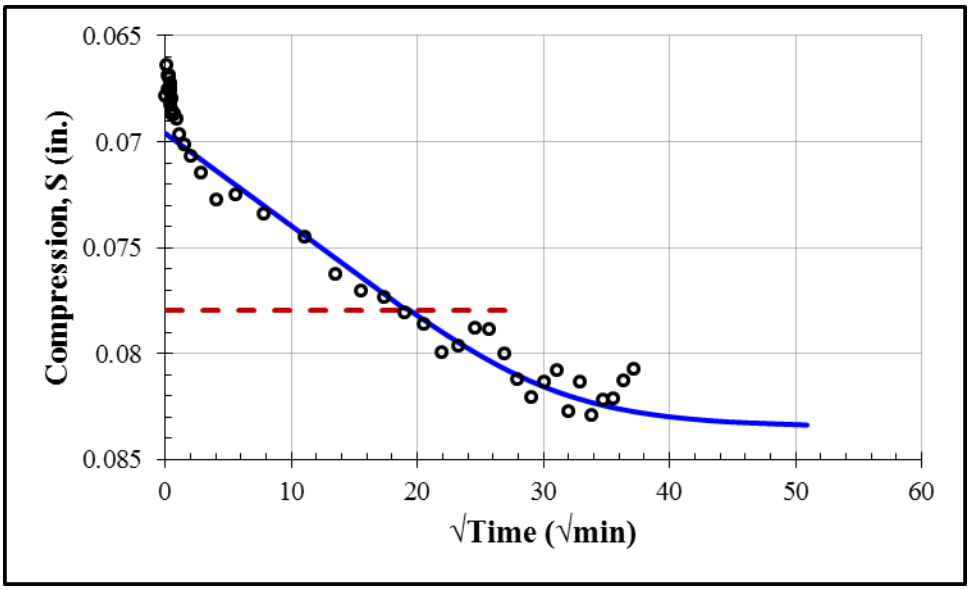

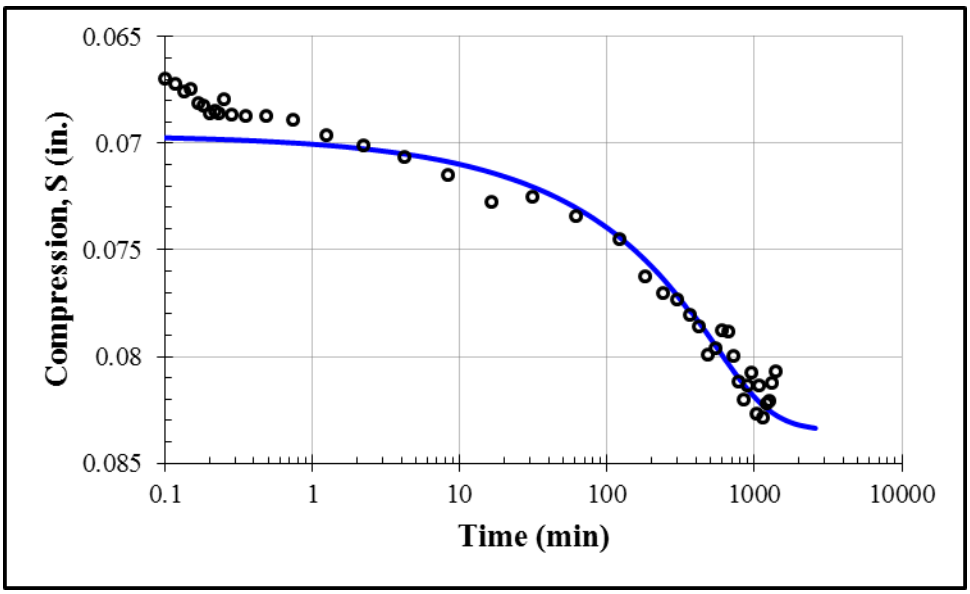

Second Loading: 16000 psf				
S_0 (in.)	S_{100} (in.)	c_v (in^2/min)	k (ft/day)	t_{50} (min)
0.0829	0.0959	0.00015	1.9 x 10^{-9}	147

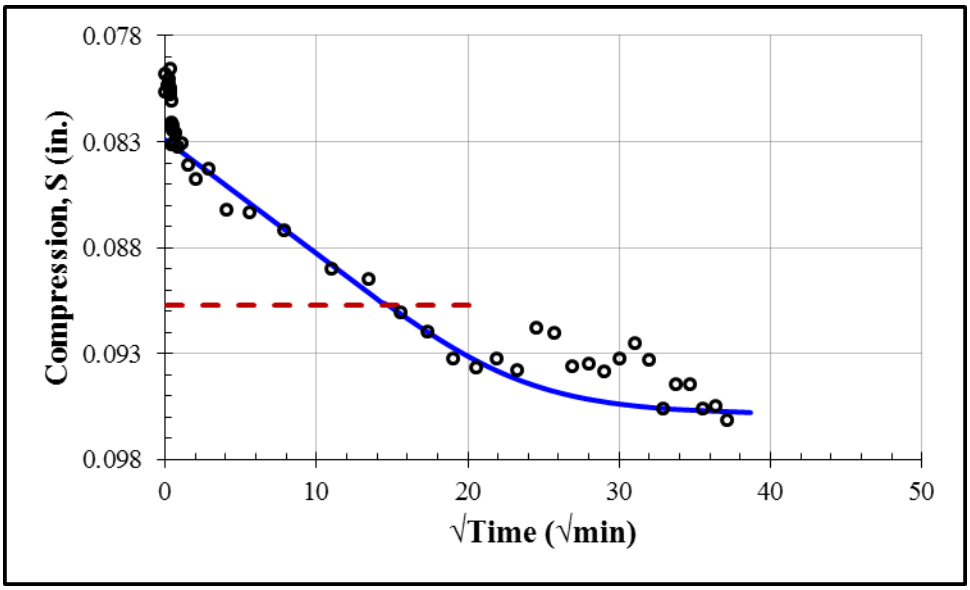

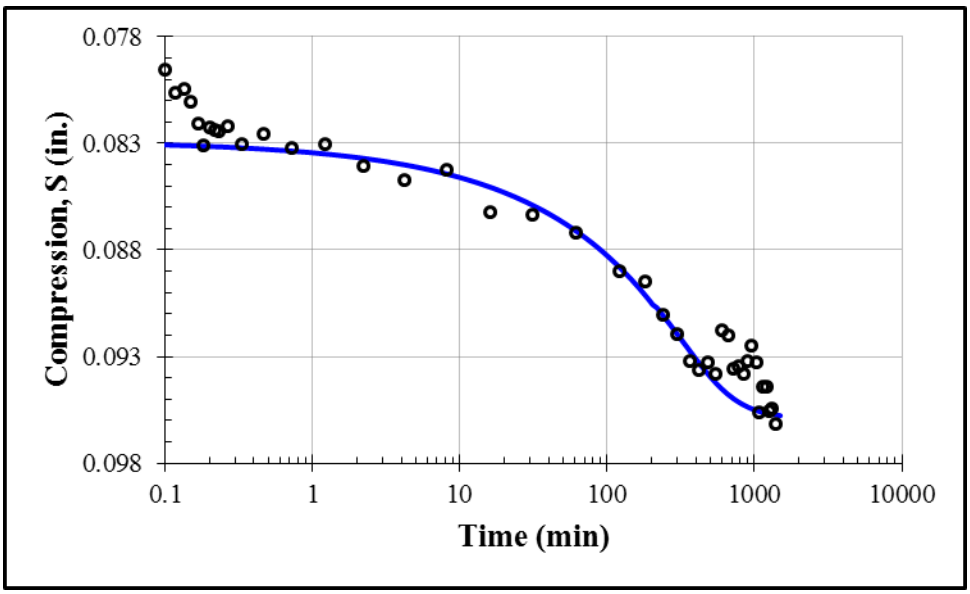

Second Loading: 32000 psf				
S_0 (in.)	S_{100} (in.)	c_v (in^2/min)	k (ft/day)	t_{50} (min)
0.0985	0.1146	0.00015	1.1 x 10^{-9}	140

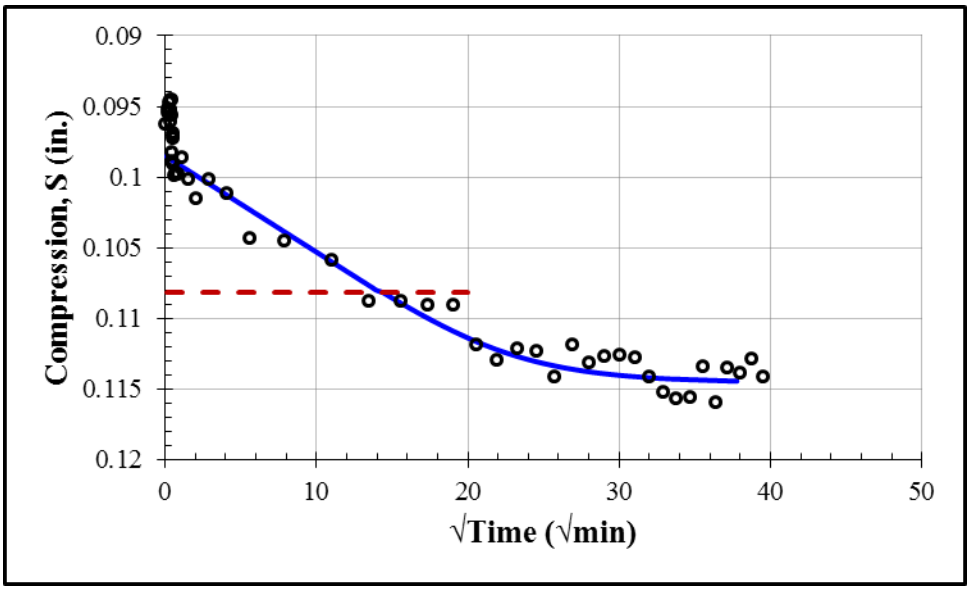

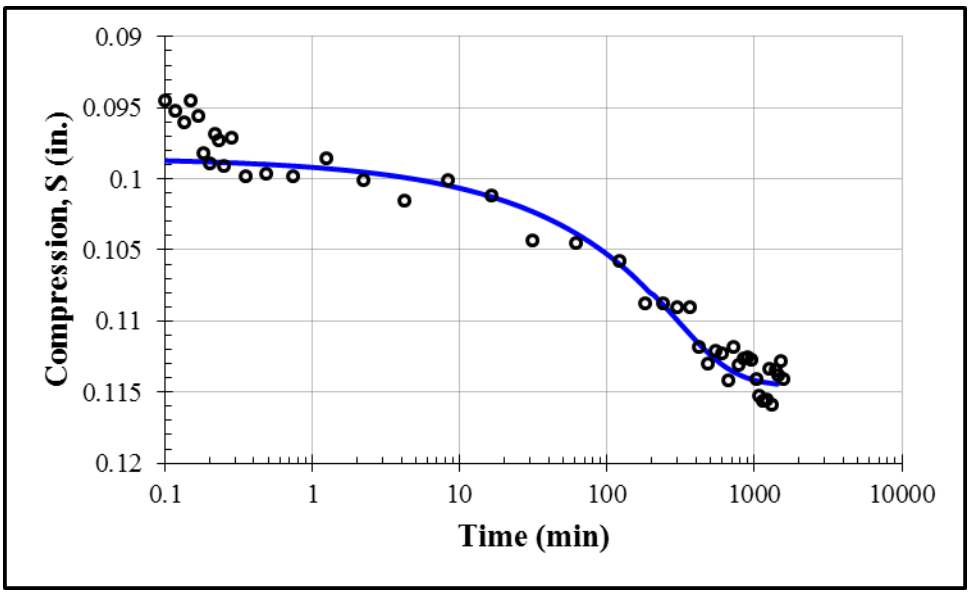

Second Loading: 64000 psf				
S_0 (in.)	S_{100} (in.)	c_v (in^2/min)	k (ft/day)	t_{50} (min)
0.1199	0.1338	0.0002	6.4 x 10^{-10}	99

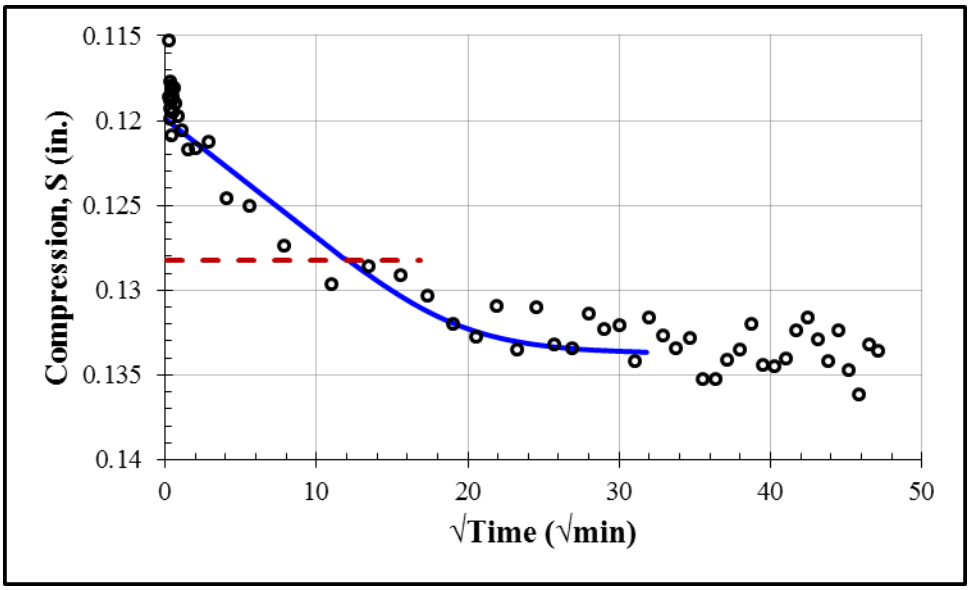

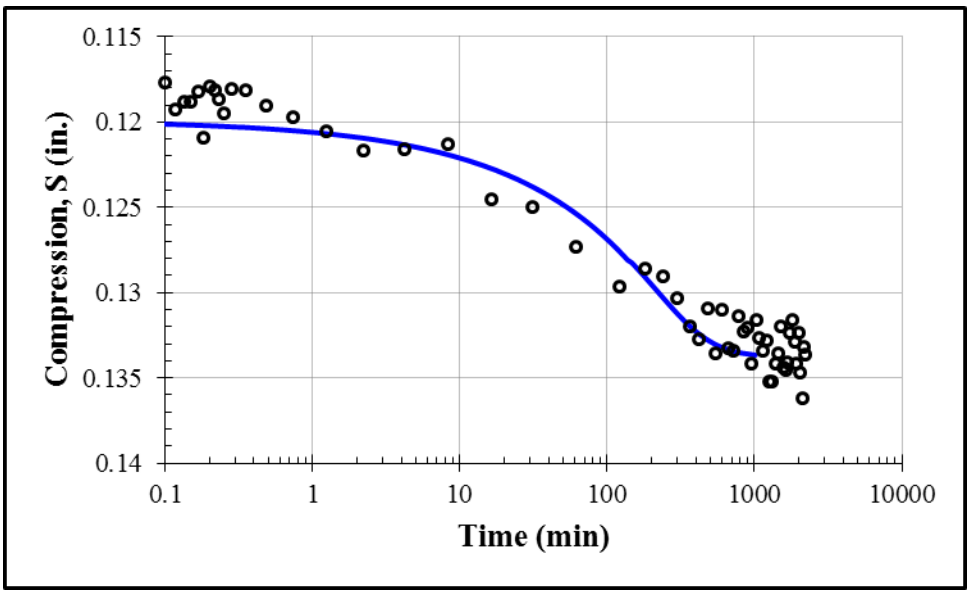

Second Unloading: 16000 psf				
S_0 (in.)	S_{100} (in.)	c_v (in^2/min)	k (ft/day)	t_{50} (min)
0.1295	0.1140	0.00035	8.4×10^{-10}	53

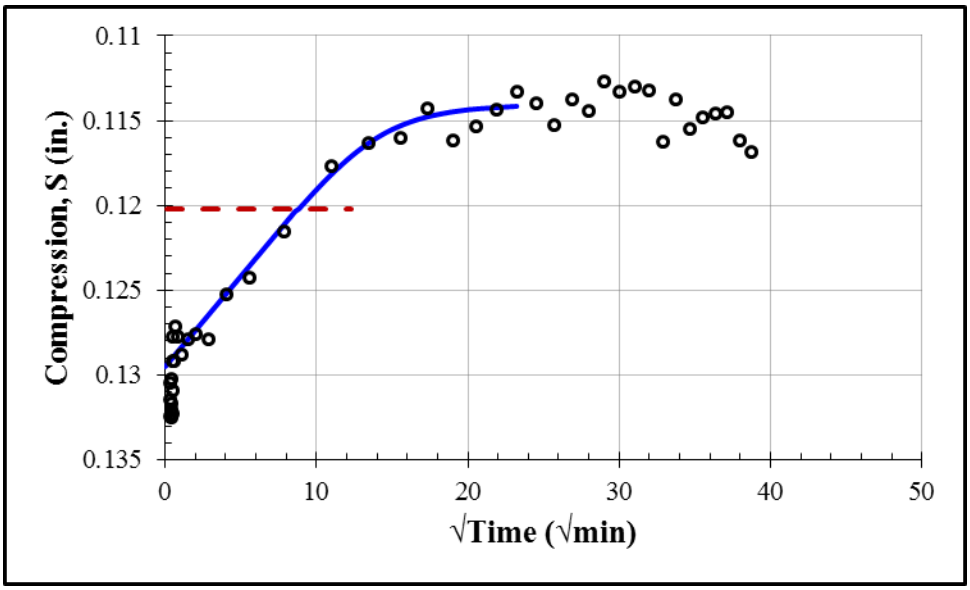

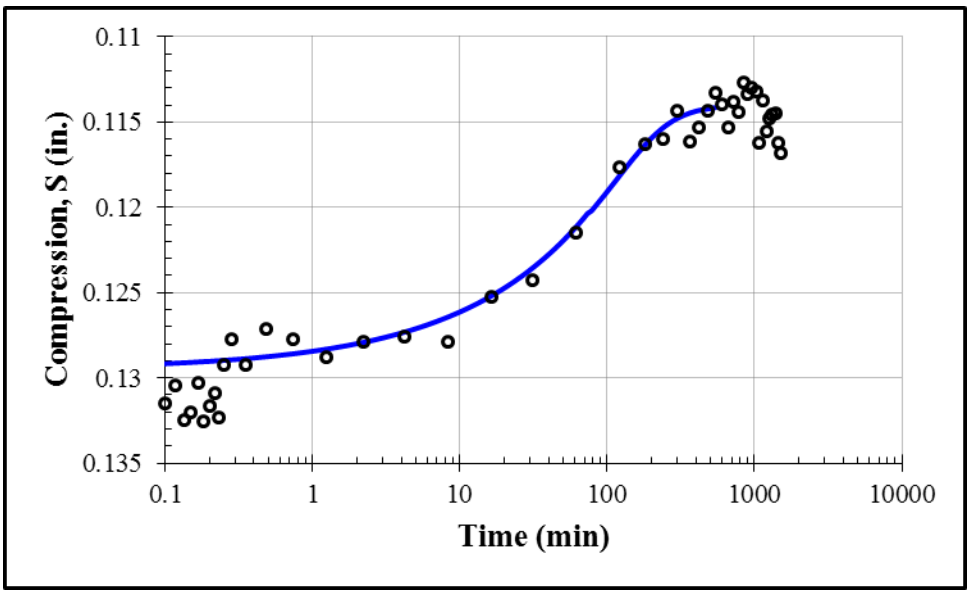

Second Unloading: 4000 psf				
S_0 (in.)	S_{100} (in.)	c_v (in^2/min)	k (ft/day)	t_{50} (min)
0.1135	0.0895	0.00025	3.8 x 10^{-9}	79

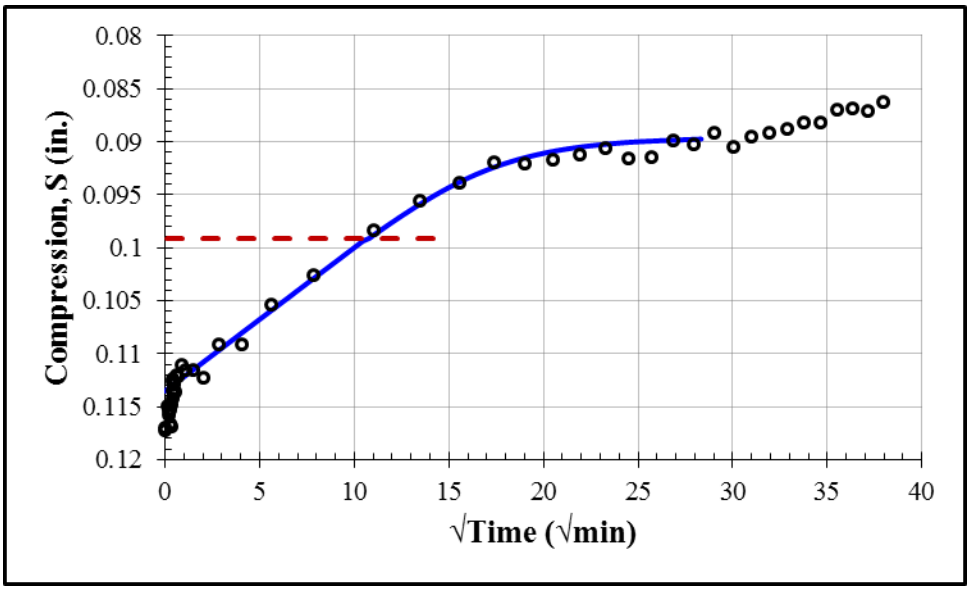

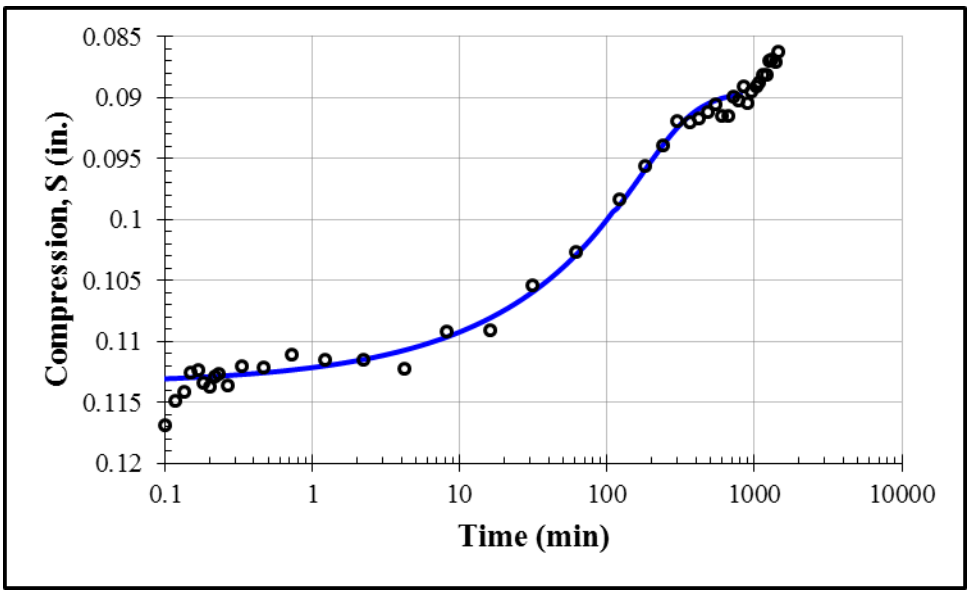

Second Unloading: 1000 psf				
S_0 (in.)	S_{100} (in.)	c_v (in^2/min)	k (ft/day)	t_{50} (min)
0.0832	0.0615	0.00015	8.4 x 10^{-9}	145

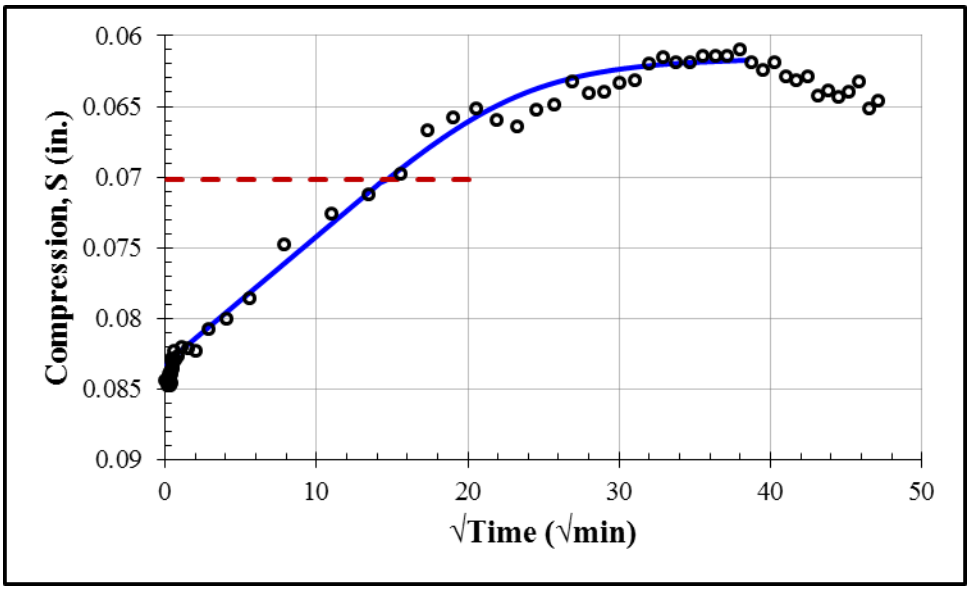

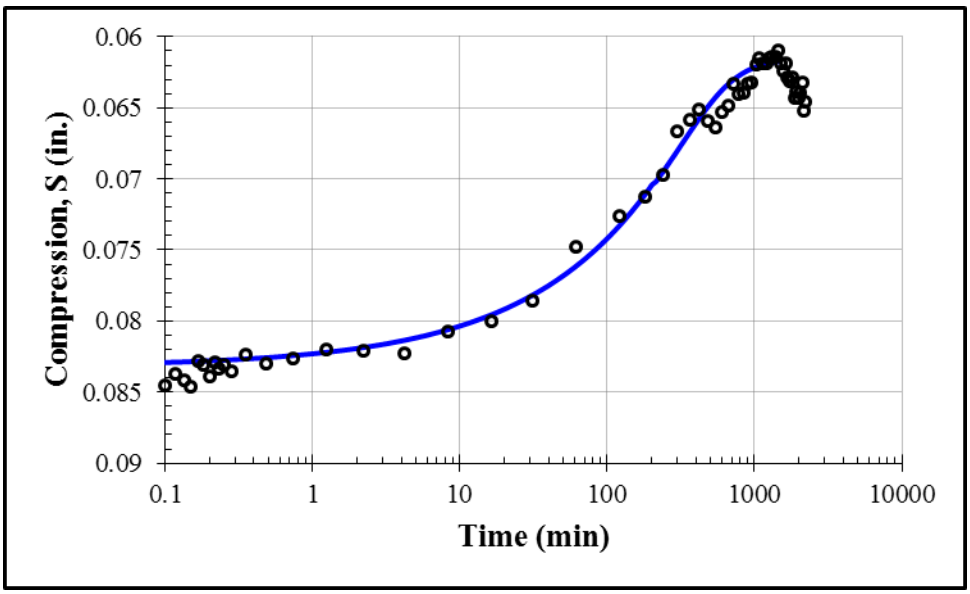

Second Unloading: 250 psf				
S_0 (in.)	S_{100} (in.)	c_v (in^2/min)	k (ft/day)	t_{50} (min)
0.0648	0.0482	0.00015	2.6×10^{-8}	154

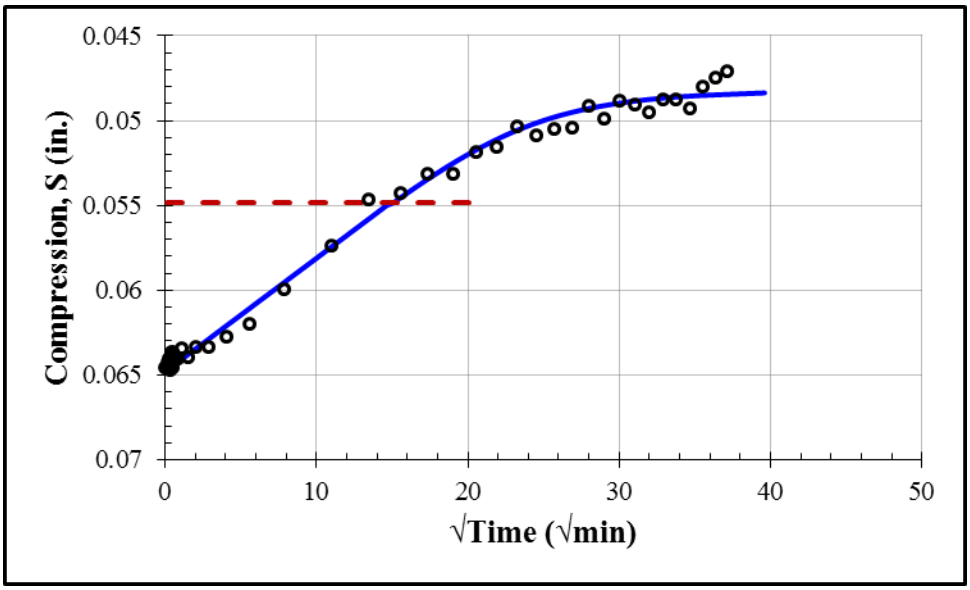

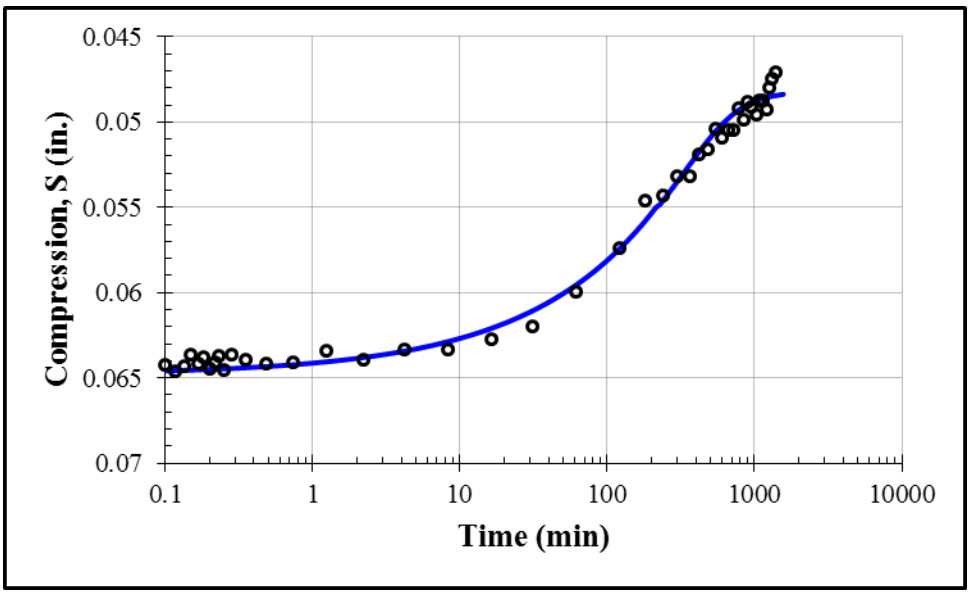

Appendix D: Consolidation Test 3

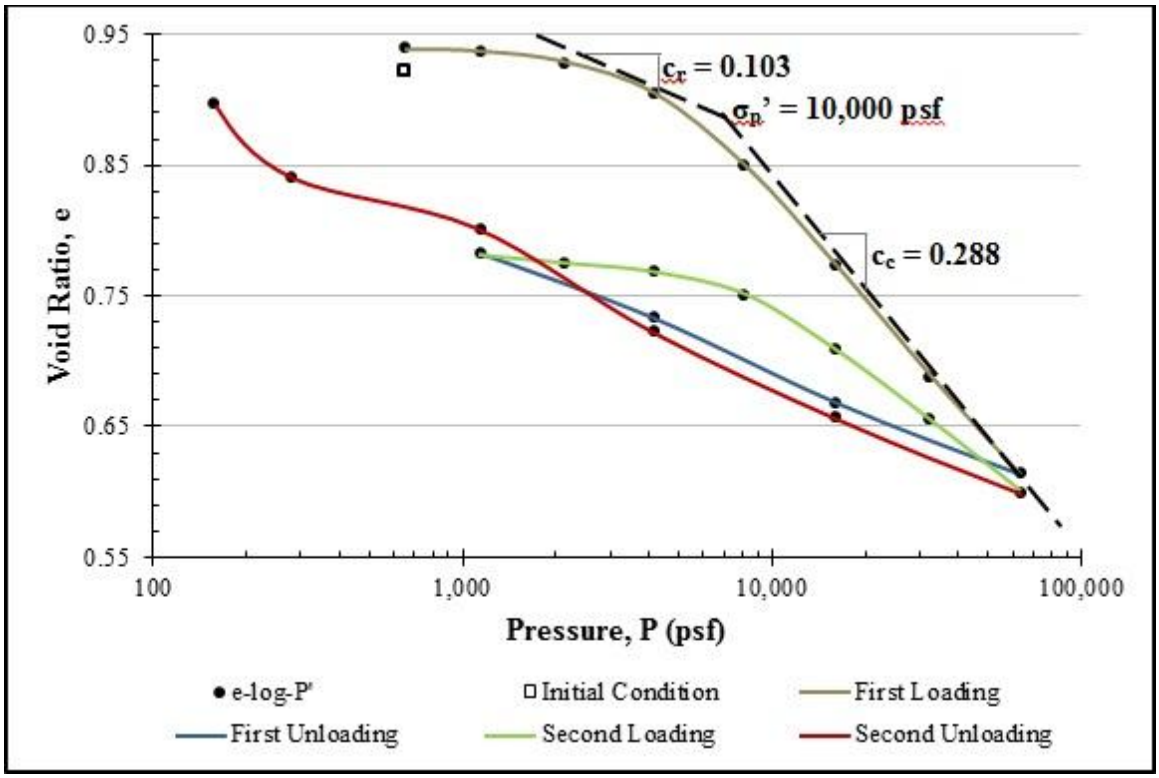

$$c_c = -\frac{e_2 - e_1}{\log(\sigma_2 / \sigma_1)} = -\frac{0.641 - 0.842}{\log(50000/10000)} = 0.288$$

$$c_r = -\frac{e_2 - e_1}{\log(\sigma_2 / \sigma_1)} = -\frac{0.901 - 0.942}{\log(5000/2000)} = 0.103$$

$$R_c = \frac{c_c}{1 + e_0} = \frac{0.288}{1 + 0.9019} = 0.151$$

$$R_r = \frac{c_r}{1 + e_0} = \frac{0.103}{1 + 0.9019} = 0.054$$

Inundation: 625 psf				
S_0 (in.)	S_{100} (in.)	c_v (in^2/min)	k (ft/day)	t_{50} (min)
-0.0017	-0.0064	0.00033	2.1 x 10^{-5}	83

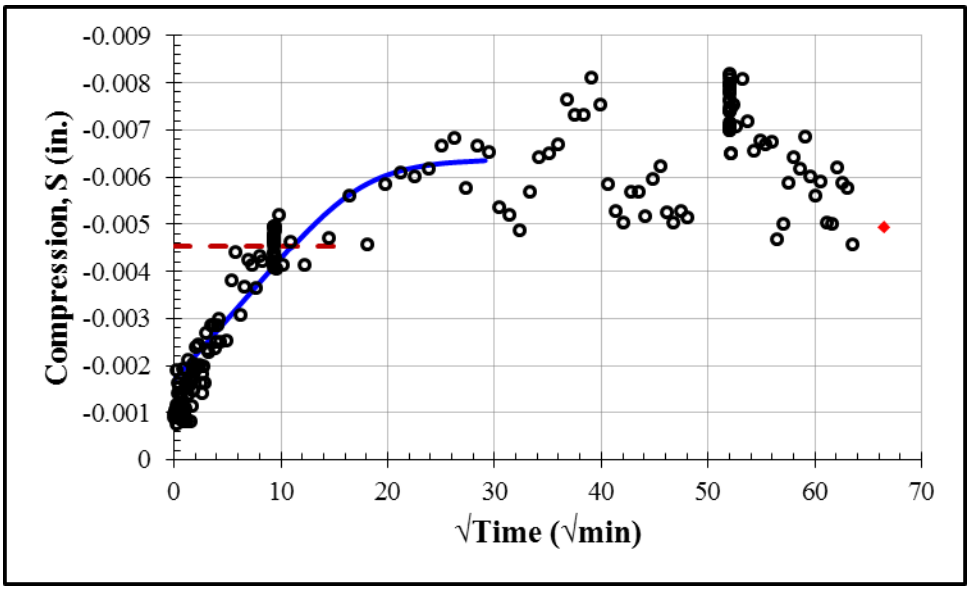

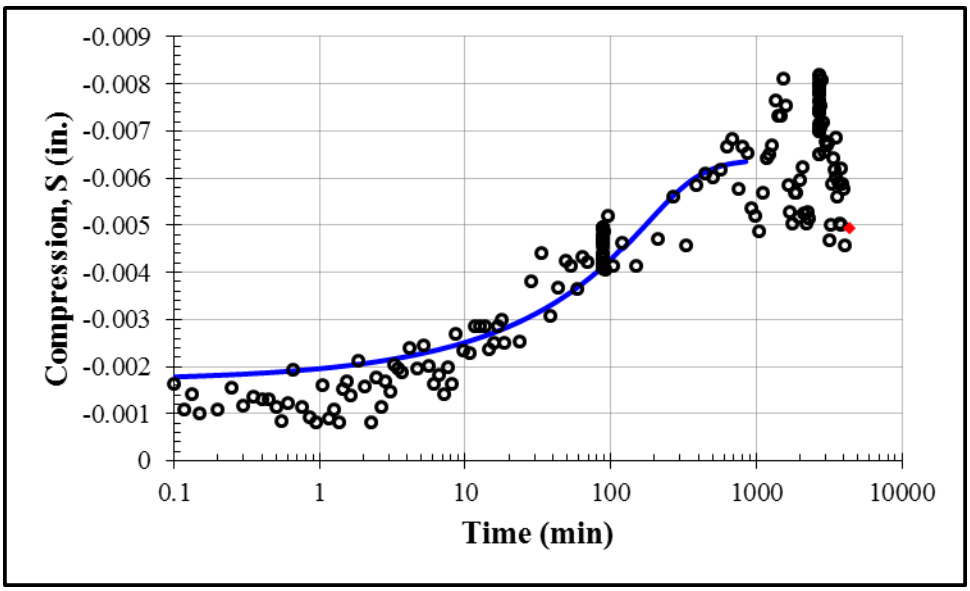

First Loading: 1125 psf				
S_0 (in.)	S_{100} (in.)	c_v (in^2/min)	k (ft/day)	t_{50} (min)
-0.0047	-0.00355	0.0002	3.9 x 10^{-9}	139

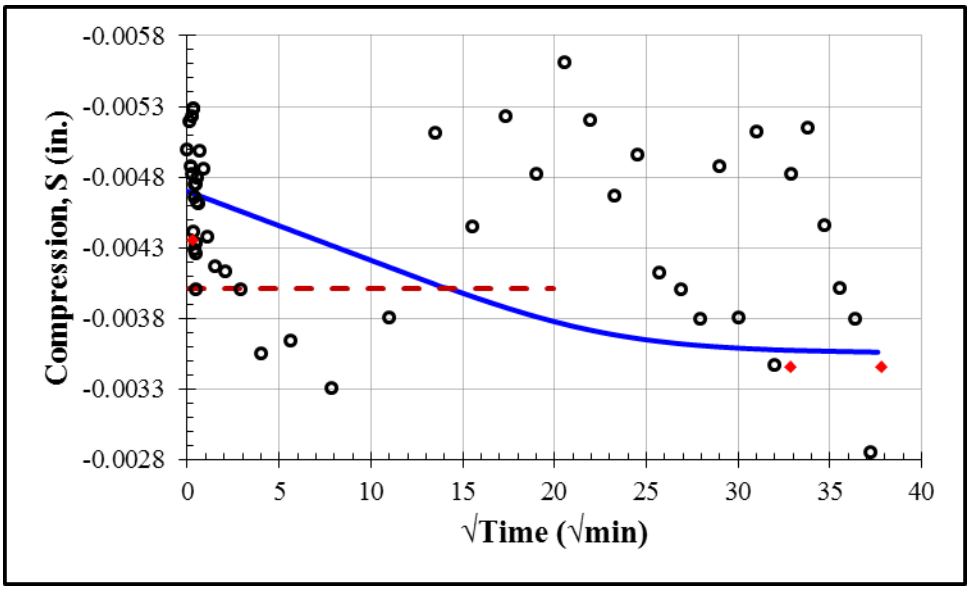

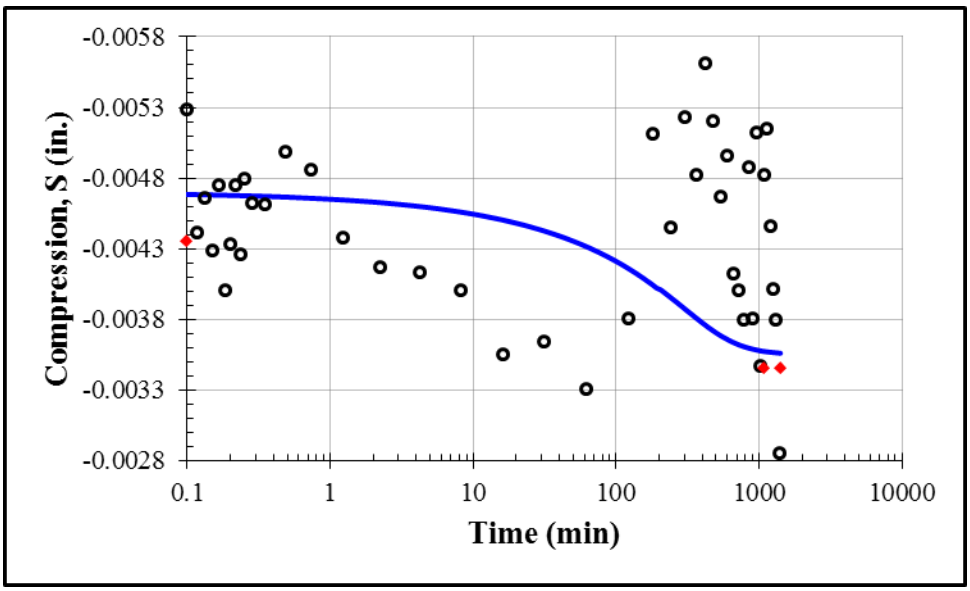

First Loading: 2125 psf				
S_0 (in.)	S_{100} (in.)	c_v (in^2/min)	k (ft/day)	t_{50} (min)
-0.0220	0.0023	0.00019	6.8 x 10^{-9}	145

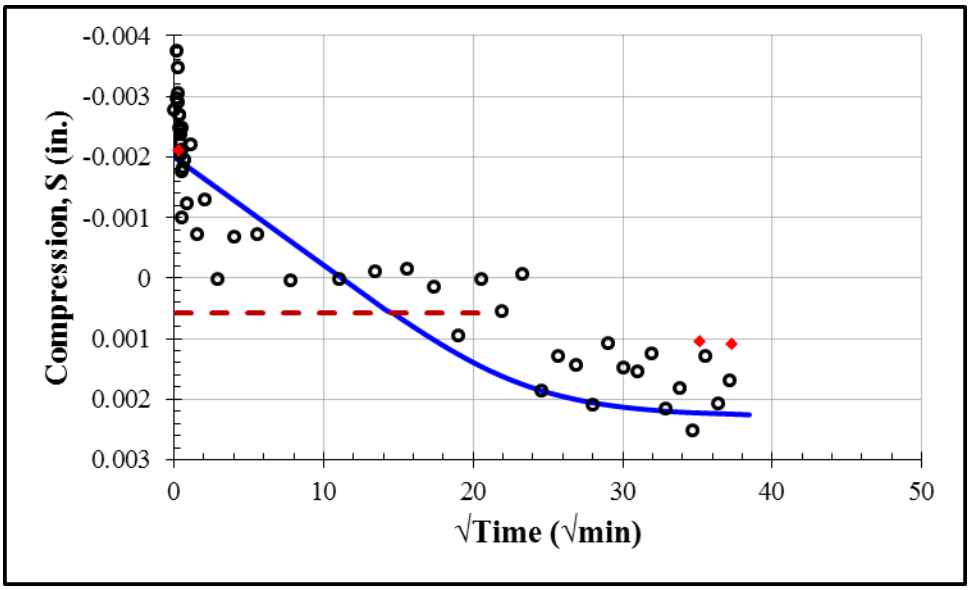

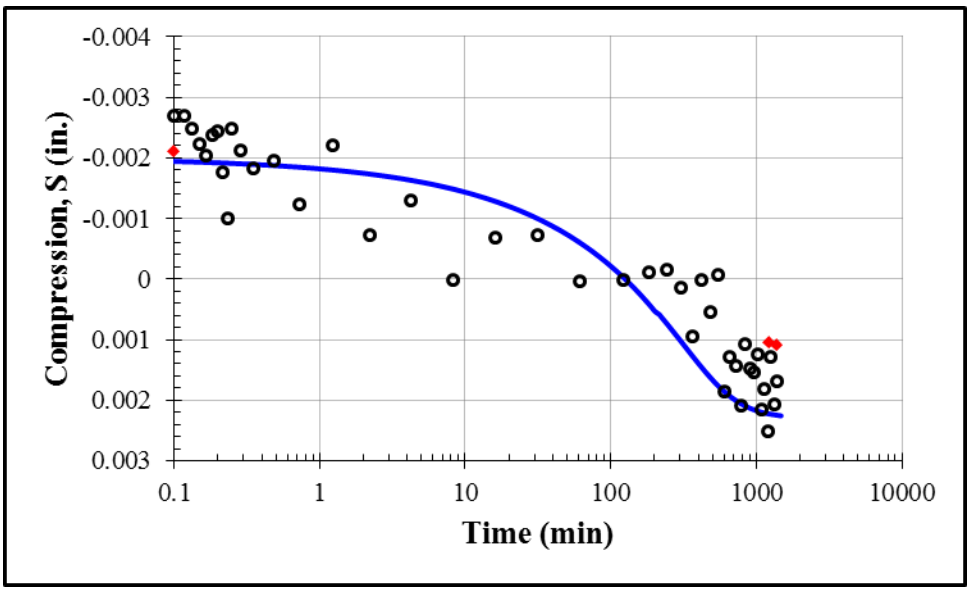

First Loading: 4125 psf				
S_0 (in.)	S_{100} (in.)	c_v (in^2/min)	k (ft/day)	t_{50} (min)
0.0040	0.0140	0.00015	6.2 x 10^{-9}	182

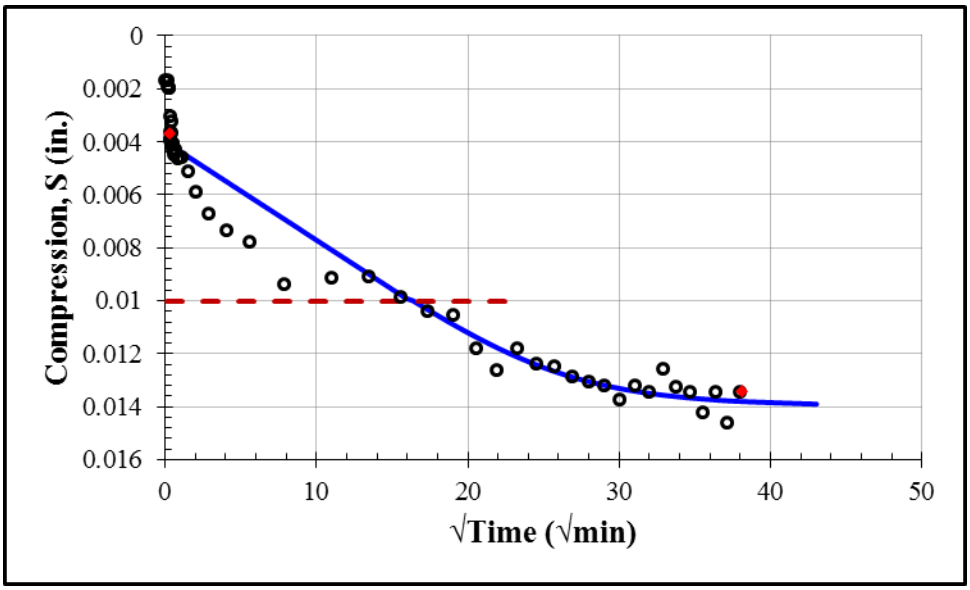

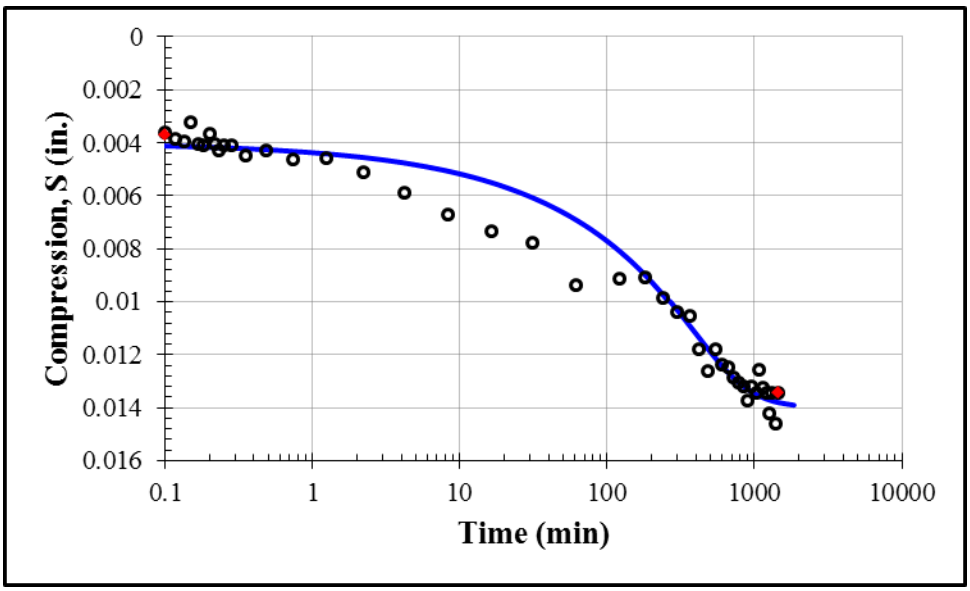

First Loading: 8125 psf				
S_0 (in.)	S_{100} (in.)	c_v (in^2/min)	k (ft/day)	t_{50} (min)
0.0172	0.0381	0.00018	7.7 x 10^{-9}	147

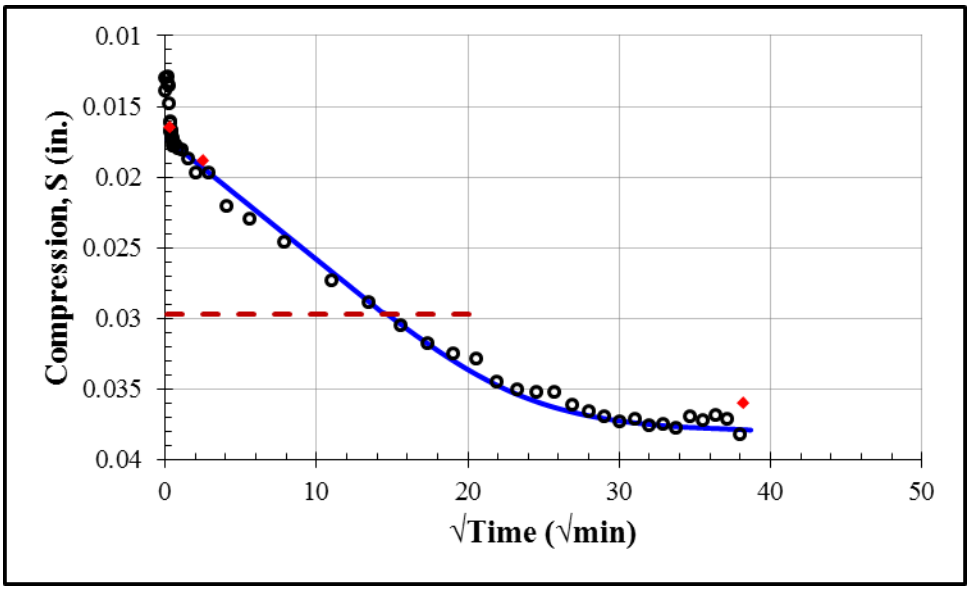

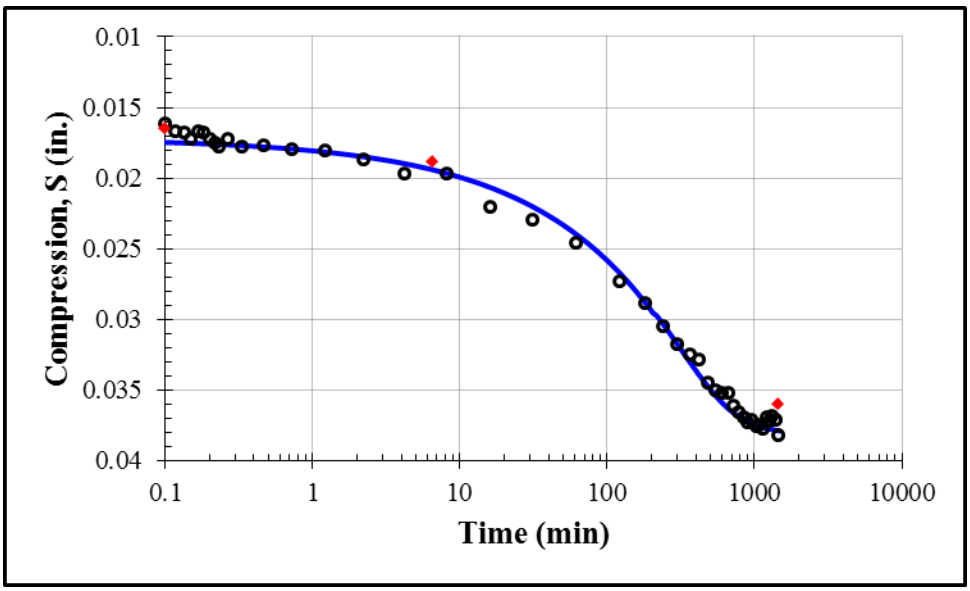

First Loading: 16125 psf				
S_0 (in.)	S_{100} (in.)	c_v (in^2/min)	k (ft/day)	t_{50} (min)
0.0412	0.0705	0.00014	4.1 x 10^{-9}	176

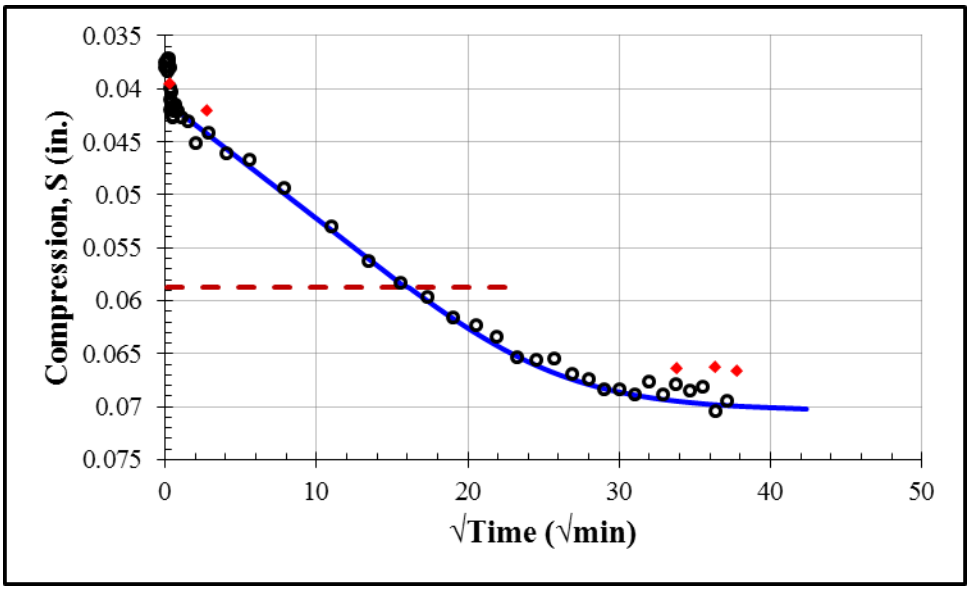

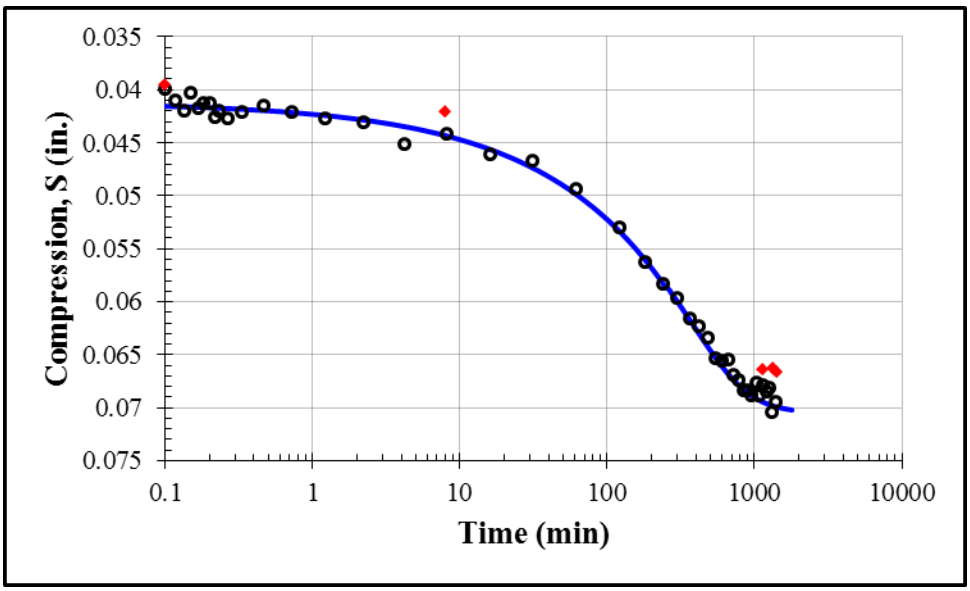

First Loading: 32125 psf				
S_0 (in.)	S_{100} (in.)	c_v (in^2/min)	k (ft/day)	t_{50} (min)
0.0721	0.1072	0.0001	1.7 x 10^{-9}	226

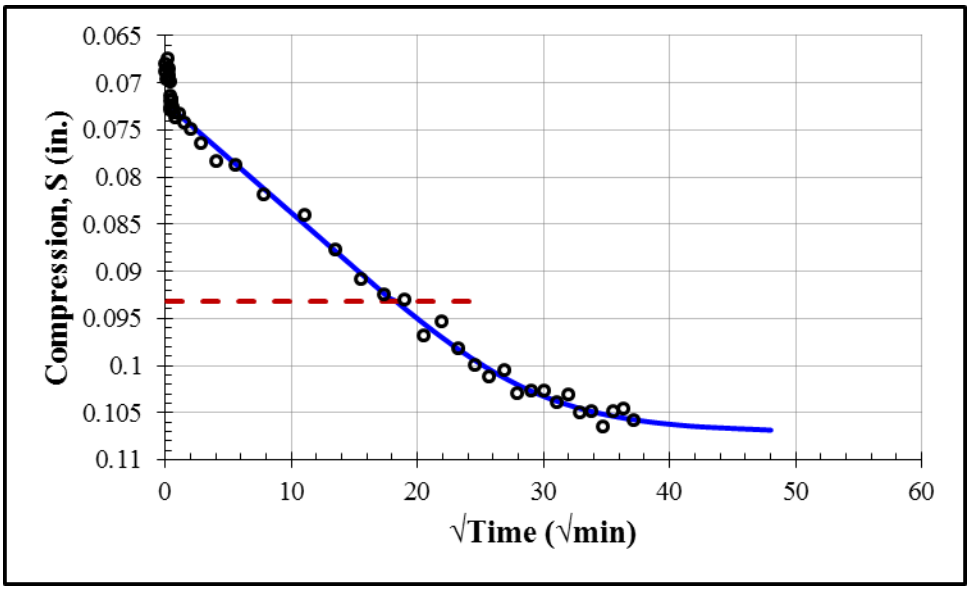

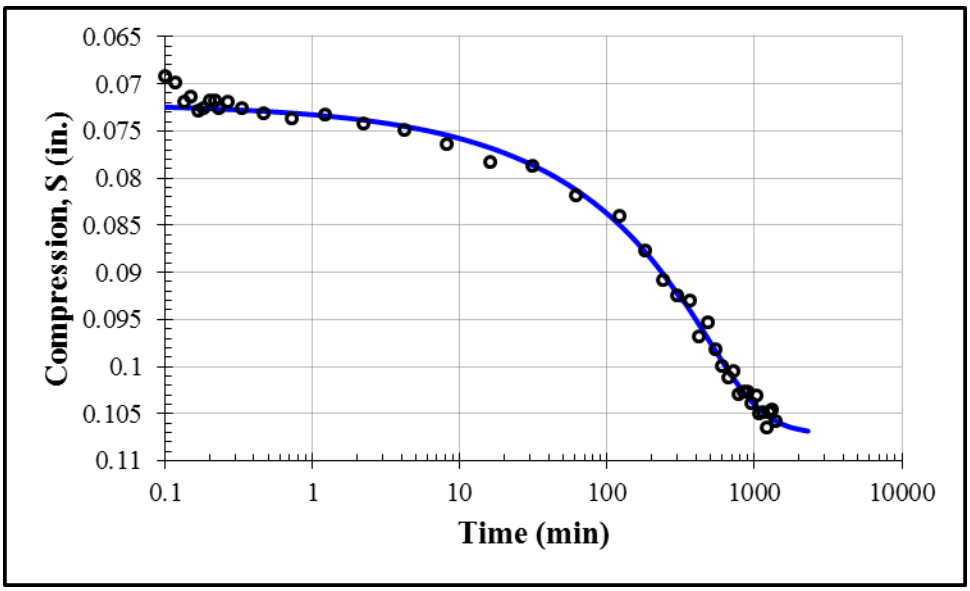

First Loading: 64125 psf				
S_0 (in.)	S_{100} (in.)	c_v (in^2/min)	k (ft/day)	t_{50} (min)
0.1095	0.1394	0.00013	9.0×10^{-10}	156

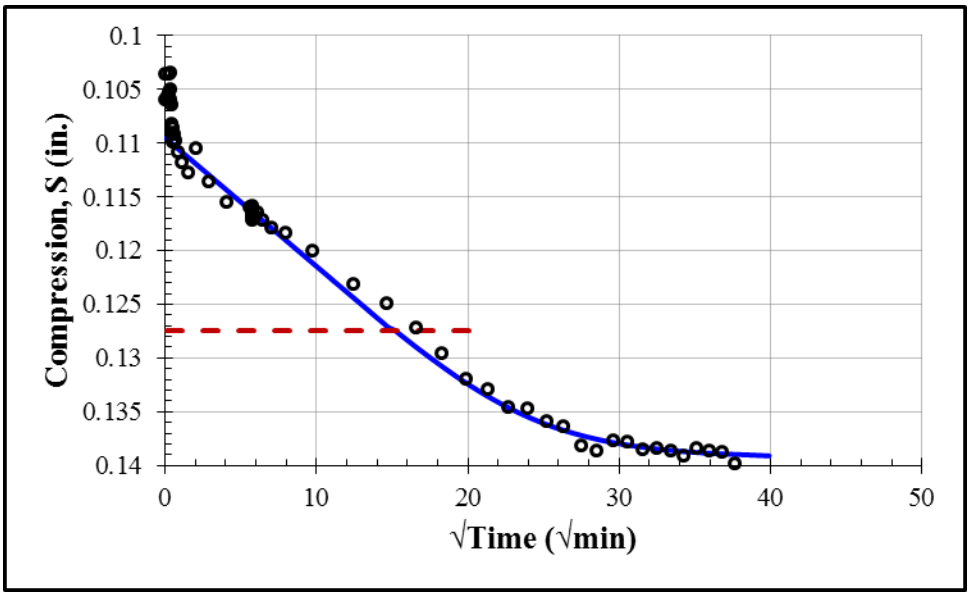

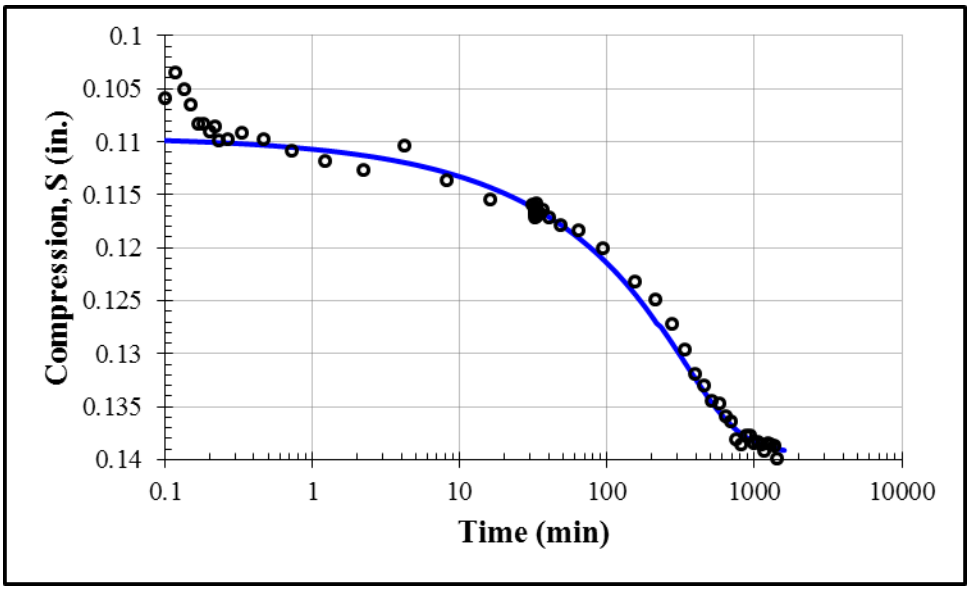

First Unloading: 16125 psf				
S_0 (in.)	S_{100} (in.)	c_v (in^2/min)	k (ft/day)	t_{50} (min)
0.1334	0.1136	0.00006	1.8×10^{-10}	300

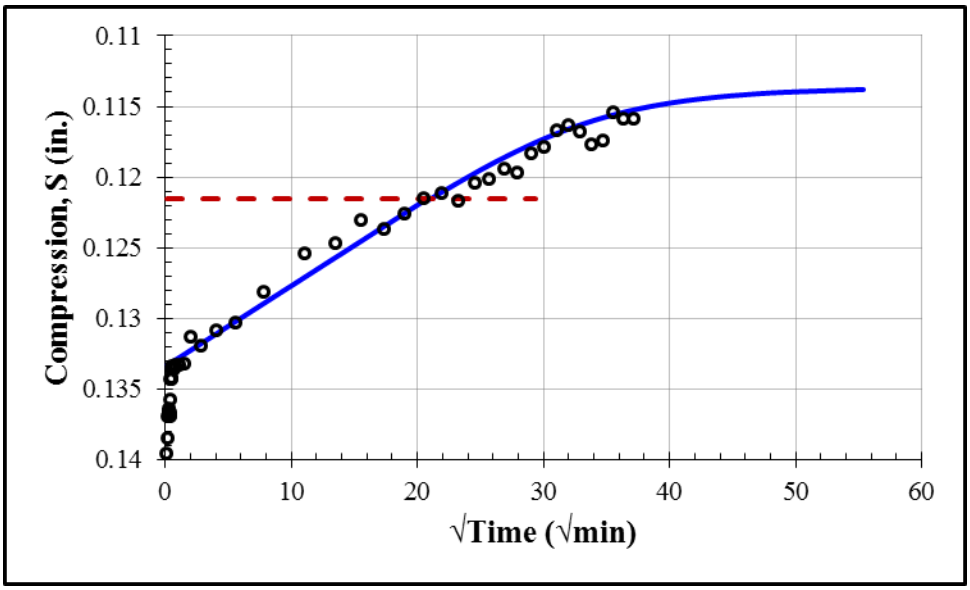

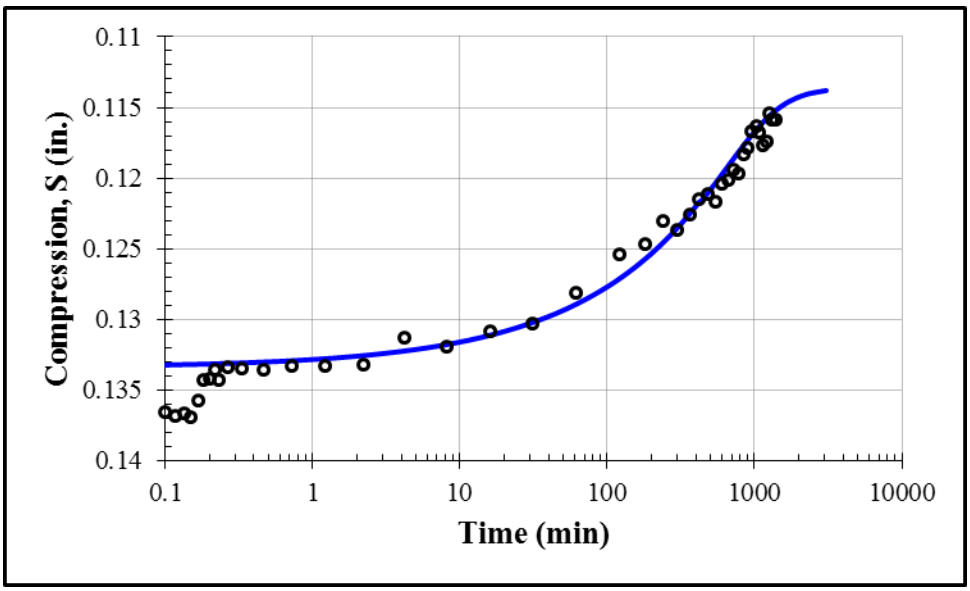

First Unloading: 4125 psf				
S_0 (in.)	S_{100} (in.)	c_v (in^2/min)	k (ft/day)	t_{50} (min)
0.1120	0.0850	0.000045	7.7×10^{-10}	435

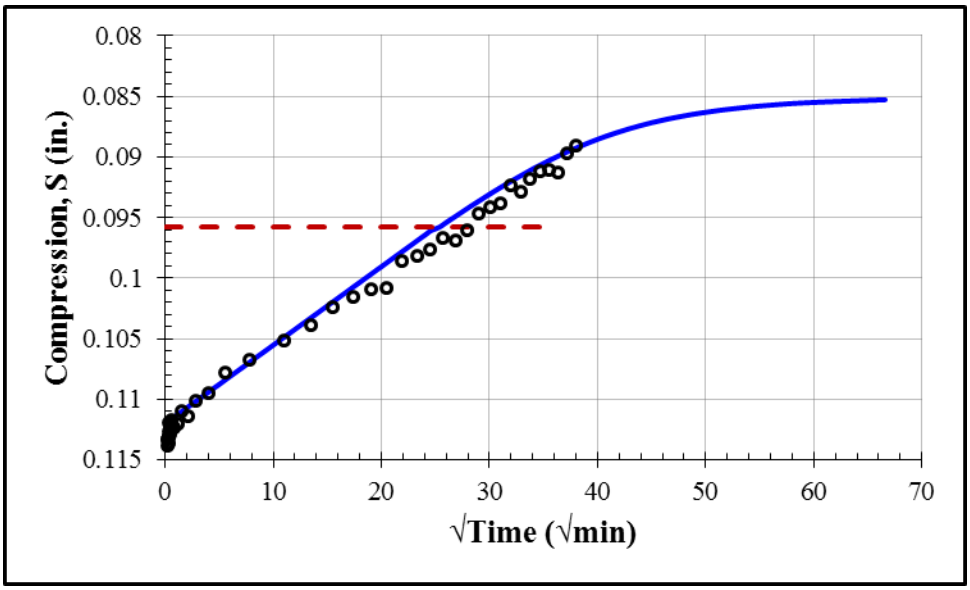

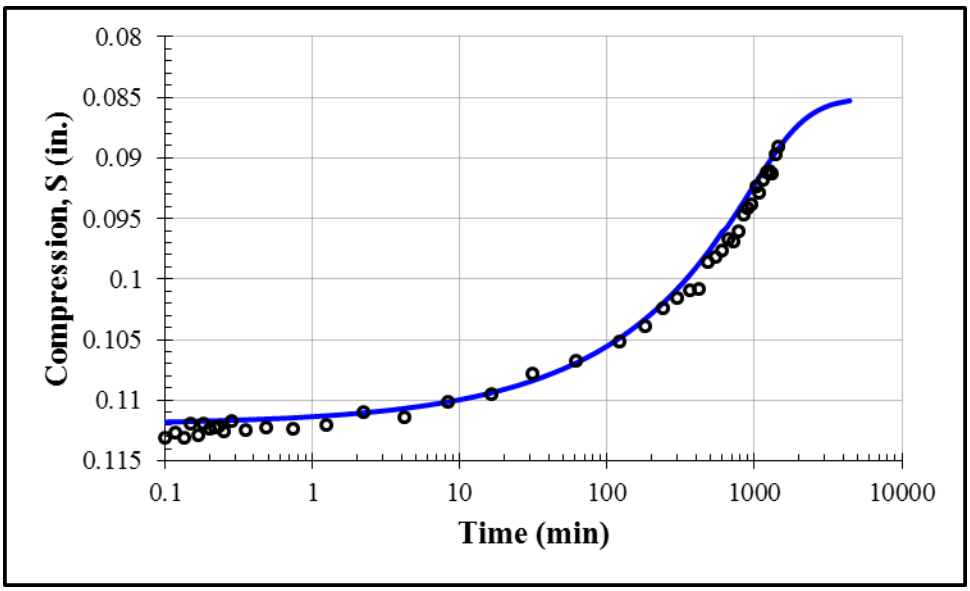

First Unloading: 1125 psf				
S_0 (in.)	S_{100} (in.)	c_v (in^2/min)	k (ft/day)	t_{50} (min)
0.0873	0.0640	0.000045	2.7 x 10^{-9}	472

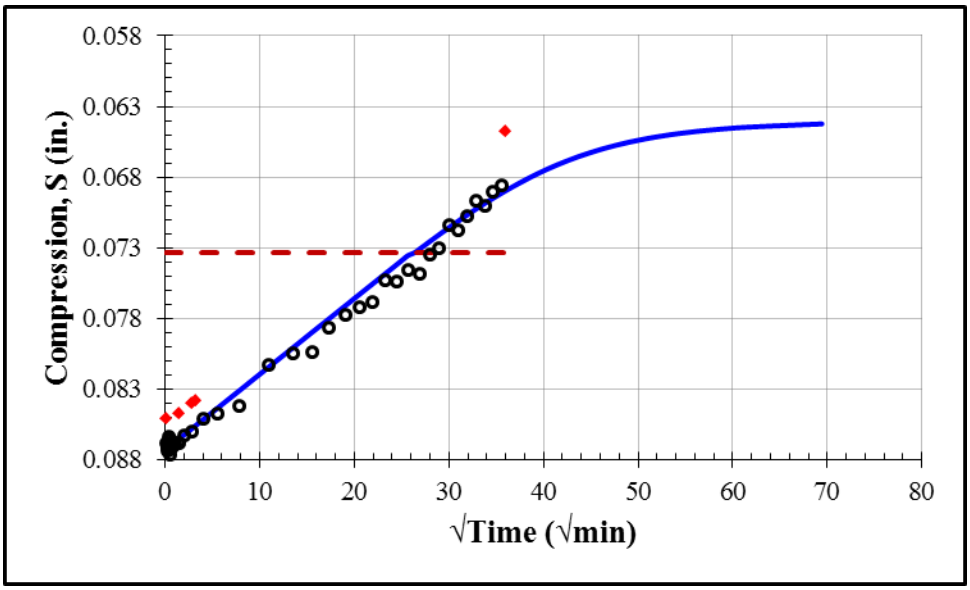

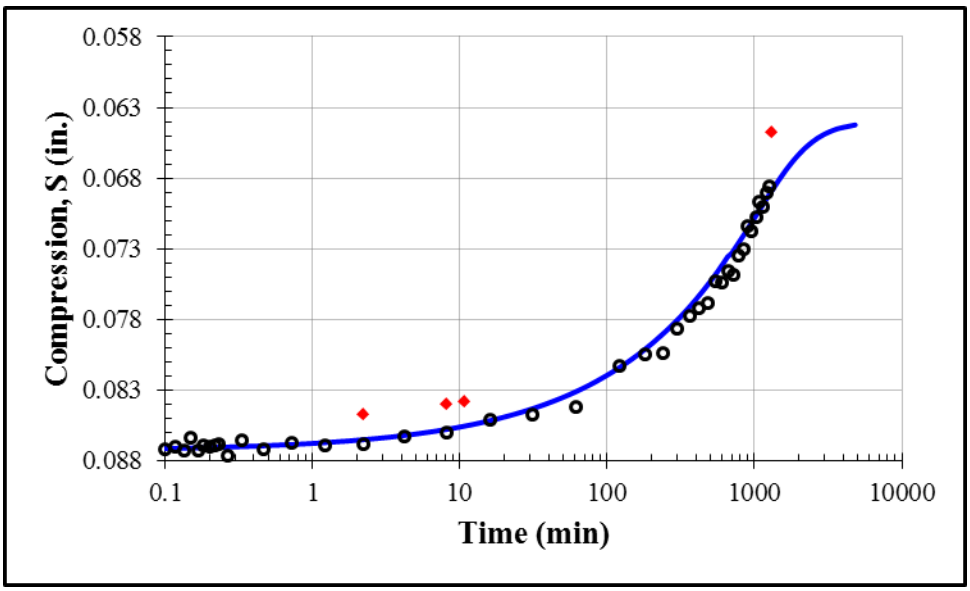

Second Loading: 2125 psf				
S_0 (in.)	S_{100} (in.)	c_v (in^2/min)	k (ft/day)	t_{50} (min)
0.0695	0.0674	0.00015	2.5 x 10^{-9}	150

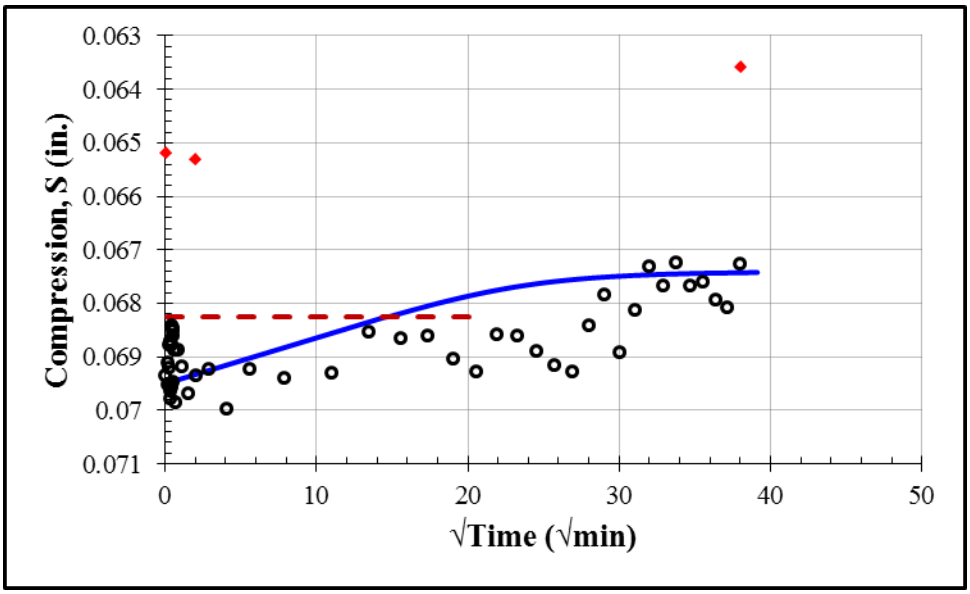

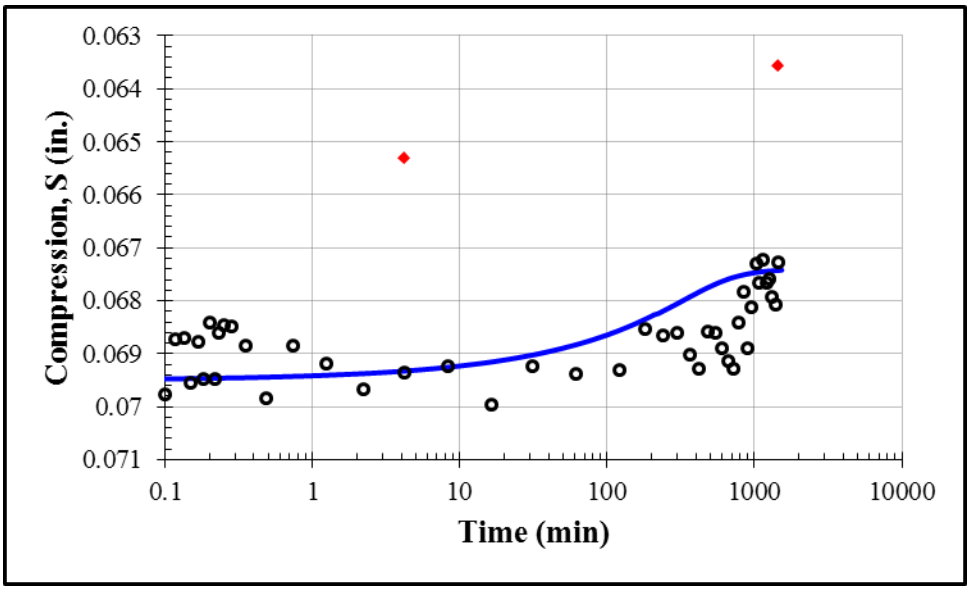

Second Loading: 4125 psf				
S_0 (in.)	S_{100} (in.)	c_v (in^2/min)	k (ft/day)	t_{50} (min)
0.0678	0.0707	0.00015	1.7 x 10^{-9}	151

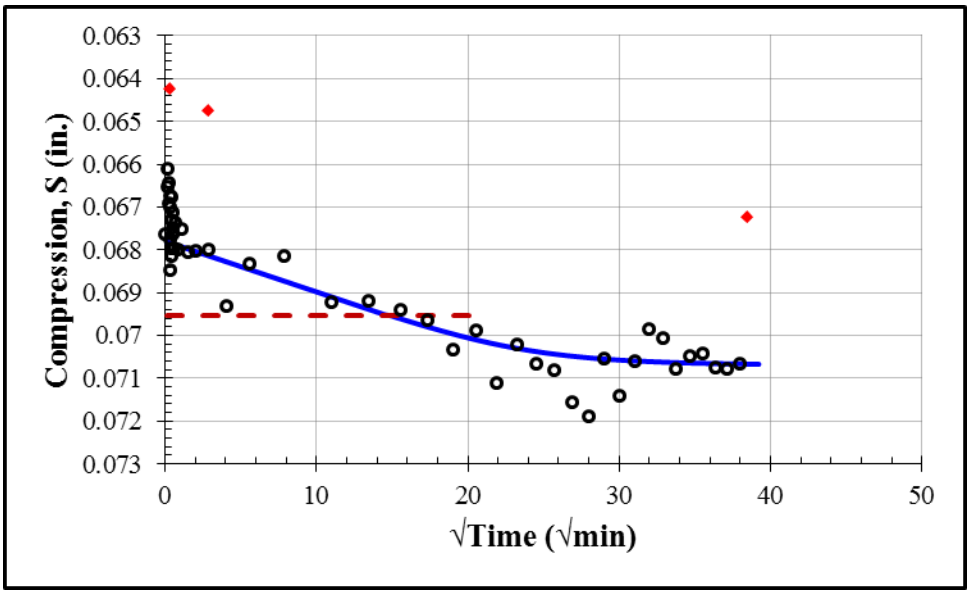

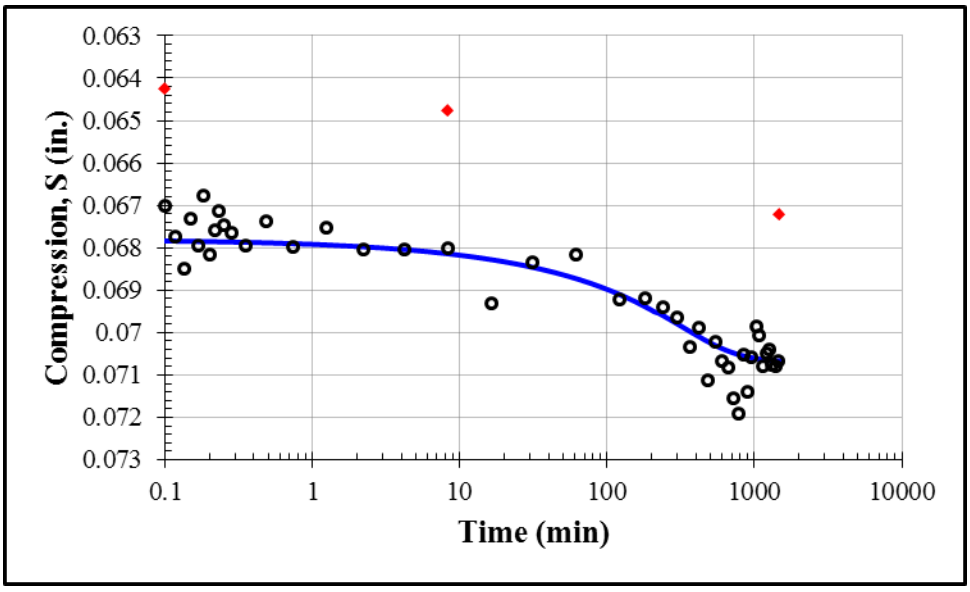

Second Loading: 8125 psf				
S_0 (in.)	S_{100} (in.)	c_v (in^2/min)	k (ft/day)	t_{50} (min)
0.0713	0.0794	0.00011	1.7 x 10^{-9}	204

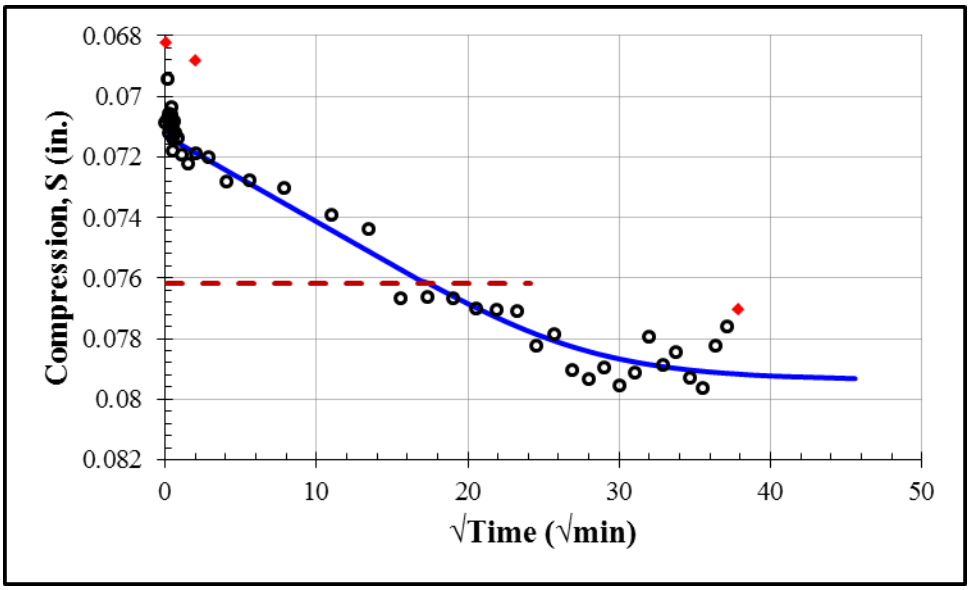

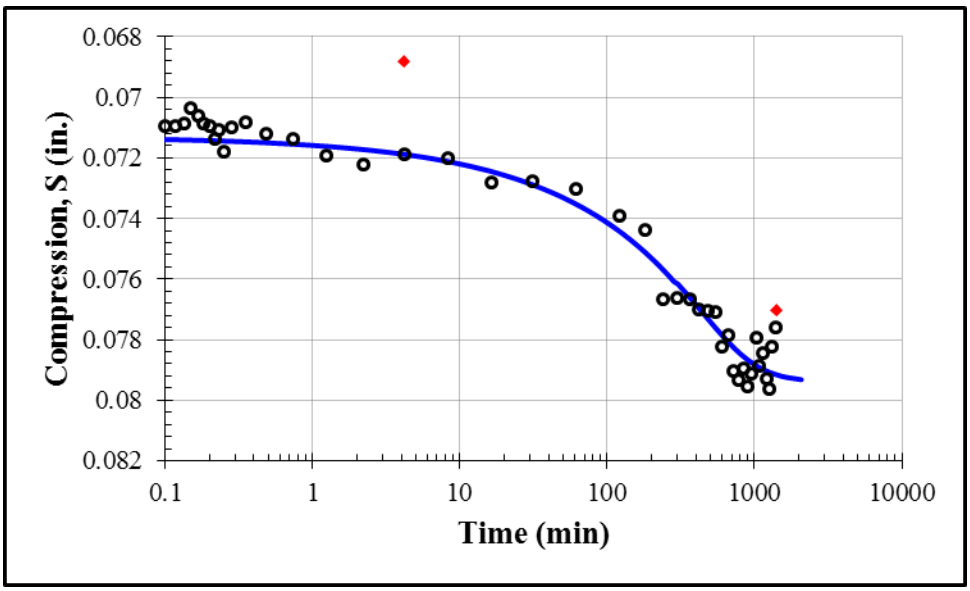

Second Loading: 16125 psf				
S_0 (in.)	S_{100} (in.)	c_v (in^2/min)	k (ft/day)	t_{50} (min)
0.0796	0.0969	0.00007	1.2 x 10^{-9}	313

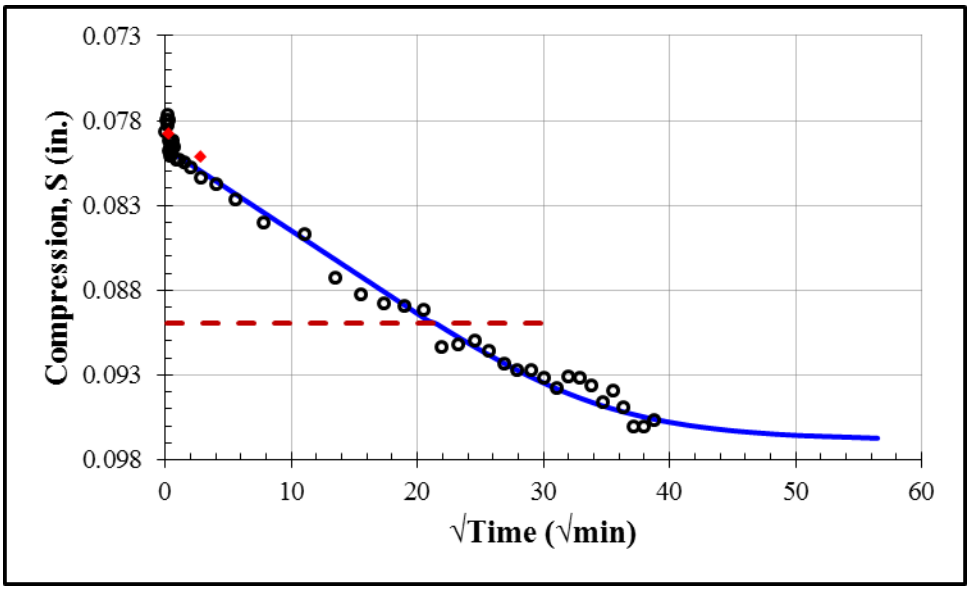

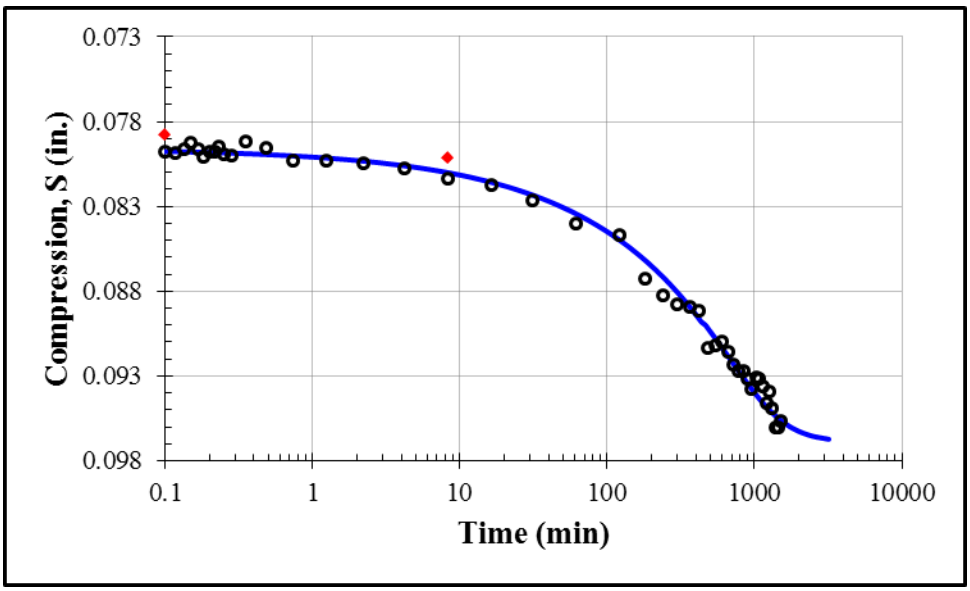

Second Loading: 32125 psf				
S_0 (in.)	S_{100} (in.)	c_v (in^2/min)	k (ft/day)	t_{50} (min)
0.0975	0.1198	0.00007	7.4 x 10^{-10}	297

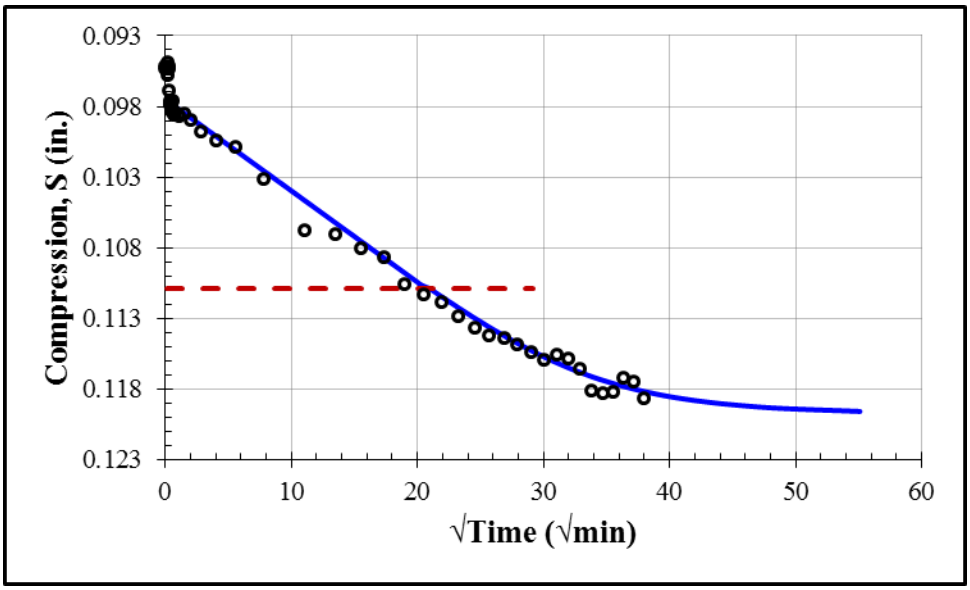

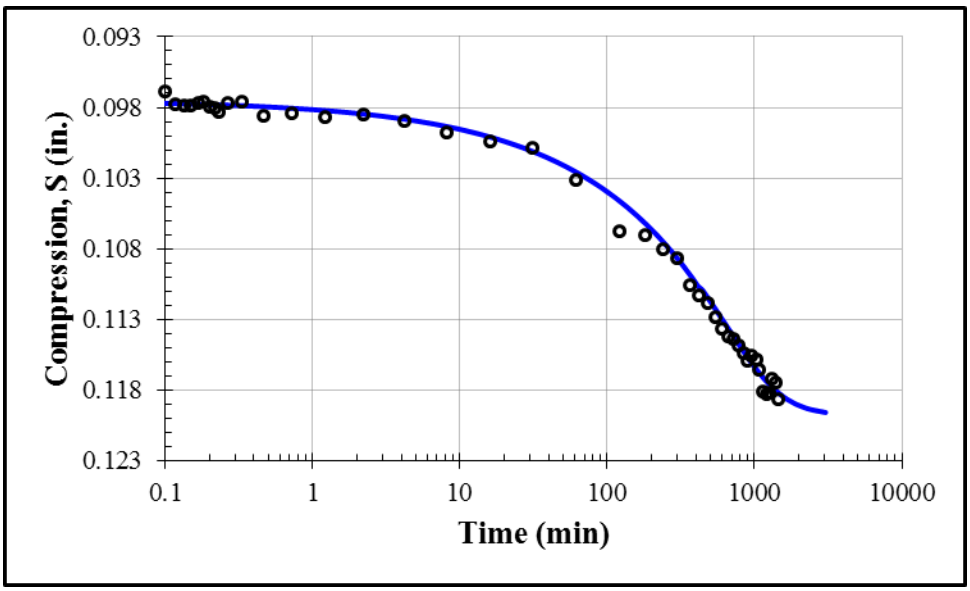

Second Loading: 64125 psf				
S_0 (in.)	S_{100} (in.)	c_v (in^2/min)	k (ft/day)	t_{50} (min)
0.1220	0.1455	0.00009	4.9×10^{-10}	215

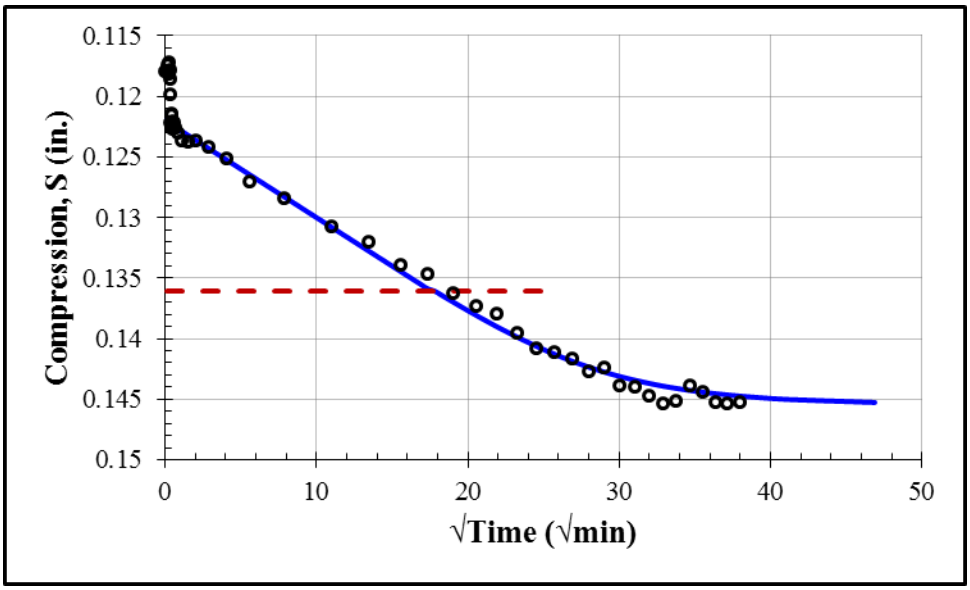

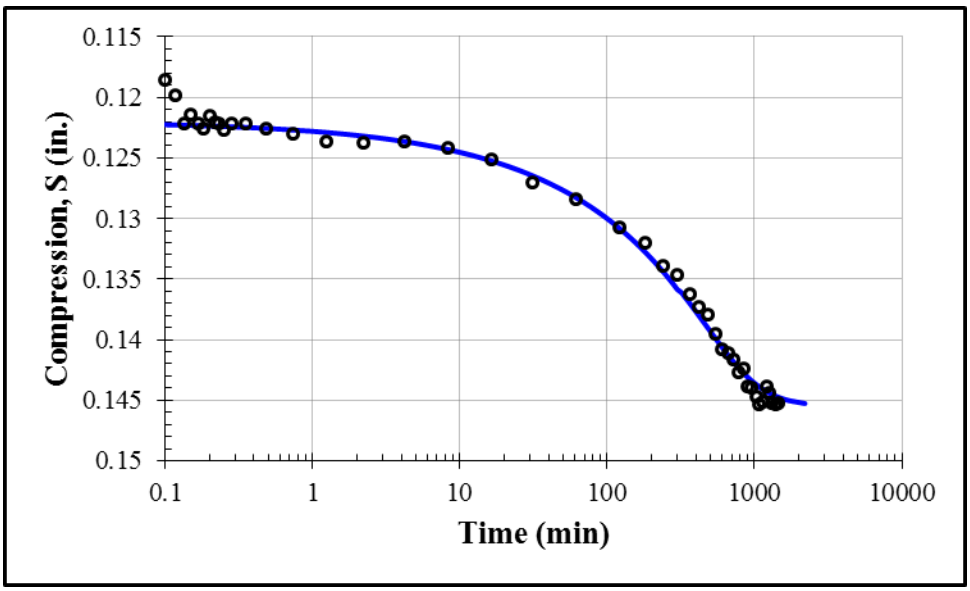

Second Unloading: 16125 psf				
S_0 (in.)	S_{100} (in.)	c_v (in^2/min)	k (ft/day)	t_{50} (min)
0.1375	0.1181	0.000075	2.2 x 10^{-10}	237

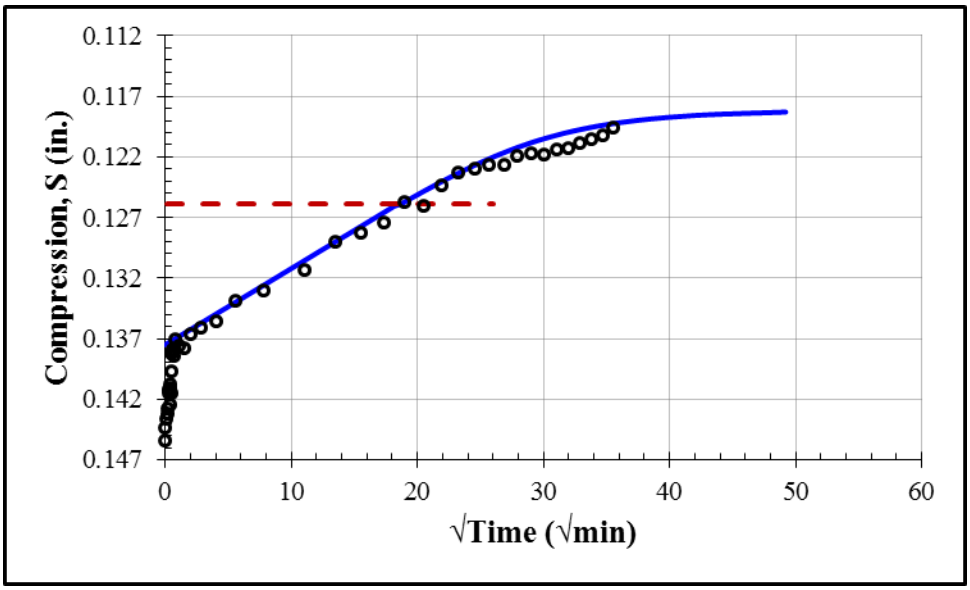

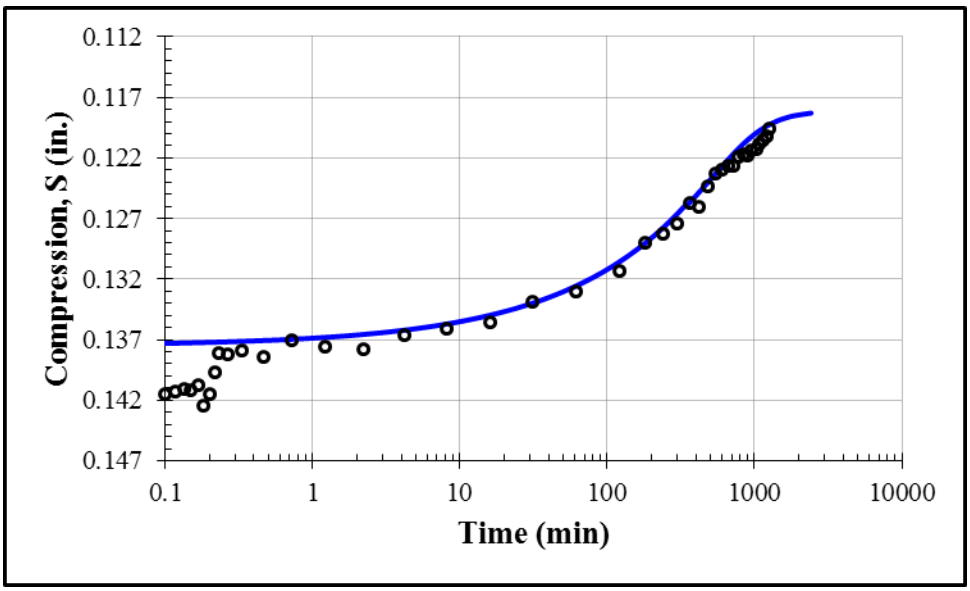

Second Unloading: 4125 psf				
S_0 (in.)	S_{100} (in.)	c_v (in^2/min)	k (ft/day)	t_{50} (min)
0.1163	0.0896	0.000048	8.1×10^{-10}	402

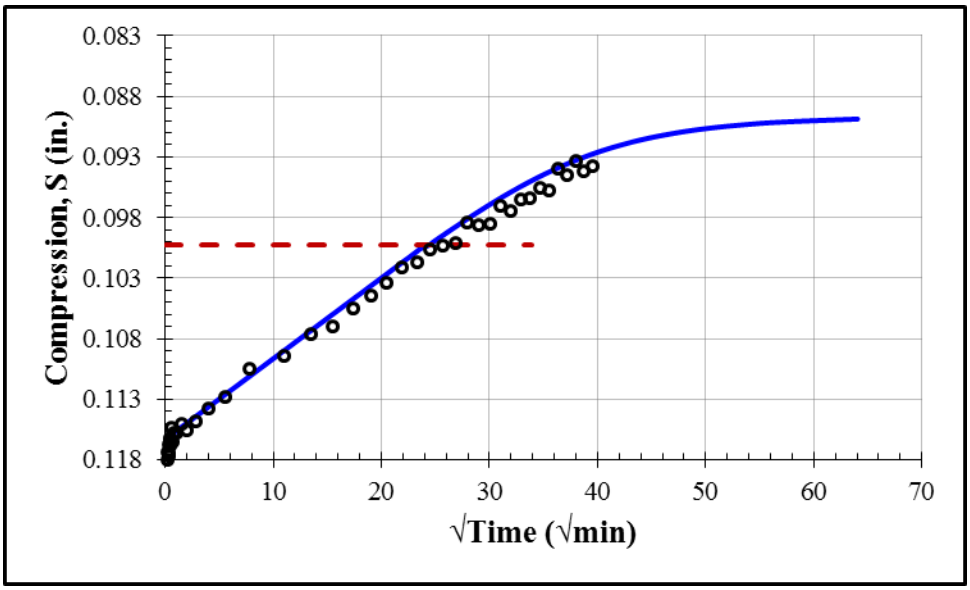

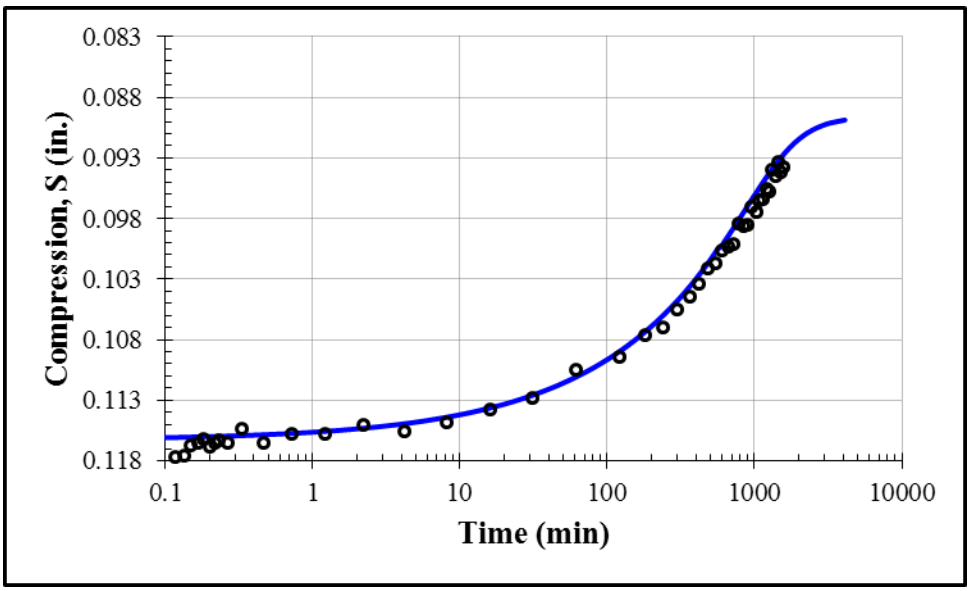

Second Unloading: 1125 psf				
S_0 (in.)	S_{100} (in.)	c_v (in^2/min)	k (ft/day)	t_{50} (min)
0.0918	0.0572	0.00002	1.8 x 10^{-9}	1049

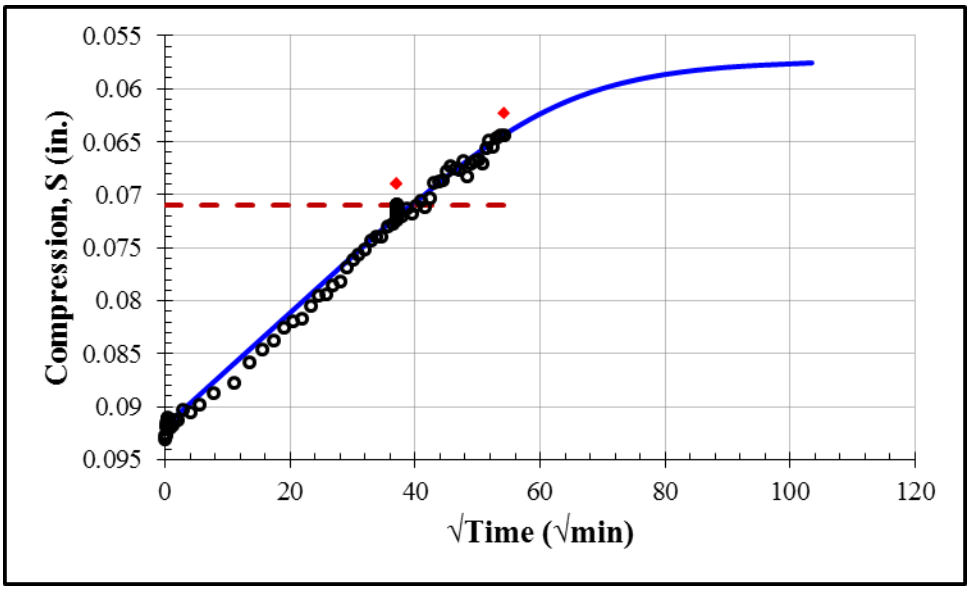

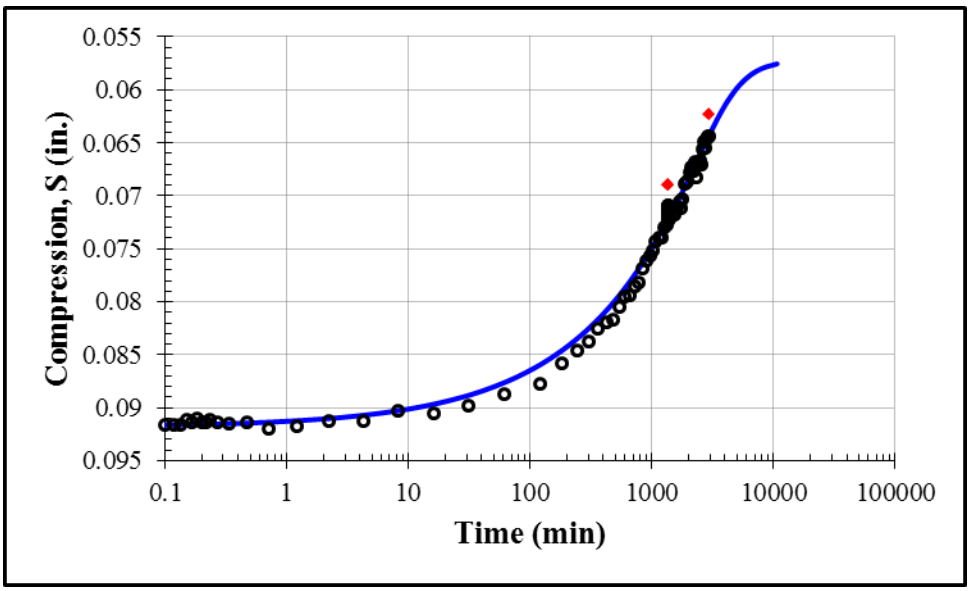

Second Unloading: 250 psf				
S_0 (in.)	S_{100} (in.)	c_v (in^2/min)	k (ft/day)	t_{50} (min)
0.0632	0.0405	0.00002	4.1 x 10^{-9}	1141

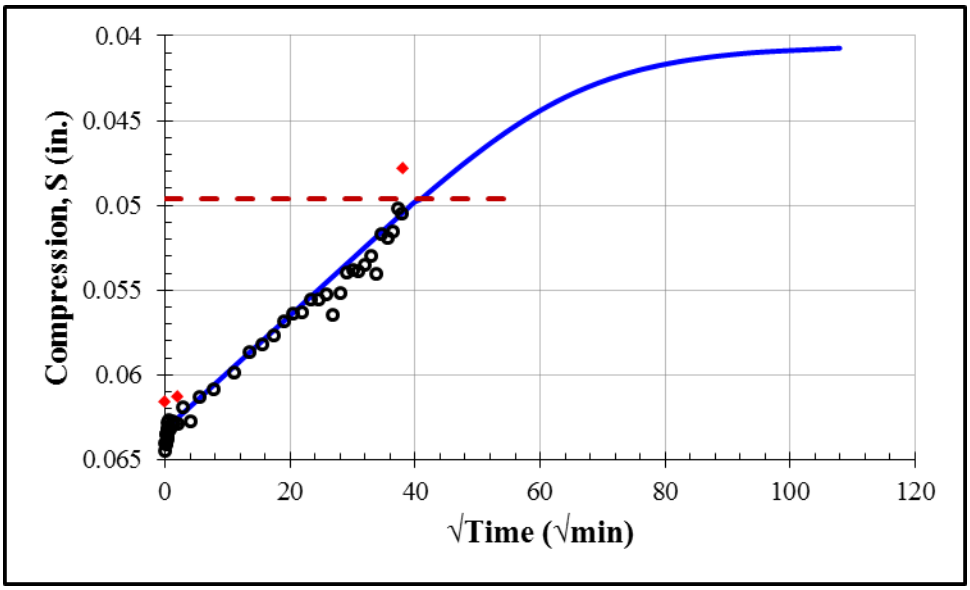

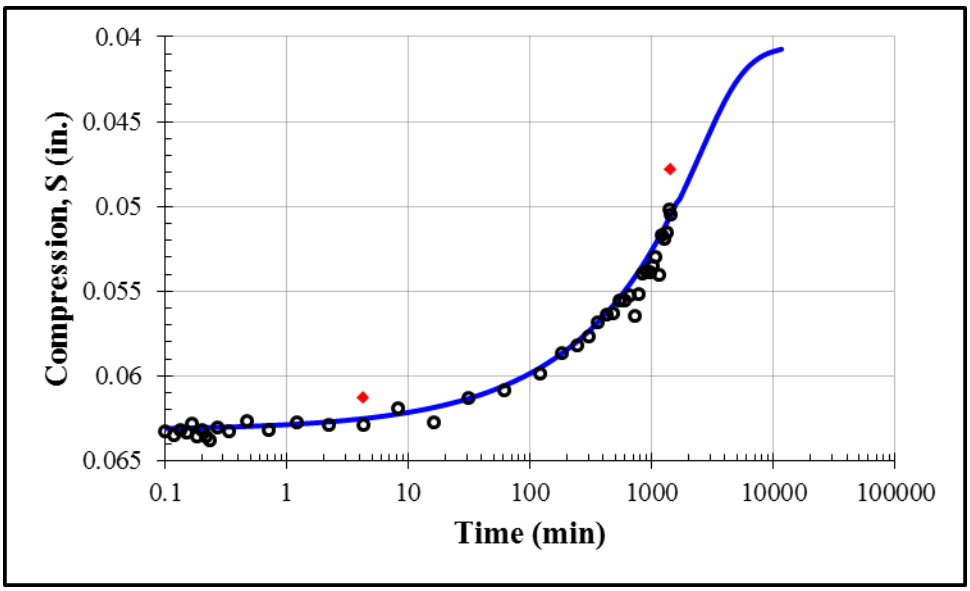

Second Unloading: 125 psf				
S_0 (in.)	S_{100} (in.)	c_v (in^2/min)	k (ft/day)	t_{50} (min)
0.0498	0.0175	0.000014	2.9 x 10^{-8}	1704

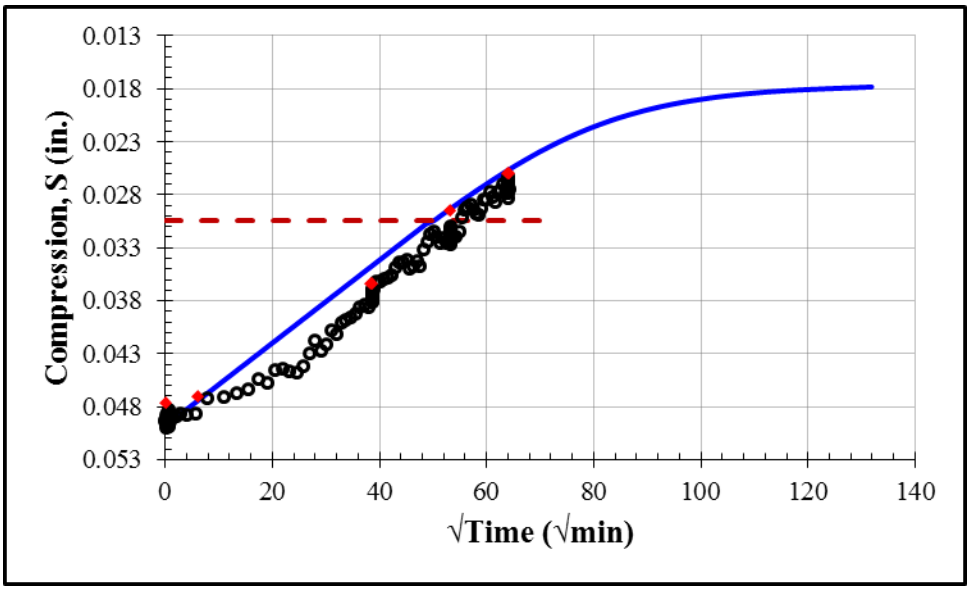

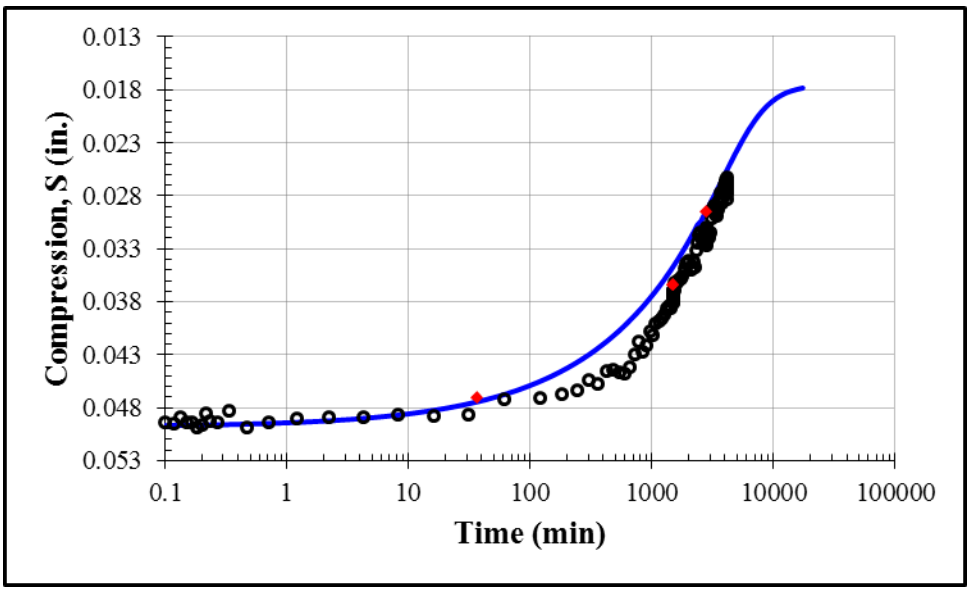

Appendix E: Consolidation Test 4

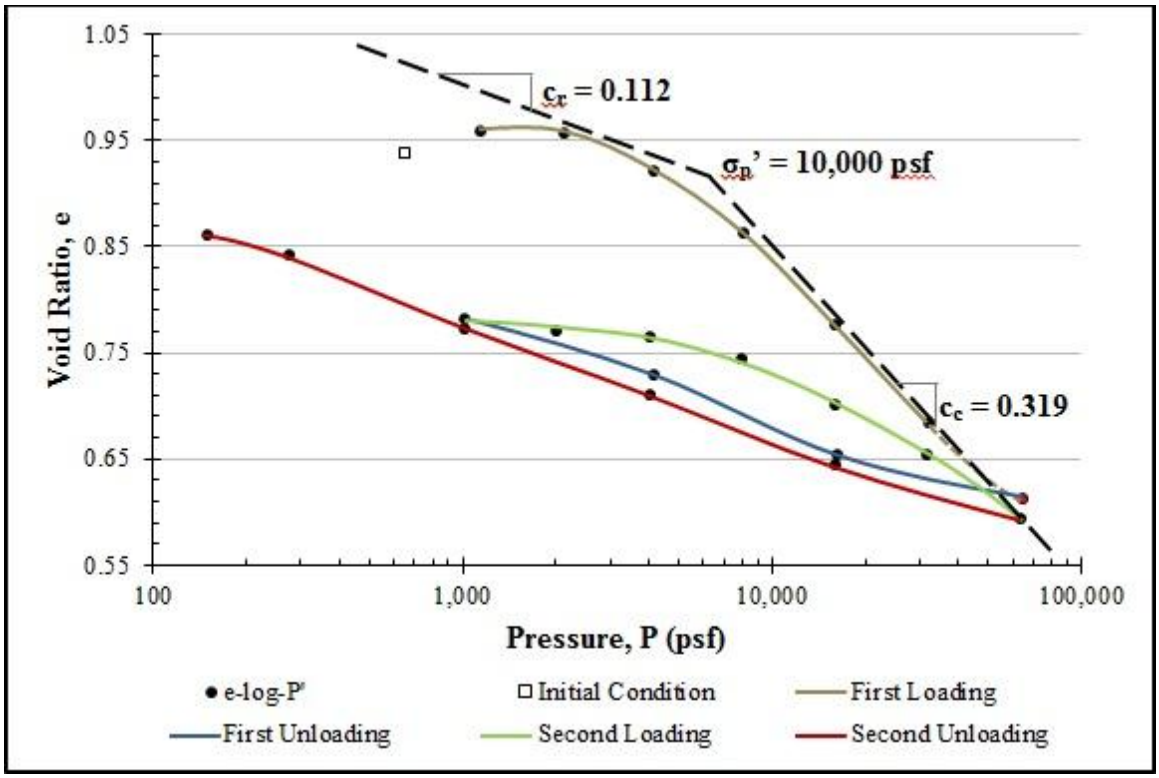

$$c_c = -\frac{e_2 - e_1}{\log(\sigma_2 / \sigma_1)} = -\frac{0.628 - 0.851}{\log(50000/10000)} = 0.319$$

$$c_r = -\frac{e_2 - e_1}{\log(\sigma_2 / \sigma_1)} = -\frac{0.950 - 1.028}{\log(3000/600)} = 0.112$$

$$R_c = \frac{c_c}{1 + e_0} = \frac{0.319}{1 + 1.0454} = 0.156$$

$$R_r = \frac{c_r}{1 + e_0} = \frac{0.112}{1 + 1.0454} = 0.055$$

Soaking at Constant Volume Starting at 625 psf				
S_0 (in.)	S_{100} (in.)	c_v (in^2/min)	k (ft/day)	t_{50} (min)
0.0000	0.0006	0.000067	6.6×10^{-10}	421

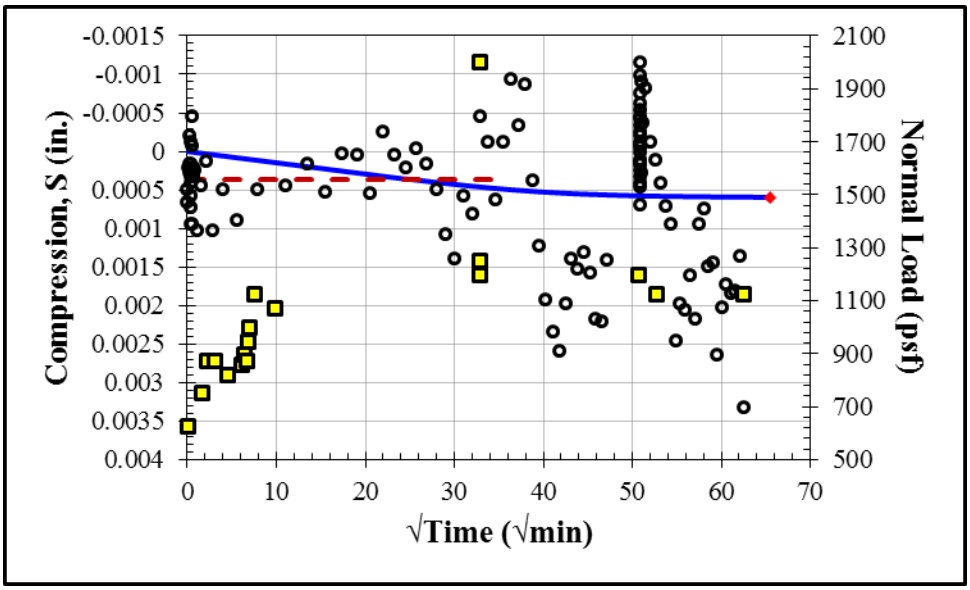

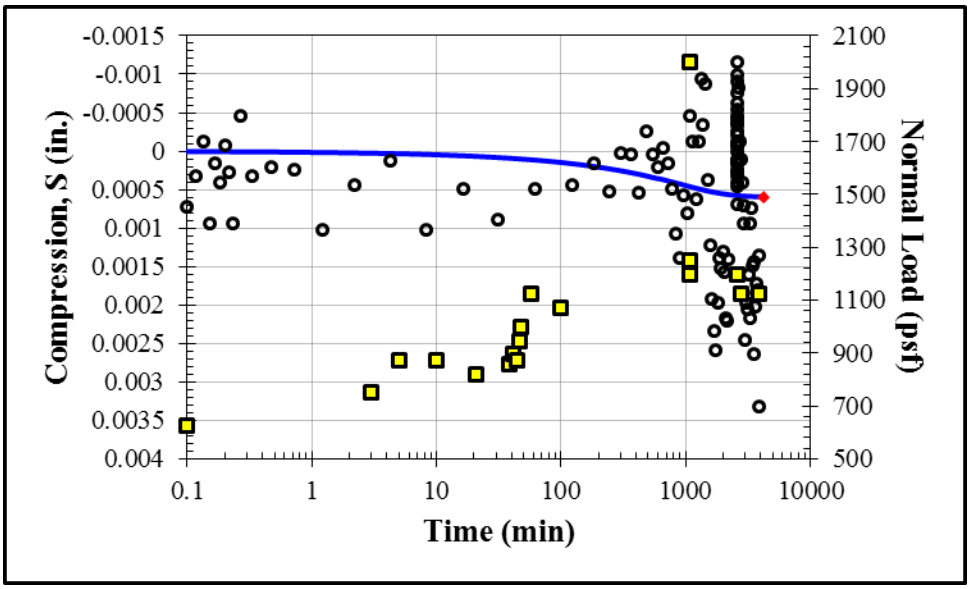

First Loading: 2125 psf				
S_0 (in.)	S_{100} (in.)	c_v (in^2/min)	k (ft/day)	t_{50} (min)
0.0028	0.0058	0.00015	3.7 x 10^{-9}	187

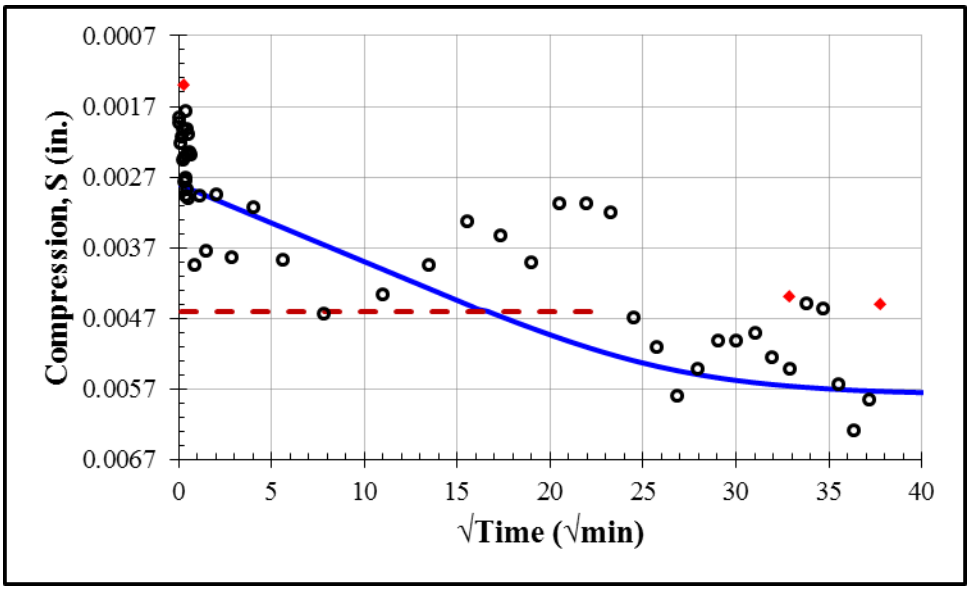

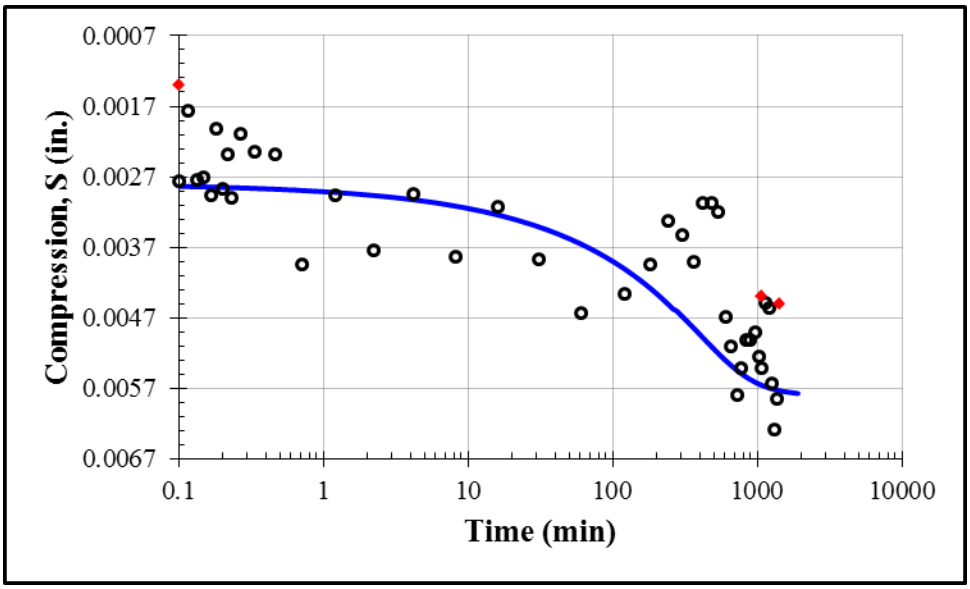

First Loading: 4125 psf				
S_0 (in.)	S_{100} (in.)	c_v (in^2/min)	k (ft/day)	t_{50} (min)
0.0093	0.0223	0.00015	7.9 x 10^{-9}	185

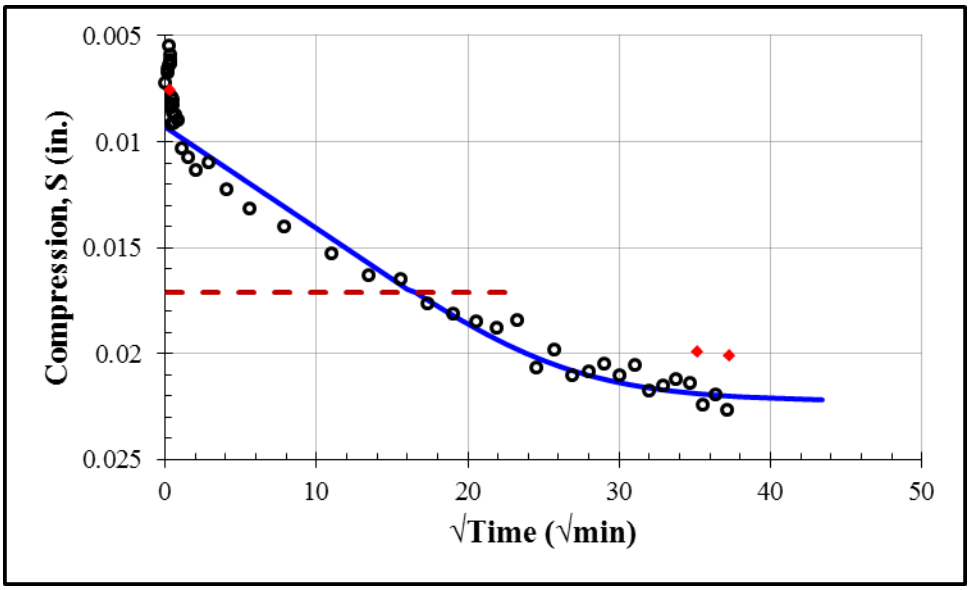

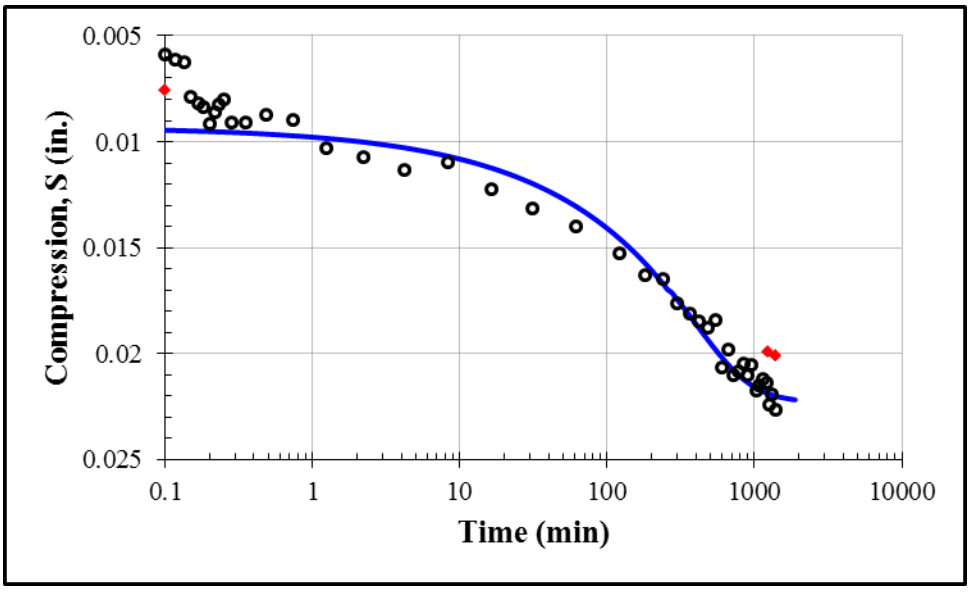

First Loading: 8125 psf				
S_0 (in.)	S_{100} (in.)	c_v (in^2/min)	k (ft/day)	t_{50} (min)
0.0253	0.0478	0.00013	5.8 x 10^{-9}	205

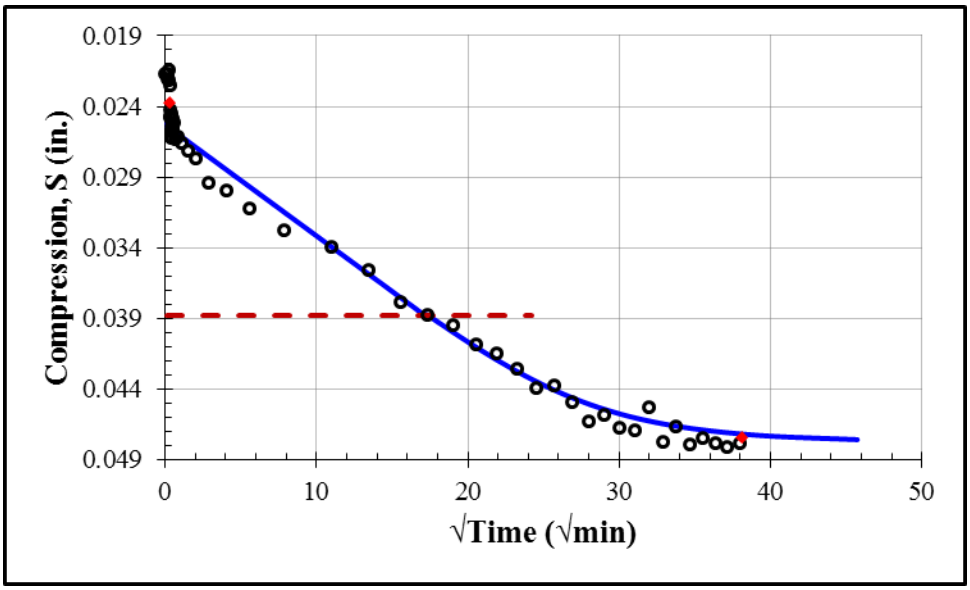

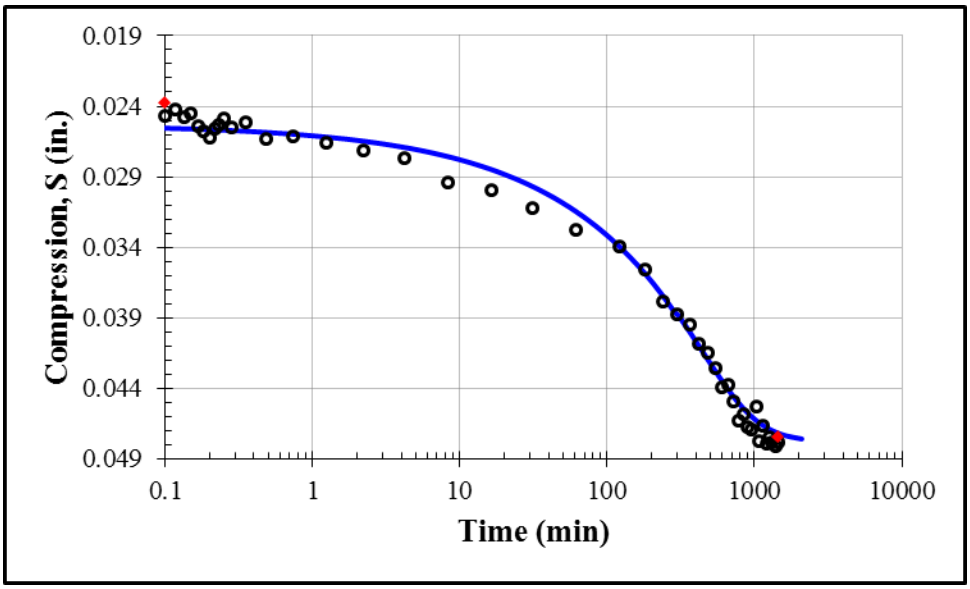

First Loading: 16125 psf				
S_0 (in.)	S_{100} (in.)	c_v (in^2/min)	k (ft/day)	t_{50} (min)
0.0507	0.0849	0.00011	3.6 x 10^{-9}	225

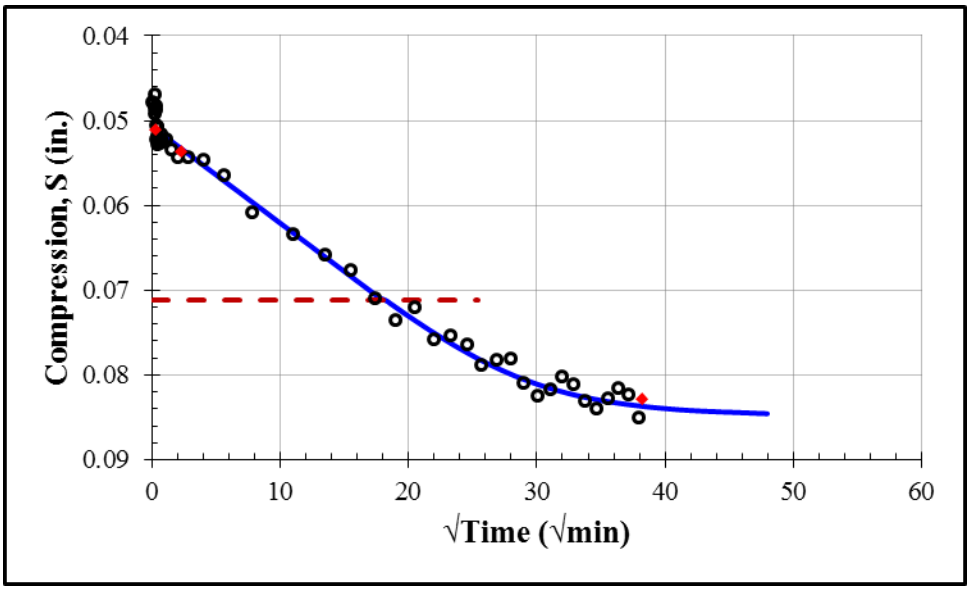

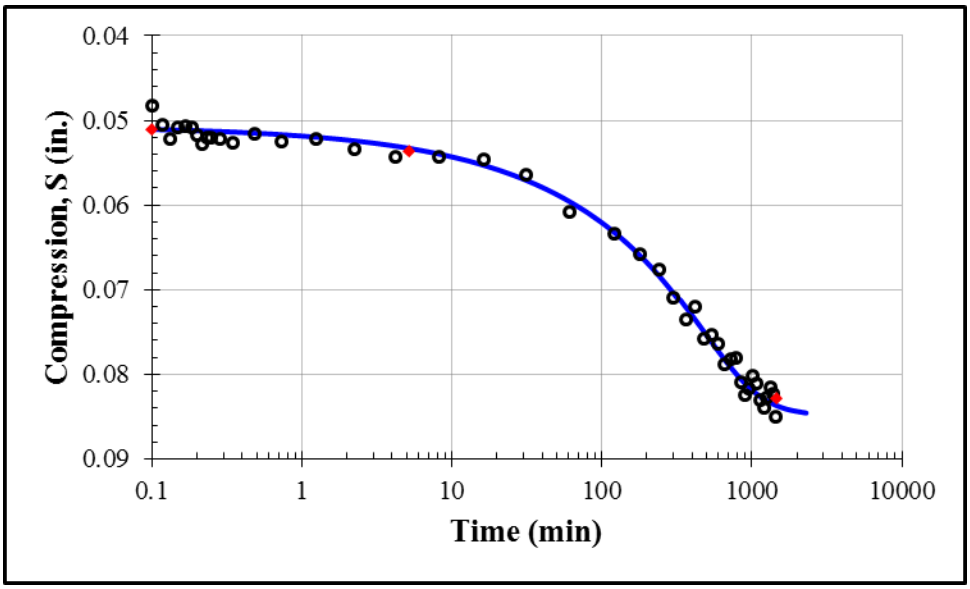

First Loading: 32125 psf				
S_0 (in.)	S_{100} (in.)	c_v (in^2/min)	k (ft/day)	t_{50} (min)
0.0867	0.1238	0.0001	1.7 x 10^{-9}	223

Note: LVDT lost contact during this increment. Dial gage readings were used instead.

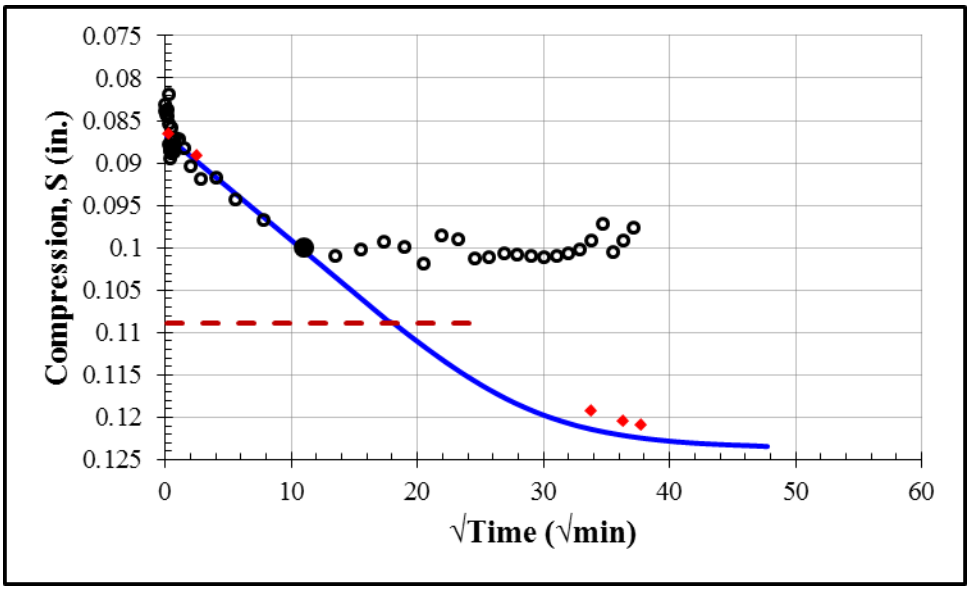

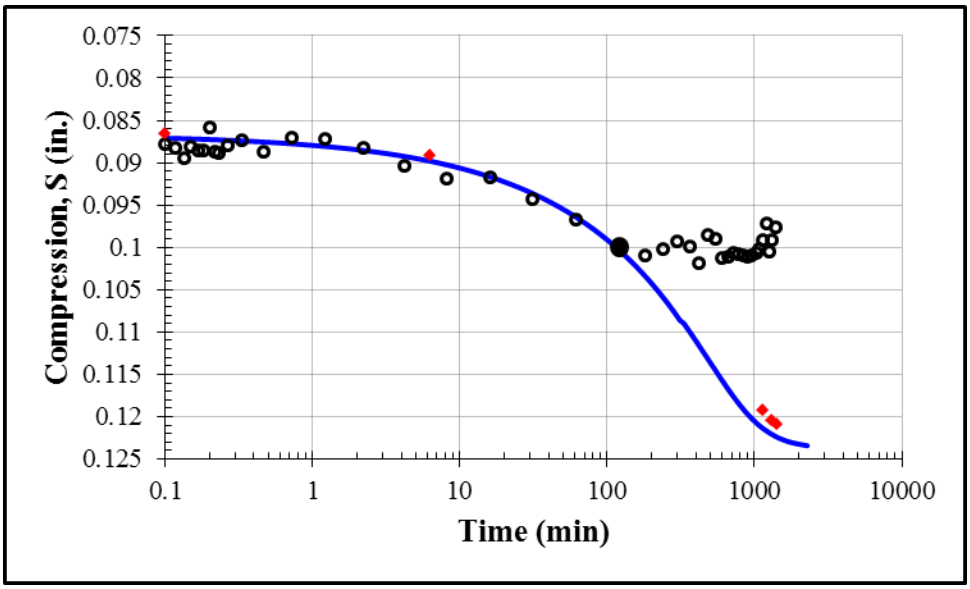

First Loading: 64125 psf				
S_0 (in.)	S_{100} (in.)	c_v (in^2/min)	k (ft/day)	t_{50} (min)
0.1262	0.1555	0.00013	8.6×10^{-10}	166

Note: LVDT and dial gage lost contact. Curve was predicted based on past experience.

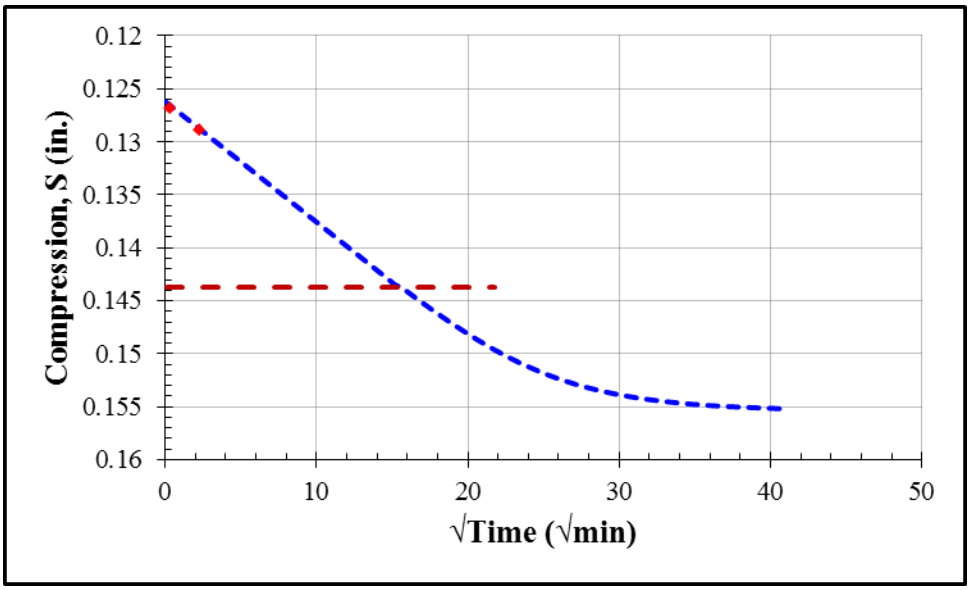

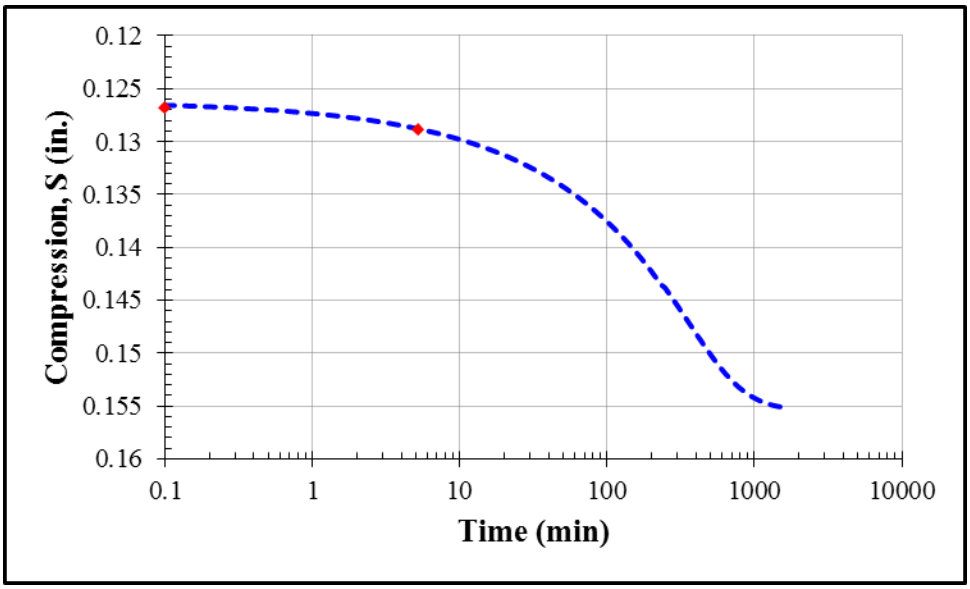

First Unloading: 16125 psf				
S_0 (in.)	S_{100} (in.)	c_v (in^2/min)	k (ft/day)	t_{50} (min)
0.1532	0.1331	0.000085	2.6×10^{-10}	207

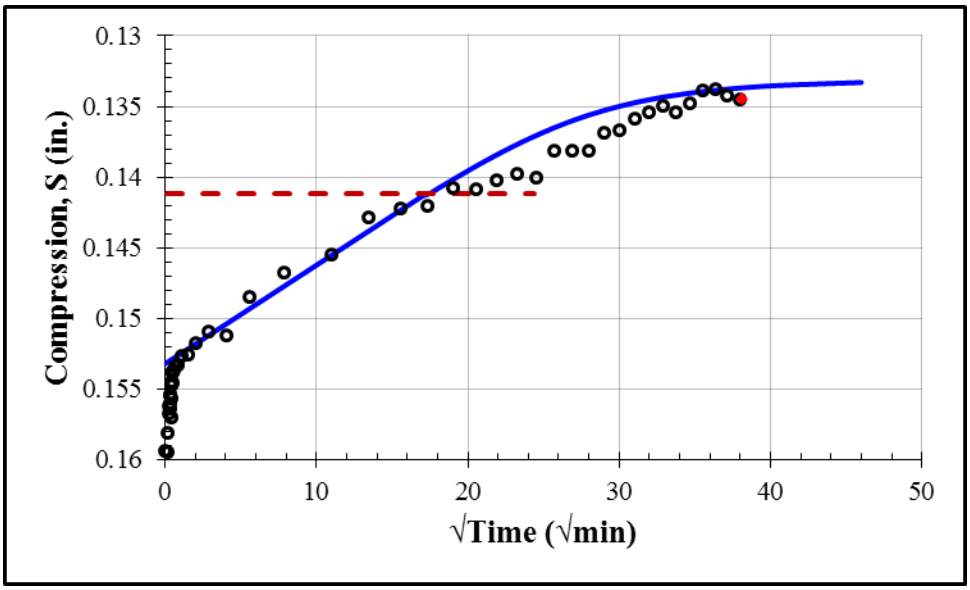

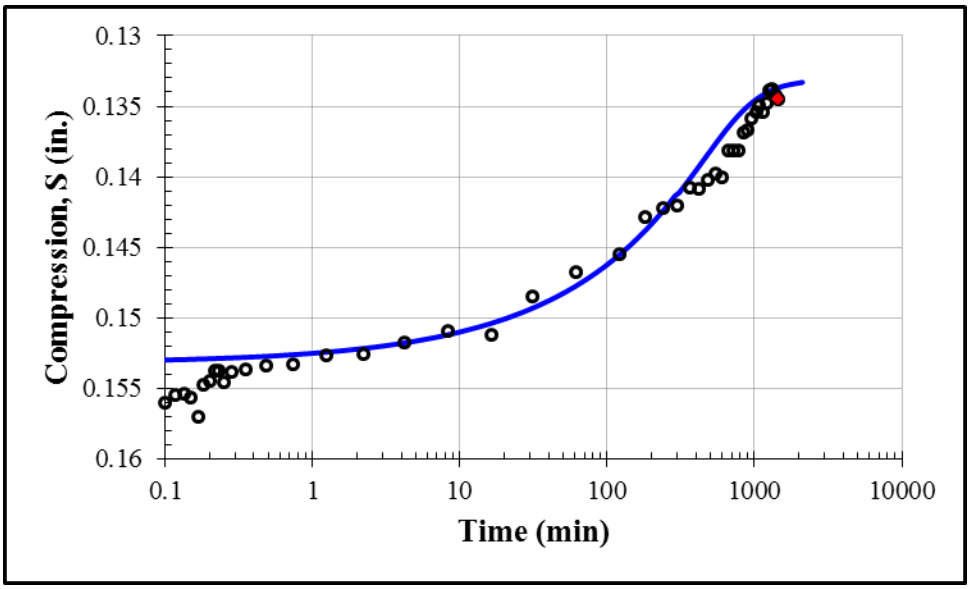

First Unloading: 4125 psf				
S_0 (in.)	S_{100} (in.)	c_v (in^2/min)	k (ft/day)	t_{50} (min)
0.1294	0.1010	0.000042	7.3×10^{-10}	456

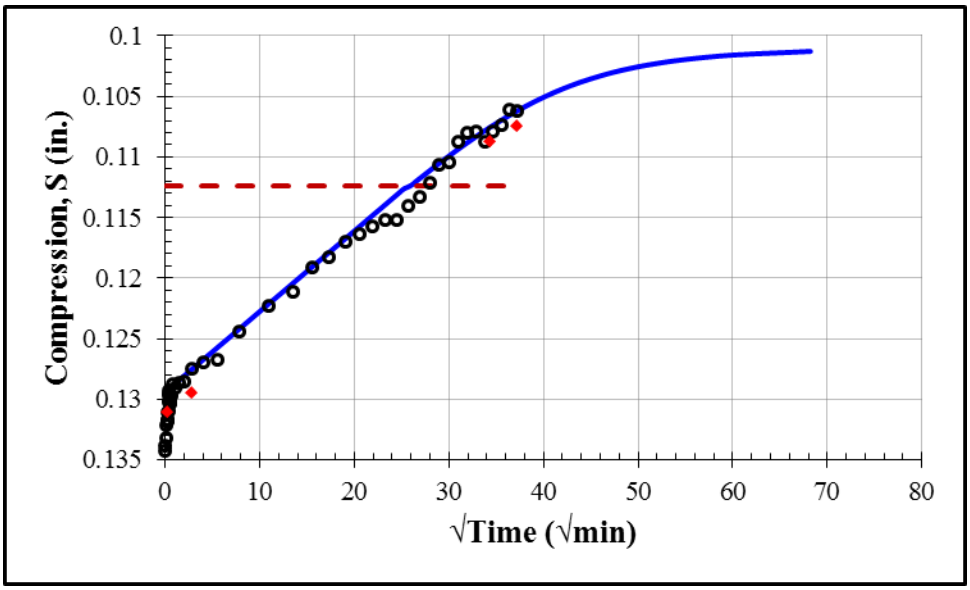

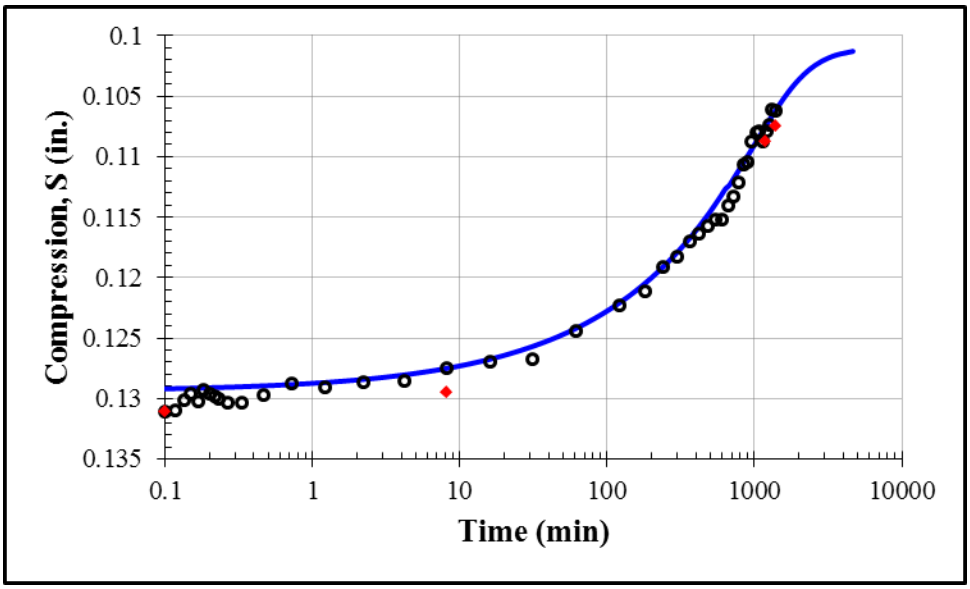

First Unloading: 1000 psf				
S_0 (in.)	S_{100} (in.)	c_v (in^2/min)	k (ft/day)	t_{50} (min)
0.1046	0.0780	0.00004	2.6 x 10^{-10}	524

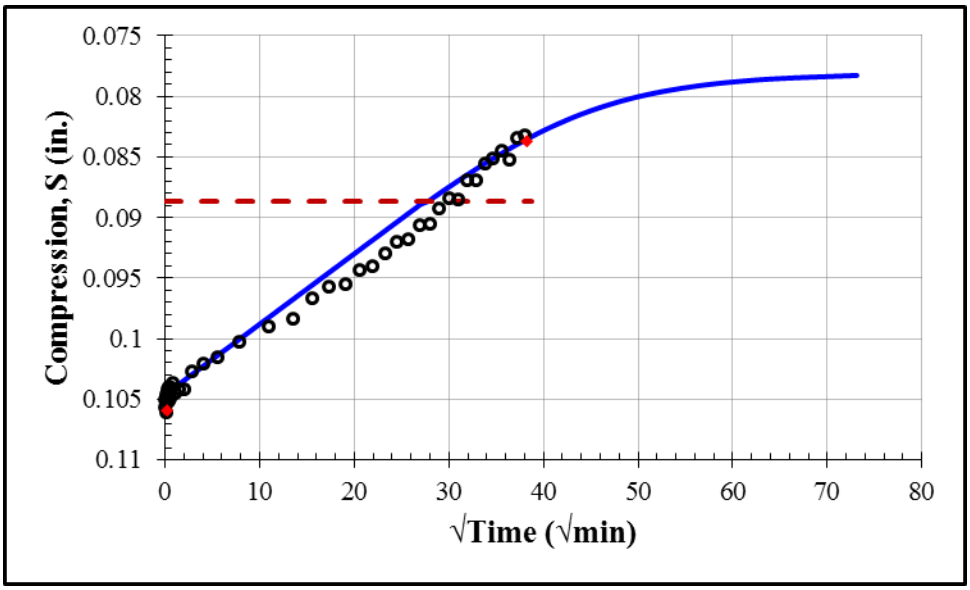

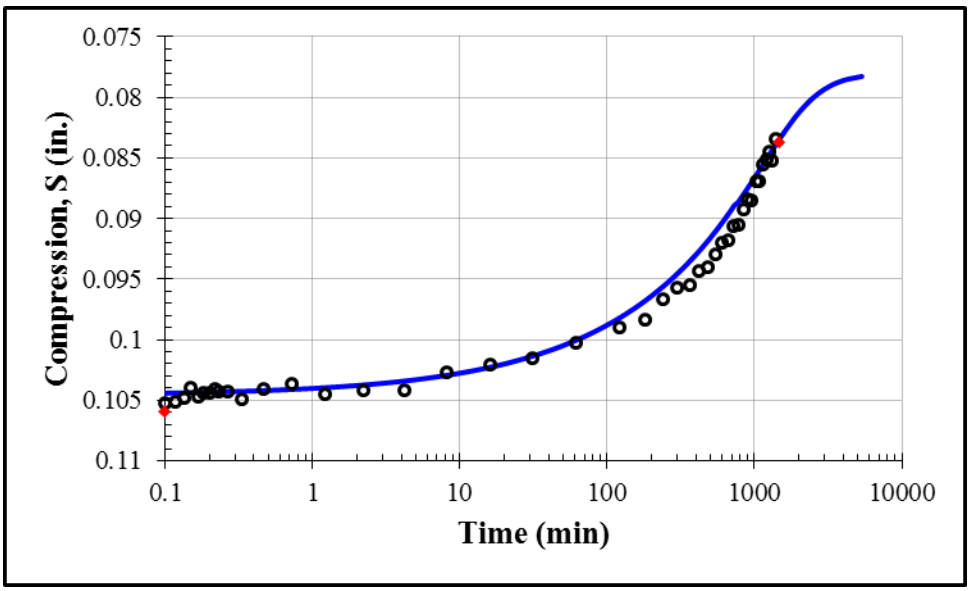

Second Loading: 2000 psf				
S_0 (in.)	S_{100} (in.)	c_v (in^2/min)	k (ft/day)	t_{50} (min)
0.0820	0.0832	0.00015	1.4 x 10^{-9}	149

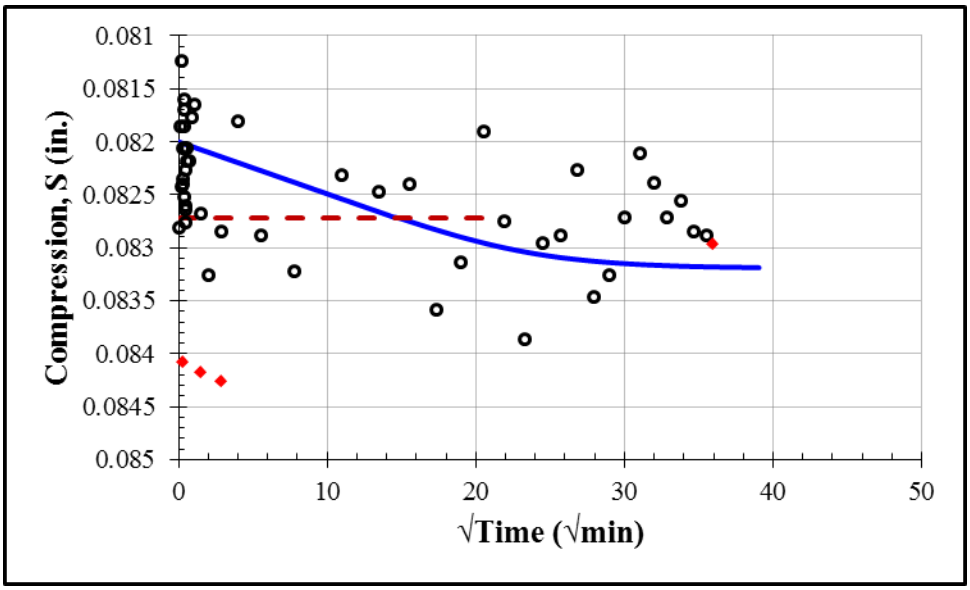

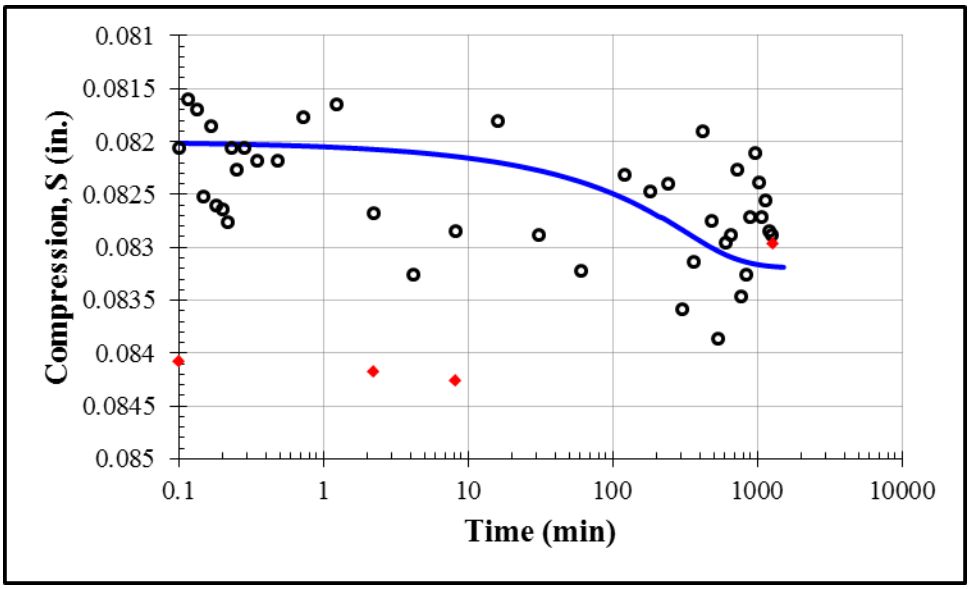

Second Loading: 4000 psf				
S_0 (in.)	S_{100} (in.)	c_v (in^2/min)	k (ft/day)	t_{50} (min)
0.0834	0.0865	0.0001	1.2 x 10^{-9}	224

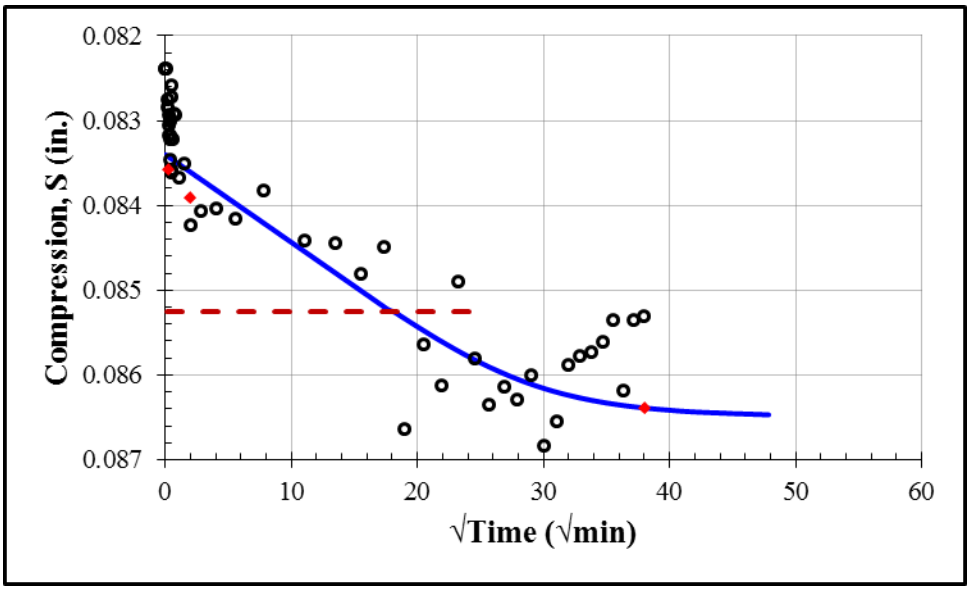

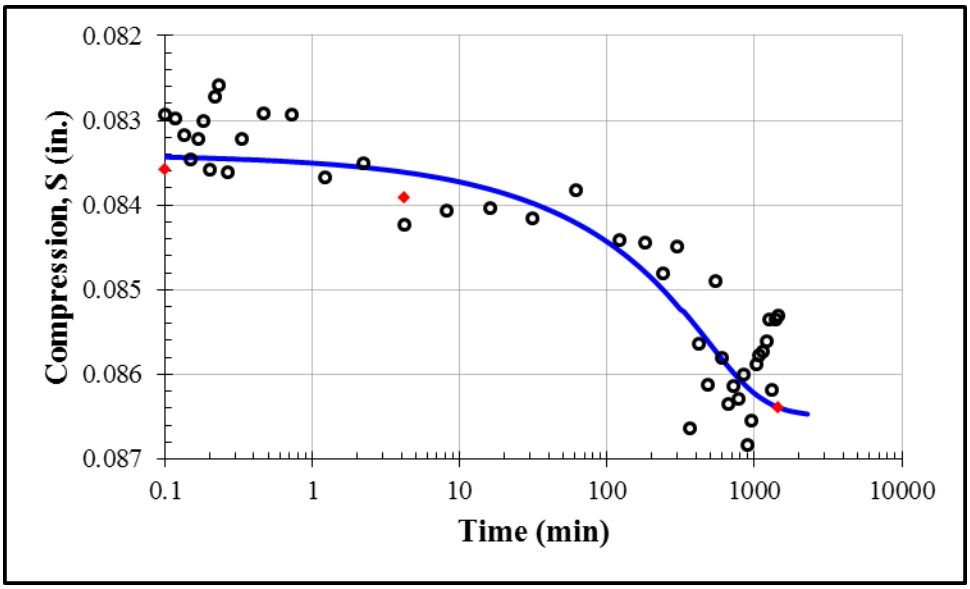

Second Loading: 8000 psf				
S_0 (in.)	S_{100} (in.)	c_v (in^2/min)	k (ft/day)	t_{50} (min)
0.0863	0.0960	0.00012	2.2 x 10^{-9}	185

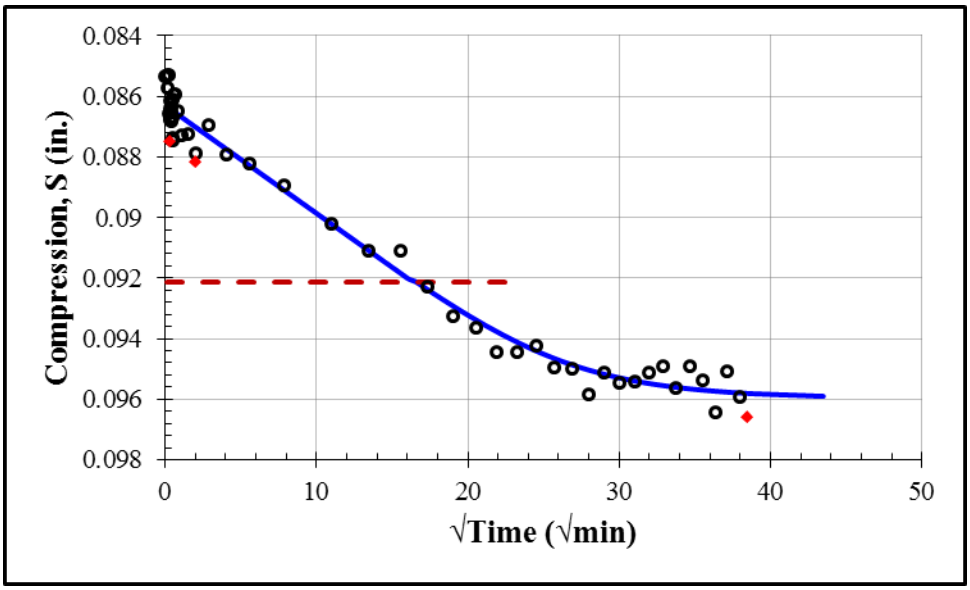

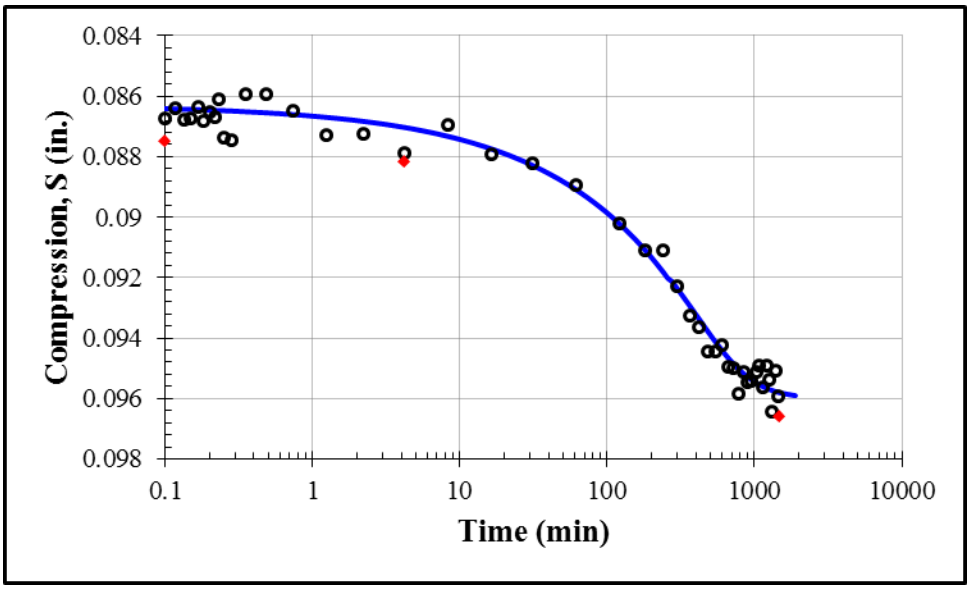

Second Loading: 16000 psf				
S_0 (in.)	S_{100} (in.)	c_v (in^2/min)	k (ft/day)	t_{50} (min)
0.0973	0.1150	0.000065	1.1 x 10^{-9}	332

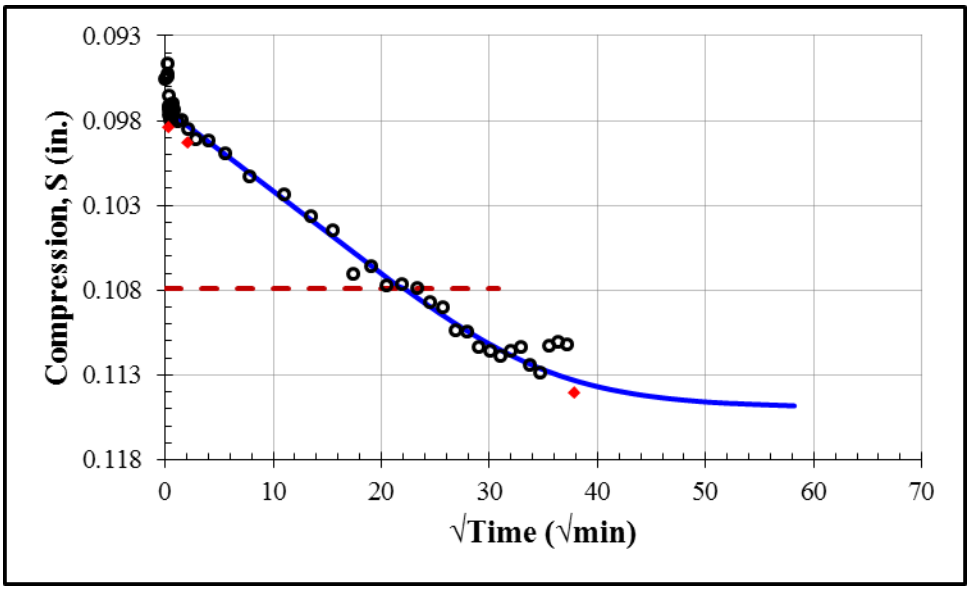

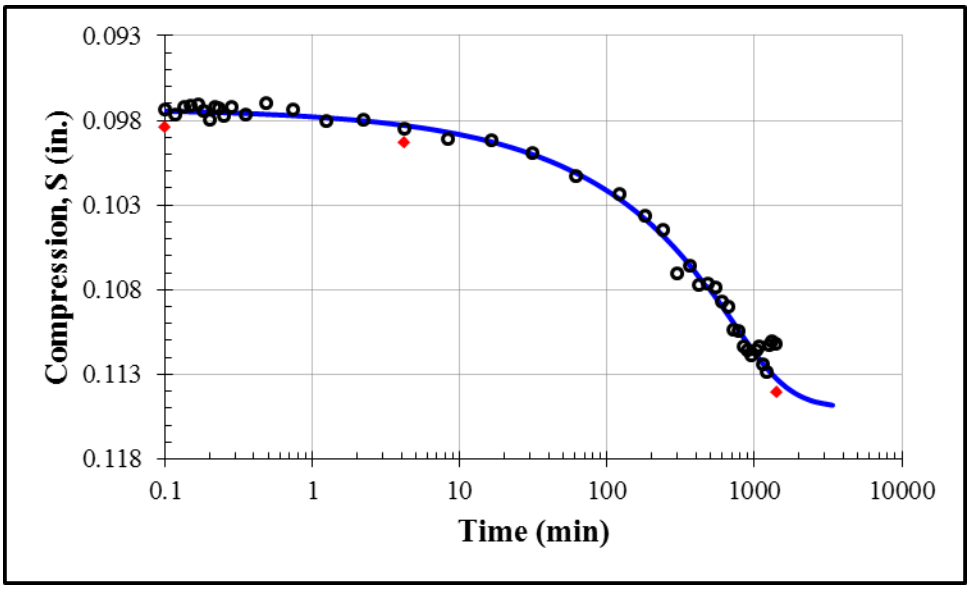

Second Loading: 32000 psf				
S_0 (in.)	S_{100} (in.)	c_v (in^2/min)	k (ft/day)	t_{50} (min)
0.1139	0.1354	0.00008	7.9 x 10^{-10}	257

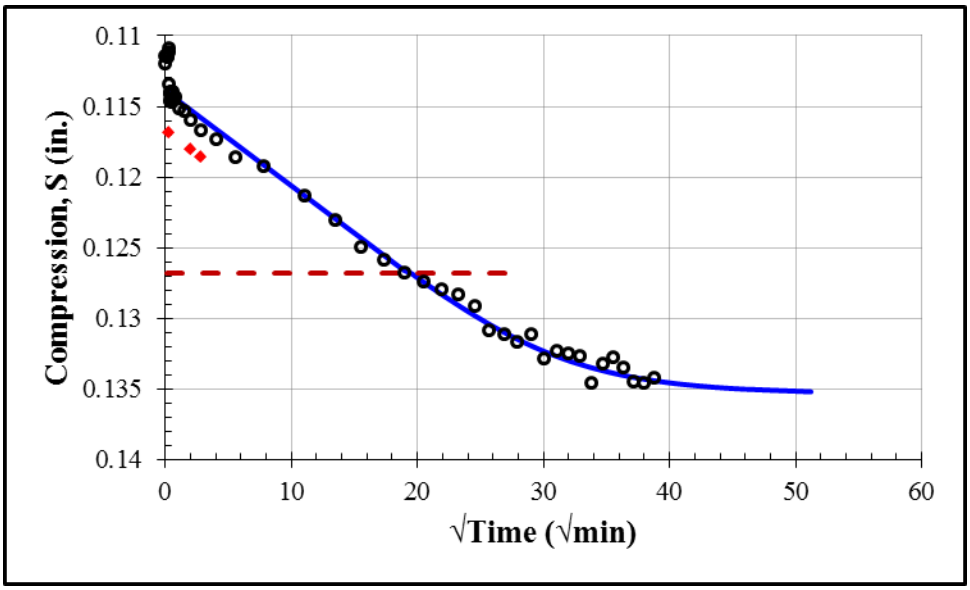

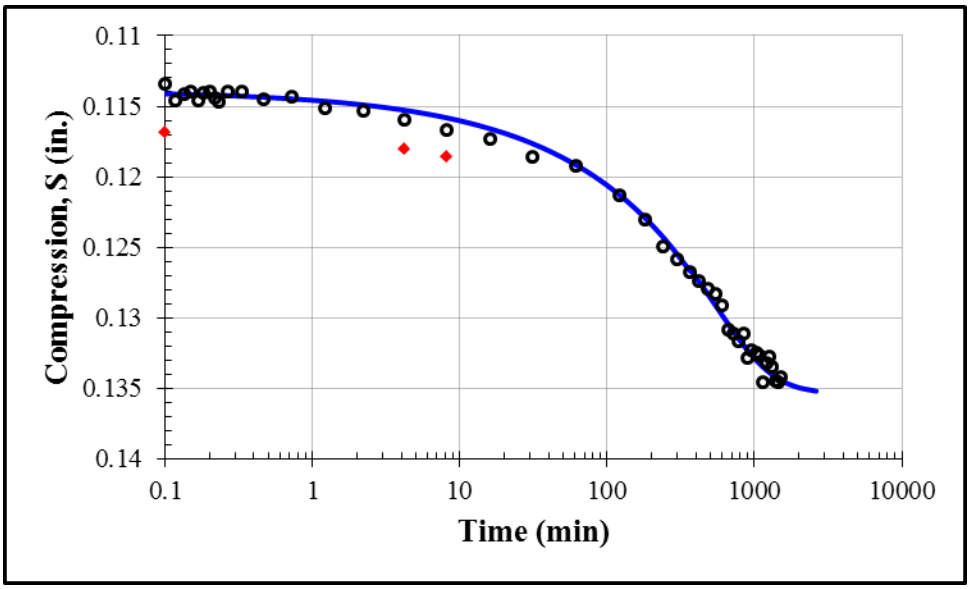

Second Loading: 64000 psf				
S_0 (in.)	S_{100} (in.)	c_v (in^2/min)	k (ft/day)	t_{50} (min)
0.1385	0.1626	0.000083	4.5×10^{-10}	231

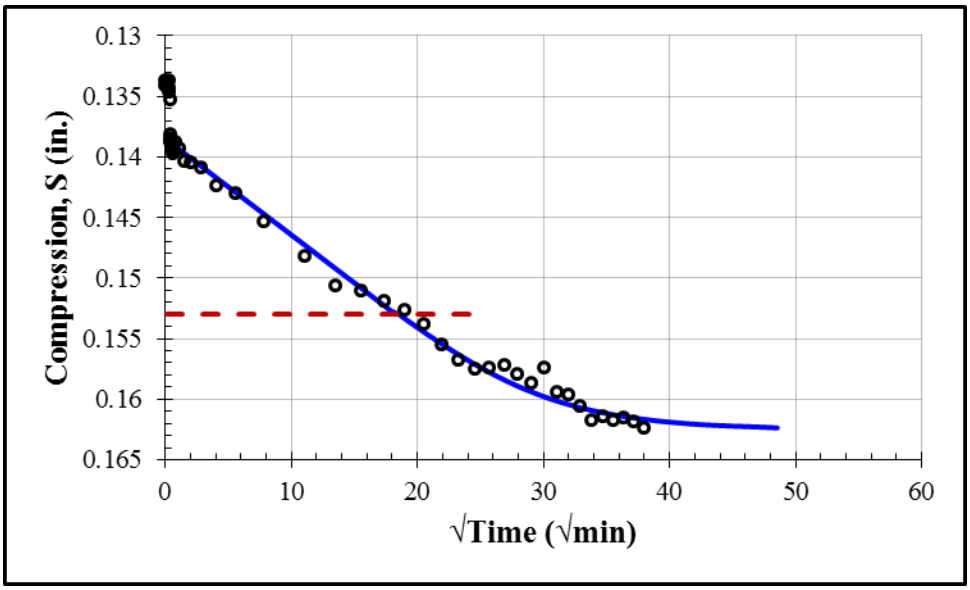

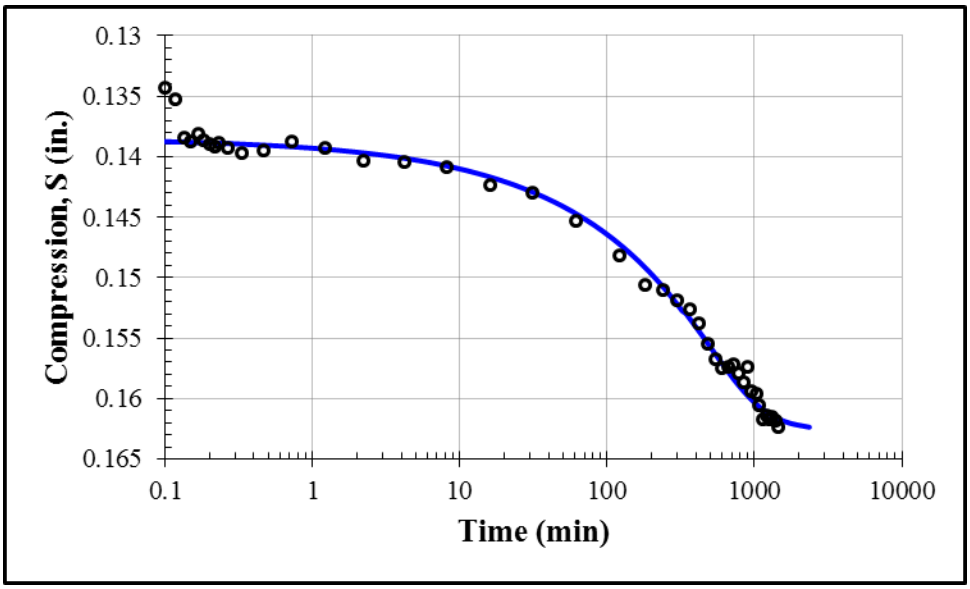

Second Unloading: 16000 psf				
S_0 (in.)	S_{100} (in.)	c_v (in^2/min)	k (ft/day)	t_{50} (min)
0.1538	0.1375	0.00009	2.2 x 10^{-10}	194

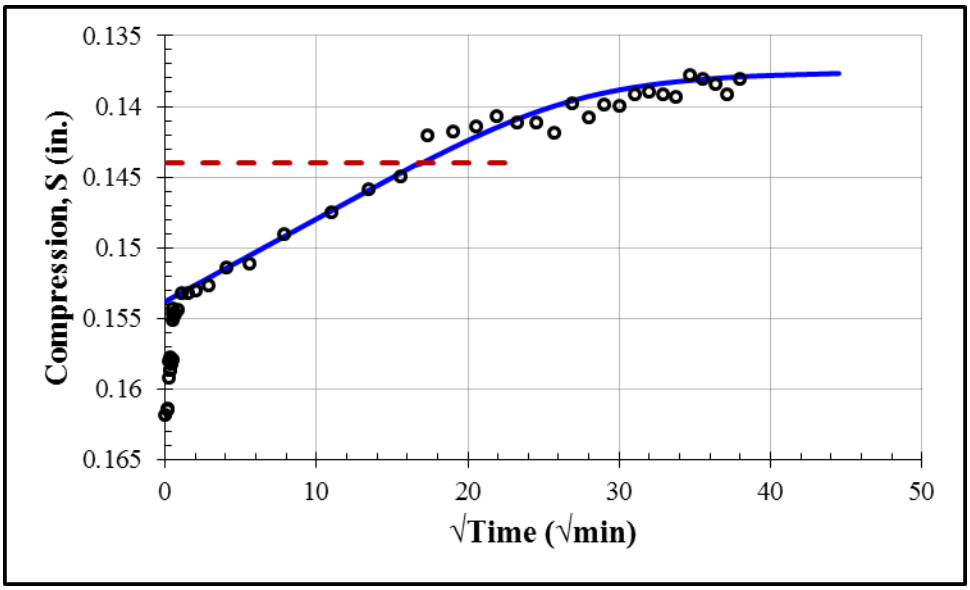

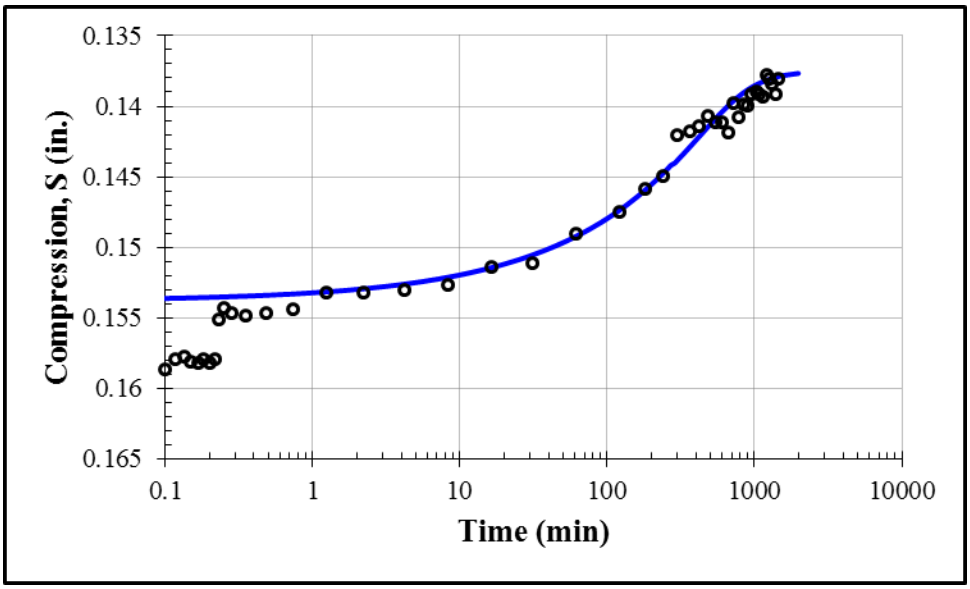

Second Unloading: 4000 psf				
S_0 (in.)	S_{100} (in.)	c_v (in^2/min)	k (ft/day)	t_{50} (min)
0.1348	0.1093	0.00006	9.4×10^{-10}	315

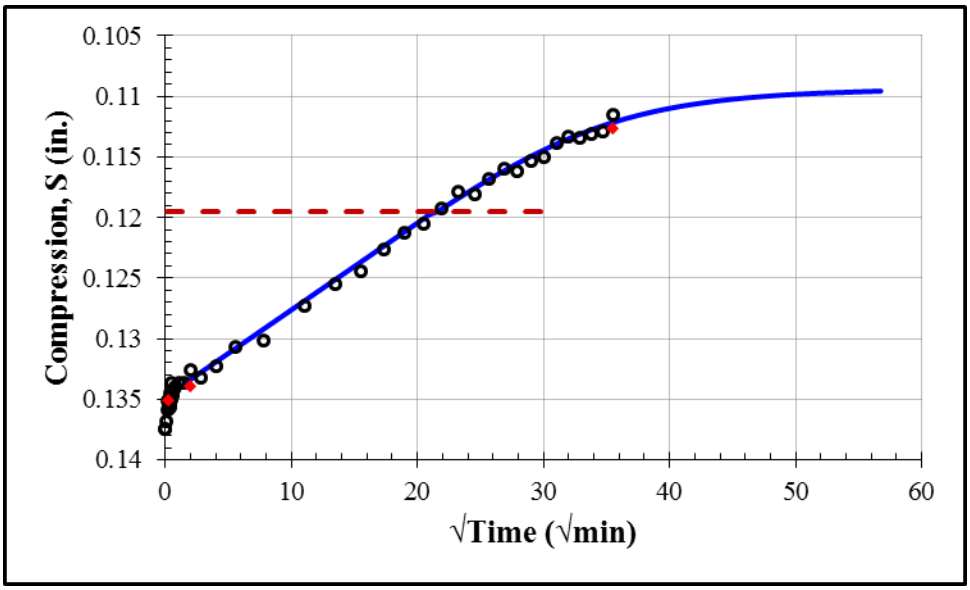

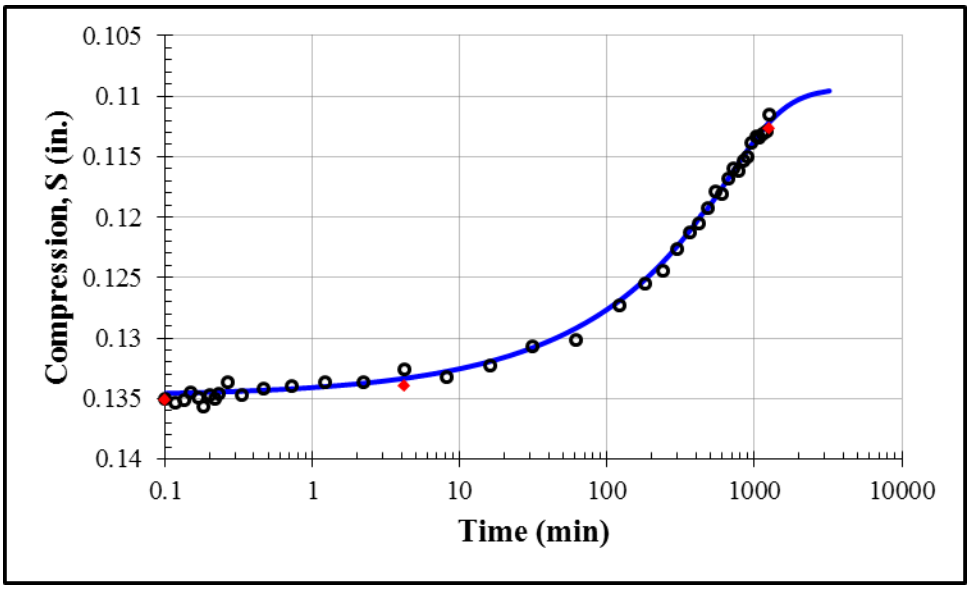

Second Unloading: 1000 psf				
S_0 (in.)	S_{100} (in.)	c_v (in^2/min)	k (ft/day)	t_{50} (min)
0.1098	0.0820	0.000035	2.4 x 10^{-9}	588

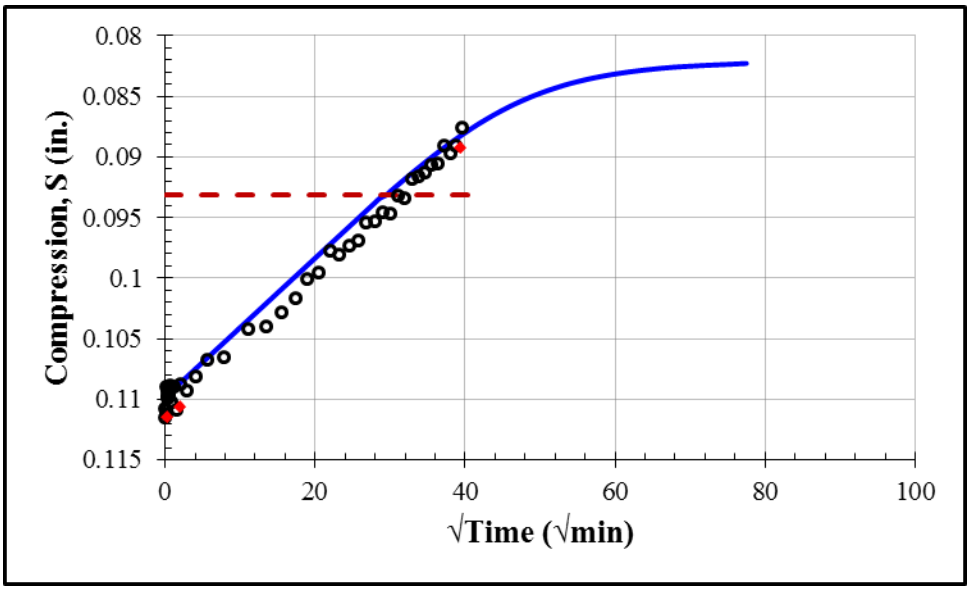

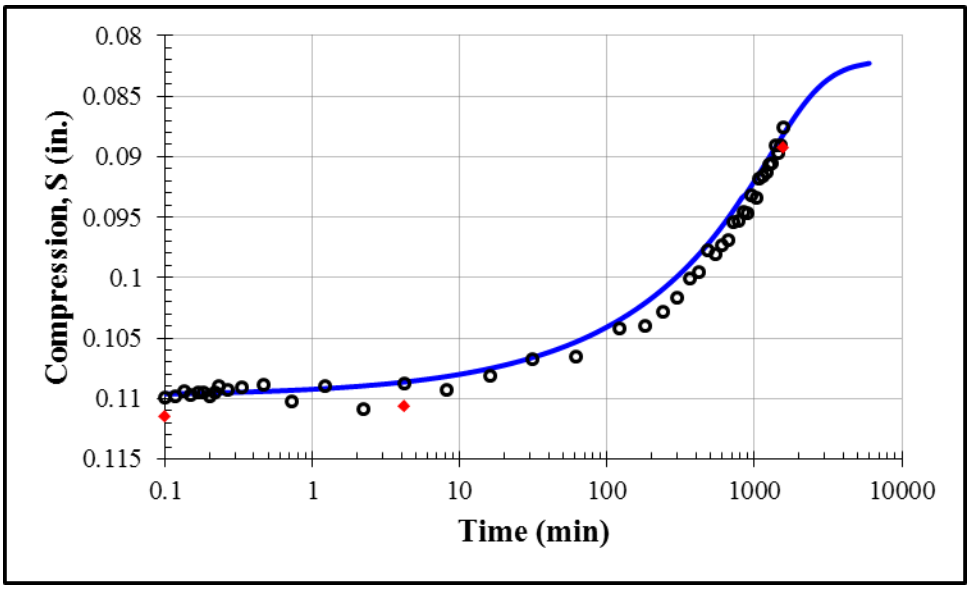

Second Unloading: 250 psf				
S_0 (in.)	S_{100} (in.)	c_v (in^2/min)	k (ft/day)	t_{50} (min)
0.0892	0.0529	0.000019	7.1 x 10^{-9}	1164

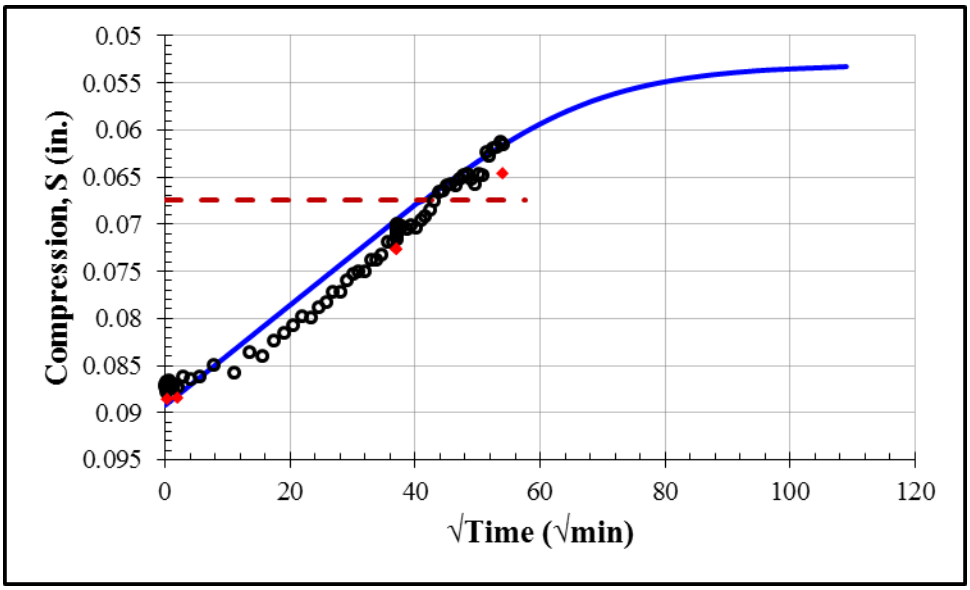

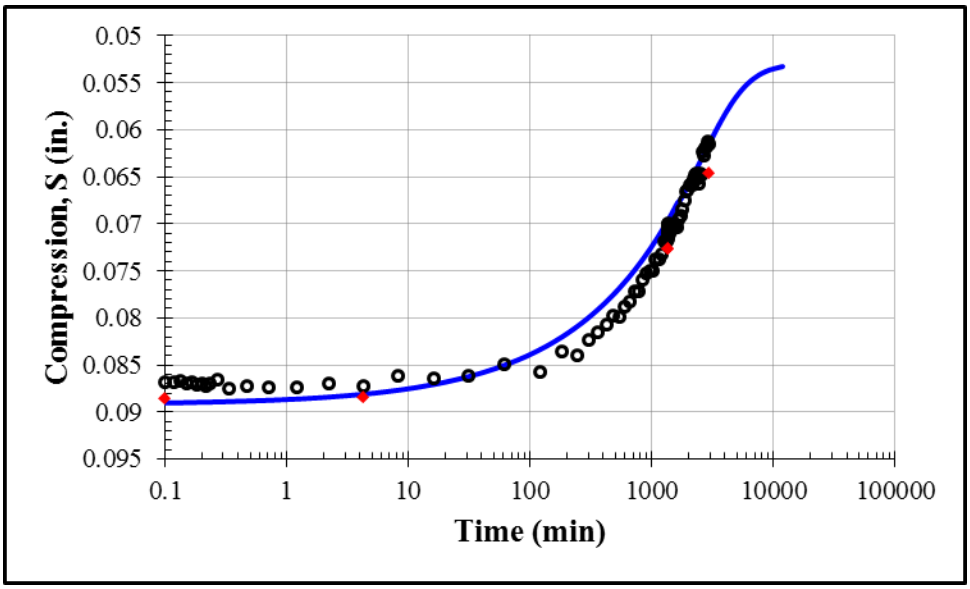

Second Unloading: 125 psf				
S_0 (in.)	S_{100} (in.)	c_v (in^2/min)	k (ft/day)	t_{50} (min)
0.0892	0.0529	0.000019	1.4×10^{-8}	1164

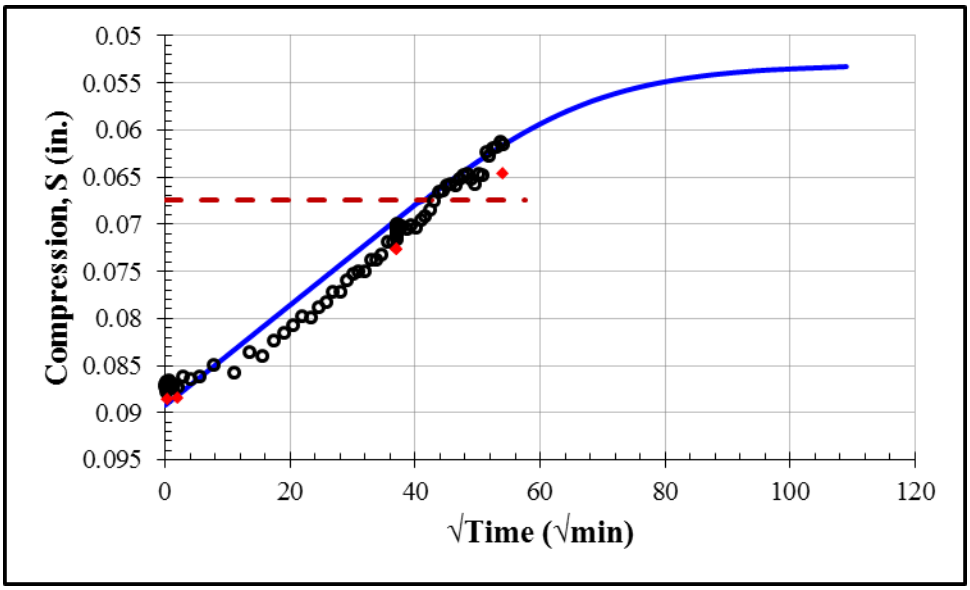

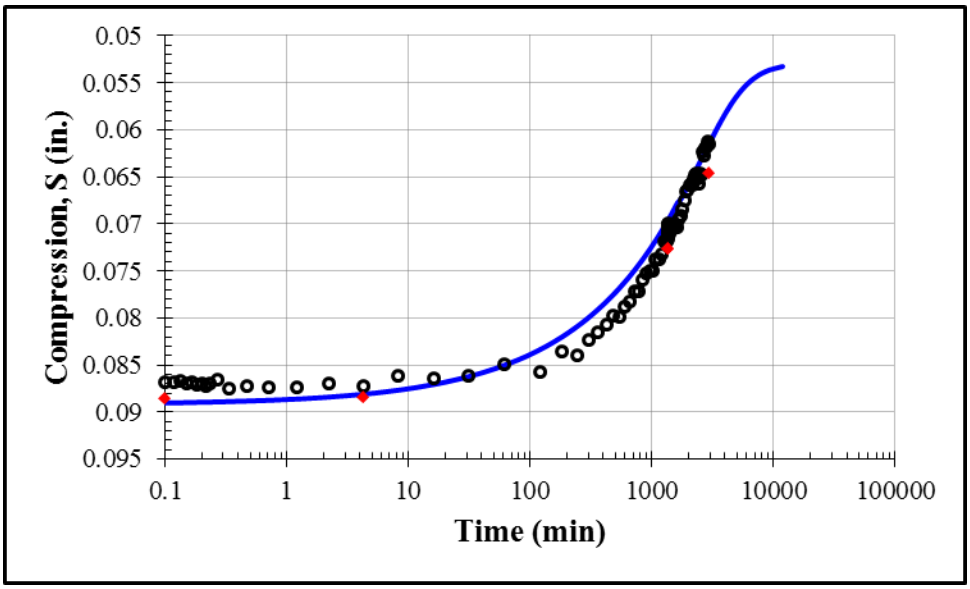

Appendix F: Consolidation Test 5

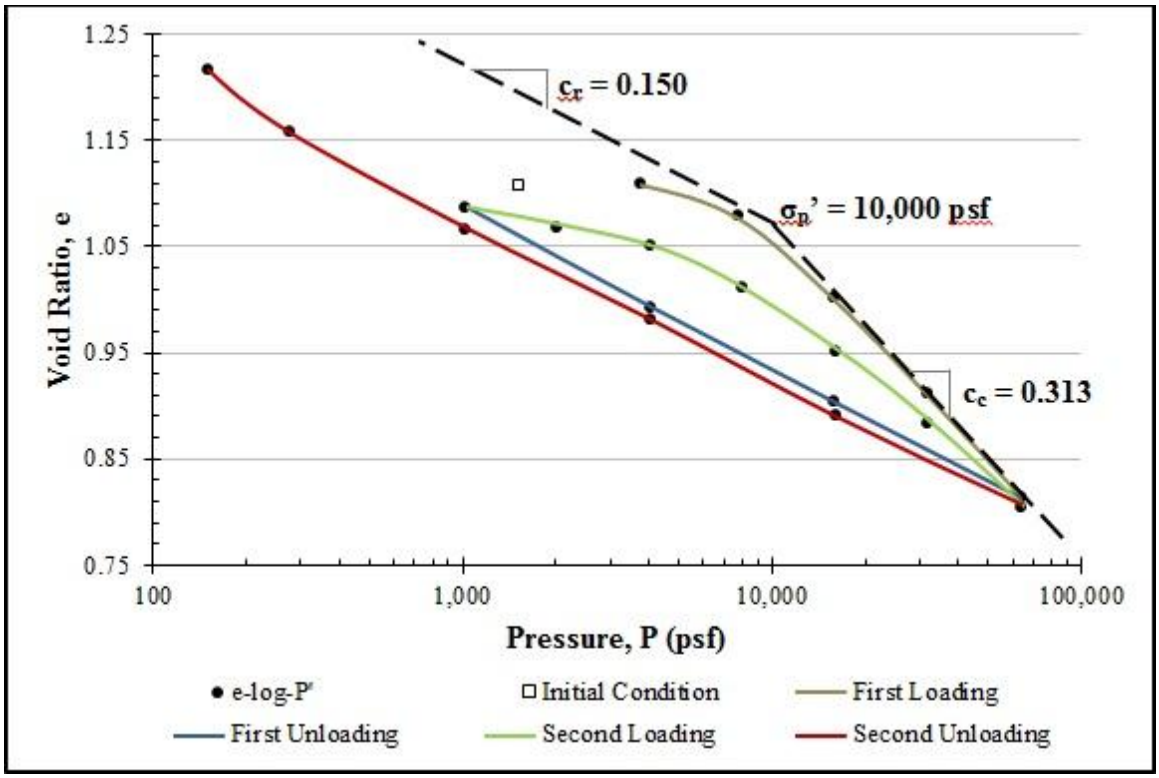

$$c_c = -\frac{e_2 - e_1}{\log(\sigma_2 / \sigma_1)} = -\frac{0.788 - 1.071}{\log(80000/10000)} = 0.313$$

$$c_r = -\frac{e_2 - e_1}{\log(\sigma_2 / \sigma_1)} = -\frac{1.071 - 1.235}{\log(10000/800)} = 0.150$$

$$R_c = \frac{c_c}{1 + e_0} = \frac{0.313}{1 + 1.1076} = 0.149$$

$$R_r = \frac{c_r}{1 + e_0} = \frac{0.150}{1 + 1.1076} = 0.071$$

Soaking at Constant Volume Starting at 1500 psf				
S_0 (in.)	S_{100} (in.)	c_v (in^2/min)	k (ft/day)	t_{50} (min)
0.0000	0.0012	0.000067	3.0×10^{-10}	395

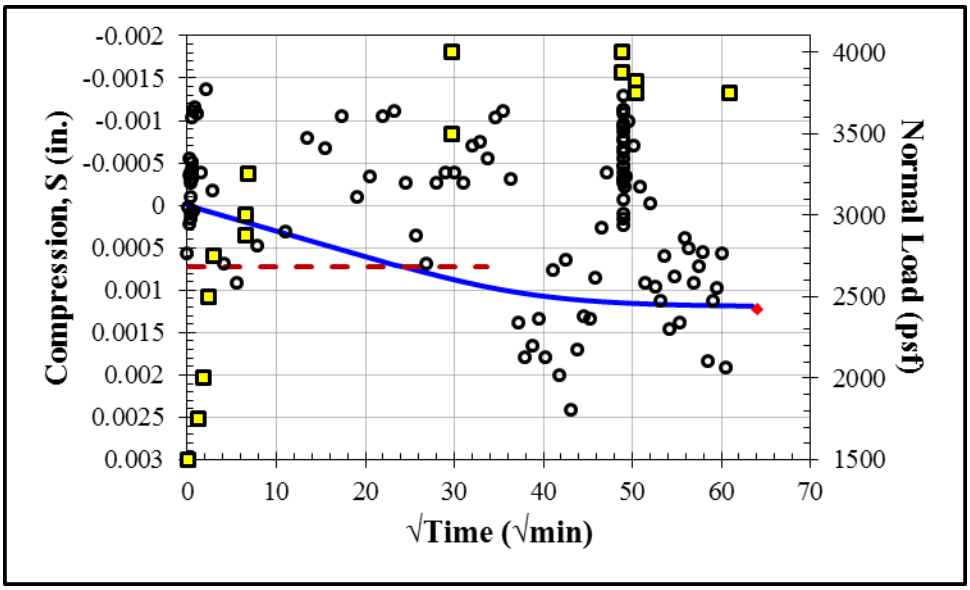

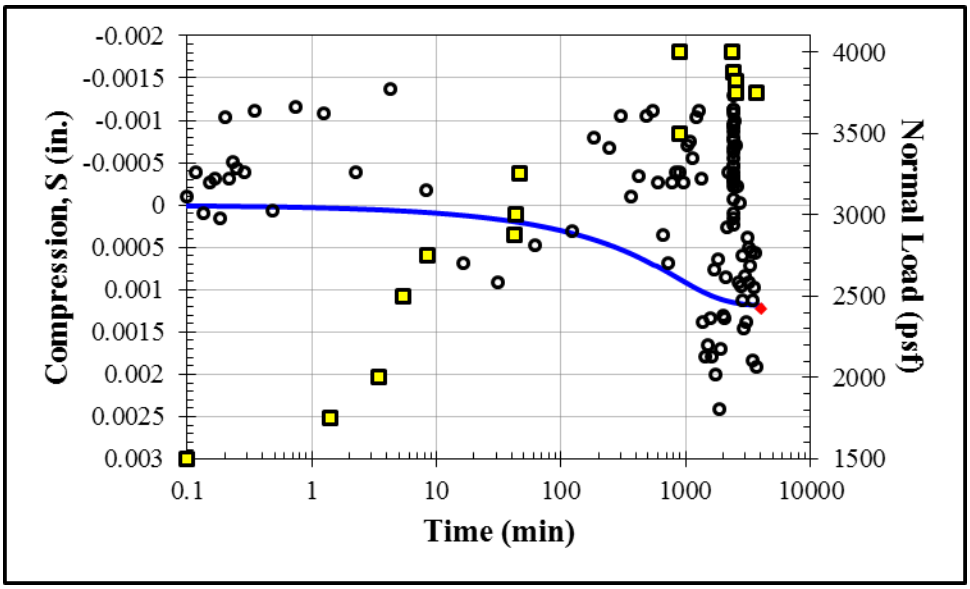

First Loading: 7750 psf				
S_0 (in.)	S_{100} (in.)	c_v (in^2/min)	k (ft/day)	t_{50} (min)
0.0056	0.0144	0.001	1.9 x 10^{-8}	26

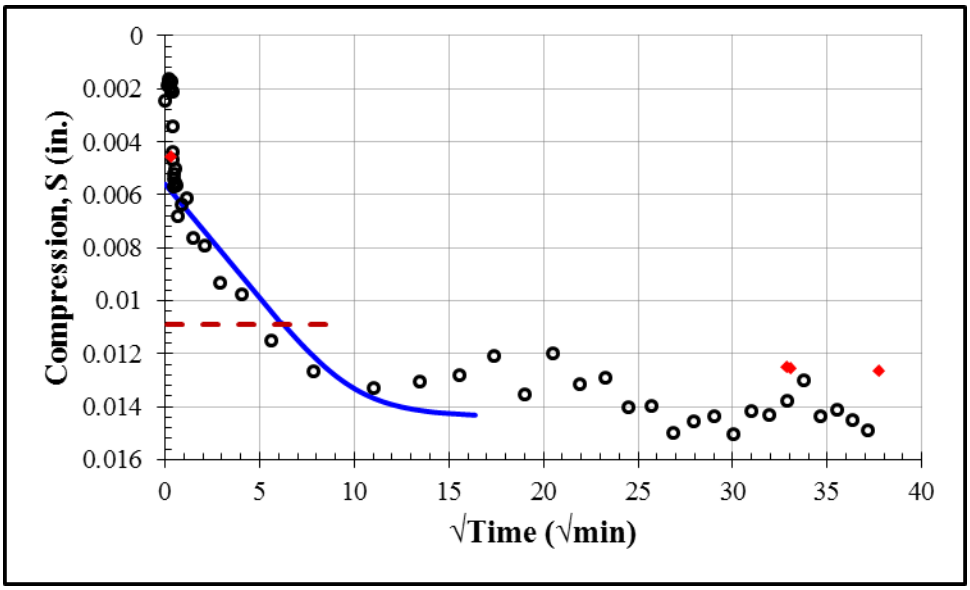

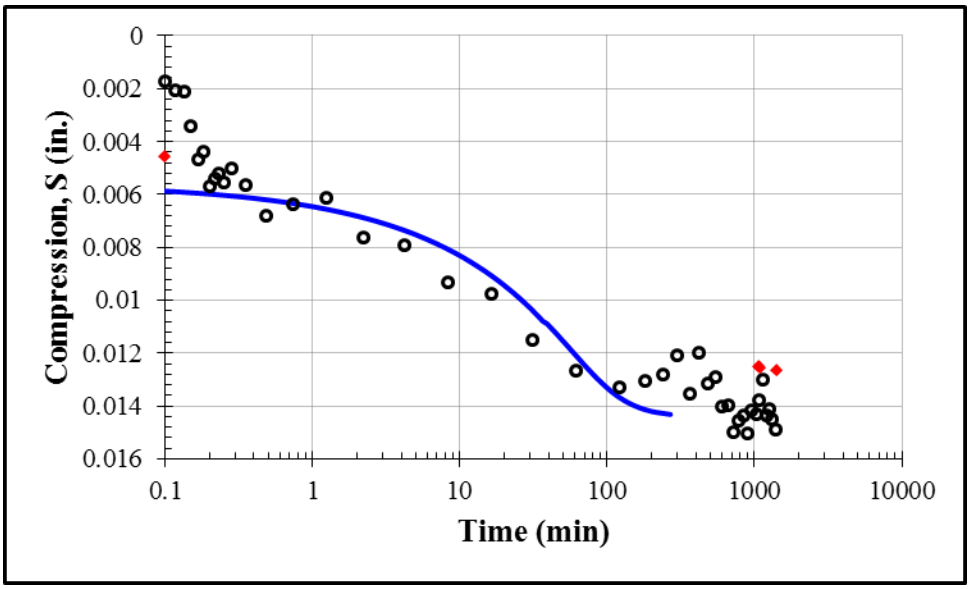

First Loading: 15750 psf				
S_0 (in.)	S_{100} (in.)	c_v (in^2/min)	k (ft/day)	t_{50} (min)
0.0205	0.0435	0.00035	8.3 x 10^{-8}	73

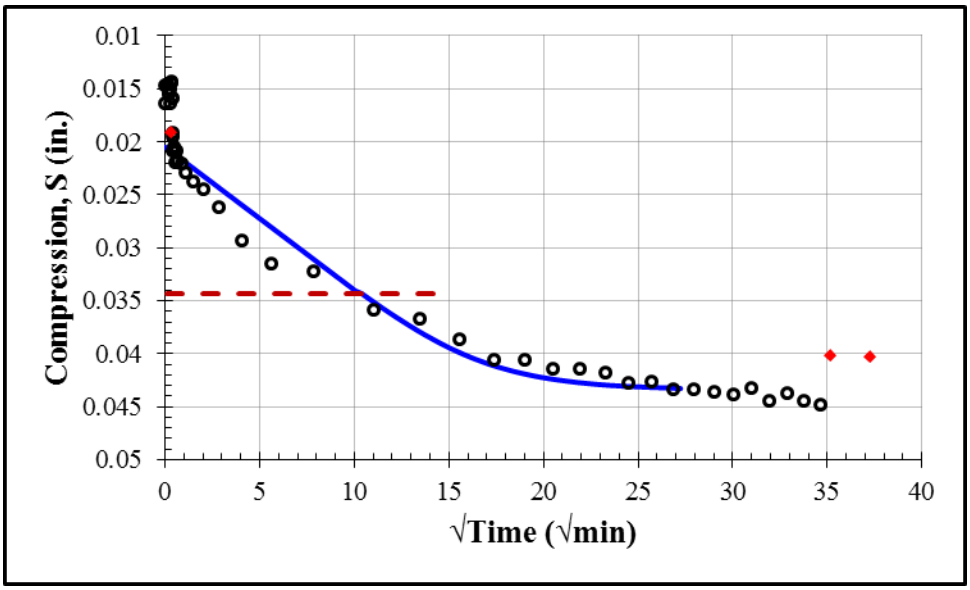

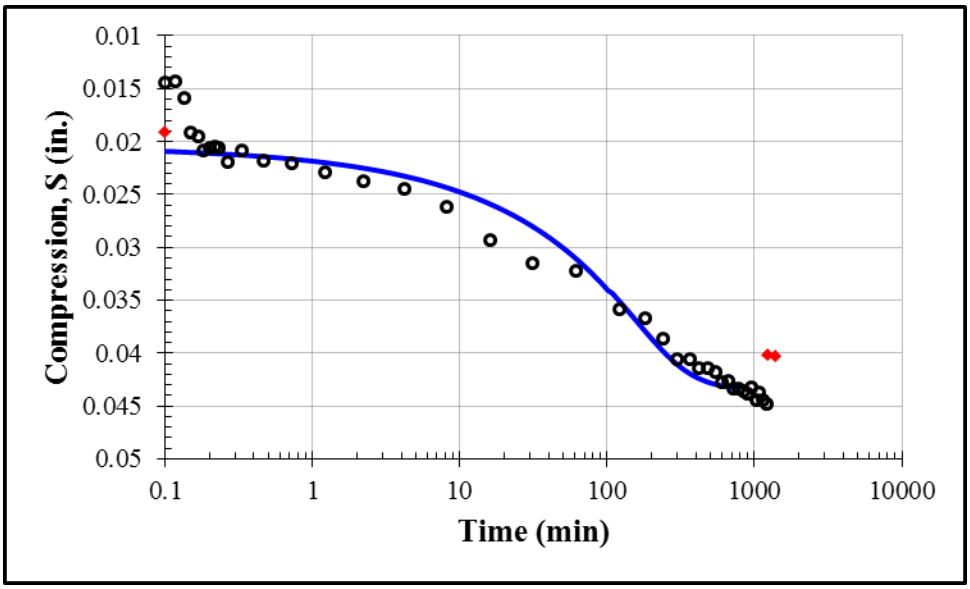

First Loading: 31750 psf				
S_0 (in.)	S_{100} (in.)	c_v (in^2/min)	k (ft/day)	t_{50} (min)
0.0491	0.0787	0.00018	2.7 x 10^{-9}	130

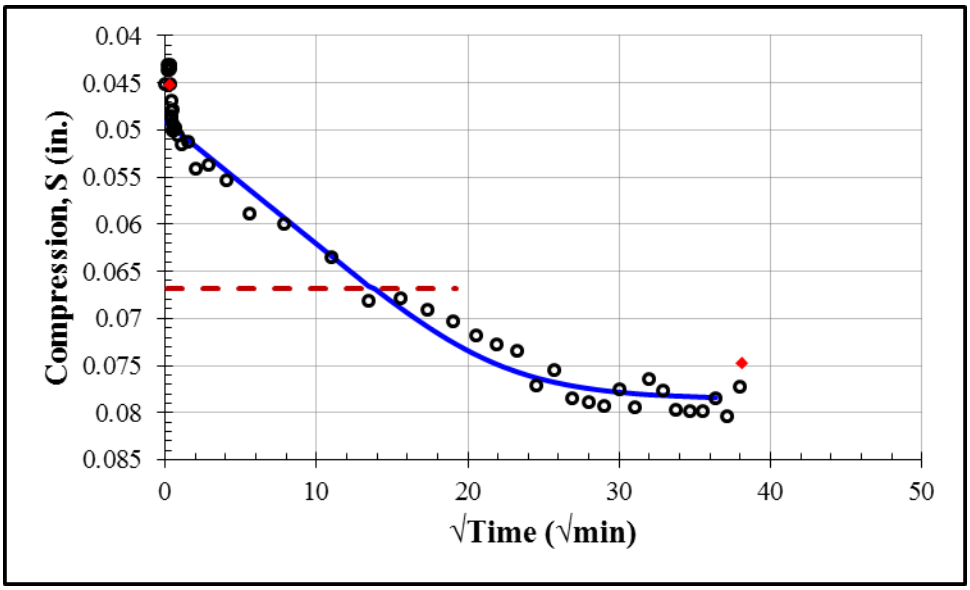

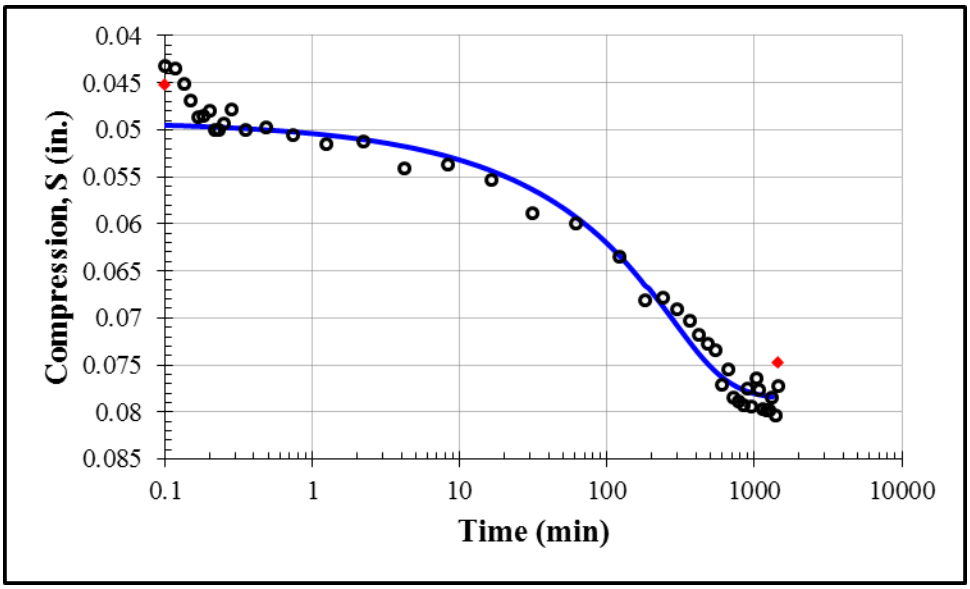

First Loading: 63750 psf				
S_0 (in.)	S_{100} (in.)	c_v (in^2/min)	k (ft/day)	t_{50} (min)
0.0810	0.1168	0.0001	8.6×10^{-10}	212

Note: The LVDT lost contact during this load increment. The dial gage was used instead.

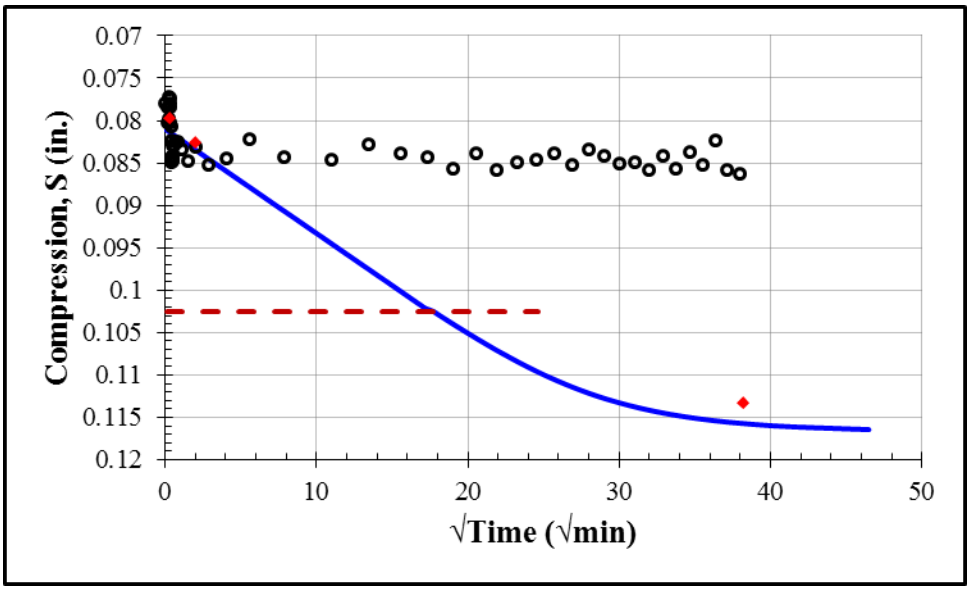

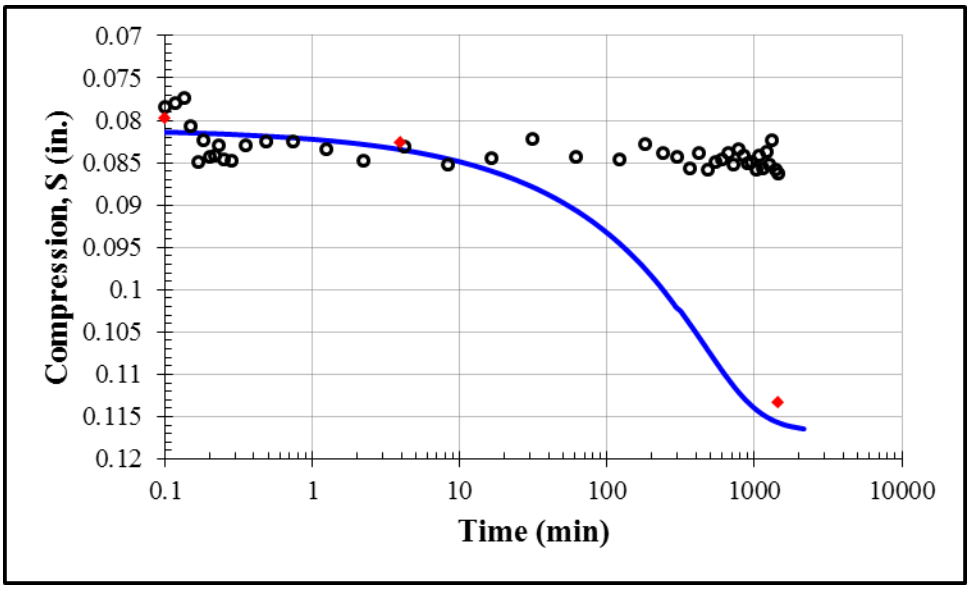

First Unloading: 15750 psf				
S_0 (in.)	S_{100} (in.)	c_v (in^2/min)	k (ft/day)	t_{50} (min)
0.1085	0.0802	0.00009	4.1 x 10^{-10}	230

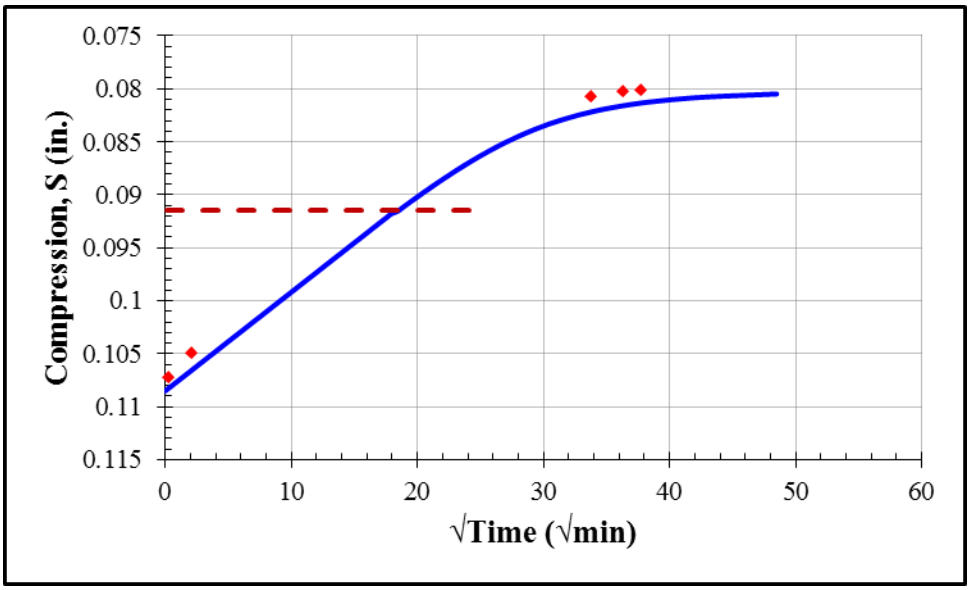

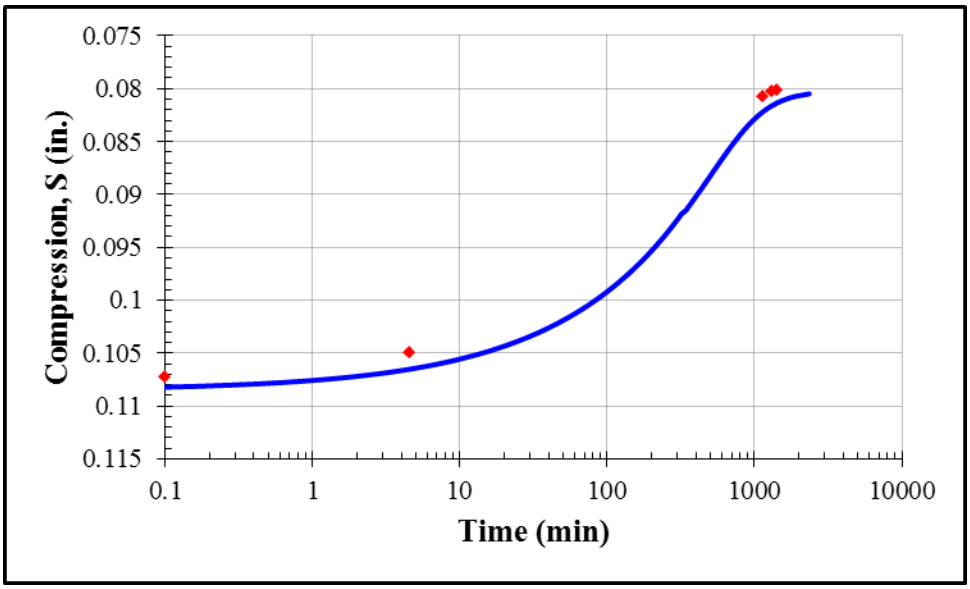

Second Unloading: 4000 psf				
S_0 (in.)	S_{100} (in.)	c_v (in^2/min)	k (ft/day)	t_{50} (min)
0.0784	0.0465	0.00006	1.3×10^{-9}	346

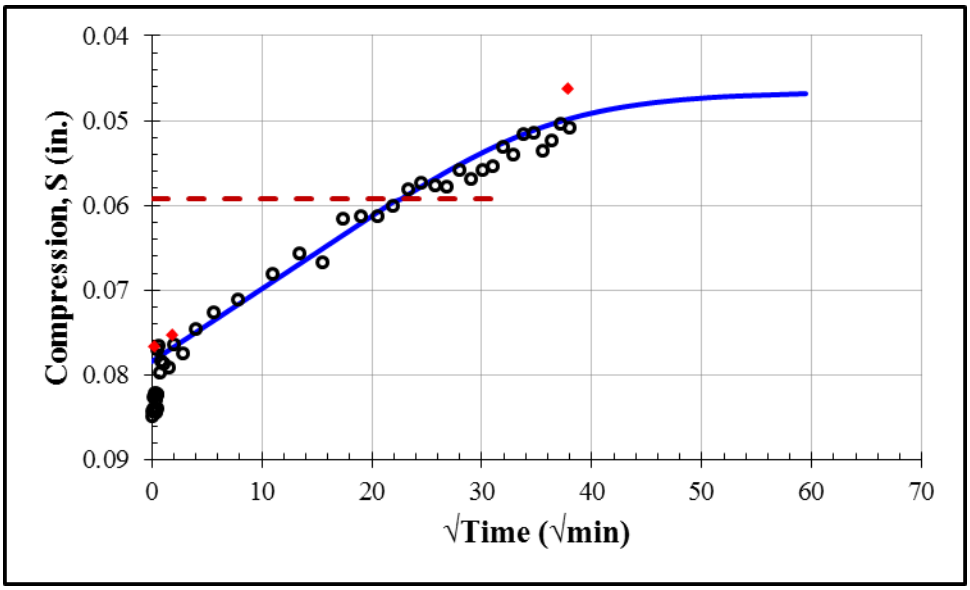

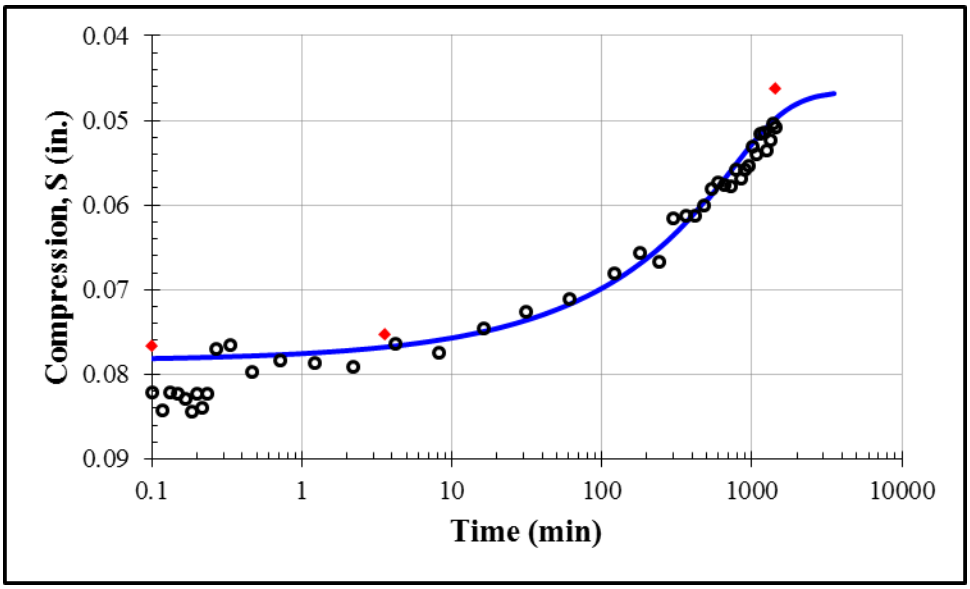

First Unloading: 1000 psf				
S_0 (in.)	S_{100} (in.)	c_v (in^2/min)	k (ft/day)	t_{50} (min)
0.0462	0.0110	0.000065	6.3 x 10^{-9}	356

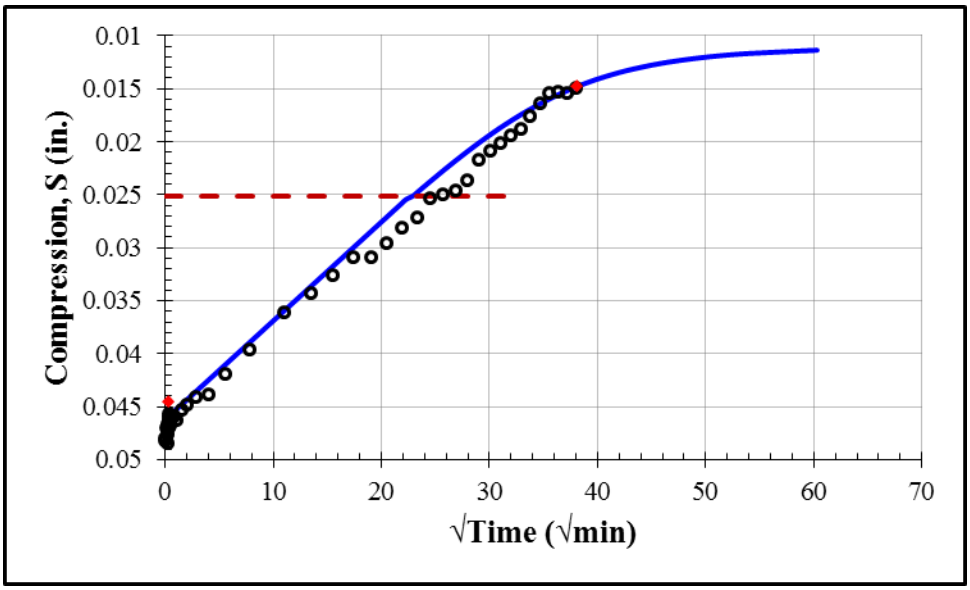

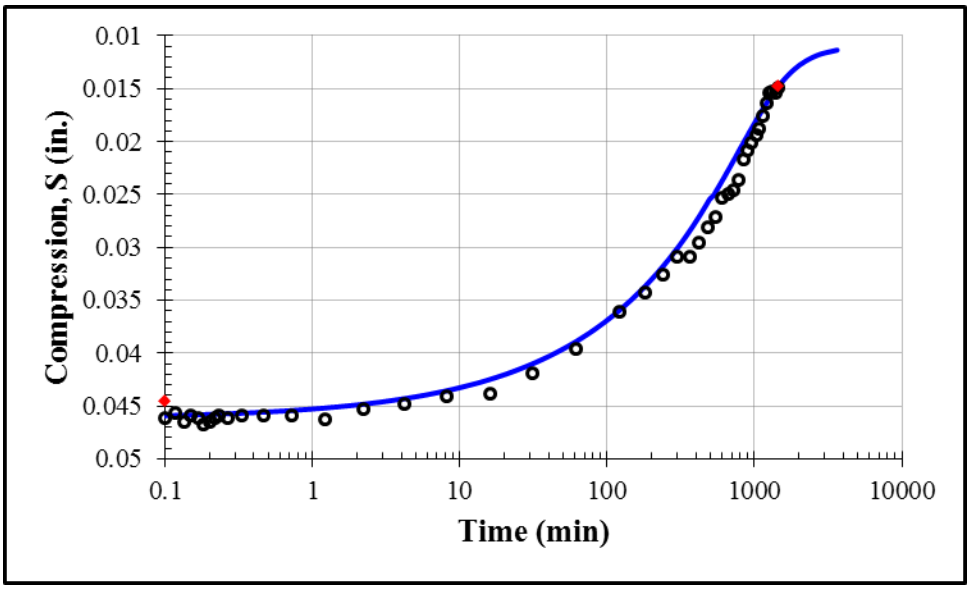

Second Loading: 2000 psf				
S_0 (in.)	S_{100} (in.)	c_v (in^2/min)	k (ft/day)	t_{50} (min)
0.0150	0.0178	0.00015	3.5 x 10^{-9}	170

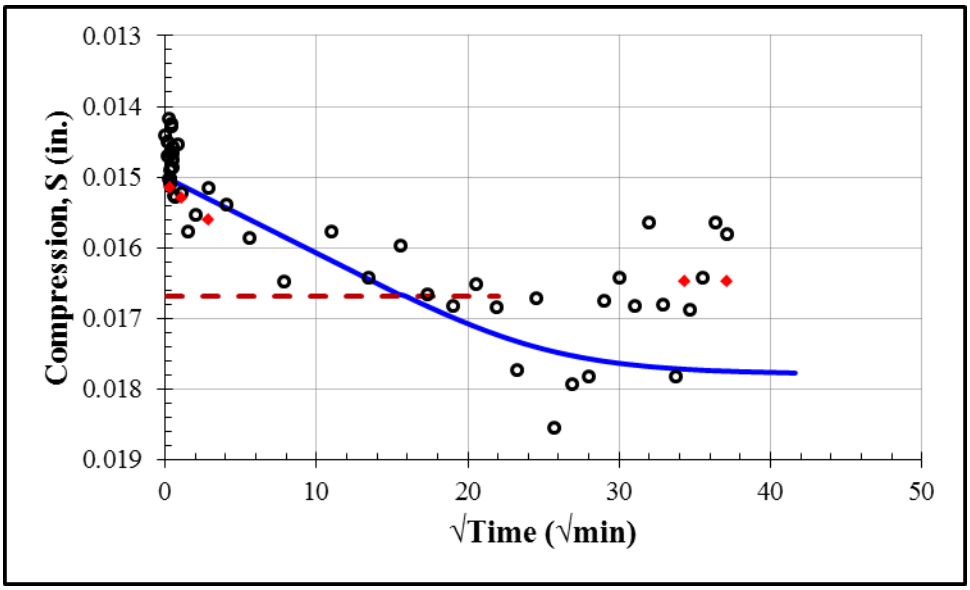

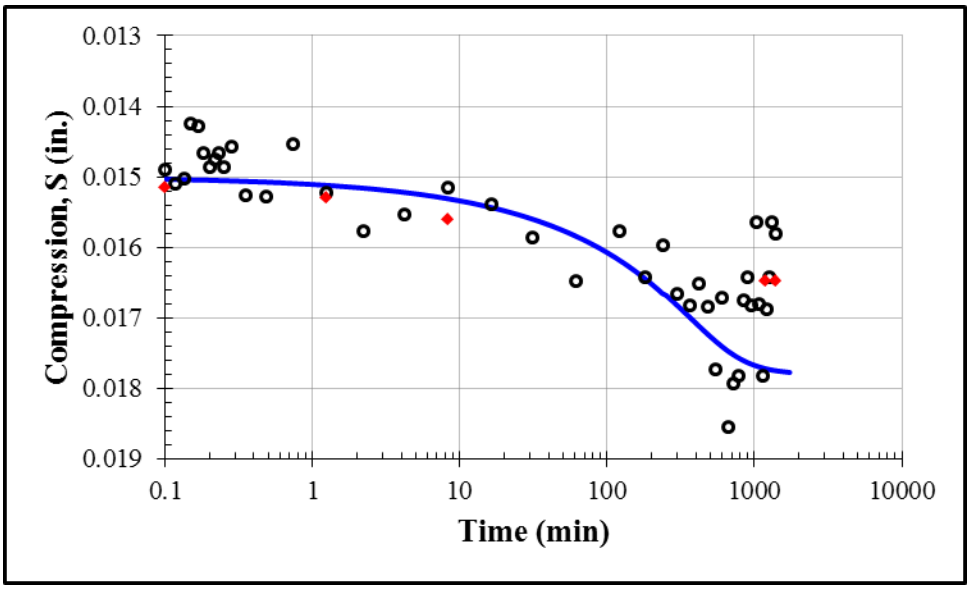

Second Loading: 4000 psf				
S_0 (in.)	S_{100} (in.)	c_v (in^2/min)	k (ft/day)	t_{50} (min)
0.0161	0.0248	0.0002	7.2 x 10^{-9}	127

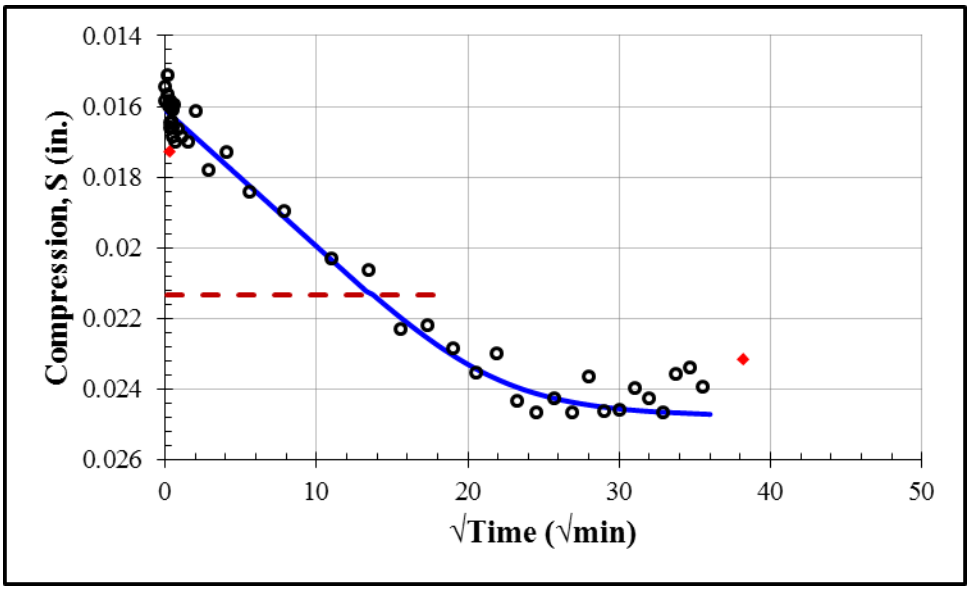

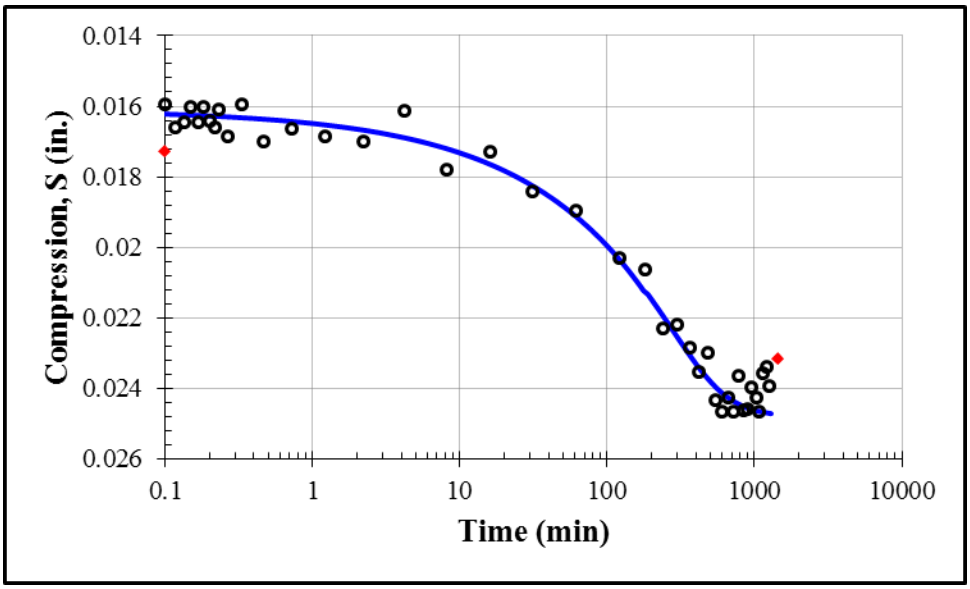

Second Loading: 8000 psf				
S_0 (in.)	S_{100} (in.)	c_v (in^2/min)	k (ft/day)	t_{50} (min)
0.0231	0.0399	0.00016	5.5 x 10^{-9}	156

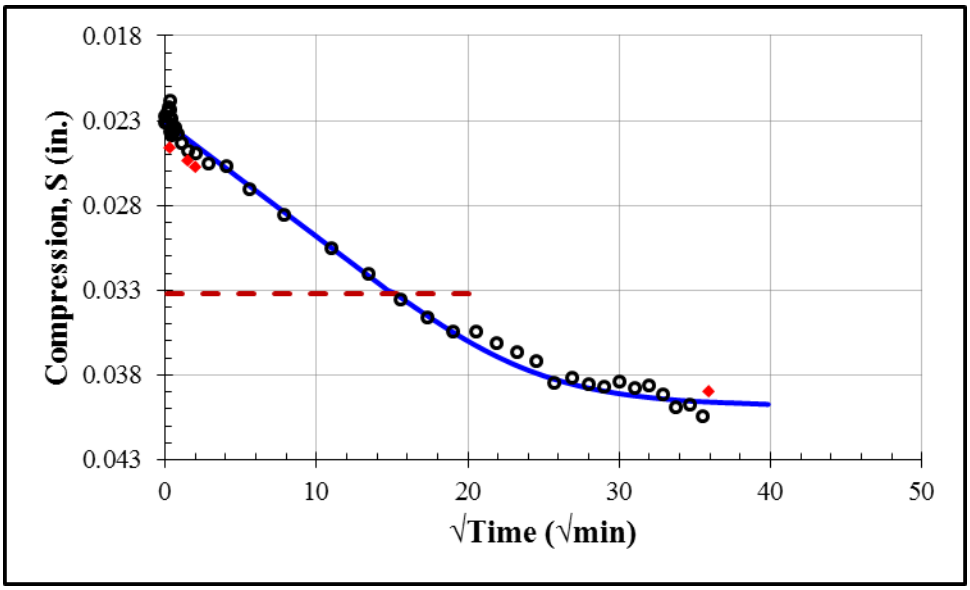

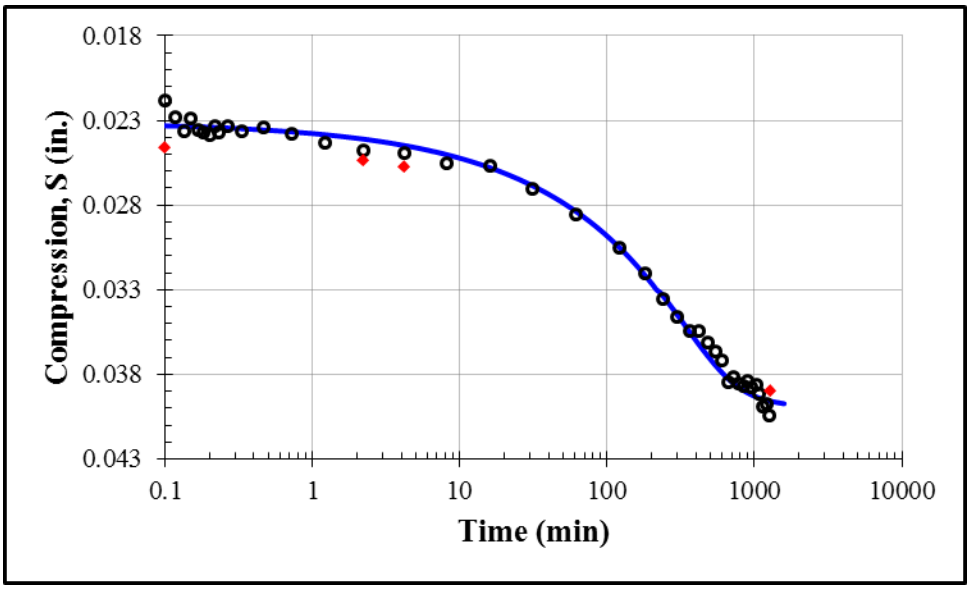

Second Loading: 16000 psf				
S_0 (in.)	S_{100} (in.)	c_v (in^2/min)	k (ft/day)	t_{50} (min)
0.0415	0.0631	0.00013	2.8 x 10^{-9}	182

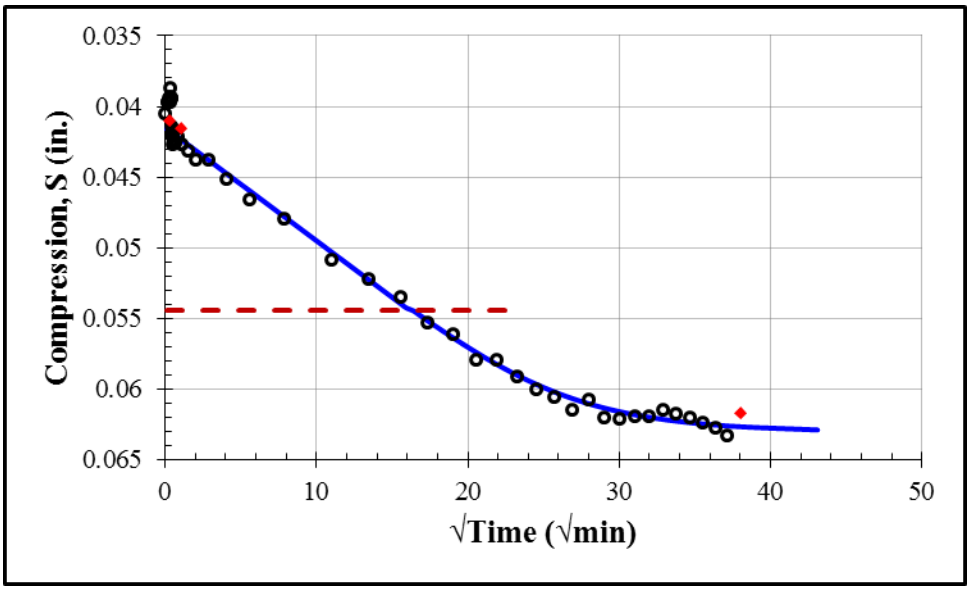

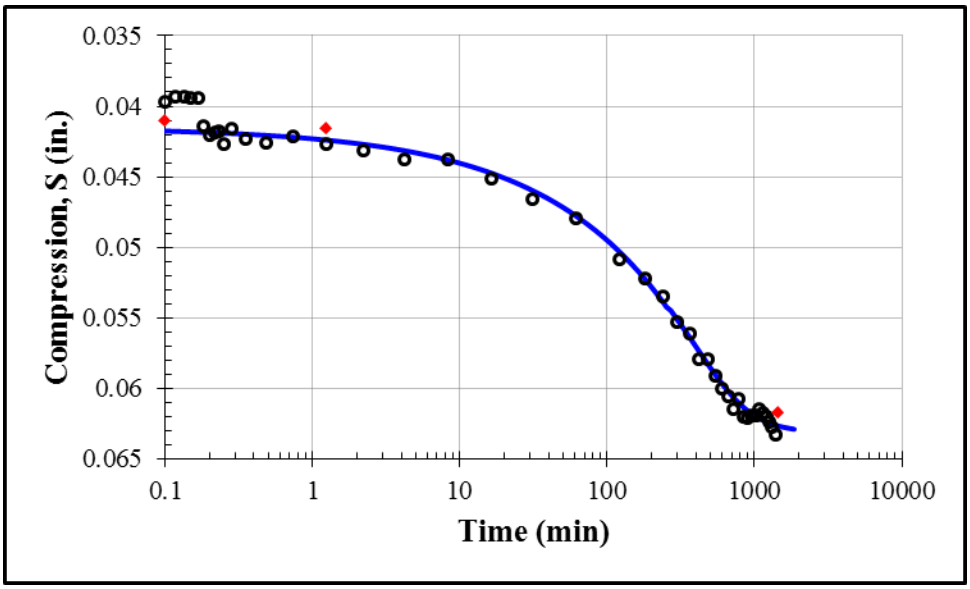

Second Loading: 32000 psf				
S_0 (in.)	S_{100} (in.)	c_v (in^2/min)	k (ft/day)	t_{50} (min)
0.0647	0.0889	0.00016	1.9×10^{-9}	139

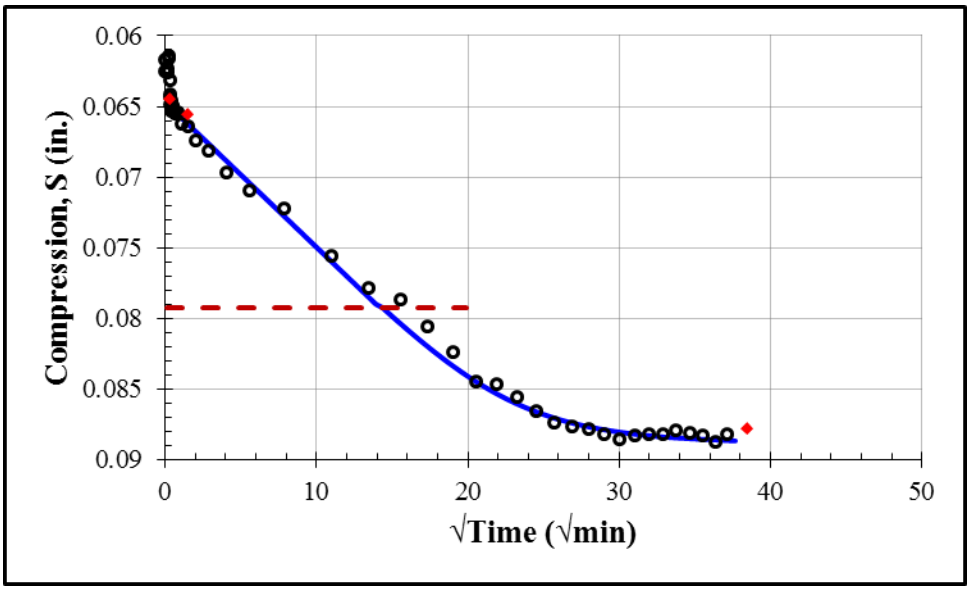

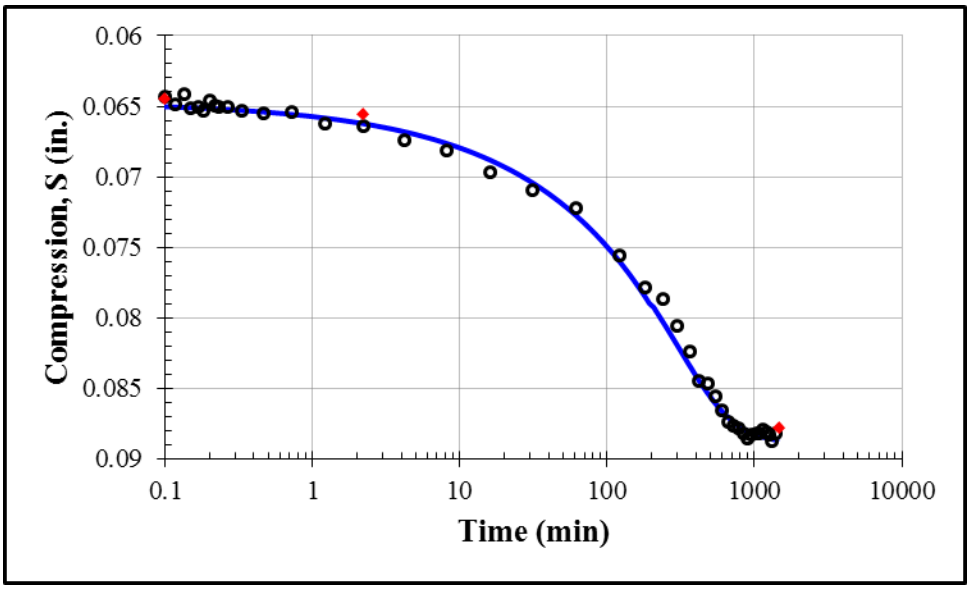

Second Loading: 64000 psf				
S_0 (in.)	S_{100} (in.)	c_v (in^2/min)	k (ft/day)	t_{50} (min)
0.0932	0.1198	0.00013	8.3×10^{-10}	157

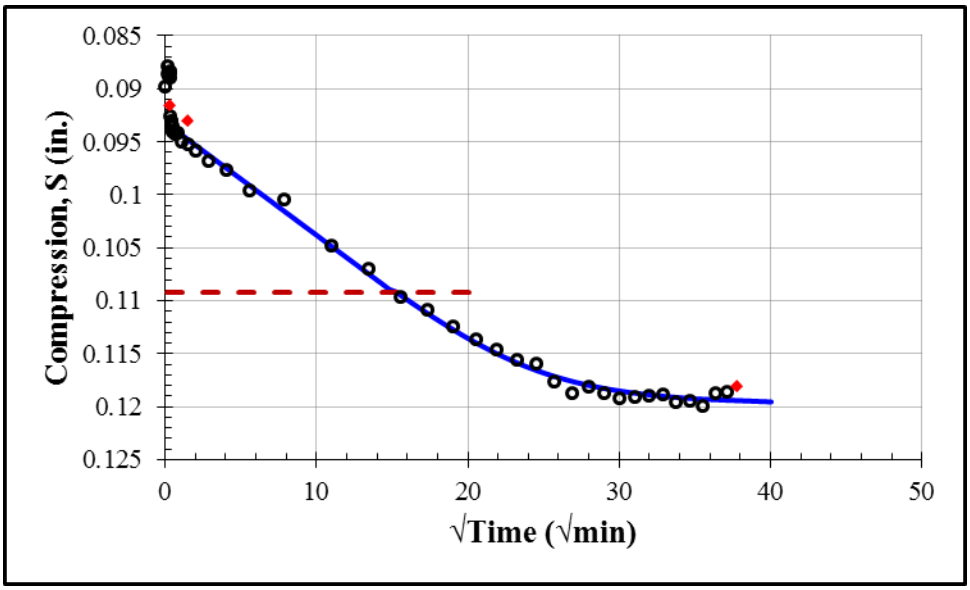

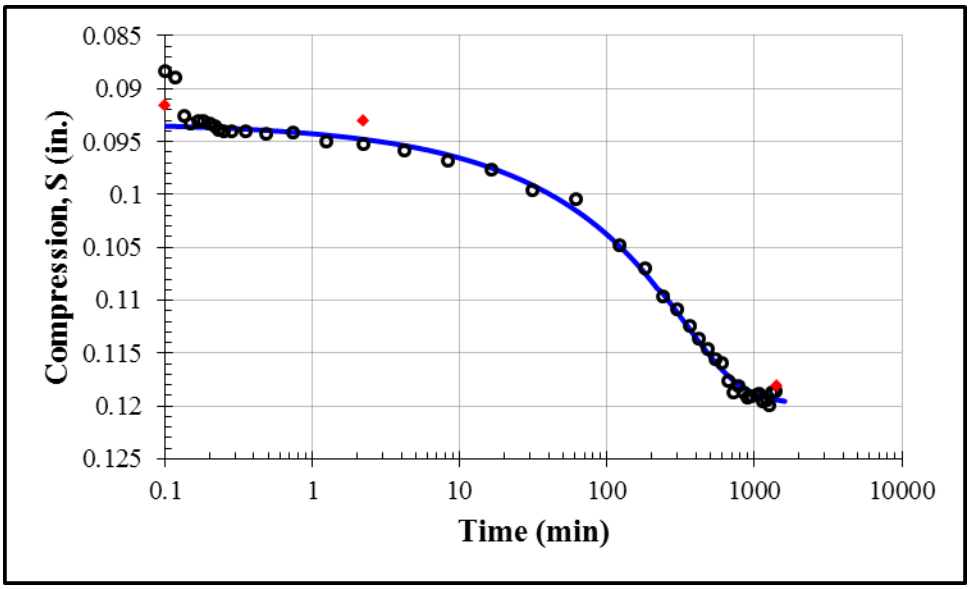

Second Unloading: 16000 psf				
S_0 (in.)	S_{100} (in.)	c_v (in^2/min)	k (ft/day)	t_{50} (min)
0.1130	0.0850	0.00012	5.4 x 10^{-10}	156

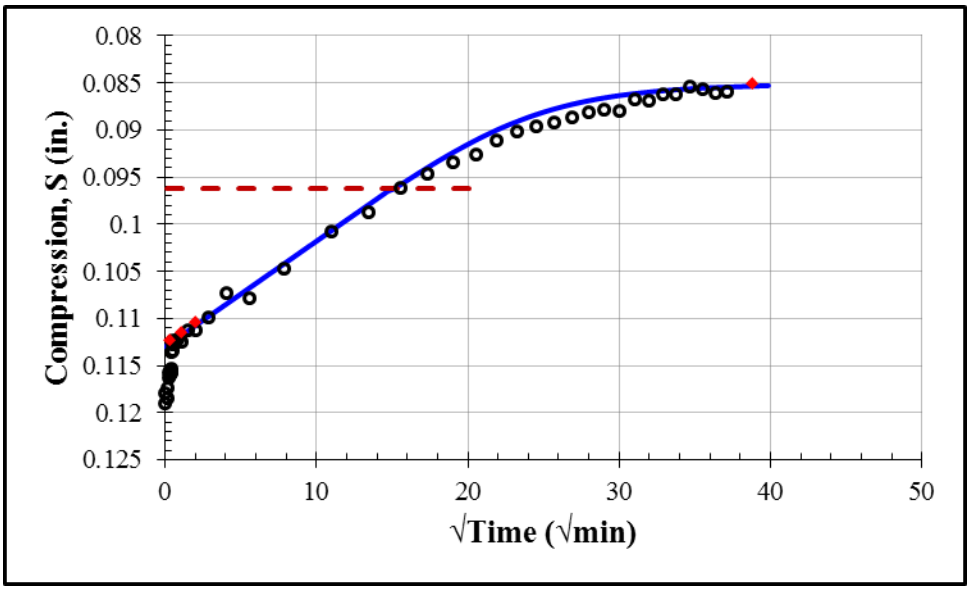

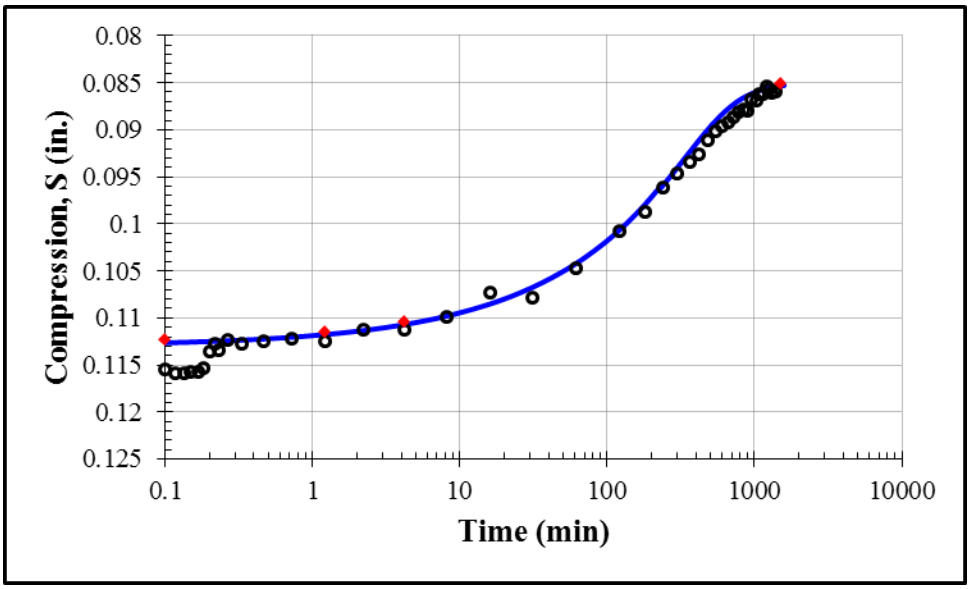

Second Unloading: 4000 psf				
S_0 (in.)	S_{100} (in.)	c_v (in^2/min)	k (ft/day)	t_{50} (min)
0.0825	0.0505	0.000085	1.8 x 10^{-9}	243

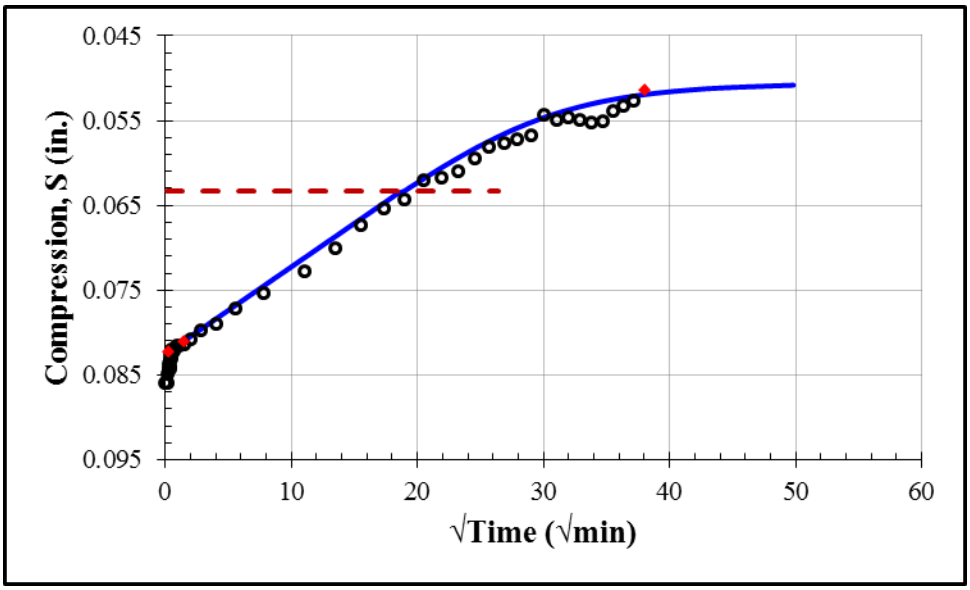

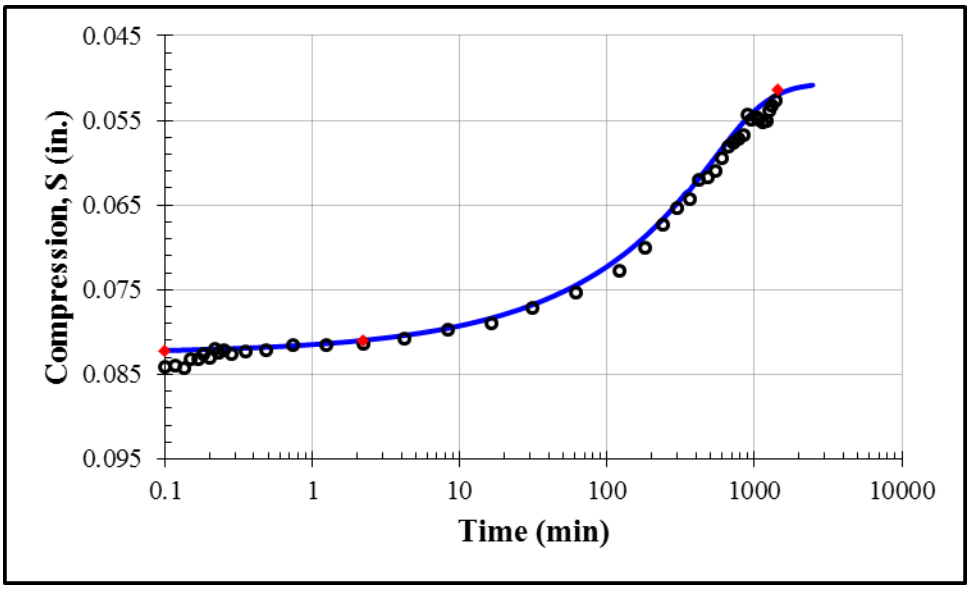

Second Unloading: 1000 psf				
S_0 (in.)	S_{100} (in.)	c_v (in^2/min)	k (ft/day)	t_{50} (min)
0.0506	0.0187	0.00006	5.2 x 10^{-9}	381

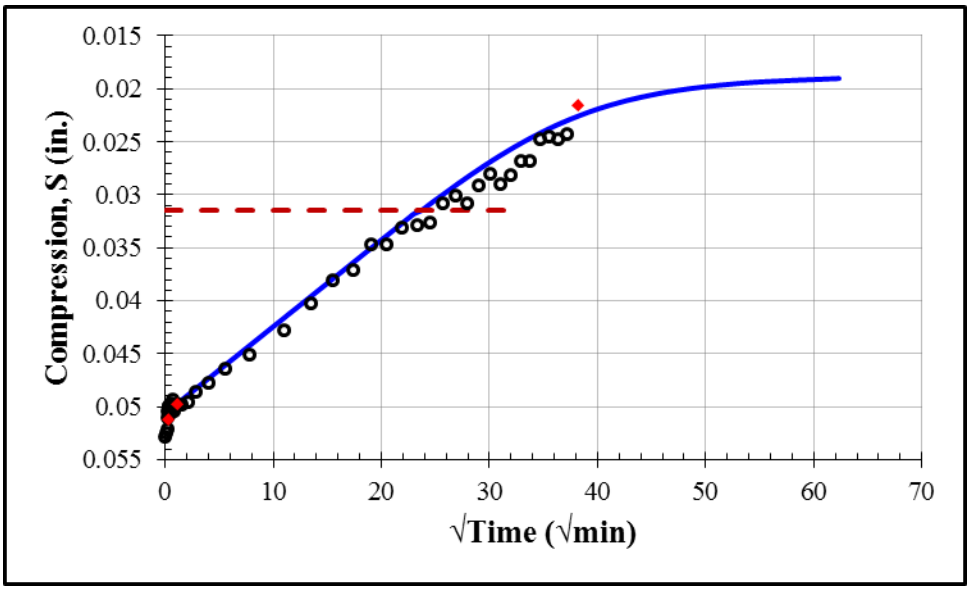

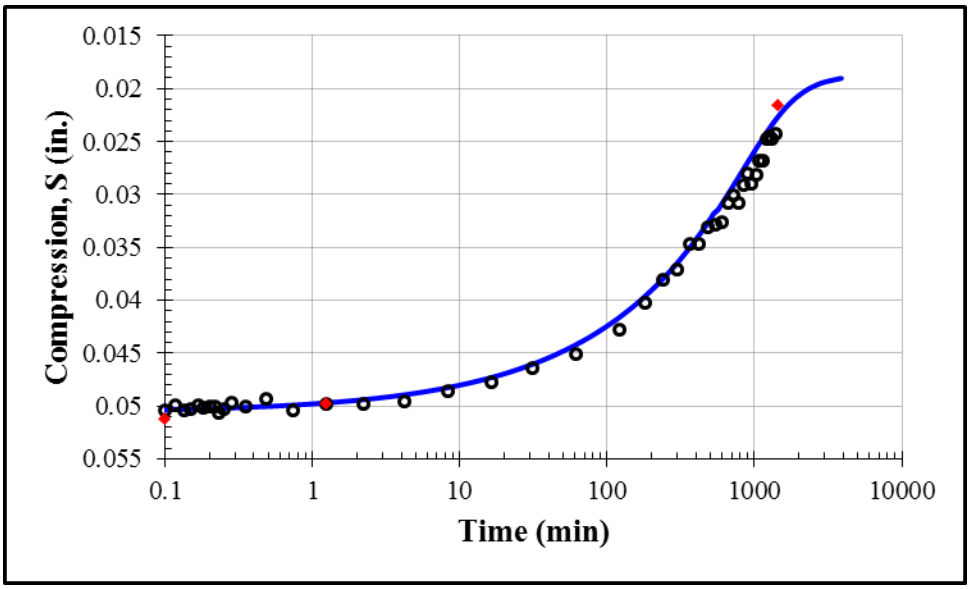

Second Unloading: 250 psf				
S_0 (in.)	S_{100} (in.)	c_v (in^2/min)	k (ft/day)	t_{50} (min)
0.0240	-0.0145	0.000055	2.4 x 10^{-8}	452

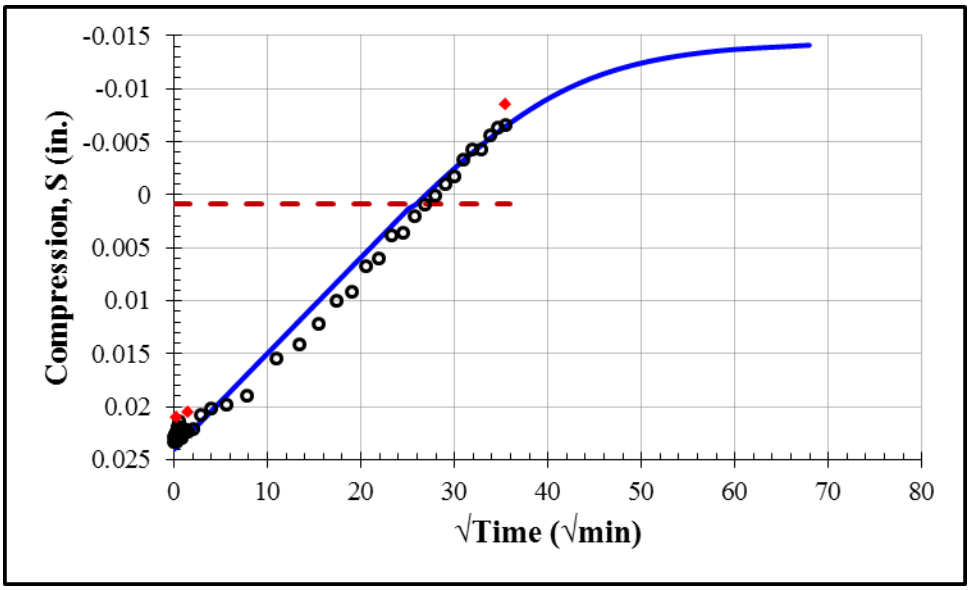

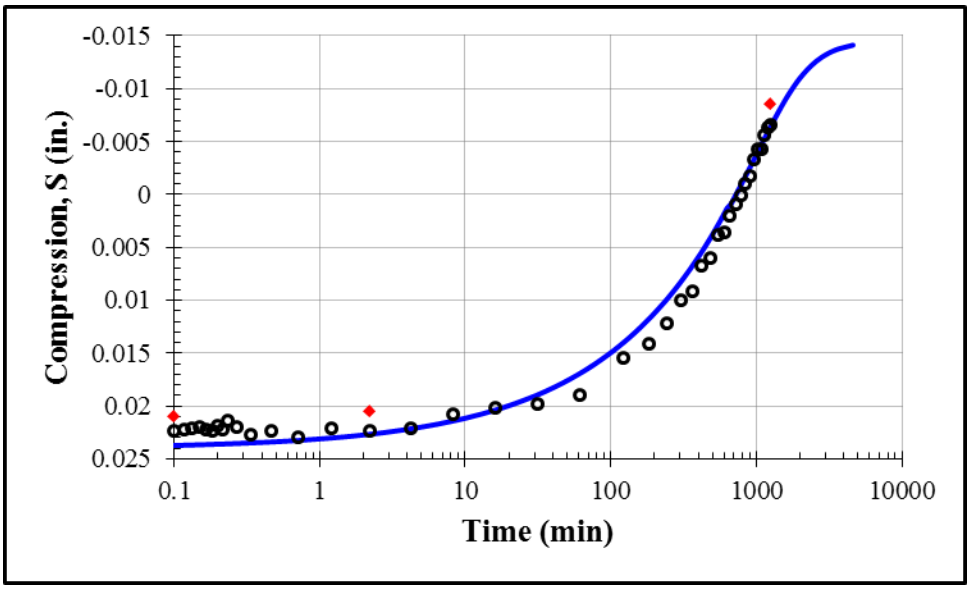

Second Unloading: 125 psf				
S_0 (in.)	S_{100} (in.)	c_v (in^2/min)	k (ft/day)	t_{50} (min)
-0.0075	-0.0358	0.000041	8.1 x 10^{-8}	661

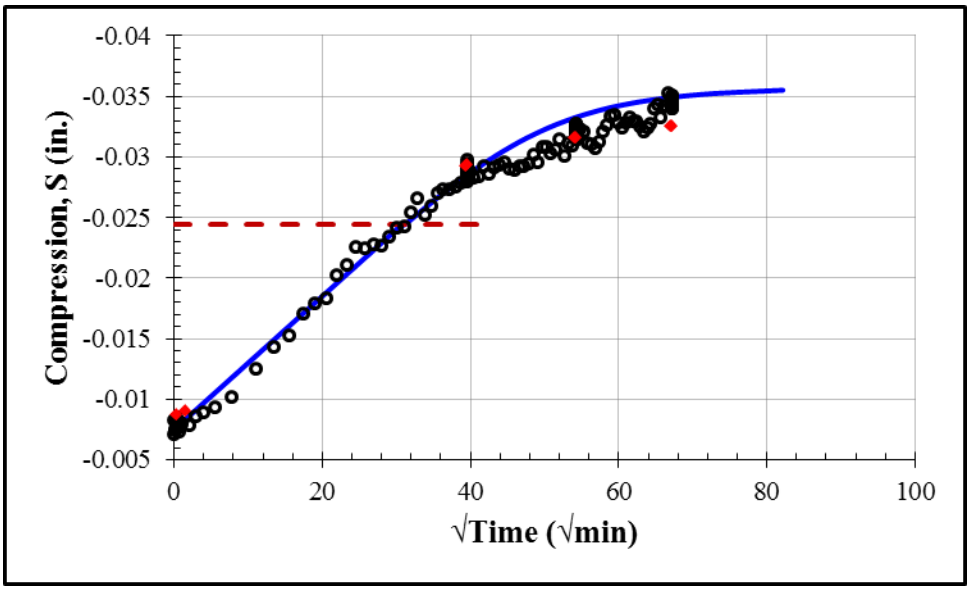

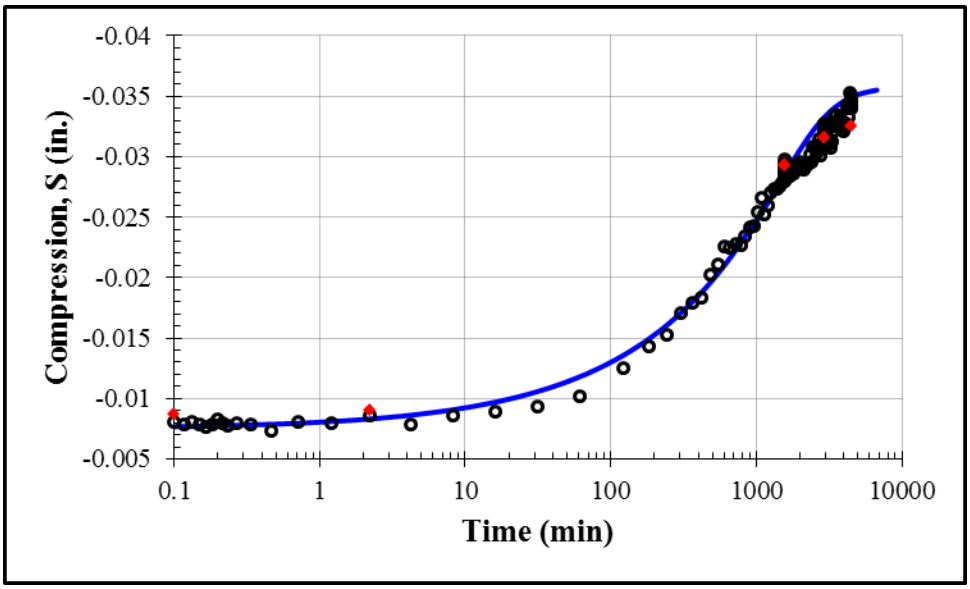

Appendix G: Unconsolidated Undrained Triaxial Test Results

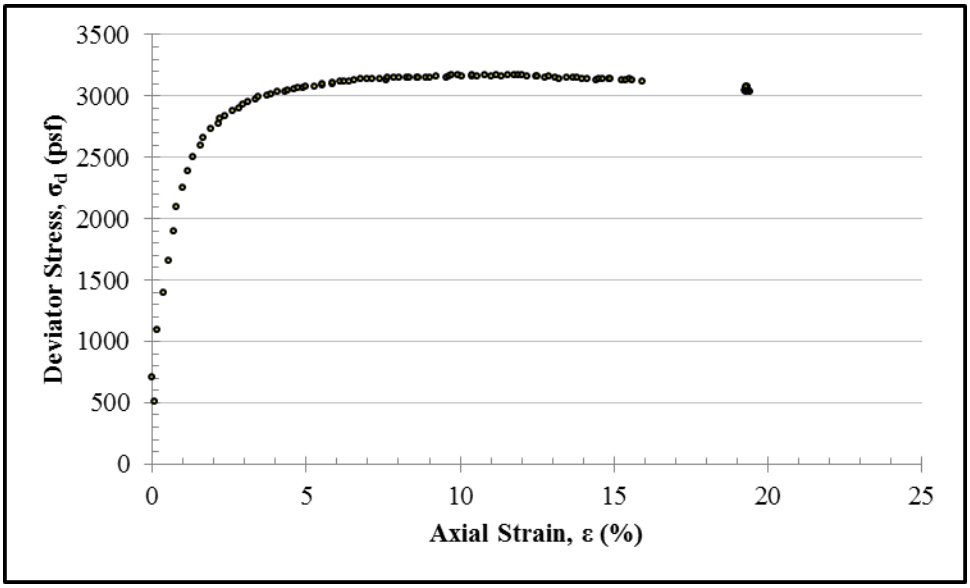

S_u (psf)	1587 psf

Boring ID	B-3
Depth (ft)	4 – 5
Description	dk brown
Confining Pressure (psi)	5
Strain Rate (%/min)	0.7
Average Sample Diameter (in.)	1.43
Average Sample Height (in.)	2.93
Moisture Content (%)	28.4
Unit Dry Weight (pcf)	-
Failure Type	-
Peak Deviator Stress (psf)	3174
Axial Strain at Peak (%)	10.8

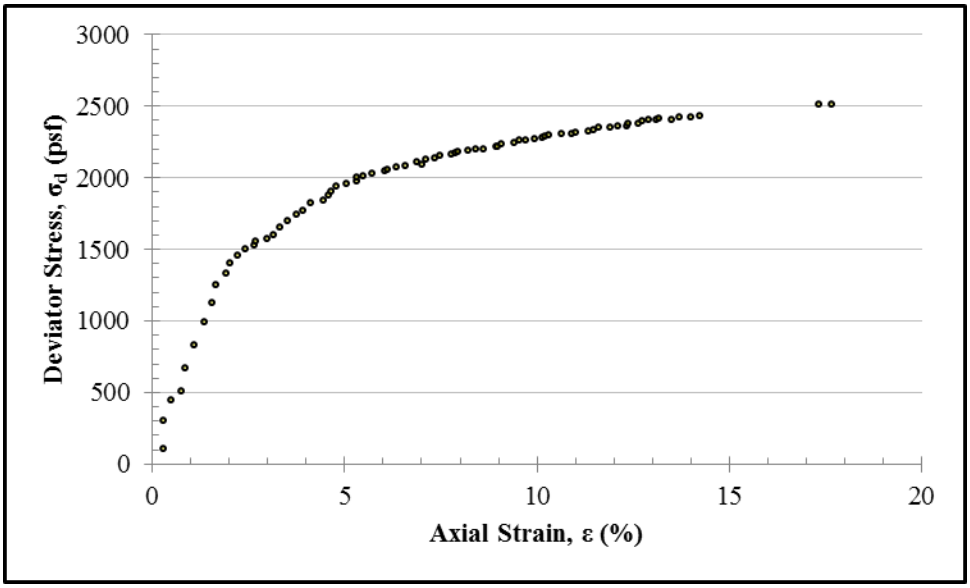

S_u (psf)	1257 psf

Boring ID	B-3
Depth (ft)	8 – 10
Description	tan
Confining Pressure (psi)	9
Strain Rate (%/min)	0.75
Average Sample Diameter (in.)	1.48
Average Sample Height (in.)	2.74
Moisture Content (%)	38.7
Unit Dry Weight (pcf)	-
Failure Type	-
Peak Deviator Stress (psf)	2514
Axial Strain at Peak (%)	17.3

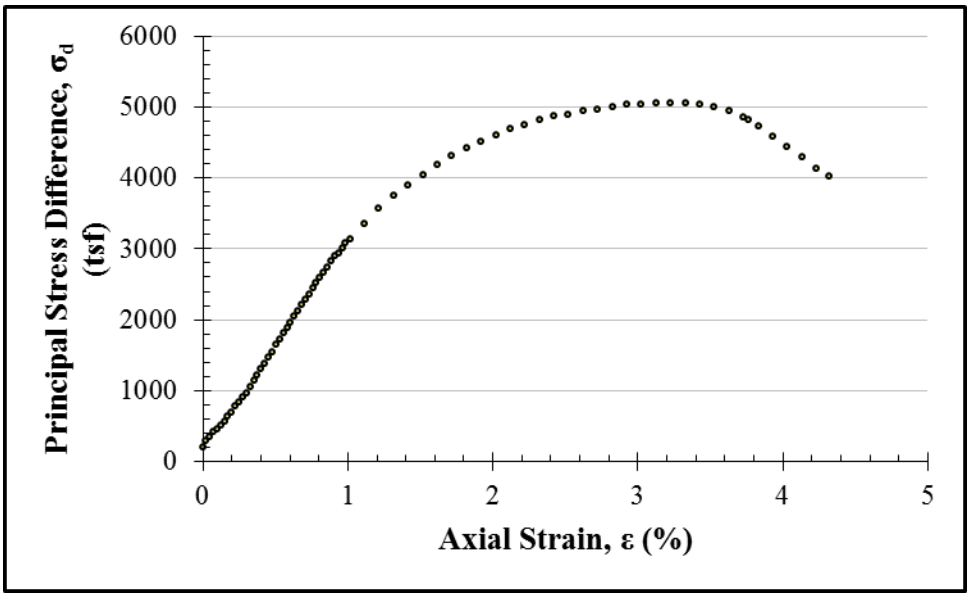

S_u (psf)	2350

Boring ID	B-2
Depth (ft)	8 – 10
Description	tan
Confining Pressure (psi)	10
Strain Rate (%/min)	0.5
Average Sample Diameter (in.)	2.74
Average Sample Height (in.)	5.74
Moisture Content (%)	23.2
Unit Dry Weight (pcf)	80
Failure Type	Multi
Peak Deviator Stress (psf)	12.0
Axial Strain at Peak (%)	4.5

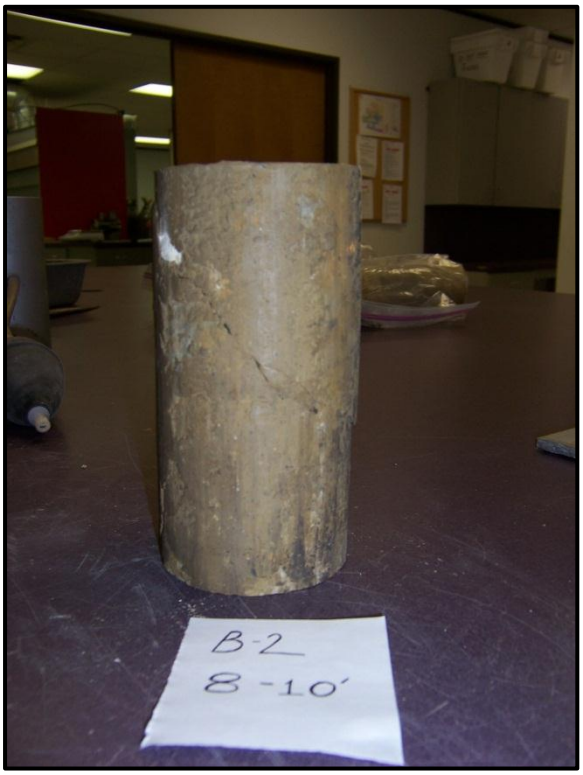

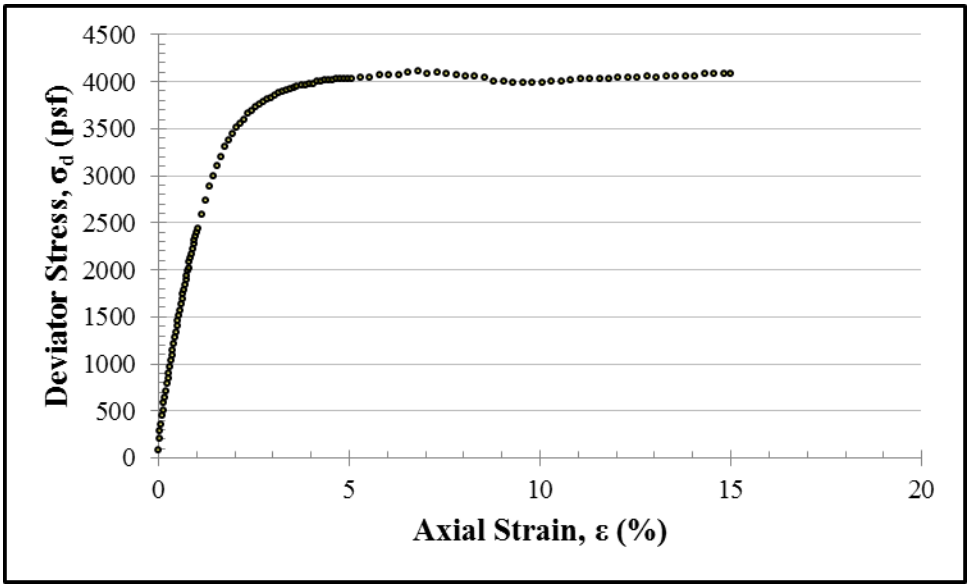

S_u (psf)	2055 psf

Boring ID	B-2
Depth (ft)	13 – 15
Description	tan
Confining Pressure (psi)	14
Strain Rate (%/min)	0.5
Average Sample Diameter (in.)	2.73
Average Sample Height (in.)	5.54
Moisture Content (%)	37.3
Unit Dry Weight (pcf)	83
Failure Type	Multi
Peak Deviator Stress (psf)	4111
Axial Strain at Peak (%)	6.8

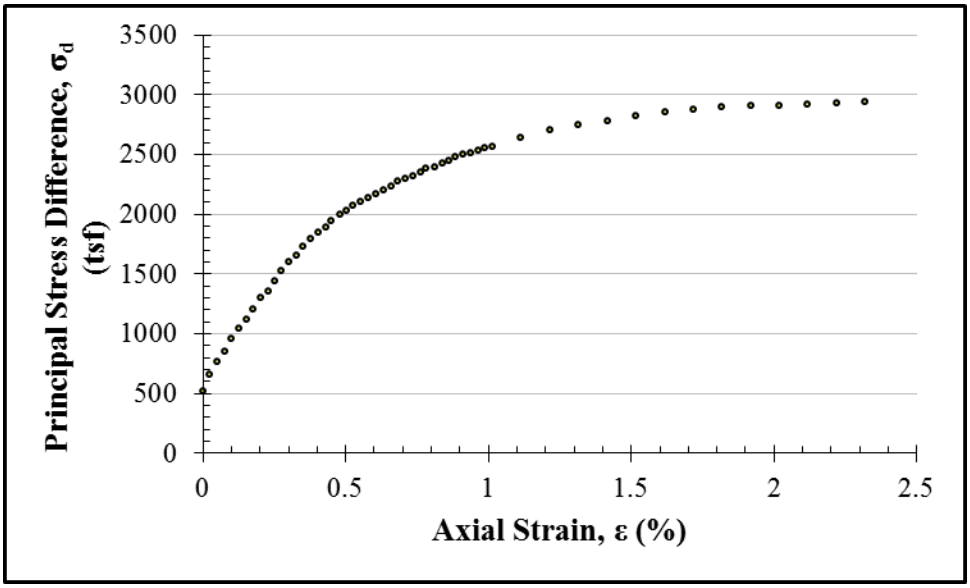

S_u (psf)	1470

Boring ID	B-2
Depth (ft)	18 – 20
Description	dk brown
Confining Pressure (psi)	19
Strain Rate (%/min)	0.5
Average Sample Diameter (in.)	2.73
Average Sample Height (in.)	6.01
Moisture Content (%)	38.8
Unit Dry Weight (pcf)	82
Failure Type	Shear
Peak Deviator Stress (psf)	2934
Axial Strain at Peak (%)	2.32

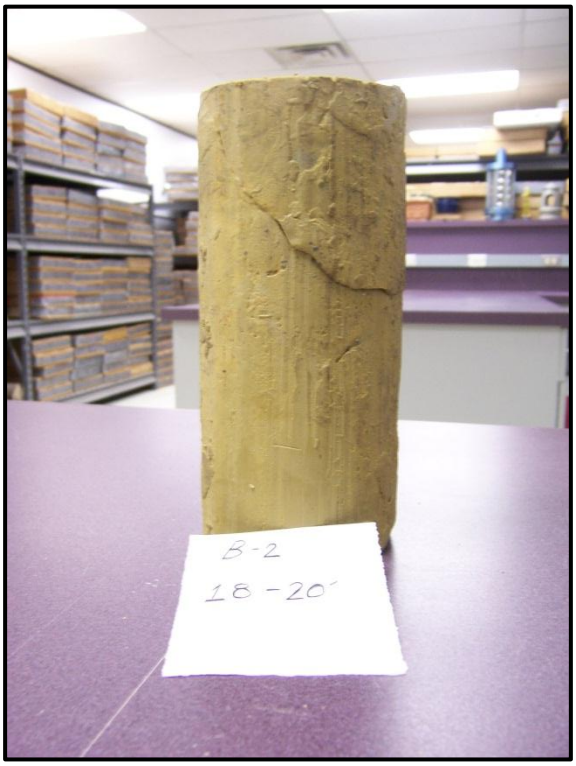

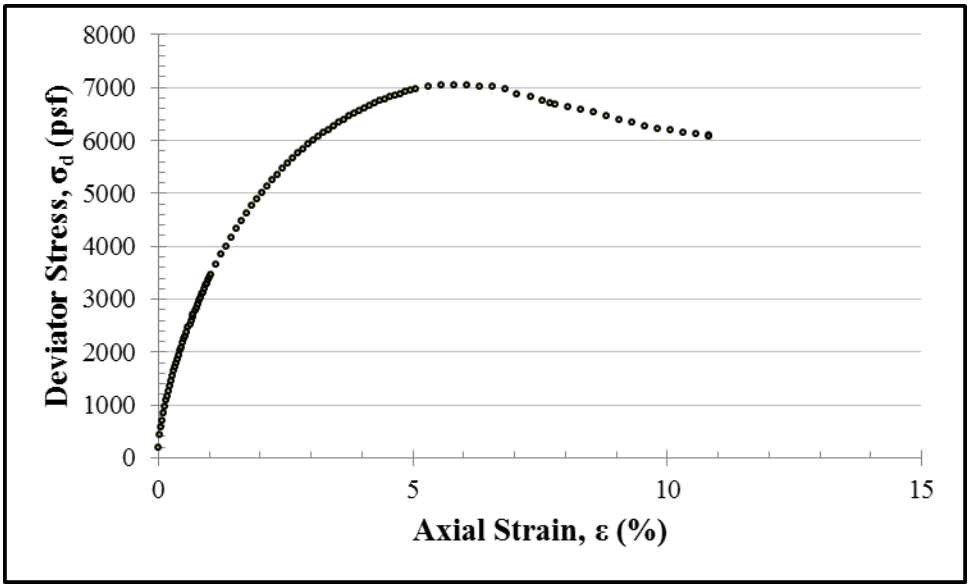

S_u (psf)	3527

Boring ID	B-3
Depth (ft)	23 – 25
Description	tan
Confining Pressure (psi)	24
Strain Rate (%/min)	0.5
Average Sample Diameter (in.)	2.77
Average Sample Height (in.)	5.33
Moisture Content (%)	39.8
Unit Dry Weight (pcf)	81
Failure Type	Multi
Peak Deviator Stress (psf)	7054
Axial Strain at Peak (%)	5.8

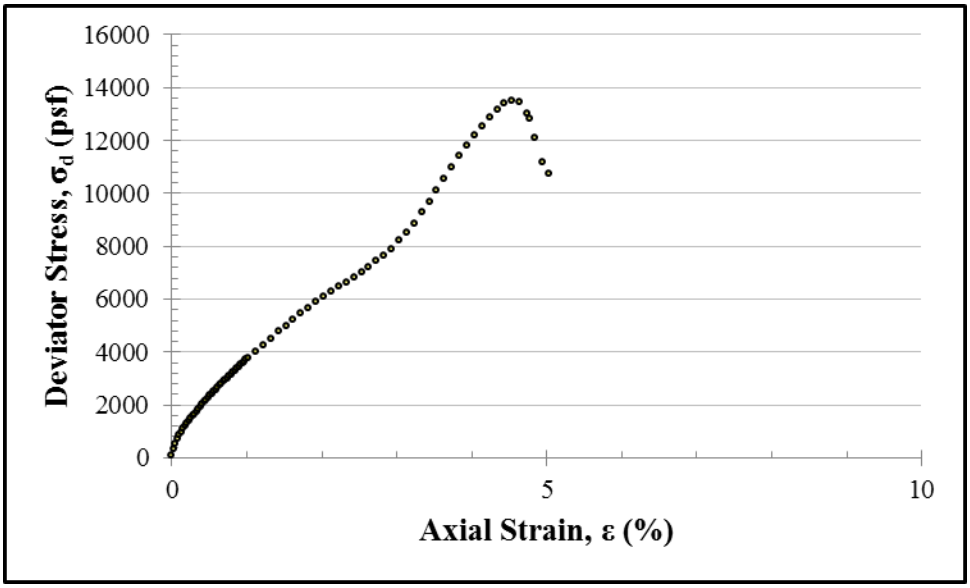

S_u (psf)	6753

Boring ID	B-3
Depth (ft)	33 – 35
Description	stiff
Confining Pressure (psi)	34
Strain Rate (%/min)	0.5
Average Sample Diameter (in.)	2.76
Average Sample Height (in.)	5.79
Moisture Content (%)	30.2
Unit Dry Weight (pcf)	92
Failure Type	Shear
Peak Deviator Stress (psf)	13507
Axial Strain at Peak (%)	4.54

Note: The horizontal crack shown above occurred during trimming. The actual shear surface was not as obvious.

Appendix H: Direct Shear Test Results

Test 1: Peak Shear at 750 psf		
Initial Moisture Content $w_{c,i}$ (%)	Failure Moisture Content $w_{c,f}$ (%)	Nominal Shear Stress at Failure, τ_f (psf)
23.4	25.6	1300

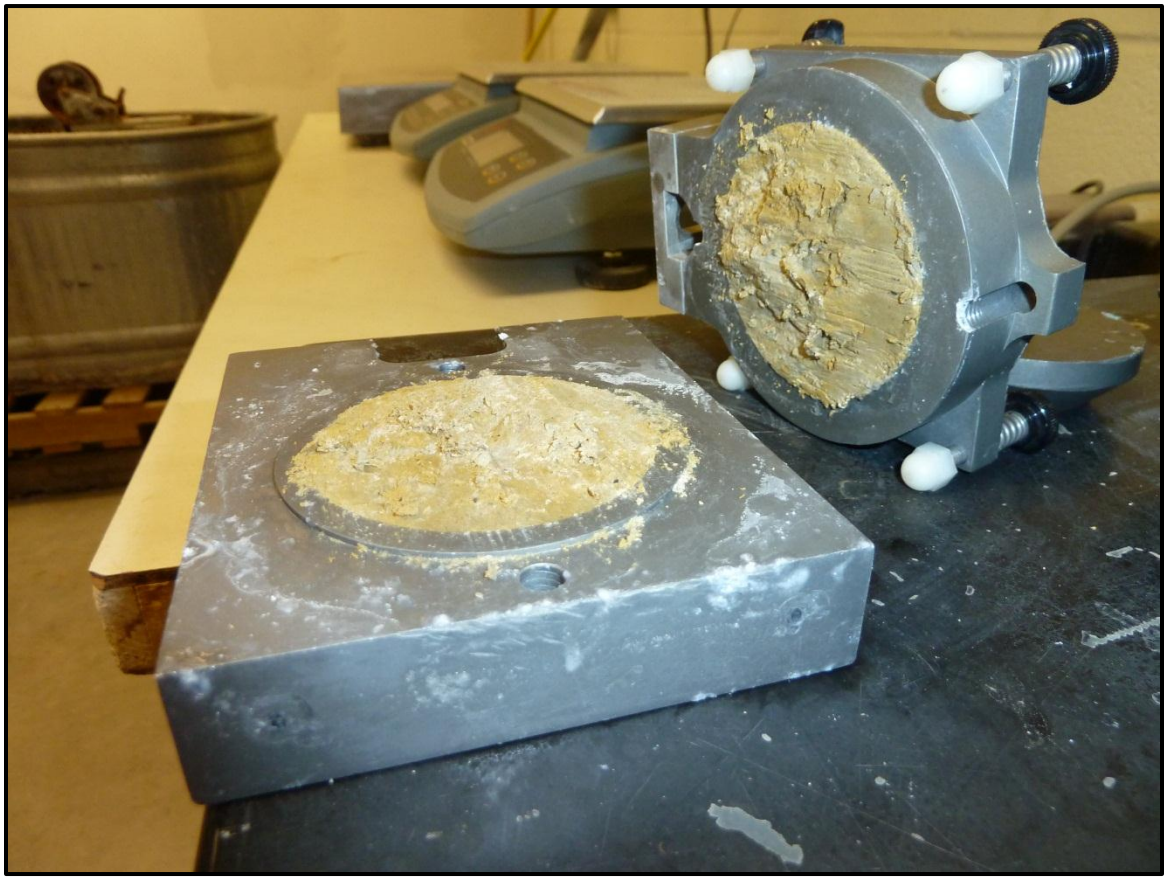

Test 1: 1st Residual Shear at 750 psf		
Initial Moisture Content $w_{c,i}$ (%)	Failure Moisture Content $w_{c,f}$ (%)	Nominal Shear Stress at Failure, τ_f (psf)
25.6	27.6	382

Test 1: 2nd Residual Shear at 750 psf		
Initial Moisture Content $w_{c,i}$ (%)	Failure Moisture Content $w_{c,f}$ (%)	Nominal Shear Stress at Failure, τ_f (psf)
27.6	27.8	270

Test 1: Residual Shear at 1500 psf		
Initial Moisture Content $w_{c,i}$ (%)	Failure Moisture Content $w_{c,f}$ (%)	Nominal Shear Stress at Failure, τ_f (psf)
27.8	27.1	600

Test 1: Peak Shear at 3000 psf		
Initial Moisture Content $w_{c,i}$ (%)	Failure Moisture Content $w_{c,f}$ (%)	Nominal Shear Stress at Failure, τ_f (psf)
27.1	26.1	1185

Test 2: Peak Shear at 1500 psf		
Initial Moisture Content $w_{c,i}$ (%)	Failure Moisture Content $w_{c,f}$ (%)	Nominal Shear Stress at Failure, τ_f (psf)
24.8	23.8	1758

Test 2: 1st Residual Shear at 1500 psf		
Initial Moisture Content $w_{c,i}$ (%)	Failure Moisture Content $w_{c,f}$ (%)	Nominal Shear Stress at Failure, τ_f (psf)
23.8	26.0	1011

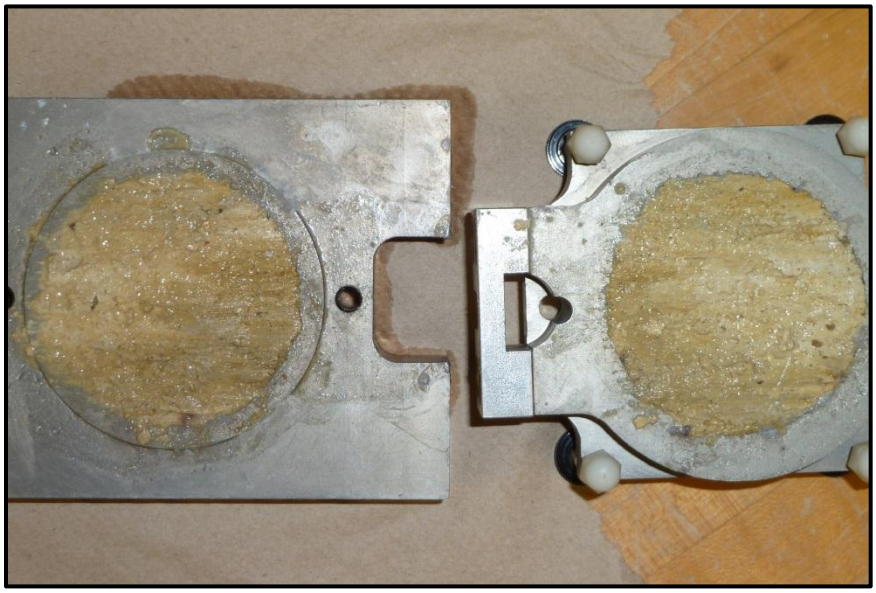

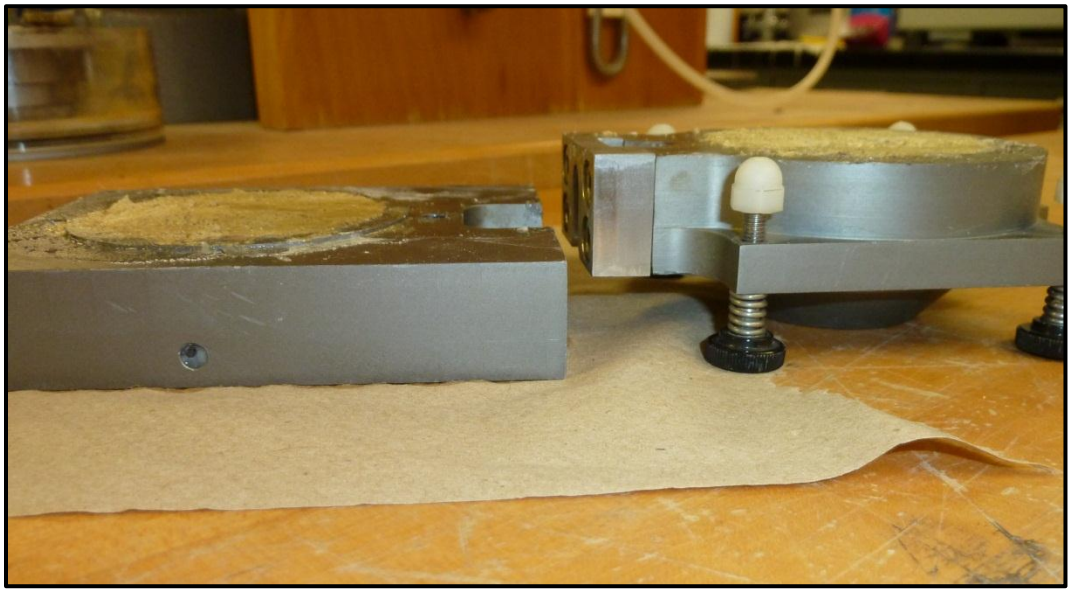

Test 2: 2nd Residual Shear at 1500 psf		
Initial Moisture Content $w_{c,i}$ (%)	Failure Moisture Content $w_{c,f}$ (%)	Nominal Shear Stress at Failure, τ_f (psf)
26.0	26.4	1082

Test 2: Residual Shear at 3000 psf		
Initial Moisture Content $w_{c,i}$ (%)	Failure Moisture Content $w_{c,f}$ (%)	Nominal Shear Stress at Failure, τ_f (psf)
26.4	28.2	1644

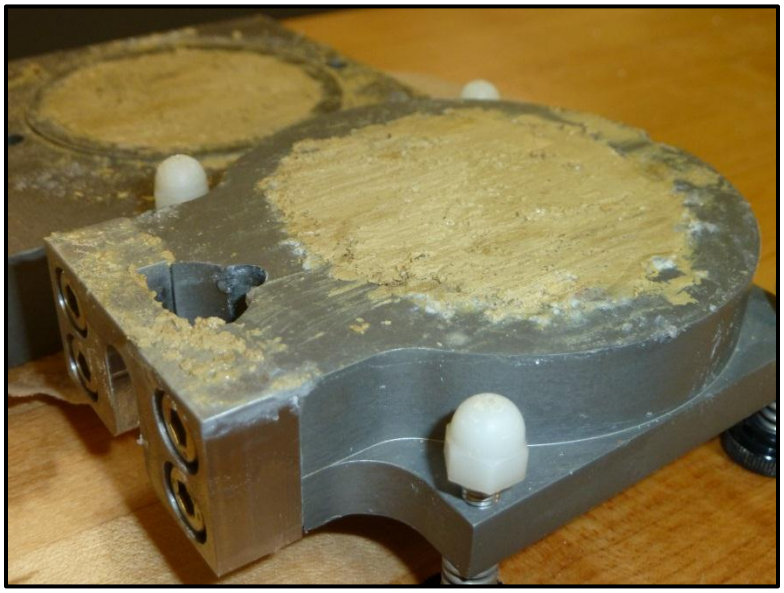

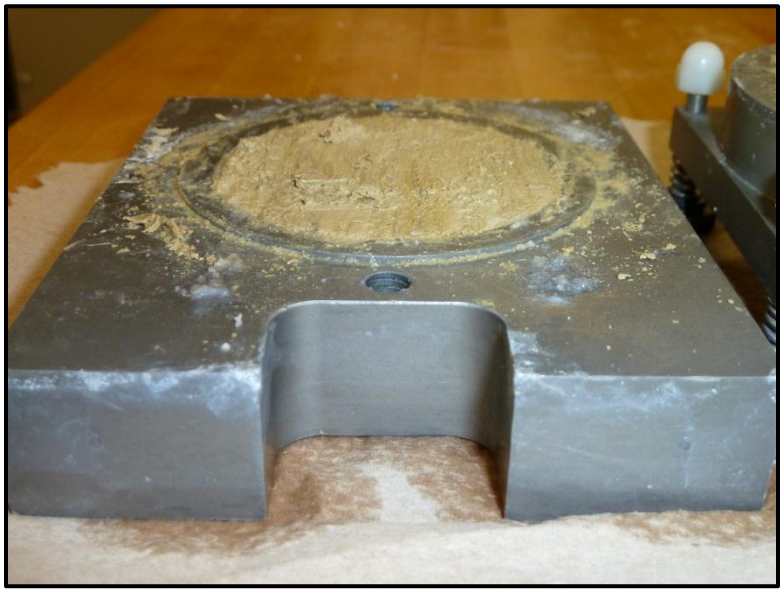

Test 2: 1st Residual Shear at 6000 psf		
Initial Moisture Content $w_{c,i}$ (%)	Failure Moisture Content $w_{c,f}$ (%)	Nominal Shear Stress at Failure, τ_f (psf)
28.2	24.8	2766

Test 2: 2nd Residual Shear at 6000 psf		
Initial Moisture Content $w_{c,i}$ (%)	Failure Moisture Content $w_{c,f}$ (%)	Nominal Shear Stress at Failure, τ_f (psf)
24.8	28.4	2860

Test 3: Peak Shear at 3000 psf		
Initial Moisture Content $w_{c,i}$ (%)	Failure Moisture Content $w_{c,f}$ (%)	Nominal Shear Stress at Failure, τ_f (psf)
21.8	26.1	2061

Note: Top half of specimen was ejected from shear box while separating halves after peak shear.

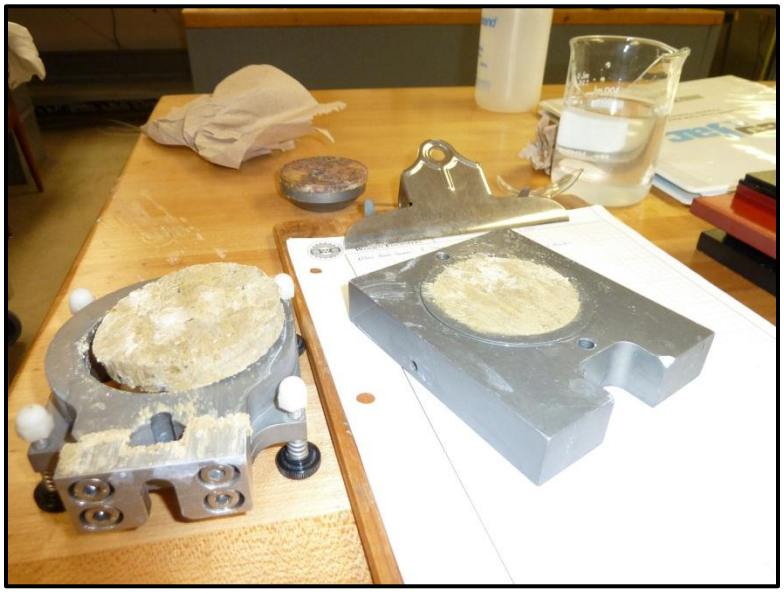

Test 3: 1st Residual Shear at 3000 psf		
Initial Moisture Content $w_{c,i}$ (%)	Failure Moisture Content $w_{c,f}$ (%)	Nominal Shear Stress at Failure, τ_f (psf)
26.1	28.9	1634

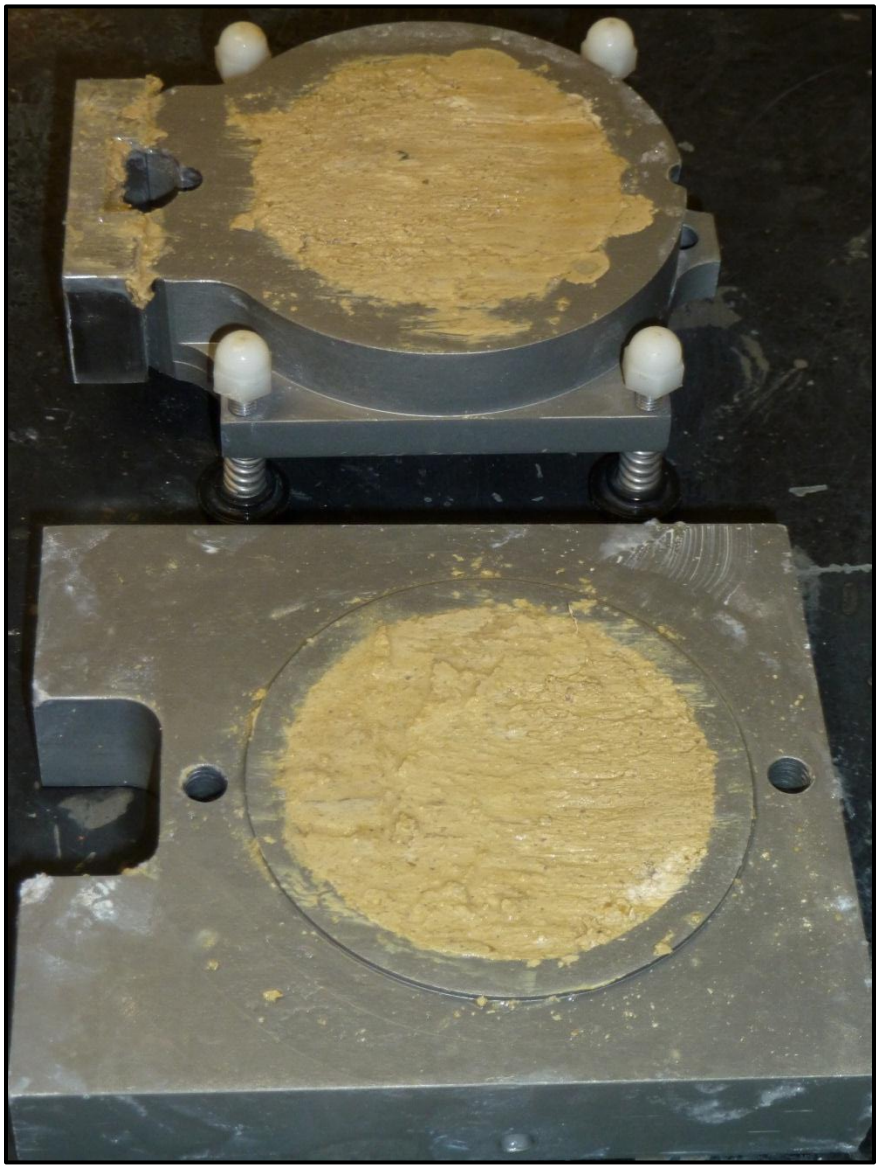

Test 3: 2nd Residual Shear at 3000 psf		
Initial Moisture Content $w_{c,i}$ (%)	Failure Moisture Content $w_{c,f}$ (%)	Nominal Shear Stress at Failure, τ_f (psf)
28.9	28.7	1471

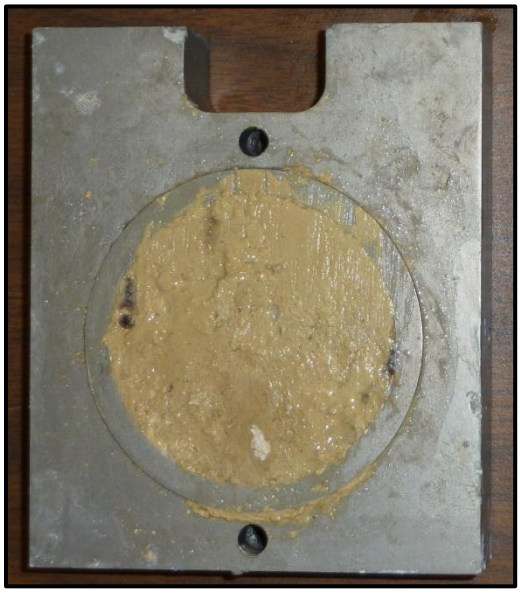

Test 3: Residual Shear at 6000 psf		
Initial Moisture Content $w_{c,i}$ (%)	Failure Moisture Content $w_{c,f}$ (%)	Nominal Shear Stress at Failure, τ_f (psf)
28.7	29.1	2705

References

Allen, J. A. 2005. Forced Ventilated Swell-Shrink Test for Potential Vertical Expansive Soil Movement. M.S. Thesis, The University of Texas at Austin.

ASTM D1586 "Standard Test Method for Standard Penetration Test (SPT) and Split-Barrel Sampling of Soils"

ASTM D2216 "Standard Test Methods for Laboratory Determination of Water (Moisture) Content of Soil and Rock by Mass"

ASTM D2435 "Standard Test Methods for One-Dimensional Consolidation Properties of Soils Using Incremental Loading"

ASTM D2487 "Standard Practice for Classification of Soils for Engineering Purposes (Unified Soil Classification System)"

ASTM D2850 "Standard Test Method for Unconsolidated-Undrained Triaxial Compression Test on Cohesive Soils"

ASTM D3080 "Standard Test Method for Direct Shear Test of Soils Under Consolidated Drained Conditions"

ASTM D422 "Standard Test Method for Particle-Size Analysis of Soils"

ASTM D4318 "Standard Test Methods for Liquid Limit, Plastic Limit, and Plasticity Index of Soils"

ASTM D4546 "Standard Test Methods for One-Dimensional Swell or Settlement Potential of Cohesive Soils"

Beal, A. O. 1964. Stratigraphy of the Taylor Formation (Upper Cretaceous), East-Central Texas. Baylor Geological Studies Bulletin No. 6, Baylor University.

Burford, S. O. 1928, Characteristics of the Taylor Marl of Travis County, Texas. M.A. Thesis, The University of Texas at Austin.

Chen, F. H. 1988. Foundations on Expansive Soils. American Elsevier Science Publication, New York.

Daksanamurthy, V. and Raman, V. 1973. A Simple Method of Identifying an Expansive Soil, Soil and Foundations. Japanese Society of Soil Mechanic and Foundation Engineering. 13(1): 97 – 104.

Dellinger, G. 2011. The Use of Time Domain Reflectometry Probes for Moisture Monitoring of a Drilled Shaft Retaining Wall in Expansive Clay. M.S. Thesis, The University of Texas at Austin.

Fredlund, D. G., Hasan, J. U. and Filson, H. L. 1980. The Prediction of Total Heave. 4th International Conference on Expansive Soils. American Society of Civil Engineers.

Funk, A. C. 1975. The Relationships of Engineering Properties to Geochemistry in the Taylor Group, Travis County, Texas. M.A. Thesis, The University of Texas at Austin.

Garner, L. E. and Young, K. P. 1976. Environmental Geology of the Austin Area: An Aid to Urban Planning. Austin: Bureau of Economic Geology, University of Texas at Austin.

Jonas, E. C. and Brown, T. E. 1959. Analysis of Interlayer Mixtures of Three Clay Mineral Types by X-ray Diffraction. Jour. Sed. Petrology, v. 29: 77 – 86.

Joshi, R. P. and Katti, R. K. 1980. Lateral Pressure Development Under Surcharges. 4th International Conference on Expansive Soils. American Society of Civil Engineers.

Katti, R. K. and Katti, A. R. 1994. Behaviour of Saturated Expansive Soil and Control Methods. New Delhi Central Board of Irrigation and Power. A. A. Balkema, Rotterdam, pp 33 – 42.

Kayyal, M. K. 1986. Effects of Wetting and Drying on Long-Term Strength of Compacted Taylor Marl Clay. M.S. Thesis, The University of Texas at Austin.

Kodikara, J., Barbour, S. L. and Fredlund, D. G. 1999. Changes in Clay Structure and Behaviour Due to Wetting and Drying. Proceedings of the 8th Annual Austrailian-New Zealand Conference on Geomechanics, Hobart. pp 179 – 186.

Marr, S. A. 2003. A Practical Method for Modeling Expansive Soil Behavior. M.S. Thesis, The University of Texas at Austin.

Mitchell, J. K. and Kenichi, S. 2005. Fundamentals of Soil Behavior, Third Edition. John Wiley & Sons, Inc.

Nelson, J. D. and Miller, D. J. 1992. Expansive Soils: Problems and Practice in Foundation and Pavement Engineering. John Wiley & Sons, Inc.

Olson, R. E. 2009. Incremental Vertical-Flow Consolidation Test. Class Notes, The University of Texas at Austin.

Popescu, M. 1980. Behavior of Expansive Soils with a Crumb Structure. 4th International Conference on Expansive Soils. American Society of Civil Engineers.

Long, J. H. and Reese, L. C. 1983. An Investigation of the Behavior of Vertical Piles in Cohesive Soils Subjected to Repetitive lateral Loads. Geotechnical Engineering Report GR83-7. Geotechnical Engineering Center, the University of Texas at Austin.

Reese, L. C., Isenhower, W. M. and Wang, S. T. 2006. Analysis and Design of Shallow and Deep Foundations. John Wiley & Sons, Inc.

Seed, H. B., Woodward, R. J., Jur. and Lundgren, R. 1962. Prediction of Swelling Potential for Compacted Clays. Journal of Soil Mech. Found. Div., American Society of Civil Engineers, 88 (SM3):53-87.

Skempton, A. W. 1953. The Colloidal Activity of Clays. Proceedings of the 3rd International Conference on Soil Mechanics and Foundation Engineering, Switzerland. V.1:57 -61.

Skempton, A.W. and LaRochelle, P. 1965. The Bradwell Slip: A Short-Term Failure in London Clay. Geotechnique, 15:3, pp 221-242.

Stark, T. D. and Eid, H. T. 1994. Drained Residual Strength of Cohesive Soils. ASCE, Journal of Geotechnical Engineering, 120, 856-871.

Stark, T. D. and Eid, H. T. 1997. Slope Stability Analyses in Stiff Fissured Clay. ASCE, Journal of Geotechnical and Geoenvironmental Engineering, 123(4), 335-343.

Tawfiq, S. and Nalbantoglu, Z. 2009. Swell-Shrink Behavior of Expansive Clays. 2nd International Conference on New Developments in Soil Mechanics and Geotechnical Engineering, Nicosia, North Cyprus, 28 – 30 May, 2009.

Tex-101-E "Test Procedure for Preparing Soil and Flexible Base Materials for Testing"

Tex-132-E "Test Procedure for Texas Cone Penetration"

Terzaghi, K. and Peck, R. 1943. Soil Mechanics in Engineering Practice. New York, John Wiley & Sons, Inc.

Tipple, G. L. 1975. Clay Minerology and Atterberg Limits of the Taylor Group in the Vicinity of Austin, Texas. M.A. Thesis, The University of Texas at Austin.

TxDOT Geotechnical Manual. 2000. Texas Department of Transportation, Bridge Division, Austin, Texas.

Van-Hue, N. 1966. The Effects of Repeated Loading on the Strength and Deformation of Taylor Marl Clay Stabilized with Lime. M.S. Thesis, The University of Texas at Austin.

Walcott, C. D. 1901. Twenty-First Annual Report of the United States Geological Survey to the Secretary of the Interior, 1899-1900. Part VII – Texas. pp. 336-338.

Young, K. 1965. A Revision of Taylor Nomenclature, Upper Cretaceous, Central Texas. Bureau of Economic Geology, Geology Circular 65-3.